



**HAL**  
open science

# WIND DEVICES INTEGRATED INTO BUILDING FACADES

David Serero

► **To cite this version:**

David Serero. WIND DEVICES INTEGRATED INTO BUILDING FACADES: Modeling and performative study of innovative wind devices integrated into the architecture of buildings for energy production. Environmental Sciences. Université Paris Est, 2021. English. NNT: . tel-04116480

**HAL Id: tel-04116480**

**<https://theses.hal.science/tel-04116480>**

Submitted on 4 Jun 2023

**HAL** is a multi-disciplinary open access archive for the deposit and dissemination of scientific research documents, whether they are published or not. The documents may come from teaching and research institutions in France or abroad, or from public or private research centers.

L'archive ouverte pluridisciplinaire **HAL**, est destinée au dépôt et à la diffusion de documents scientifiques de niveau recherche, publiés ou non, émanant des établissements d'enseignement et de recherche français ou étrangers, des laboratoires publics ou privés.

PARIS-EST UNIVERSITY  
DOCTORAL SCHOOL

Doctoral thesis  
in Architecture of

David Serero

# WIND DEVICES INTEGRATED INTO BUILDING FACADES

Modeling and performative study of innovative  
wind devices integrated into the architecture  
of buildings for energy production

under the direction of :  
Robert LE ROY, Jean-Denis PARISSÉ and co-supervised by Loïc Couton

Defended on Wednesday January 13, 2021  
ENSA Paris-Val de Seine - 3 Quai Panhard Levassor - Paris 13<sup>e</sup>

Jury members:

**Laurent Lescop**, Professor at ENSA d'Architecture de Nantes, Architect, Rapporteur  
**Julien Weiss**, Professor at the Technical University of Berlin, Rapporteur  
**Sandrine Aubrun**, Professor at the Ecole Centrale de Nantes, examiner  
**Loïc Couton**, Professor at ENSA Paris-Malaquais  
**Robert Leroy**, Professor at ENSA Paris-Malaquais  
**and Jean Denis Parisse**, Lecturer, HDR at the University of Aix-Marseille



# SUMMARY

SUMMARY .....	3
FOREWORD .....	9
SUMMARY .....	11
1. GENERAL INTRODUCTION.....	13
PART 1 WIND AND ARCHITECTURE .....	13
1. HISTORICAL LANDMARKS IN THE USE OF WIND FOR VENTILATION AND ENERGY PRODUCTION .....	14
2. IMPACT OF WIND TURBINES ON THE TERRITORIES .....	15
1.3. SCIENTIFIC STATE OF THE ART .....	15
1. ANALYSIS OF BUILDING TYPOLOGIES IN URBAN AREAS: THE EXAMPLE OF PARIS .....	16
PART 2 METHODOLOGY OF ANALYSIS AND WIND SURVEYS IN URBAN AREAS .....	23
2. INTRODUCTION.....	23
2.1.WIND MAPPING AND GEOGRAPHICAL POTENTIAL ANALYSIS .....	23
2.2.METHODOLOGY OF ANEMOMETRIC DATA COLLECTION IN URBAN AREAS .....	24
2.3. COMPARATIVE ANALYSIS OF WIND ENERGY SYSTEMS .....	25
2.4.CONCLUSION .....	28
PART 3 MODELING AND PERFORMANCE EVALUATION OF DEVICES.....	29
3. INTRODUCTION.....	30
1. PRINCIPLES OF AIR MOVEMENT IN URBAN AREAS.....	30
1. PHYSICAL PRINCIPLES OF FLUID MECHANICS .....	32
2. METHOD OF MODELING AND DEFINITION OF INITIAL CONDITIONS OF THE SIMULATION .....	35
3. NUMERICAL SIMULATION OF A BUILDING ROOFING SYSTEM WITH 3 TYPES OF INITIAL CONDITIONS .....	36
4. Conclusion.....	36
PART 4 METHODOLOGY FOR INTEGRATING DEVICES INTO ARCHITECTURAL ENVELOPES.....	36
4.0 INTRODUCTION.....	37
1. PRESENTATION OF THE METHODOLOGY .....	37

2.	NUMERICAL MODELLING - THEORETICAL STUDY 1 : A LOW VOLUME IN AN OPEN AREA .....	37
3.	THEORETICAL STUDY 2 : VERTICAL ACCELERATORS - BUILDING PLAN WITH FOIL TYPE V1.....	38
4.	THEORETICAL STUDY 3 : ACROTHERIAL DEVICES .....	38
5.	THEORETICAL STUDY 4: A HOUSING BUILDING IN AN URBAN SUBURB - BUILDING AT 136 AVENUE PARMENTIER, 75011 PARIS .....	39
6.	THEORETICAL STUDY 4 : AN IGH BUILDING IN A SALES SITE.....	39
7.	ASSESSMENT OF THESE 4 STUDIES .....	39
8.	STUDY OF WIND TURBINES ADAPTED TO ARCHITECTURAL INTEGRATION .....	43
PART 5 DESIGN AND ARCHITECTURAL INTEGRATION OF DEVICES.....		46
1.	INTRODUCTION .....	46
2.	PRESENTATION OF THE ARCHITECTURAL DESIGN METHOD .....	46
3.	TYPES OF INTEGRATED TURBINES AND EXPERIMENTAL STUDY MODELS .....	48
4.	QUANTIFICATION OF THE POWER OF THE DEVICES .....	48
5.	PRINCIPLE ESTIMATION OF THE GLOBAL ENERGY PRODUCED IN A TYPICAL CITY .	49
6.	ACTIONABLE DENDROGRAMS FOR DESIGN SUPPORT.....	50
7.	EXAMPLES OF ARCHITECTURAL INTEGRATION OF WIND POWER GENERATION DEVICES .....	51
7.1.	Old or heritage buildings.....	51
8.	CREATION OF AN OPEN ACCESS LIBRARY OF WIND ENERGY DEVICE MODELS ON A COLLABORATIVE BIM PLATFORM .....	51
6.	GENERAL CONCLUSION.....	51
APPENDIX 1: INITIAL STUDY OF THE RESEARCH: CONSTRUCTION OF AN EXPERIMENTAL WIND TUNNEL AND CALIBRATION OF THE NUMERICAL MODEL OF THE SIMULATION		
APPENDIX 2: DATA SHEETS OF WIND ENERGY CAPTURE DEVICES.....		51
APPENDIX 3: EXISTING BUILDING-INTEGRATED WIND ENERGY SYSTEMS .....		51
APPENDIX 4: EXAMPLE OF A WIND TURBINE STUDY USING A GENERATIVE DESIGN TOOL (FUSION 360).....		52
APPENDIX 5: A CALCULATION REPORT OF THE STARCCM+ SIMULATION .....		52
BIBLIOGRAPHIC REFERENCES .....		53
INDEX OF ILLUSTRATIONS.....		54





## ACKNOWLEDGEMENTS

In the four years of development of this work, a large number of people, institutions and laboratories have contributed to this research, in simple telephone conversations, meetings, or sometimes by spending long hours analyzing or rereading this work. These exchanges, reflections and hypotheses have deeply nourished the thesis and have led to the maturity of the work.

I will not be able to name all these people here and I apologize in advance to those I have forgotten to mention.

I would first like to thank the people who supervised this research: Robert Leroy for his particular attention to the work and to the methodological approach in the different stages of the project.

Jean-Denis Parisse of the Ecole de l'Air for his precious support in the steps of this work and for having carefully followed my experiments and my training on the numerical simulation of fluids in particular on the STARCCM+ software.

And, in particular, Loïc Couton who strongly participated in initiating this work and encouraged me in starting the thesis. For 3 years, from 2013 to 2016, we jointly conducted a research seminar at the Paris-Malaquais School of Architecture on the design of smart envelopes. This seminar, which fascinated the students, raised on several occasions, the strong potential of building facades for the control of interior ambiances, but especially their potential for the production and distribution of energy to the whole building.

Gilles Bouchet from the IUSTI laboratory and teacher at the Ecole des Ponts was able to verify the calculation hypotheses, the results of the numerical simulations and the evaluation of the generated powers. His access to a computer farm allowed me to obtain results on simulations that I could not calculate with my limited means (or that would have taken several weeks of calculation).

I thank the GSA laboratory of ENSA Paris-Malaquais and its director Maurizio Brocato for their support and the exchanges we had throughout this work.

As well as the EVCAU laboratory, of ENSA Paris Val-de-Seine, and all its members for all their support and help in the multiple experiments of wind survey and analysis that I did on this large building of the urban campus of Paris-Diderot. This building was an important study site because of its location on a clear and windy axis at the edge of Paris.

The school of architecture Paris Val-de-Seine and its director Philippe Bach who allowed me to use the computer laboratories for the calculation of many simulations and for the installation on the roof of the school of several connected anemometers.

The Ecole des Ponts, for giving me access to their formidable research library, which is essential for the bibliographic work, and for allowing me to use their physical wind tunnel. Unfortunately, due to the COVID 19 health crisis, this possibility could not be fully explored in this study.

Pascal Terracol and Stéphanie Boufflet, who, as part of the thesis monitoring committee, took the time to comment on the work with great intelligence and kindness and to answer the questions of method raised by the research.

Margarita Ferrucci, from Soufflerie Eiffel for her pertinent remarks on the choice of case study sites and her advice on the implementation of the connected anemometers for wind analysis.

Coralie Betbeder from Ecole Polytechnique, for her help in setting up numerical simulations.

The Netatmo company, for letting me hijack their products and implement them in an experimental way on construction sites in order to generate a valuable data cloud for this research.

The Fablab of the Paris Val-de-Seine school and the Fablab of Volumes and in particular Corentin Boiteau for the digital printing of dozens of models of turbines and buildings in order to test on a reduced scale the results of our analyses and their architectural integration.

I would also like to thank all the owners, contractors, construction companies who allowed me to visit, survey, photograph or measure buildings, towers, windmills, water pumps for the needs of this research such as: the Syndical Council of 136 Avenue Parmentier (which authorized me to install several anemometers as early as 2016 on the roof of this building), the Community of Communes Bayeux Intercom for the readings on the roof of the Bayeux media library, the University of Grenoble Alpes for the measurements on the Climat Planète research center, the windmills of Pla San Jordi in Majorque, the windmill of Coudrey (14), the public affairs center of San Francisco, USA, the Marina Bay Sands hotel of Singapore and its kinetic wind façade, the wind tower of the gardens of Dolat-abad in Yazd in Iran, the great Aeolus, the vertical axis wind turbine of Cap-Chat in Montreal.

And all the collaborators of the SERERO agency who participated in the fabrication of physical models, wind turbine prototypes and the long calculations of simulations, and in particular: Mahdi Derakhshan, Hsin-Yu Chen and Camille Ballon.

I would also like to thank the members of the jury of this thesis who all accepted, without any hesitation, to participate in the defense of this research and in the long process of evaluation of this work: Sandrine Aubrun, Julien Weiss and Laurent Lescop.

## FOREWORD

This work aims at obtaining a doctorate in architecture. This relatively recent device has been dominated by the historical or social studies of architecture and is still the subject of debate in French schools of architecture, particularly at a time when the status of teacher-architects is being aligned with that of teacher-researchers at the university: What is a thesis in architecture? Is it a discipline of the social sciences, or of engineering? Is an architectural work not already an act of research? If the architect develops in certain cases new knowledge on the art of building, does he not generate an artistic approach that does not constitute a contribution to the practice or to the methods of design?

These questions remain unanswered, and each architecture dissertation contributes to the clarification and definition of this type of doctorate.

My research has taken the singular axis of relying on **a double body of knowledge**: architectural design and fluid mechanics, allowing architecture to get out of its isolation between Arts and Engineering and to propose a cross-fertilization of these disciplines. The approach is therefore transdisciplinary, and aims to shift the field of study of fluid mechanics by studying the impact of wind in hyper-localized areas of large buildings, and to inform the architectural design on the change of airflow inevitable at the periphery of its envelope.

Could we propose a new approach to design by combining the tools of analysis and calculation of fluid mechanics phenomena with the expertise of an architect in the urban sector?

This research, halfway between architecture and engineering, is facilitated by **emerging digital tools**, which allow the realization of building data that would have been difficult to envisage before. This information constitutes a **"project design environment"** aiming to "profile", to draw the building, according to **a performative method, rather than on a simple artistic approach**.

The method of architectural design that architects use: parallel design from one scale to another of the project, refinement of the global meaning of the project to its finest expression in the architectural details, realization of prototypes and prefiguration of the assembly of materials of the project, are proven methods to analyze, understand and design a space.

However, in spite of the efforts and hours spent to improve my technical knowledge in fluid mechanics, I cannot be considered as a specialist in the subject. The calculation method, the boundary conditions and initial conditions, the choice of the calculation algorithm have a major importance in the accuracy of the results. Details in these elements can easily make the calculation deviate from the real behavior and seriously degrade the accuracy of the calculation. The complete acquisition of this knowledge is beyond the time frame of this research.

On the other hand, the possibility for the architect to interact directly with the analysis tools allows him to better understand the impact of each of his choices on the environment of the project, its urban and territorial context. It now seems obvious that if digital data constitute a new body of research, researchers must learn to master their analysis and manipulation. **The architect-researcher** thus establishes data generation and analysis devices, and develops an informed design mode of the Design by Data type.



## SUMMARY

Cities, because of their wide variety of building heights, streets corridors and open spaces, have an important potential in the creation of wind acceleration zones. For a long time, airflows generated by buildings have been seen as nuisance for the city. This research on urban wind, by the use of advanced computer fluid dynamics modelization (CFD) showcases that one can precisely locate and evaluate the potential of accelerated airflows around buildings. How would cities look like, in the future, if architects would seize this technology and integrate micro-wind turbines to their design?

This research analyzes several architectural designs based on the airflow simulation model we developed, compares the results with on-site wind speed data survey around buildings, and presents design examples with fully integrated design of wind turbine to building. The method developed in the research aims to provide a straightforward design methodology for architects to integrate wind energy harvesting devices to their projects.

Our research proposes to address the potential of wind energy in urban city, considering that cities are now planned with high level of details 3D models, or with large scale 3D scans of buildings blocks (Lidar technology). Computer fluid dynamics simulations of large urban districts have the potential to become now part of the conceptual tools of architects and designers. Building envelopes are becoming smarter; Building's façade or rooftops are available for wind energy harvesting devices integrated to building, such as photovoltaic panels and wind turbines.

Combining connected anemometers wind survey with computational fluid dynamic (CFD) software STARCCM+, we simulated the reaction between wind and several building typologies to predict potential extracted energy by measuring wind speed acceleration (the extracted energy depends on the cube of the wind speed). The geometry of buildings contributes to wind speed enhancement.

Following an in-depth analysis on the performance and behavior of existing building that integrates these devices, we further studied devices such as "aérofoil" (an acceleration and control wing at the edge of the turbine) to accelerate wind speed to a specific point and to stabilize airflow turbulences. The aérofoil's goal is to developed strategies to compensate the unstable airflows conditions in urban environment and to optimize the wind speed amplification effect of buildings.

In conclusion, if most energy engineers have turned away from urban wind energy harvesting because of their turbulent characteristics, each building can be considered as a wind accelerator with a high potential for cities to produce renewable energy locally, closer to the consumption area.

*Keywords-*

*CFD simulation in urban environment*

*Wind energy harvesting devices*

*Net-Zero Energy Building*

*Urban wind behavior Simulation*



# 1. GENERAL INTRODUCTION

## 1. Background of the research

Without wind, would there be life on our Earth? If the winds in our atmosphere are capable of moving 150,000 tons of sand grains in a few minutes, of pumping millions of tons of water in the Netherlands, of participating in the movement and fertilization of the vegetation on our planet, their invisible force is often neglected and undervalued, except for a few spectacular episodes that they offer us during the passage of typhoons or storms... And yet, it is only wind.

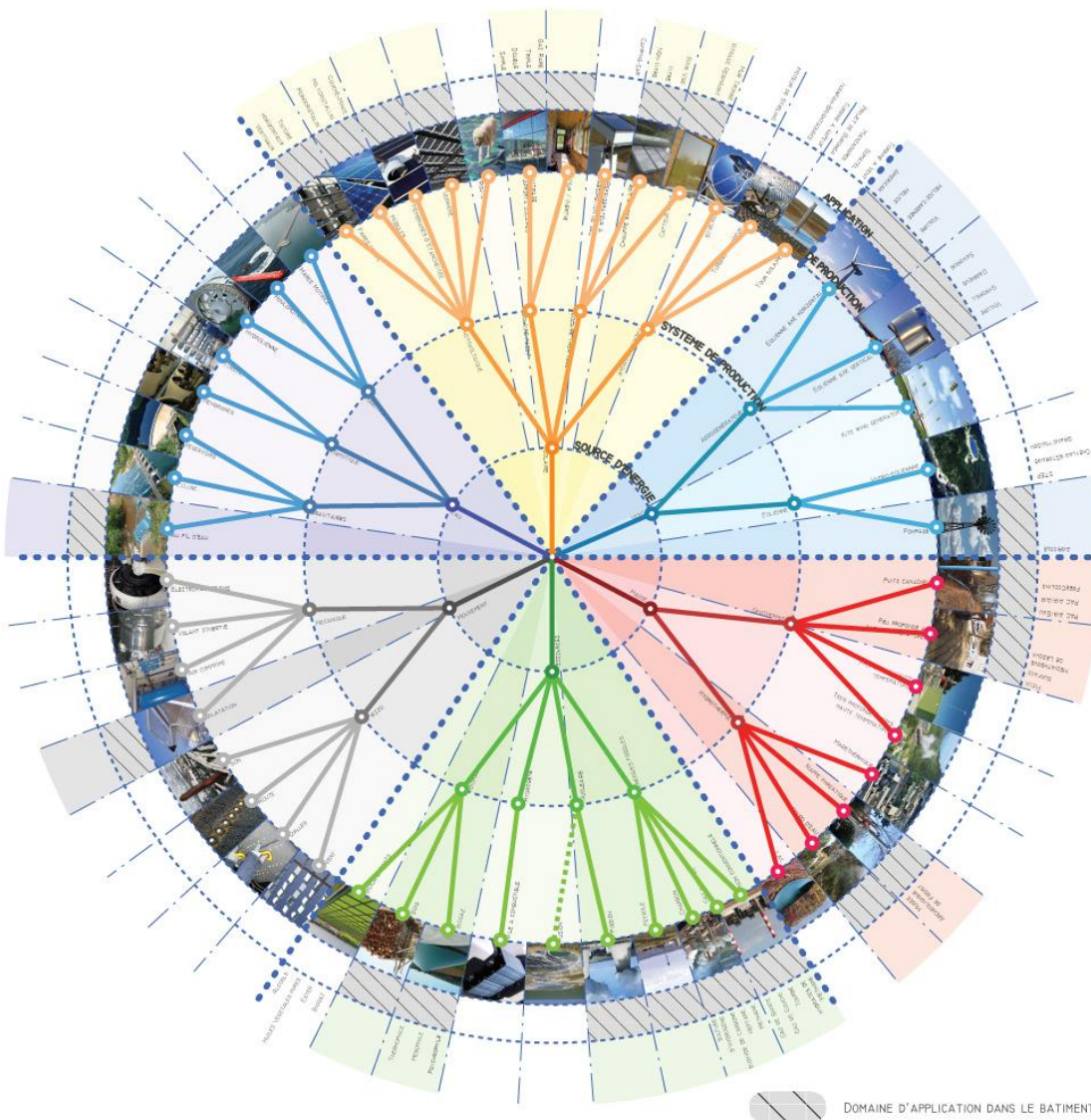


Figure 1. Mapping of renewable energy sources not currently used in buildings By D. Serero

In 1891, two years after the construction of his famous tower in Paris, Gustave Eiffel stopped building high-rise structures to concentrate exclusively on the study of the impact of winds on

buildings thanks to the wind tunnel he built in Auteuil<sup>1</sup>. He devoted the last 20 years of his life to analyzing and understanding the rules of aerodynamics and vibration of structures.

This work of Eiffel marks the change from his work as an engineer specializing in the optimization and construction of steel structures to a research of experimental simulations of wind force. Gustave Eiffel would write, "*wind is the main constraint of light structures of great height.*"<sup>2</sup> Architects and engineers would spend the next 50 years improving the strength of structures, optimizing the amount of material needed for each design, and limiting the vibratory effects of wind that can weaken them or generate whistling.

This energy from solar radiation and the displacement of very large volumes of air on our planet has a fundamental impact on our climate, but the meteorological phenomenon is complex and difficult to understand. It has often been seen as the archetype of the Chaos theory "can the flapping of a butterfly's wings in Brazil cause a tornado in Texas?"<sup>3</sup> mathematicians<sup>4</sup> and meteorologists who had access to the first computer simulations since the 1970s.

This research has taken the singular axis of relying on a double body of knowledge: architectural design and fluid mechanics allowing to propose a combined contribution of these disciplines.

Halfway between architecture and engineering, this work is facilitated by emerging digital tools, allowing the production of building data that would have been difficult to envisage before. This information constitutes a "*project design environment*" aiming at "profiling", at drawing the building, according to a performative method, rather than a simple artistic approach.

## 2. Rethinking where energy is produced

A wind of protest has been blowing for several years on the implementation of wind turbines in the landscape: The discovery of the harmful impacts on biodiversity, air pollution by micro-vibrations, kinetic effects of wind blades harmful to health, awareness of the heritage value of the great landscape and the acceleration of climate change with increasing episodes of violent winds on our planet are all points of resistance to the development of this energy on our territory.

On the other hand, the very great loss of energy by electromagnetic induction along long distance cables (30% of the energy produced by the wind turbines is lost during the transport of the energy) pushes us to consider a **bringing closer of the zones of energy production to the zones of energy consumption**. New wind turbine devices of micro-turbine type (in

---

<sup>1</sup> The Eiffel wind tunnel is located at 67 rue Boileau in Paris 16<sup>ème</sup> and is still in operation today.

<sup>2</sup> Gustave EIFFEL, *Scientific Works Performed at the 300-Meter Tower: From 1889 to 1900*, BnF collection ebooks, 2016, 318 pp.

<sup>3</sup> Title of the conference given by the American meteorologist Edward Lopez in 1972 at the American Association for the Advancement of Science. The computer simulations that he carried out as early as 1963 make him one of the precursors of this typical phenomenon of the chaos theory.

<sup>4</sup> Henri Poincaré and Pierre-Simon de Laplace, mathematicians precursors of the chaos theory. This theory assumes that a very small deviation on a parameter can have a significant influence on the resulting situation at a later date.

particular with vertical axis) allow us to consider the reuse of an **urban and built territory** for the diffuse and continuous production of renewable energy.

The arrival of gearless direct drive wind turbines (which limits noise and maintenance of the gearbox) combined with the emergence of connected objects can form the **basis of a new space of sharing and exchange of energy geolocated in real time**. The control of demand and resource make us move to the new paradigm of micro-decentralization of energy production in order to meet the challenges of smoothing wind power production (related to wind surges).

These problems of deployment of wind energy on our territories, raise several working hypothesis to rethink this operation:

- Could we work on the landscape of our cities in order to propose a better integration of these devices in an urban panorama?
- Could we bring the places of energy production closer to the places of consumption?
- Can our buildings become energy collectors, and integrate a field of smaller grouped wind turbines rather than a few large ones?

### 3. Objectives of the research

While studying the past uses of wind, from the first windmills, to the development of urban micro-wind turbines, and analyzing new paradigms such as energy sharing and exchange, or anemometer readings in urban sites, we defined four main objectives for the thesis:

- 1 - Measuring and sharing hyper-localized wind data in urban areas (free access, Open data type)
- 2- Development of a scientific and architectural method for modeling wind flow and evaluating its speed around buildings
- 3- On the basis of this analysis, design of architectural devices for energy production in coherence with the architecture of the building.
- 4- Definition of a simplified method of "manual" type to help the architectural design of integrated energy production devices: the dendrogram

These objectives allow, in the logic of the architectural project, to accompany the designer from the analysis of the site to the integration of wind energy systems in his project. The data on the site will be the basis for developing a reflection and a methodology of design of energy production systems embedded in the project.

### 4. Methodologies deployed in the research

As part of my architectural practice on the performance of architectural envelopes, I have studied, on several occasions, the possibility of transforming buildings into supports for wind energy capture devices (see Figure 1). These attempts are one of the factors that motivated this research work. The techniques of numerical aerodynamic simulation, offer a new horizon to analyze these phenomena of flow and interaction of particles. Since 2015, and in particular since my work at the Villa Medici on the simulation of acoustic effects in a performance space<sup>5</sup>, I am convinced of the need **to develop new tools for the analysis of physical phenomena to rethink our way of designing** buildings.

The first step of the research is to establish a state of the art through bibliographic and technical research. A lot of research has been done on the optimization, evaluation or design of wind energy production systems. Much less research exists on the issue of embedded micro-wind turbines, and even less on the mode of wind survey in urban sites.

One of the objectives of this research is to categorize the different types of wind in urban areas and to identify their flow patterns around buildings. To do so, we implemented **a method of urban wind data collection**, which allows us to establish a map of urban winds. For this, we used connected ultrasonic anemometers that were installed at several study sites. The continuous wind data provided at each of these points is then used as a reference for the numerical simulation of the airflow.

In this research, we have also used a **method of numerical simulation using the software STAR CCM +**. These simulations are made from 3D models of buildings and urban areas, which we have modeled (Revit, Rhinoceros). The calculation environment is parameterized according to the wind conditions of the experiment and the type of result sought. This method allows to develop the complete volumetric model of the wind behavior on a roof area, or an urban block in its entirety.

Thirdly, we have established a nomenclature of the main micro-wind turbine devices and their type of implementation in urban sites. By identifying the wind spectra, we can define the choice and performance of energy collection devices that could be implanted on the building. We can also determine the method of attachment to the roof or facade, the type of wind, the altimetry of the device in relation to the level of the roofs, and the potential nuisance in the surrounding area.

In spite of the important efforts made within the framework of this research to improve my technical knowledge in fluid mechanics, I cannot be considered as a specialist in urban aerodynamics. The calculation method, the boundary conditions and initial conditions, the choice of the calculation algorithm have a capital importance in the precision of the results. Several elements, in the initial conditions, or in the calculation method have sometimes been simplified to fit in reasonable calculation times of less than 3 to 5 days.

## 5. Presentation of the plan

This research is structured around five parts:

---

<sup>5</sup> David SERERO, "Acoustic domes with variable geometry", *Journal of the French Academy in Rome Villa Medici*, 04/2006 p.

The first part, **Wind and Architecture**, reviews the first uses of wind in the emergence of renewable energy. In particular, this chapter allows us to discover the variety of wind devices adapted to urban sites.

The second part focuses on the **methodology of architectural integration of energy production devices**. This chapter makes an extensive study of building typologies in eclectic urban sites and proposes an approach to the phenomenon of wind turbulence in urban sites.

Several of these building typologies have been the subject of multiple anemometric measurements performed specifically for this research. The installation of connected anemometers on a building allows to prefigure an urban network to collect and share wind data in real time.

The third part: **Modeling and the performative evaluation of the devices** sets up the experimental model used to carry out the aerodynamic studies of this research. We have privileged, following several experiments, a numerical simulation of the devices, calibrated and compared to wind measurements by ultrasonic anemometers (carried out on half a dozen buildings located in the Greater Paris).

The fourth part studies several cases of implementation of these devices and a **performative evaluation of several prototypes**, combining 3D modeling of the envelopes with a digital wind tunnel simulation using the STAR CCM+ software. The digital analysis of the architectural form allows for the adjustment of the project's profiling and this is presented on 3D printed study models.

The **fifth part** presents a large number of architectural integration simulations in existing buildings or those under construction. This chapter presents the basis of a "manual" dedicated to architects and designers allowing to quickly evaluate the interest of integrating a wind energy collector in a building.

In summary:

1 - Wind and architecture, reviews the state of the art on the subject and defines the research problem

2 - Wind mapping, presents the methods of wind mapping and the difficulties in obtaining hyperlocal data in urban areas

3 - Airflow numerical simulation method, presents the method and the airflow calculation mode implemented on STAR-CCM+.

4 - Methodology for the design of wind devices, develops a large number of calculations and experiments to profile and design wind gas pedals

5 - Architectural integration and dendrogram, develops the architectural approach of these systems and establishes the elements of a design guide

Conclusion and perspectives, summarizes the research and some development perspectives of this work



# PART 1

## WIND AND ARCHITECTURE

*From the first uses of wind to renewable energy*



### Contents:

- History of wind energy and building ventilation
- Analysis of the problems generated by traditional wind turbines
- Studies of building typologies in the urban landscape: the example of Paris



WIND AND ARCHITECTURE .....	19
2. HISTORICAL LANDMARKS IN THE USE OF WIND FOR VENTILATION AND ENERGY PRODUCTION .....	23
2.1. FROM THE FIRST WINDMILLS TO OFFSHORE WIND TURBINES.....	23
2.2. From the first windmills to offshore generators .....	23
2.3. The first windmills - Two examples in Iran .....	24
2.4. Case study of wind towers called Badgir .....	25
2.5. The emergence of the windmill.....	28
• Tower mills .....	29
• Pivot or candlestick mills.....	29
• The cavier mills .....	30
• Evaluate the power of windmills .....	30
2.6. From the Cleveland Wind Turbine to Modern Wind Turbines.....	32
2.7. The evolution of offshore wind installations.....	35
2.8. The expected technological breakthrough of the floating farshore wind turbine .....	36
2.9. Advantages and disadvantages of offshore wind technology.....	36
2.10. Limitations encountered in their use .....	36
2.11. Manufacturers and operators on a global scale.....	37
2.12. Energy production of offshore wind farms .....	37
2.13. Development area and seascape .....	37
2.14. Key dates in the development of offshore parks .....	38
2.15. The future of this technology .....	38
2.16. Evolution of wind behavior analysis devices .....	39
• TYPES OF WIND TUNNELS.....	39
- Eiffel wind tunnel.....	39
- Aerodyne Wind Tunnel.....	43
- Wind Tunnel of Saint Cyr .....	44



## 2. HISTORICAL LANDMARKS IN THE USE OF WIND FOR VENTILATION AND ENERGY PRODUCTION

### 2.1. FROM THE FIRST WINDMILLS TO OFFSHORE WIND TURBINES

This chapter, entitled Winds and Architecture, is developed along 3 axes:

- First, a historical and technical synthesis of the history of wind energy
- Secondly, the analysis of the problems generated by traditional wind turbines
- Third, studies of building typologies in the urban landscape, taking the example of Parisian buildings.

Many devices have been developed by men to produce energy by using natural phenomena such as wind, tides, water currents.

Whether it is the draining of polders in the Netherlands, the production of flour by windmills or the development of maritime navigation, wind has always been an important and fascinating source of development of human activity and a witness of man's intelligence to use local resources. Sports-related inventions such as kitesurfing, or hydrofoil boat racing are interesting examples of man's mastery of the wind for the discovery of the territory or for simple pleasure.

### 2.2. From the first windmills to offshore generators

From ancient times, from Babylon to the coasts of Persia, windmills spread first through the Middle East, before being established in Egypt. Around the year 1000, windmills were used as tools to grind cereals (rotating stone millstone), to extract oil or to pump the water necessary for the irrigation of crops. They replaced tedious and repetitive human work. At the end of the 19th century, Germany had more than 18,000 of them on its territory, and Finland 20,000. We are interested here in some singular elements of the history of wind control and the creation of the first wind turbines until their most recent development.

In the VIII<sup>ème</sup> century, in Iran, the creation of "wind walls" or windmills constitutes the architectural identity of certain cities in the desert. The remarkable example of the city of Yazd in Iran and its wind chimneys called Badgir make it possible to ventilate, as early as the VIII<sup>ème</sup> century, houses by the use of geothermal air currents (passing through the horizontal wells of cooling). This constitutes the birth of air conditioning by simple air movement (convection based on the temperature between hot and cold). These examples show that, very early on, the management of the wind around the building participates in the climatic and architectural design of these buildings, just like that of the houses in the landscape of Brittany or Provence linked to the great pendular winds (Mistral, the west winds).

### 2.3. The first windmills - Two examples in Iran



Figure 2. The raw earth windmills of the city of Nashtifan in eastern Iran



Figure 3. The vertical blades of the raw earth windmills partly go up against the wind and limit the speed of the device, src: National Geographic, photo Reza Azizfarkhani

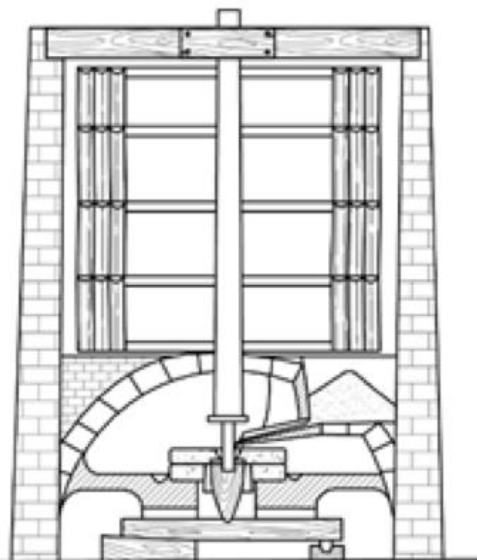
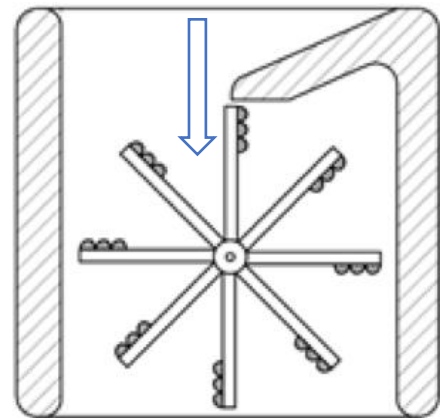


Figure 4. Schéma de fonctionnement des moulins de Nashtifan, relevé par WHC UNESCO



One of the main characteristics of the city of Nashtifan<sup>6</sup> is the strong wind that reaches it. This is most likely the origin of its name, which is derived from the word Nish Toofan (sting of the storm). Due to the natural elements of the region, wind turbines (see figure 2 and 3) are among the inventions that were developed early and have been used for centuries. As wind speeds can sometimes reach 120 km/h, these turbines were built perpendicular to the wind direction to maximize their efficiency. They were the subject of a complete study by Moshtaghe Gohari<sup>7</sup>.

<sup>6</sup> Nashtifan, a city located in the eastern part of Iran

<sup>7</sup> Kambiz MOSHTAGHE GOHARI, *Morphogenesis of Iranian windmills, techniques for managing wind in an architectural manner*, These de doctorat, Paris Est, 2018.

About 30 of these windmills are scattered around the region and can reach a height of 15 to 20 meters. From my research, it seems that these types of windmills were built during the Safavid dynasty and are usually constructed of clay, straw and wood. The wooden blades of these mills turn the grinding stones in an earthen room. Each of the windmills consists of 8 rotating chambers, each housing 8 vertical blades (essentially a slotted wall) (See Figure 4). Once the chambers have begun to rotate under the influence of the wind, the main axle of the wind turbine turns and engages the grinders. The vibrations created by this rotation gradually move the grain from its storage container to the grain mills, which turn it into flour.<sup>8</sup>

**These windmills are among the oldest in the world** and the idea of building windmills in other countries, especially in the Netherlands, probably originated in Iranian architecture. These windmills were invented in eastern Persia around 500 to 900 AD. The first example found is that of vertical sails made of bundles of reeds or wood attached to the central vertical stem by horizontal struts. The disadvantage of these windmills is that, since the wind panels turn horizontally, only one side of the device absorbs the wind energy, while the other half of the device turns against the wind and limits the speed of rotation of the mill.

#### 2.4. Case study of wind towers called Badgir

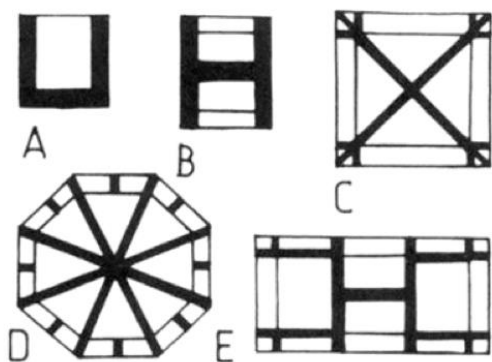


Figure 5. Cross-sectional drawings of five typical wind tower types in Yazd city at the vent level. A. Unidirectional. B. Bidirectional. C. Four-way. D. Octagonal with two vents on each side. E. Four-way with two "false" vents on opposite sides.

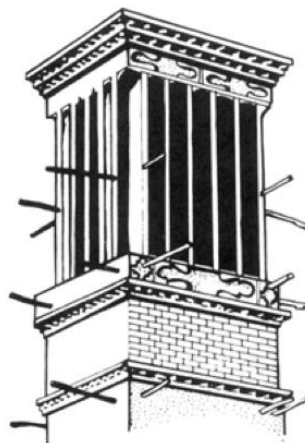


Figure 6. A wind turbine in Yazd with wooden poles on which scaffolding is attached for maintenance purposes.

Yazd is known as "šahr -e- bādġīrhā," the city of wind towers, and is famous for the number and variety of its wind towers, some of which date from the Timurid period<sup>9</sup>. The wind catchers here are brick towers that typically rise 30 cm to 5 m above the roof, although the tallest Bādġīr in the world, built at Bāġ-e-Dawlatābād in Yazd, rises 33.35 m above the roof of the garden pavilion it serves.

Wind towers have openings at the top on one, two, or up to 8 of its sides (Figure 5 and 6) and were decorated with richly carved brick, mud plaster, or lime plaster. The most common use of wind catchers is to cool and ventilate the first floor and basement living rooms of houses in the summer<sup>10</sup>. Air trapped in the tower vents is cooled as it descends and cools the occupants in the rooms below by convection and evaporation (Figure 7). When there is little or no wind, the

<sup>8</sup> BĀDGĪR - *Encyclopaedia Iranica*, <http://www.iranicaonline.org/articles/badgir-traditional-structure-for-passive-air-conditioning>,

<sup>9</sup> O'KANE, "The Madrasa al-GhiyāsĀiyya at Khargird," in , 1976, p. 85.

<sup>10</sup> S ROAF, "Windcatchers," in *Windcatchers in Living with the Desert*, 1982, pp. 57-70-.

air rises in the tower, whose walls are heated by the sun, drawing cool, moist air from the courtyard and basement through the summer rooms<sup>11</sup>. Wind tower ventilation is especially important in basements, where nighttime, afternoon, and summer nights are spent. Wind catchers are also built on the living quarters of caravanserais, on the prayer rooms of mosques, and on water cisterns, where they effectively cool the stored water by evaporation.

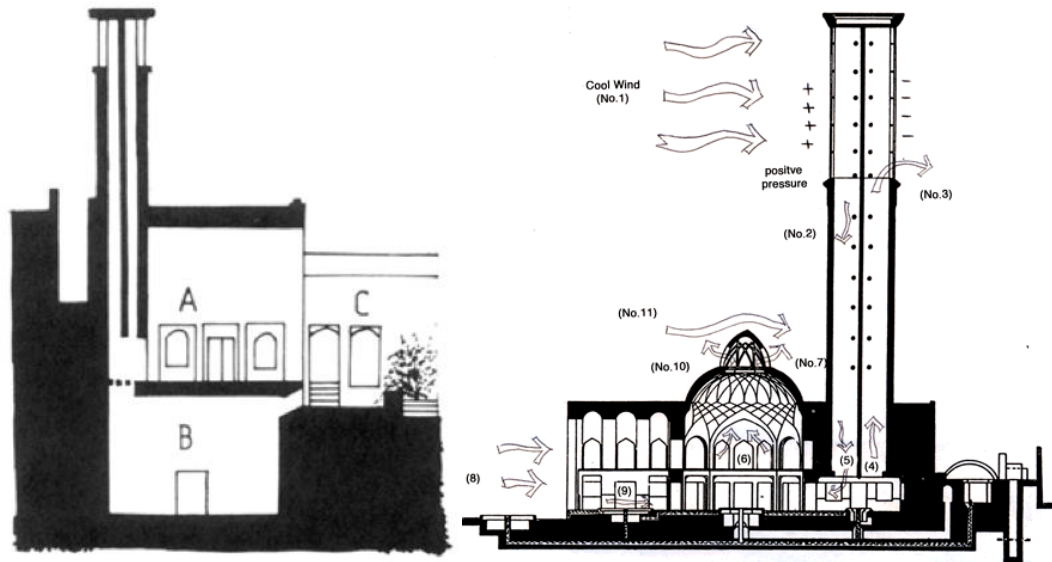


Figure 7. Cross section through a wind catcher serving the main summer rooms of a house in Yazd. A. *Ṭālār*. B. Basement. C. Courtyard with pool by H. Ahmadikia.

The main part of this architecture is the very large Badgir with a height of 33.35 m and an octagonal plan. This Badgir (See figure 7) captures the cold winds (1) at a higher level, in all directions, and channels them (2, 5) into the interior spaces. The dry, warm wind (5) will pass over a pond with a fountain and become cool and moist with evaporation. The cool, moist air (6) then enters the room. There is an increase in air pressure on the windward side (1) and a decrease on the leeward side (3), so that the Badgir captures air on the windward side and draws in air on the leeward side, thus ventilating the interior. A developed study of the ventilation and

<sup>11</sup> BAHADORI, "Passive Cooling Systems in Iranian Architecture," *in* , 1978, p. 144.

cooling principle and numerical modeling of the Bagdirs principle was done by Iranian architect Dehghan Kamaragi<sup>12</sup> in 2014.

This building has a dome on the central hall, which helps ventilation, hot air rises under the dome and comes out through its vents, it occurs by stack effect without wind, but if there is wind, the wind increases ventilation in two ways. First, the wind on the dome creates a negative pressure near the passages and this negative pressure draws air in. Air (8) enters through the large windows via ponds and a garden, this is another ventilation aid. Again, as with the Badgir, the chimney effect also works on cold nights and hot days.

The effect of the sun on this dome is also useful. During the day, the sun heats this dome. (See Figure 8) This heat is then transferred to the surrounding air by convection and radiation, so that this warm air rises and draws in cool air from the basement. The final strategy used here to cool the system is the vegetation around the building. It cools and gives oxygen to the air.

The elements that make up the wind tower are as follows: Each element of a wind tower plays a role in the overall functioning of the device. A wind tower in order, from bottom to top, is made up of the following elements: 1) chimney, 2) rod, 3) catgut and chain, 4) shelf.

1. Chimney: The chimney part of the tower is usually an incomplete pyramid shape. The different proportions of the upper part of the wind sensor are arranged with this part. In some cases, its height is as high as a person and in others, it is a few meters high.

2. Stem: the part of the wind tower is located between the shelf and the room is called the "stem"; the higher the wind, the higher the "stem" is also. According to the regions and climates, the height of the "stem" adapts and seeks to capture a continuous wind that blows high; the beauty of this part mainly depends on the brick decoration.

3. Catgut and chain: the catgut and chain are located between the "peduncle" and the tray.

4. Shelf: The head of the wind tower is the shelf, which includes the blades, the air ventilation duct. The common types of geometric figures of the shelf include an elongated rectangle, vertical, horizontal and square. Shelves are usually open at the front. In addition, this feature is modified depending on the wind direction, however, two shelves would generally be considered for each type of air duct to the room (see Figure 5, Diagram C or D).<sup>13</sup>

---

<sup>12</sup> Gholamreza DEGHAN KAMARAGI, *Ventilation and Cooling Systems in Traditional Persian Gulf Architecture*, *op. cit.*

<sup>13</sup> "BĀDGĪR - Encyclopaedia Iranica," *op. cit.*

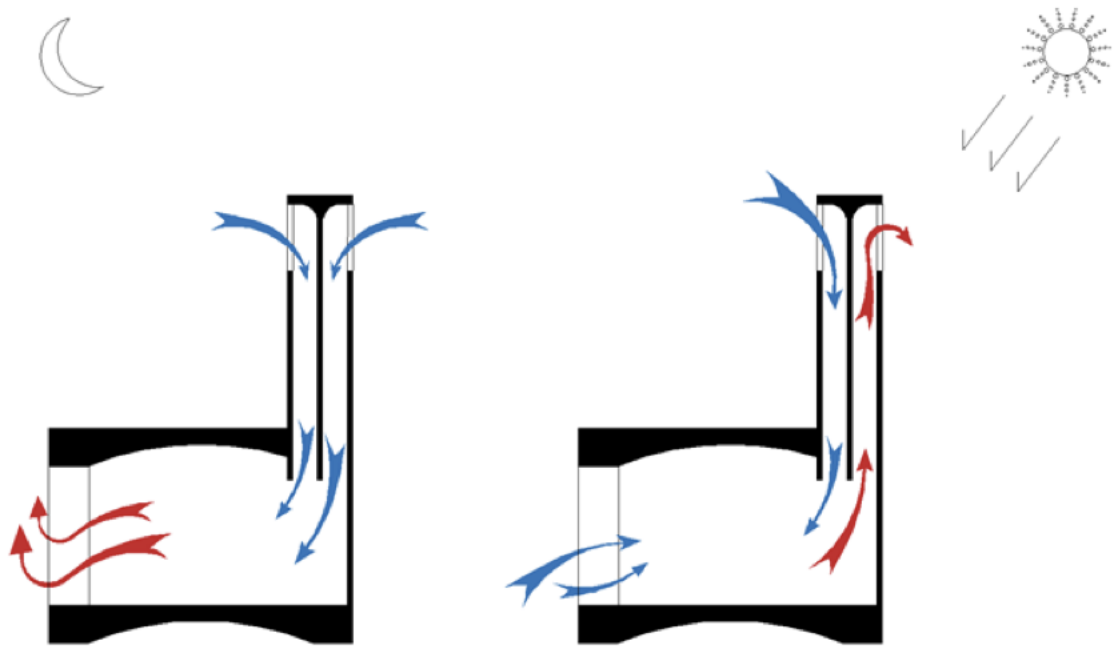


Figure 8. Schematic of the wind tower operation according to day and night. ( drawn by D. Serero)

## 2.5. The emergence of the windmill

Coming from the Iranian plateaus, the first **windmills** arrived in Europe from the IX century, and became commonplace little by little until the XII<sup>ème</sup> century. If in the East, it was only used to **grind grains**, in Europe, it will gradually assume other roles, such as **making oil, brewing sheets, sawing stone or wood, making paper pulp or grinding cereals, ...**



Figure 9. Windmill in Schiedam, the Netherlands ( photo D. Serero)

There are 3 types of **windmills** which constitute the vast majority of the mills used:

- The mill tower
- The pivot mill or candlestick
- The Cavier mill

- *Tower mills*

The **tower mill** (see Figure 9) is the most common type of mill in France. Even if its silhouette varies according to the region, it generally has a fixed **stone or brick** body, sometimes covered with rough or painted cement. Its roof can rotate **360°**, supports the wings and houses the spinning wheel and the lantern.



Figure 10. The Moidrey mill in Pontorson (Manche), Photograph D. Serero on May 27, 2018, it is a "tower mill" type mill.



Figure 11. Detail of the blades whose angle can vary according to the wind speed. ( D. Serero)

Located 5 km from Mont Saint-Michel, the **Moidrey mill** (dating from 1806) is one of the most interesting examples of these mills in France (see figure 10). Following its restoration in 2003, it was classified by UNESCO as a world heritage site in 2007. In activity since its restoration, it has become a place of animation and historical visits on the work of the millers who make flour from buckwheat, wheat and rye.



Figure 12. The Cassel (North) "pivot" type mill (Photo by PAT 2013, [www.moulins-a-vent.net](http://www.moulins-a-vent.net))



Figure 13. The "cavier" type mill-cavier of Aigremonts in Bléré (Indre-et-Loire) (Photo by PAT 2013, [www.moulins-a-vent.net](http://www.moulins-a-vent.net))

- *Pivot or candlestick mills*

The **pivot mill or candlestick mill** (see figure 12) is a type of mill that appeared in France from the 12th century onwards, it is the oldest mill recorded in France. It is characterized by a **wooden**

**cage** that can turn on a **vertical pivot** carved in an oak trunk. They are particularly typical of the North, as well as the East of France.

The **mill of Cassel** (See figure 12) built in the XIIIth century is perched at the top of the Mount Cassel, is a symbol of the city. It is the last representative of its kind in the region, where once stood about twenty **wooden mills on a pivot**.

- *The cavier mills*

The **cavier mill**, halfway between the pivot mill and the tower mill, (see figure 13) is a typical type of mill in the **Anjou region**. It has a small wooden cage called a **hucherolle** supporting the **wings**, pivoting 360°, atop a conical masonry tower.

Built in 1848, then restored between 2004 and 2007 by the municipality of Bléré, the **windmill** of Aigremonts, nearly 18 meters high, is of the **cavier** type. It was originally built on a cellar structure, adapted to the double activity of its owner, winemaker and miller. An association, "Les Amis du Moulin des Aigremonts", offers visits and educational demonstrations of its operation.

- *Evaluate the power of windmills*

It is not easy to estimate the power of these old windmills. However, the surveys made by the engineer Charles-Augustin Coulomb in 1781 in Lille on several windmills of the time allows to compare them and to estimate their power. In his study the engineer gives the wind speed and power of these mills for different modes of operation.

A computer simulation<sup>14</sup> of a windmill with a diameter of 24.6 m and a sail area of 80 m<sup>2</sup> was carried out using the modern theory of the "blade element" as explained by Albert Betz<sup>15</sup> in 1926. The calculation gives the power and torque of the windmill as a function of the wind, or, which amounts to the same thing, using dimensionless expressions, to the coefficient of performance  $C_p$  (ratio of power output to theoretical wind power) as a function of the feedforward ratio  $X$  (ratio of wing tip speed  $R\omega$  to wind speed  $V$ ) :

$$P = \frac{1}{2} \rho \cdot A \cdot V^3 \cdot C_p$$

with  $\rho$  = density of the air

$A$  = area swept by the rotor

The accuracy of the calculation is limited by the approximate knowledge of the aerodynamic data of a wing, here the asymmetrical Flemish wing with a leading edge windscreen.

From this study, it is possible to calculate the power of windmills equipped with different wings: flat wings with constant angle of incidence, flat wings with angle of incidence variable with the distance to the center, and Flemish wings.

---

<sup>14</sup> Philippe BRUYERRE, " Power of windmills ", *Le Monde des Moulins*, 08/07/2019

<sup>15</sup> Albert BETZ, *Windenergie und ihre Ausnutzung durch Windmühlen, Göttingen, Vandenhoed & Ruprecht, 1926. A detailed presentation of the blade element theory is given in: JOURIEH Munif, Développement d'un modèle représentatif d'une éolienne afin d'étudier l'implantation de plusieurs machines sur un parc éolien, Thèse de Doctorat de Mécanique, Arts et Métiers ParisTech, Paris, 2007, p. 51-57. <https://pastel.archives-ouvertes.fr/pastel-00003390/>, 1926.*

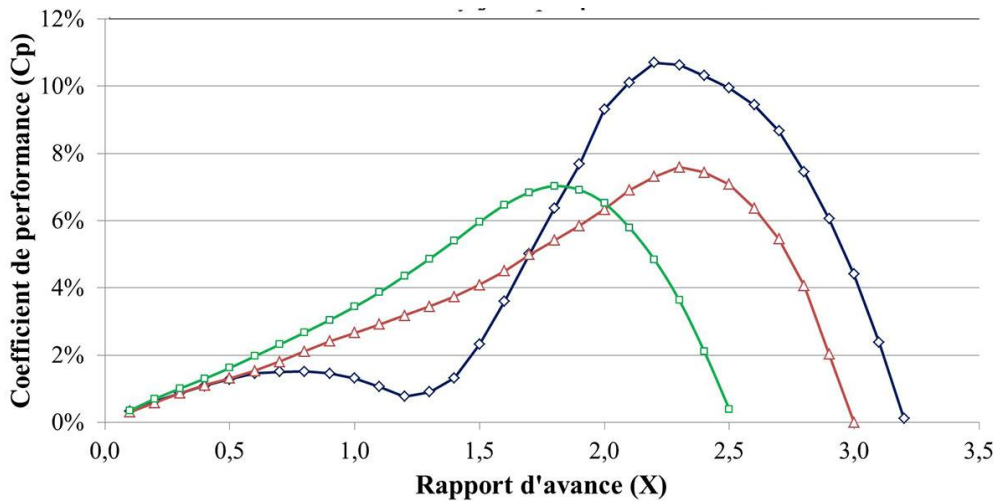


Figure 14 Power curves of three main types of mills (black, Flemish mill; red, symmetrical wing mill with variable inclination; green, symmetrical wing mill with constant inclination<sup>16</sup> .

This is the power available on the mill shaft, the useful power being obtained by evaluating the friction losses on the bearings, the power transmission losses (losses of more than 40% for wooden gears) and the losses of the driven machine (hydraulic losses in the case of a pump).

The change from symmetrical, constant-tilt wings to variable-tilt wings slightly increases the coefficient of performance, which is achieved for a higher feed ratio. The latter mill will turn faster than the former for the same wind speed. Switching from the variable tilt to the flamingo wing increases the coefficient of performance more strongly, while the feed ratio remains comparable.

The improvement of the windmill blades allows to increase their specific speed (speed of rotation in a given wind), their coefficient of performance as well as their diameter. The combined impact of these different factors on the power of a windmill is very important as shown in the following table (see figure 14).

Type de moulin	Diamètre	Puissance maximale dans un vent de 6,5 m/s
Moulin à ailes symétriques et inclinaison constante	10 m	900 W
Moulin à ailes symétriques et inclinaison variable	15 m	2 300 W
Moulin flamand (ailes asymétriques et planche à vent)	24,6 m	8 600 W

Figure 15 Power of different types of windmills in a 6.5 m/s wind<sup>17</sup>

This analysis shows that the power of a windmill varies greatly, from one to ten, depending on the type of wings used (speed of rotation and performance) and the diameter of the rotor, which also depends on the type of wings (stability of operation) (See Figure 15).

<sup>16</sup> Philippe BRUYERRE, "Power of the windmills", *op. cit.*

<sup>17</sup> *Ibid.*

## 2.6. From the Cleveland Wind Turbine to Modern Wind Turbines

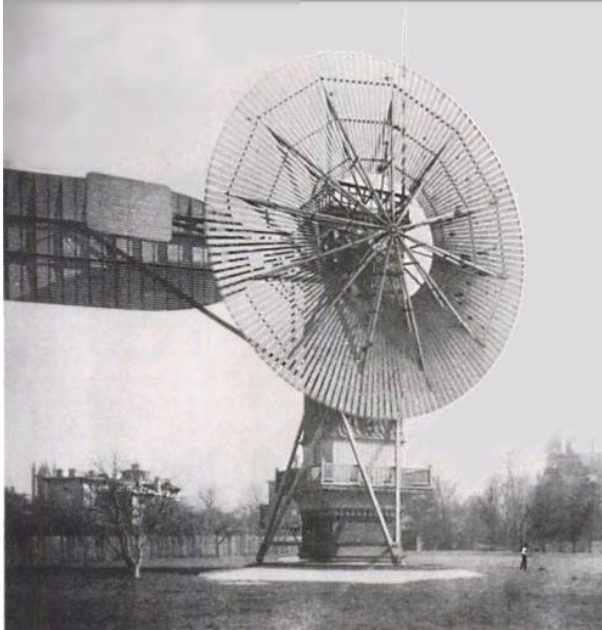


Figure 16. 1888 The Cleveland wind turbine, an electrical first

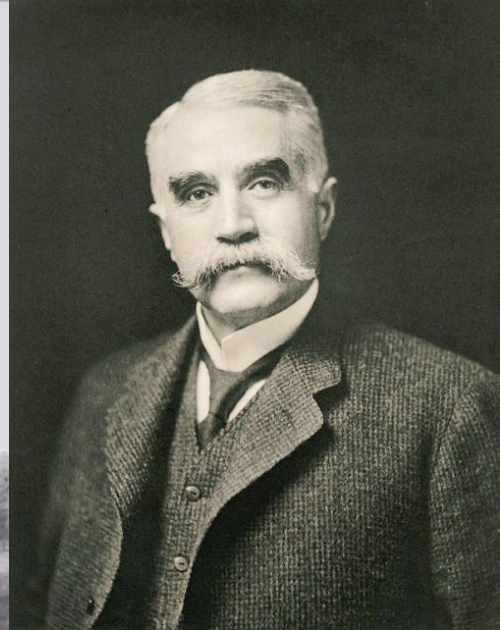


Figure 17. Portrait of Charles Brush, the inventor of the first electricity-generating wind turbine

In 1888, in Cleveland (in the Midwestern state of the United States) (See figure 16), engineer Charles Brush (See figure 17) managed to power his home from a wooden mill using a giant wind turbine 18 meters high and 17 meters in diameter. The first automatic wind turbine for electricity generation was started at this time.

A wind turbine uses the kinetic energy of the wind to convert it into electricity. When a wind turbine produces electricity, it can also be called a wind generator.<sup>18</sup>

It should be noted that the large diameter slows down the motion and the number of blades balances the pressures between the top and bottom of the turbine. A major flaw in the innovation of the pioneer of the American electrical industry: The 144 blades produced only 12 kW. This is partly due to a poorly performing generator and a too slow rotation

In Denmark, at the same time, **Poul La Cour**, a meteorologist and pioneer of Danish wind energy, (1846-1908) quickly learned from his American counterpart. In 1891, his prototype built on the grounds of the Askov school (on the border with Prussia) had fewer blades to turn faster and produce more electricity. His fast rotating wind turbine, the first so-called "industrial" one, was a success. The foundations of rotor aerodynamics were laid. In 1918, ten years after his death, 3% of the energy produced in Denmark already came from wind power. The "Danish Edison" also devoted part of his research to the storage of energy, the great emerging issue, by converting the force of the wind into hydrogen via a process of electrolysis.

As mechanics and aerodynamics have progressed, the productivity of wind turbines has continued to improve. However, headwinds were blowing on its development, due to coal, then to cheap oil, and finally to uranium fission. From 1958, the deployment of the civil nuclear program generates a real stop in the development of wind energy, which will restart only in the early 2000s when the **ecological awareness related to global warming**. The prototype of Lucien

<sup>18</sup> *Onshore Wind Turbines: Operation, Issues and Major Players*,

Romani and EDF of wind turbine with double blades installed in Nogent-le-Roi (Eure-et-Loir) in 1958 is very quickly forgotten. In 1963, Lucien Romani and the BEST (see figures 18 and 19) presented to the Direction of Studies and Researches of EDF a project of wind generator likely to be erected without the intervention of a monumental crane and to function then without permanent personnel.



Figure 18. Machine of 35 m, 1 000 kW, Neyrpic wind turbines of Saint-Rémy-des-Landes. (Source: <http://eolienne.cavey.org/>)

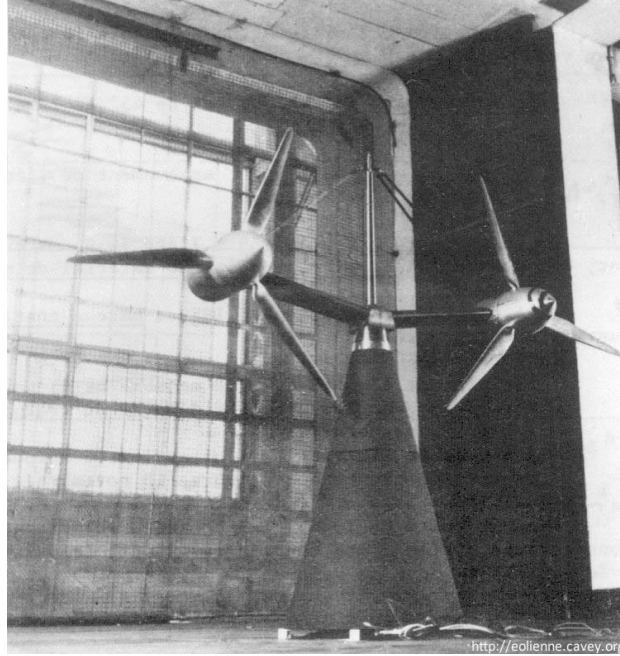


Figure 19. Model of the BEST double helix wind turbine, by the engineer Lucien Romani in 1963, Direction des Etudes et Recherches d'EDF a wind turbine project (Source: <http://eolienne.cavey.org/communs>)

It was the result of long preliminary studies, carried out with the help of the Laboratoire Central des Ponts et Chaussées, the LBTP, the O.N.E.R.A., Breguet, the CIMT, Sud-Aviation, the Entreprise Générale Industrielle, Neyrplast, Alstom, the Société des Monteurs-Levageurs, etc...

It was planned to have two counter-rotating wind turbines of 32 meters in diameter, close to each other and located in the same plane on a truncated cone-shaped tower made of thin reinforced concrete veil. Each propeller would have driven, via a gearbox, a synchronous generator of 1000 kW.

Tests conducted at the Breguet wind tunnel in Vélizy proved that this arrangement provided a 10% gain over two analogous propellers placed far apart.

Economic studies conducted by EDF's Equipment Department showed that, based on an average use of 2,150 hours/year, the cost of the energy produced would have been 30 to 50% higher than that of energy produced from oil.

The project was aborted despite the large budget spent on its development.



Figure 20. Gedser turbine in Denmark, on a reinforced concrete mast the origin of today's wind turbines (source: <https://fr.wind-turbine-models.com/>)



Figure 21. Danish engineer Johannes Juul (1887 -1969) (source: <http://www.windsofchange.dk/JohannesJuul.png>)

In 1957, the Danish Johannes Juul (see figure 21) developed his Gedser turbine (see figure 20) with a power of 200 kW. This three-bladed turbine, equipped with an electromagnetic steering system and an asynchronous generator, with emergency aerodynamic brakes activated by centrifugal force in case of overspeed, was the first to produce alternating current. This model has largely inspired the design of current wind turbines. After two oil crises, renewable energies have again the wind in their sails and the wind farms do not cease to expand, from the 70s in Denmark and the United States, on land and sea. Between 2000 and 2012, the global production of electricity from wind is multiplied by 28 (the global production of wind is then 1 039 Twh).

From 2016, new calls for tenders are launched by the French state for the creation of giant wind farms at sea, so-called "offshore" farms<sup>19</sup> (especially in the North Sea).



Figure 22. Kentish Flats offshore wind farm, off the British coast of Kent (@Vattenfall-Robin Dawe)

<sup>19</sup> The term "offshore" literally means "off shore", as opposed to *onshore* wind turbines.

An offshore wind turbine, i.e. one installed at sea, converts the force of the wind into electricity. Offshore wind turbines work on the same principle as traditional land-based models.

The wind turns the blades, usually three. These drive a generator that transforms the mechanical energy created into electrical energy, following the principle of a dynamo. The main difference between a marine and a terrestrial model of wind turbine is the nature of the foundations, which allow it to be fixed in the ground or anchored to the seabed (except in the case of "floating" wind turbines). Offshore wind turbines must also be very robust to withstand harsh marine conditions.

Offshore wind turbines (see Figure 22) are most often grouped together in a "wind farm" of between 20 and 50 turbines of several megawatts (MW) each. Traditional offshore wind farms are generally not installed in areas where the depth exceeds 40 meters.

Some "farshore" installations, i.e. offshore (more than 30 kilometers from the coast), with floating bases, are currently in the design phase.

## 2.7. The evolution of offshore wind installations

If the first prototypes of offshore wind turbines were simple copies of onshore wind turbines, the machines have gradually been adapted to the sea. Current technological developments, and in particular the expected evolution of machines in size and power, are characteristic of offshore wind turbines.

In a few years, there has been a strong increase in the performance of these devices. For example, the Thorntonbank wind farm, installed in 2008 off the coast of Ostend (Belgium), uses 5 MW turbines. **Wind turbines with a unit power of 8 MW are now being developed and 10 MW models are being studied.**

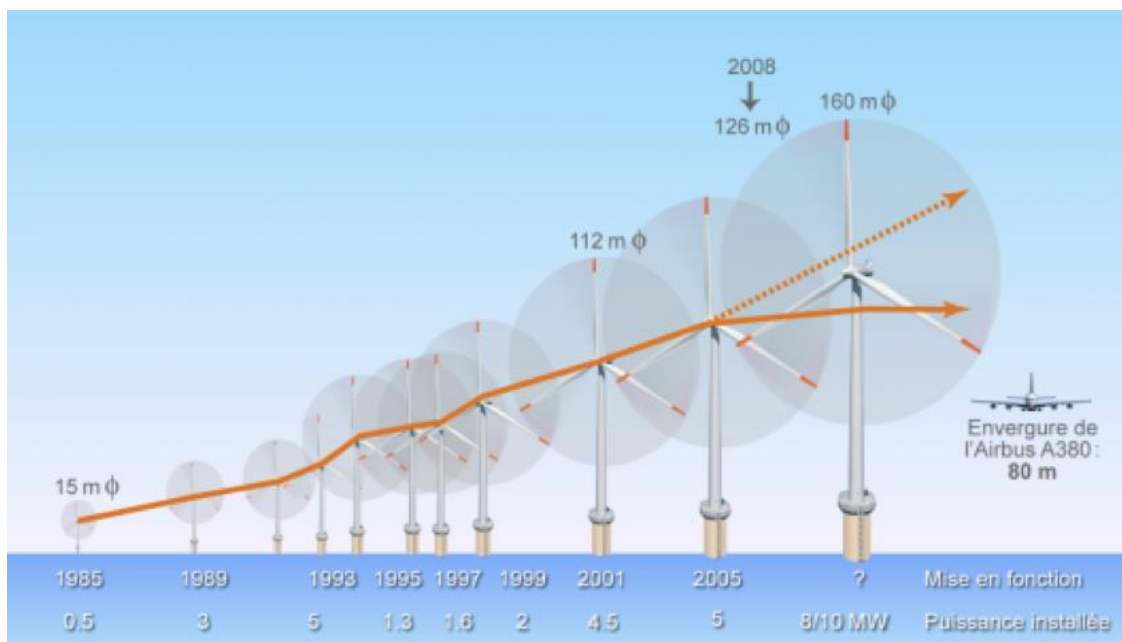


Figure 23. Evolution of the size and power of offshore wind turbines (@Connaissance des Énergies / [https://www.connaissancedesenergies.org/sites/default/files/eolien\\_offshore.infographie\\_zoom.png](https://www.connaissancedesenergies.org/sites/default/files/eolien_offshore.infographie_zoom.png))

Offshore wind turbines are also increasingly differentiated from onshore wind turbines by their technical design adapted to the marine environment. Although they look the same, their operating conditions are different (see Figure 23). The marine foundations are the most notable

aspect of their particularities since they must be anchored or driven into the seabed. They must also resist corrosion, storms and the forces created by the surrounding water masses.

## 2.8. The expected technological breakthrough of the floating *farshore* wind turbine

The first offshore wind projects consisted of installing wind turbines in shallow or medium depth waters, from 5 to 40 meters deep. Beyond this depth, it is difficult and very expensive to plant the wind turbine in the seabed or to place its base. To free oneself from the constraint of the water depth is an interesting track, especially in countries like France where the depths quickly exceed 40 meters when one moves away from the coast.

At the end of 2017, the average depth of offshore wind farms in European waters was 27.5 m, with these located on average 41 km from the coast.

Floating wind turbine projects, located several tens of kilometers from the coast and at a depth of more than 50 meters, offer interesting prospects, particularly in France (Ideol's Floatgen prototype, off the coast of Le Croisic, projects in Brittany and in the Mediterranean)<sup>20</sup>. Unlike traditional offshore wind turbines, their foundations are not sunk into the seabed but anchored by cables. This simplifies their installation and greatly reduces the need for materials.

## 2.9. Advantages and disadvantages of offshore wind technology

- Offshore wind technology has benefited from many of the recent technological advances in onshore wind, one of the most mature renewable energies.
- As the sea is flat, the winds encounter fewer obstacles and are therefore more sustained, more regular and less turbulent than on land. With the same power, an offshore wind turbine can produce up to 2 times more electricity than a land-based wind turbine.
- The sea offers large areas free of obstacles, where the installation of machines is possible, subject to consultation with other users of the sea.

## 2.10. Limitations encountered in their use

- Initial investments in offshore wind projects are significantly higher than those in onshore projects, notably because of the additional costs related to foundations and connection.
- Although winds are more constant at sea than on land, offshore wind power is also intermittent<sup>21</sup>.
- The wind turbine is mechanically subjected not only to the forces of the wind on the blades and the structure, but also to the forces created by the currents.
- The installation of wind turbines at sea is more complicated than on land. Suitable boats must be used. Maintenance of wind turbines is also more complicated and expensive than on land. If a breakdown occurs, it can take several days to repair, resulting in a loss of production.
- The electrical connection requires the installation of submarine cables to the coast which can be several kilometers away. For long distances, it is necessary to use a direct

---

<sup>20</sup> *Onshore Wind Turbines: Operation, Issues and Major Players*,  
<https://www.connaissancedesenergies.org/fiche-pedagogique/eoliennes-terrestres>,

<sup>21</sup> *Myth: All renewable electricity generation is intermittent*,

current routing<sup>22</sup> and to associate electronic power converters in order to reduce the electricity losses.

### 2.11. Manufacturers and operators on a global scale

In view of the colossal investments needed in this sector, manufacturers and operators have quickly aggregated to cope with the scale of the projects. In 2016, China's **Sewind** (which builds Siemens wind turbines in part under license) and Germany's **Siemens** were the top two offshore wind turbine builders, according to *Bloomberg New Energy Finance*<sup>23</sup> (Siemens Wind Power has since merged with Spain's Gamesa Group in April 2017). MHI Vestas is also a major offshore wind turbine manufacturer.

Denmark's Ørsted (ex-Dong Energy), Germany's EON Climate and Renewables, Sweden's Vattenfall and Denmark's DONG are the world's leading operators of offshore wind farms.

### 2.12. Energy production of offshore wind farms

The **energy density** of an offshore wind farm, i.e. the power installed per square kilometer of sea surface, allows us to understand the potential productivity of a site. It is about 8 MW/km<sup>2</sup> on average for 2 to 3 wind turbines installed per square kilometer, and reaches 15 to 20 MW/km<sup>2</sup> in very windy sites.

The **Beaufort scale** is a scale rated from 0 to 12 degrees, proposed by Admiral Beaufort in 1806 (modified in 1946), and used to measure the strength of the wind (Douglas scale).

An offshore wind turbine starts operating at a wind speed of 2 Beaufort (about 10 km/h or 3 m/s), reaches its cruising speed at 6 Beaufort (45 km/h or 12 m/s), and must be stopped at 11 Beaufort (110 km/h, 30 m/s). The ratio of the number of hours of operation at full power equivalent to the number of hours of theoretical operation in the year (8760 h) is called the **load factor**. According to WindEurope, the load factors of offshore wind farms in Europe are between **29% and 48%**<sup>24</sup>.

Offshore wind has seen significant **cost** reductions in **recent years**, as evidenced by the November 2016 award of the Danish Kriegers Flak project to Vattenfall at a price of €49.9/MWh<sup>25</sup>.

### 2.13. Development area and seascape

The exploitation of the offshore wind resource is particularly suitable for densely populated countries with difficulties in finding suitable sites on land and with a substantial and windy coastal maritime space.

Northern Europe is particularly well endowed for the exploitation of offshore wind energy, with wind speeds above 8 m/s at 50 m height, i.e. a power density above 600 W/m<sup>2</sup>. In order to prevent collisions, these wind farms are marked on nautical charts and visually, by the use of positioning lights.

---

<sup>22</sup> *Transmission of electricity AC or DC? Explanation,*

<sup>23</sup> *BNEF 2016 wind turbine manufacturers ranking,*

<sup>24</sup> *Offshore Wind,* , <https://www.ecologique-solidaire.gouv.fr/eolien-en-mer-0>, accessed July 15, 2020.

<sup>25</sup> *Ibid.*

The UK has the largest offshore wind farm in the world, ahead of Germany and China. At the end of 2016, nearly 88% of the world's offshore wind installations were located in the waters of 10 European countries<sup>26</sup>.

#### 2.14. Key dates in the development of offshore parks<sup>27</sup>

**1991:** the first offshore wind farm in Denmark is installed on the Vindeby site, 2.5 km from the coast in very shallow waters (less than 5 meters). The 11 wind turbines installed with a unit power of 450 kW are then only slightly modified onshore wind turbines.

**1990s:** Denmark and two other pioneer countries in the offshore wind sector (the Netherlands and Sweden) launch programs to harness offshore wind. These countries have extensive and shallow continental shelves suitable for the installation of offshore wind turbines.

**Mid-2000s:** the United Kingdom and Germany are also launching large-scale offshore wind farms. With the Middelgrunden wind farm, Denmark inaugurates in 2001 the largest offshore wind farm of the time and a new generation of wind turbines: 20 wind turbines of 2 MW, 180 m apart and arranged on a circular arc of 3.4 km radius. If we consider the average annual consumption of a household of about 100kW, the energy production of this park would supply a city of 20,000 inhabitants.

**2011:** France launches a first call for tenders on offshore wind energy, the results of which are announced in April 2012: 4 sites are awarded for a planned installed capacity of nearly 1,930 MW.

**2017:** more than 3.1 GW of new offshore wind capacity was installed (and connected to the grid) that year, according to WindEurope<sup>28</sup>, a record (560 new wind turbines distributed among 17 farms). This brings the installed offshore wind capacity in Europe to 15,780 MW at the end of 2017. WindEurope did not, however, communicate the associated electricity production that year.

#### 2.15. The future of this technology

**Farshore** wind energy technologies, i.e. offshore wind energy more than 30 kilometers from the coast, offer even more interesting prospects than conventional offshore wind energy. Indeed, the offshore wind is more regular and more sustained, not to mention that the sharing of maritime space is less problematic than near the coast. Because of the complexity of manufacturing and installing floating wind turbines, these technologies are still in the pre-industrial research phase.

According to Wind Europe, the offshore wind farm in Europe could have a total installed capacity of 25 GW in 2020 (compared to 15.8 GW at the end of 2017). In France, 6,000 MW of offshore wind turbines were to be installed by this date according to the objectives of the Grenelle

---

<sup>26</sup> "OFFSHORE WIND.

<sup>27</sup> "Offshore wind", *op. cit.*

<sup>28</sup> Tom REMY and MBISTROVA, "Offshore Wind in Europe Key trends and statistics 2017," *windeurope*.

Environnement<sup>29</sup> but this target is now out of reach due to various delays. The multi-year energy program (PPE)<sup>30</sup> sets a target of 3 GW offshore installed by the end of 2023<sup>31</sup>.

Various calls for tenders for offshore wind power have been held in France and the first projects are expected to be commissioned after 2020. <sup>e</sup>According to the players in the sector, France has the second largest offshore wind energy development potential in Europe after the United Kingdom.

## 2.16. Evolution of wind behavior analysis devices

From the first wind tunnels to CFD simulation

- TYPES OF WIND TUNNELS

As mentioned in the introduction of the thesis, the engineer Gustave Eiffel, like the Voisins brothers or Leonardo da Vinci, is a precursor in the study of wind, particularly thanks to his ability to understand and measure the pressure of wind on structures. In the 1890's, Eiffel, with his experience on load-bearing structures, created an experimental wind tunnel, where he could test models and prototypes of structures in order to improve their dimensioning and design. This wind tunnel (see figure 25, 26 and 27), still in operation today, will participate in the development of many experimental techniques of airflow analysis. We will briefly present here some of the important wind tunnels for the study of wind on buildings and their characteristics.

- Eiffel wind tunnel

It is built in wood and covered with canvas. The wind tunnel includes from top to bottom :

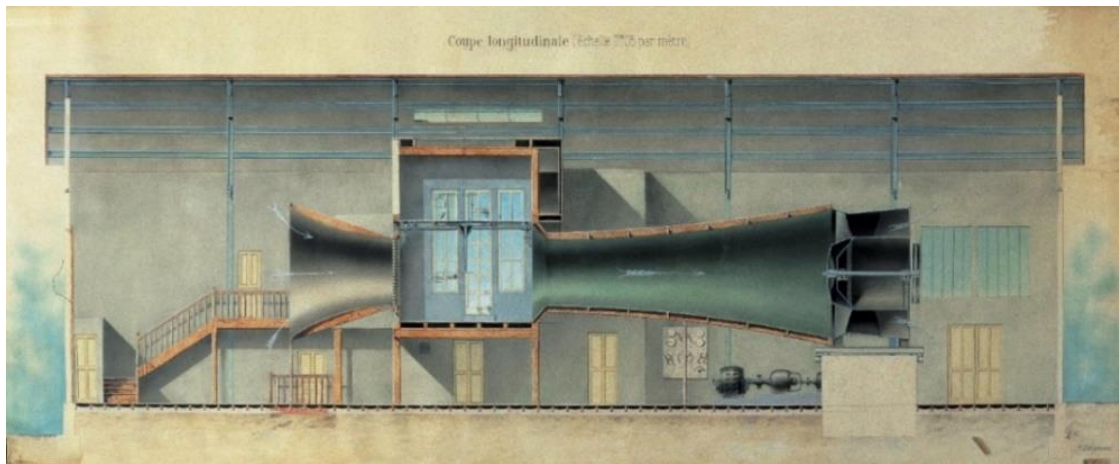
- A collector of 4 m diameter at the entrance and 2 m diameter in the experimental chamber
- An unguided vein 2 m in diameter and 2.37 m long
- A diffuser of 2 m diameter at the outlet of the experiment chamber and 4 m diameter at the fan
- A 23-blade fan of 4 m diameter (7 tons).

---

<sup>29</sup> Grenelle de l'Environnement: stakes, actors, laws of 2009 and 2010,

<sup>30</sup> Mael DANCETTE, *What is the purpose of the multi-annual energy program (PPE)? PPE (programmation pluriannuelle de l'énergie): definition and objectives*, <https://www.connaissancedesenergies.org/quoi-sert-la-programmation-pluriannuelle-de-lenergie-ppe-170324>,

<sup>31</sup> "Offshore wind", *op. cit.*



**Characteristics:**

Velocity from 0.5 m/s to 30 m/s

Turbulence rate between 1 and 2%.

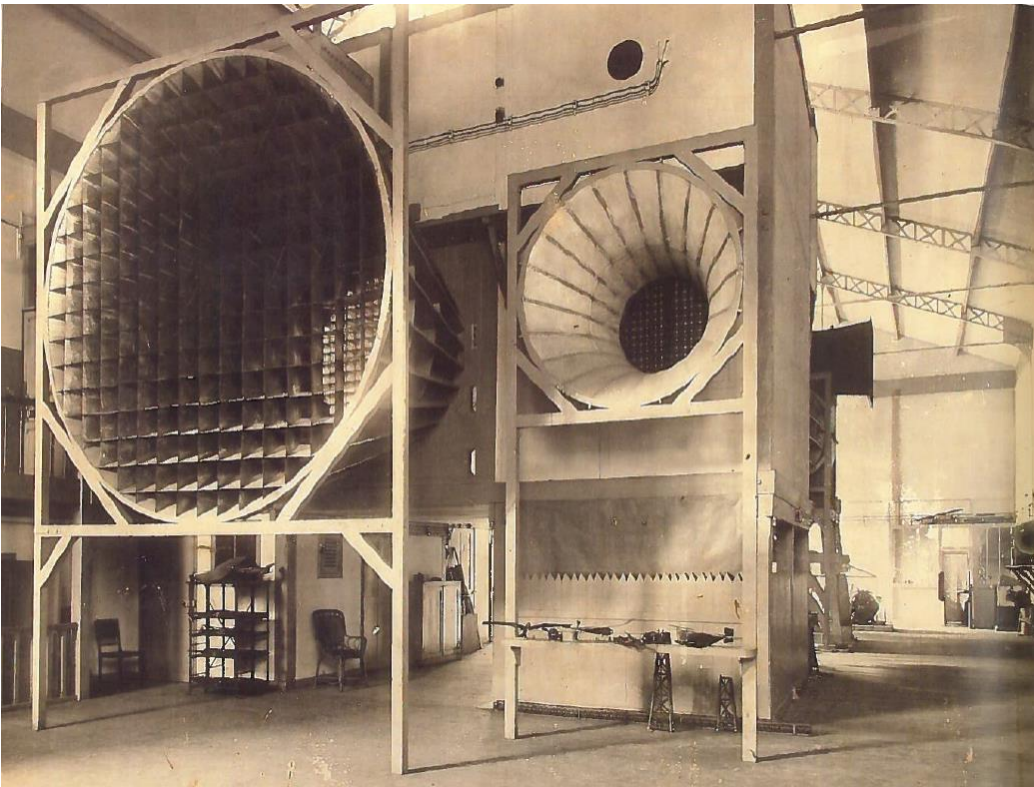
Possibility to model the turbulent atmospheric boundary layer Global acoustic pressure levels from 43 to 82 dB(A)<sup>32</sup>

Figure 24. Eiffel wind tunnel, longitudinal section of the initial configuration of the wind tunnel. Source: © Laboratoire Eiffel, with the kind permission of Mr Martin Peter

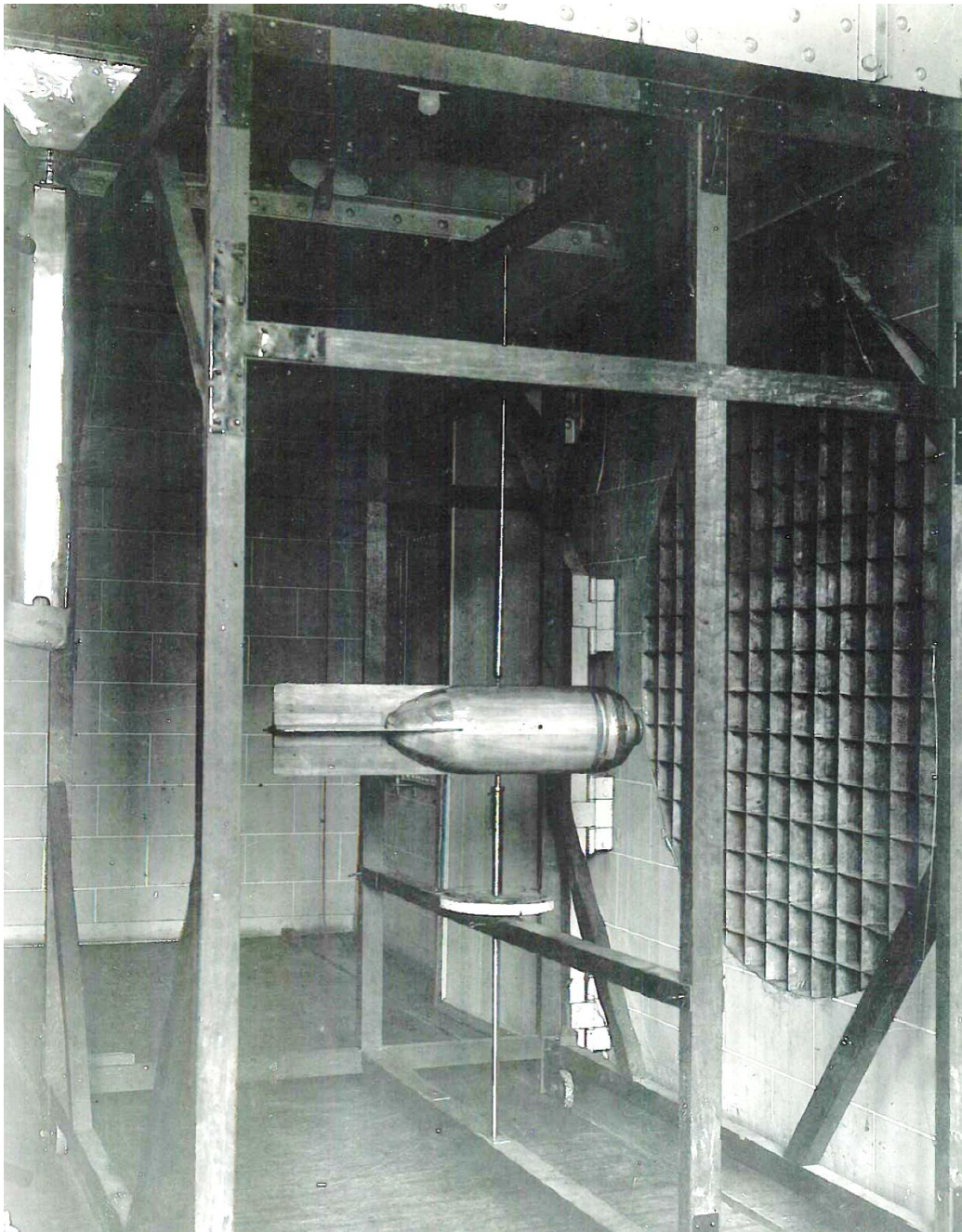


Figure 25. Motorization of the Eiffel wind tunnel, Photo D. Serero of 18/09/2016 . Source © Laboratoire Eiffel, courtesy of Mr. Martin Peter

<sup>32</sup> Eiffel Aerodynamics Laboratory,



*Figure 26. Eiffel wind tunnel by Gustave Eiffel . The wind tunnel chamber of the aerodynamic laboratory created by Gustave Eiffel in 1911. Paris XVith district, 67, rue Boileau. Source © Laboratoire Eiffel, with the kind permission of Mr Martin Peter*



*Figure 27. Eiffel wind tunnel by Gustave Eiffel , study of an aircraft, Source © Laboratoire Eiffel, courtesy of Mr Martin Peter*

- Aerodyne Wind Tunnel<sup>33</sup>

It is the wind tunnel of the IUT of Cachan, usable by the students and the members of the association which manages it (See Figures 28 and 29).

- Prototype study at scale 1, closed circuit operation, illuminated walls to visualize the air flow, very innovative sliding floor system
  - Volume of the study cut: 17.2 m<sup>2</sup>
  - Test speed: Up to 58 m/s
  - Support surface: 2.65m - 3.12m
  - Track : 1.40m - 1.65m
  - Weight: 1800 kg Front Axle, 900 kg Rear Axle

---

<sup>33</sup> "Tunnel Info - Aerodyn Wind Tunnel.



Figure 28. Wind tunnel aerodyne, Association d'études réalisations en optimisation Dynamique & Energétique ; Source : <https://aerodyne-cachan.blogspot.com/>, with the kind permission of the association



Figure 29. Aerodyne wind tunnel . Source: <https://aerodyne-cachan.blogspot.com/>, courtesy of the association

#### - Wind Tunnel of Saint Cyr<sup>34</sup>

Located in the Paris region, the S2A wind tunnel is the only one able to provide such complete aerodynamic and acoustic services. The S2A wind tunnel, a joint venture formed by PSA,

---

<sup>34</sup> Wind Tunnel "S2AScale 1/1".

Renault and the CNAM (see figure 30), can perform aerodynamic or acoustic tests on all types of vehicles or objects.

PLENUM	
Vein (vein predisposed Semi Guided)	3/4 open
the nozzle section	24 m <sup>2</sup> (6.5 x 3.7)
Length of the plenum (between sails)	22,70 m
Width of the plenum (between sails)	16,20 m
test section length	14 m
Height of the plenum	10.40 m
Maximum wind speed	240 km / h
Coefficient of contraction	6
acoustic treatment	semi-anechoic (F. cutoff = 125 Hz)
background noise level, shutdown	<44 dB (A) (noise equivalent to a library)
Maximum noise at 160 km / h	69 dB (A) (Equivalent noise in a busy street)
Volume control (ref center tray)	-3 M <X <3 m; -1.5 M <Y <1.5 m
<b>CHARACTERISTICS OF THE FLOW to control volume</b>	
Uniformity of flow 160 km / h	<0.4%
angular deviation	<0.6 ° planes XY and XZ
turbulence ratio	<0.4%
Longitudinal static pressure gradient along the X axis (Y = 0, Z = 0.25 m)	<0.001 / m -3m to + 3m <0.004 / m + 3m to 5m +
boundary layer displacement thickness	15 mm without aspiration 7 mm with aspiration



Figure 30. Souffleries de Saint Cyr . Source: Souffleries S2A; [www.soufflerie2A.com](http://www.soufflerie2A.com)

### 3. IMPACT OF WIND TURBINES ON THE TERRITORIES

The recent development of a large number of wind farms is the subject of more or less well-founded criticism. Local associations and journalists raise important criticisms of these systems (see figure 31) while the scientific literature is more measured on their impact. Here we make a first assessment of these large wind turbines in our landscape.

#### Overall environmental balance

A multi-criteria study published in 2008 in the journal *Energy & Environmental Science* considers wind power to have the best overall environmental record<sup>35</sup>. A wind turbine does not consume fresh water (access to fresh water is a major global issue), does not require pesticides, does not induce thermal pollution. It has a very small footprint (the presence of a wind turbine is compatible with agricultural activities) and a reduced impact on biodiversity. It is, moreover, available almost everywhere, in a decentralized way. It is a clean energy that does not directly produce carbon dioxide, sulfur dioxide, fine particles, long-lived radioactive waste, or any other type of air or water pollution at its site of operation.

This study has only a reduced vision of the impact of wind energy on a territory, and a more global and systemic analysis allows to better identify and weigh the weight of each of these arguments. Here is a synthesis of the main ones.

#### Visual impact

In many installations, wind turbines have been considered to be too numerous with too rapid a rotation of their blades. This is the case of the Tehachapi Pass wind farm in California, or the San Geronio wind farm (see Figure 34). Compared to the first wind farms, which were very dense, the new wind farms have their turbines spaced further apart, as they are larger in size and power. They have therefore lost their over-concentrated aspect.

Wind energy is a subject of debate in France, between supporters, who campaign for the development of wind structures, and opponents, who campaign for a moratorium on these devices, which they accuse of disfiguring the landscape and whose ecological usefulness they question.

---

<sup>35</sup> *Energy & Environmental Science*,



Figure 31. The visual impact on the landscape of a wind farm in San Geronio Pass, USA , source: Stock photos & Images (662)

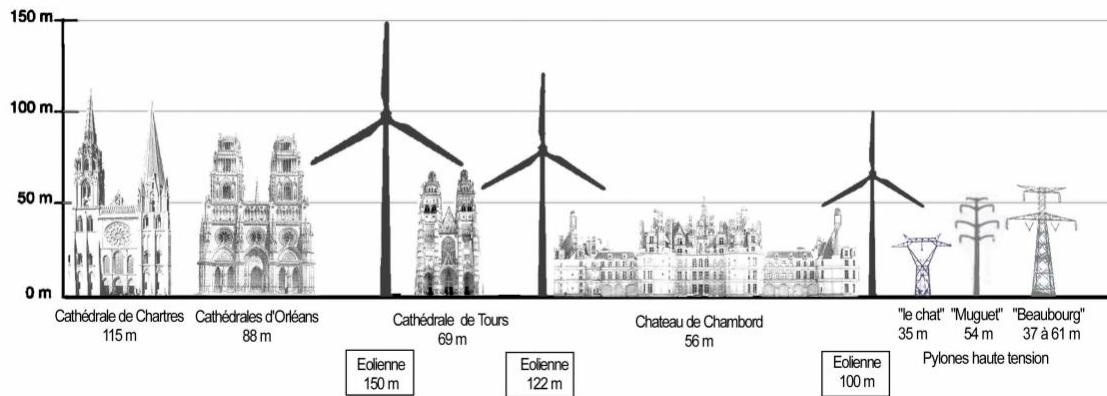


Figure 32. Comparative height of wind turbines to heritage buildings in intermediate scale cities. <sup>36</sup>



<sup>36</sup> <https://www.irca.fr/ils-vendent-leur-chateau-pour-echapper-aux-eoliennes-geantes/>

Figure 33. In Coutances, Normandy, a wind turbine is located in the axis of the city's cathedral and distorts the city's urban panorama<sup>37</sup>

### Intermittence and efficiency of wind energy

- According to the British think tank Civitas , because of the intermittence of its production, wind power would cause more greenhouse gas emissions than nuclear and gas. Its irregular production of energy requires the use of other energy sources such as coal and gas when the wind is too weak or too strong<sup>38</sup> to compensate for the drop in production. This alternation of production generates a decrease in the performance of the energy compensation plants.

### Noise impact

In 2006 and again in 2017, a National Academy of Medicine task force on wind turbines concluded that<sup>39</sup> :

*"The production of infrasound by wind turbines is, in their immediate vicinity, without danger to humans; there is no proven risk of stroboscopic visual stimulation by the rotation of the wind turbine blades."*

This has since been corrected, as the impact study now provides for noise mapping and individual measurements of the nearest residents (see Figure 33), with a minimum distance of 500 m from homes.

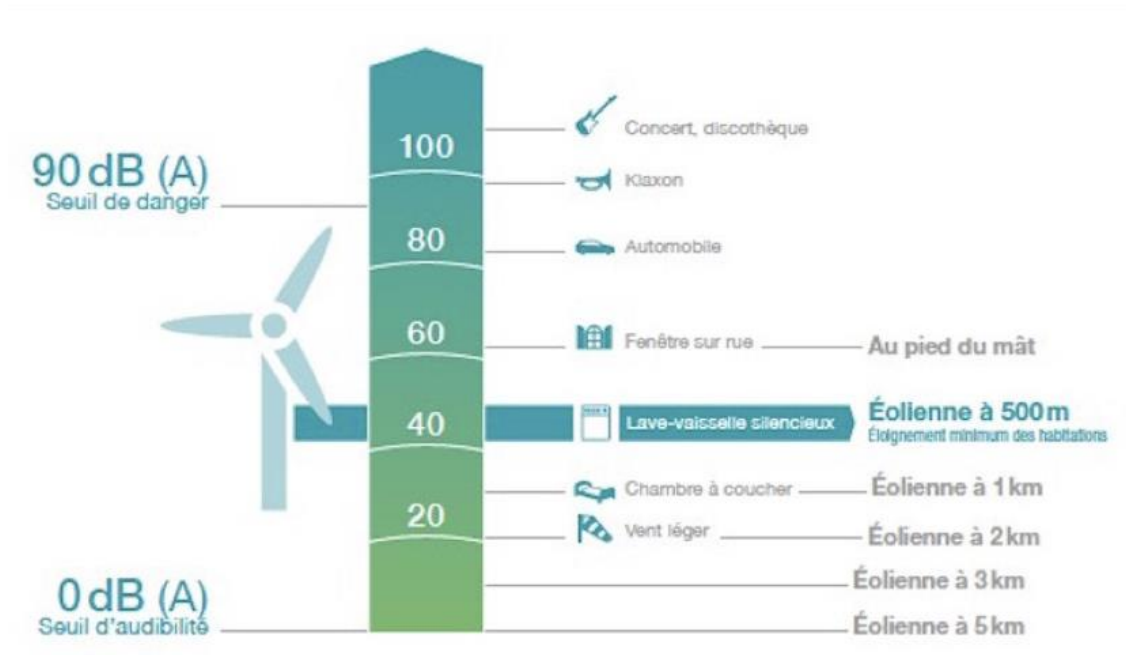


Figure 34. Comparison of noise impact (source: <https://reporterre.net/Quel-est-l-impact-des-eoliennes-sur-l-environnement-Le-vrai-le-faux>)

Concerning the distance of 500 m, the working group asked, as a precautionary measure and while waiting for the conclusion of the requested studies, that the construction of wind turbines

<sup>37</sup> <https://www.lamanchelibre.fr/actualite-52657-eolienne-et-cathedrale-la-ville-de-coutances-demande-un-droit-de-reponse-a-tf1>

<sup>38</sup> "Do wind turbines increase CO2 emissions?", *Le Monde.fr*, 10/01/2012 p.

<sup>39</sup> "Report 17-03. Health Nuisances of Onshore Wind Turbines - National Academy of Medicine | An Institution in its Time".

with a power superior to 2.5 MW be suspended, whereas there was, at this date, no terrestrial wind turbine of such power in France. This report applies moreover, a precautionary principle, without scientific basis, because the noise of a wind turbine is not related to its nominal power. This is why acoustic assessments are systematically carried out as part of an environmental impact study.

The latest generation of machines have made significant progress in terms of noise pollution and can be programmed, in particular circumstances of wind strength and direction, to reduce the impact on a nearby residential area.

In Australia, in March 2005, pediatrician David Iser found three cases of "significant problems" in a study of 25 people living within 2 km of a wind farm<sup>40</sup>.

A wind turbine produces a noise level of 55 dBA at the base of its tower, which corresponds to the noise level in an office. This noise level is generally considered acceptable. French regulations are not based on intrinsic noise, but on the notion of sound emergence, i.e. the difference between the ambient sound level and the wind turbine sound level. The aim is to remain below 5 dBA during the day and 3 dBA at night, whatever the wind speed. A new regulation reinforces this criterion by introducing the concept of spectral emergence, with emergence levels to be respected by frequency (7 dB between 125 and 250 Hz, 5 dB between 500 and 4,000 Hz). This makes it one of the strictest regulations in Europe.

On November 28, 2009, Le Monde devoted an eight-page dossier to the "wind cursed", who live near wind turbines and "suffer from stress, nausea, insomnia, dizziness, irascibility, depression...". The newspaper indicates that "the testimonies are accumulating in a disturbing way"<sup>41</sup>.

### Impact of infrasound

Large horizontal axis wind turbines generate nuisances that can have an impact for several kilometers in the direction of the outgoing air trail from the turbine. A British study from the Ratcliffe Technology Center in Nottingham shows that micro-vibrations of the air generated by the movement of the wind on the blades of a large wind turbine can pollute the air<sup>42</sup> with low-frequency sounds from periodic sources that can constitute strong sources of pollution invisible to humans and perceptible by a large number of animal species.

---

*Low frequency noise and vibration levels at a modern wind farm have been measured at distances up to 1km. Noise and vibration levels have been found to comply with recommended residential criteria even on the wind turbine site itself and the acoustic signal is below accepted thresholds of perception below 20 Hz. Nevertheless, low-level infrasonic, periodic noise from the windfarm may occasionally be detected by instrumentation at distances up to 1 km, despite other sources of noise.*

---

Several publications report the adverse health effects of low frequency and infrasound generated by wind farms<sup>43</sup>. The symptoms most often mentioned are nausea, tachycardia, tinnitus, difficulty in falling asleep and concentration. Very low frequencies and infrasound are

---

<sup>40</sup> Federation Environnement Durable - Vent du Bocage,

<sup>41</sup> The World at War with Wind Turbines,

<sup>42</sup> D. J. SNOW, *Low frequency noise and vibration measurements at a modern wind farm*, Powergen - Ratcliffe Technology Centre, 1997.

<sup>43</sup> Schomer, et al, *Wind Turbine Noise Conference, Denver, August 2013* | Waubra Foundation,

not currently taken into account in France in impact studies prior to the installation of a wind farm. The ANSES has therefore been asked to study the effects of these phenomena<sup>44</sup>.

### Impact on biodiversity

Several studies on wind turbines<sup>45</sup> show that the number of birds killed by wind turbines is negligible compared to the number that die due to other human activities (hunting...). Another study suggests that migratory birds adapt to obstacles; those birds that do not change their route and continue to fly through a wind farm would be able to avoid the blades, at least under the conditions of the study (low wind and daytime). In the United Kingdom, the Royal Society for the Protection of Birds concluded that :

"The available evidence suggests that properly positioned wind farms do not pose a significant hazard to birds."

According to the League for the Protection of Birds, with the documented exceptions of lapwing, redshank and black-tailed godwit, many species appear to be able to use the space near wind farms for nesting<sup>46</sup>.

Other studies of wind turbines show that they can have a significant impact on avifauna<sup>47</sup> :

- Loss of habitat
- Disturbance during the construction phase
- Barrier effect
- Mortality (1 to 60 birds per turbine per year)

Bats, which have been relatively neglected until now, are causing similar concerns, especially for the largest installations: bat mortality increases exponentially with the height of the tower, according to a 2007 study, while bird mortality remains stable. Indeed, in addition to the risk of direct collision, bats are sensitive to barotrauma caused by the rotation of the blades<sup>48</sup>. The mortality rate of bats due to barotrauma or collision is estimated at 1 to 69 individuals per wind turbine and per year<sup>49</sup>.

The negative impacts on wildlife were reported to us during an interview with the bat specialist, **Laurent Arthur**<sup>50</sup> of the Natural History Museum of Bourges in March 2019. He deplores a high mortality of bats in the vicinity of large wind turbines. Their ultrasonic sonar is often taken in default by the speed of the blades of large wind turbines. To date, M Arthur deplores that the data on the **mortality of birds and bats**, are not the subject of any quantification or follow-up on behalf of the installers of wind turbines or companies of production of renewable energy.

How could we develop wind turbines with very low environmental impact? Can we reduce the noise pollution, the micro-vibration effects of the air, the stroboscopic effects of the blades of these large wind turbines in the landscape?

---

<sup>44</sup> Anses - Agence nationale de sécurité sanitaire de l'alimentation, de l'environnement et du travail,

<sup>45</sup> *Wind Power and Bird Studies*,

<sup>46</sup> LPO (Ligue pour la Protection des Oiseaux),

<sup>47</sup> *Impacts of Wind Turbines on Birds - Wind Biodiversity*,

<sup>48</sup> UNITED NATIONS ENVIRONMENT PROGRAMME, Guidelines for the consideration of *bats in wind projects*. Update 2014, Bonn, UNEP/EUROBATS, 2016.

<sup>49</sup> *Impacts of Wind Turbines on Bats - Wind Biodiversity*,

<sup>50</sup> L. ARTHUR and M. LEMAIRE, *Les Chauves-souris de France Belgique Luxembourg et Suisse*, BIOTOPE, coll. "Collection Parthénope", 2009.

If it is not, a priori, opposed to wind energy, the association France Nature Environnement asks for a better consideration of the risks to which the birds are exposed<sup>51</sup>.

### Impact on wave propagation

Wind turbines have been accused of potential interference with military radars for the detection of low flying aircraft or for weather radars for the detection of precipitation. Indeed, wind turbines constitute an obstacle to the propagation of the wave. Depending on the proximity and density of the wind farm, this can be a major blockage at low altitude giving a shadow area in the data. In addition, as the blades are rotating, the radar notes their speed of movement and the data processing by Doppler filtering can not differentiate them from a moving target.

### Artificialization of soils

An onshore wind turbine base is made by pouring 1,500 tons of concrete into the ground on a steel lattice frame. In order to install the 20,000 onshore wind turbines planned for 2025 by the Energy Transition, 30 million tons of concrete would have to be poured, which is incompatible with the policy of fighting against soil artificialisation. Moreover, in France, there is no legal obligation to remove this concrete from the ground when dismantling the wind turbine<sup>52</sup>.

### Impact of dismantling

- *The foundations*

They are levelled to a depth of at least 1 m, for a total height of 2.5 to 4 meters, leaving the possibility of resuming agricultural activity on the site. In some cases, it is possible to remove the entire foundation, although the related costs are not provided for by the operators<sup>53</sup>.

- *Delivery stations*

They are removed and their foundations completely removed. Each site is then covered with soil and returned to natural vegetation or to agricultural use. This last step leaves no visible trace of the wind farm's past existence.

- *The blades*

Made of composite materials, they are difficult to recycle and recover. To date (2019), there is no treatment process in France or in Germany<sup>54</sup>. Pyrolysis processes (already tested in aeronautics) or solvolysis are being researched, which would allow recycling of both the fiber and the polymer resin, but there is no factory capable of implementing them<sup>55</sup>. Today, the burial of the blades is the only method used during the dismantling of wind turbines for their treatment.

- *The cost of dismantling*

It is assumed by the owner of the building (wind operator, SEM...) and is partly recovered through the sale of scrap metal from masts and other components. In France, article L553-3 of

---

<sup>51</sup> *Endangerment of protected species: FNE sues EDF Energies Nouvelles,*

<sup>52</sup> *Wind turbines: 30 million tons of concrete to save biodiversity - Economie Matin,*

<sup>53</sup> LUC LENOIR, *The (polluting) recycling of old German wind turbines,*

<sup>54</sup> *Ibid.*

<sup>55</sup> *How to recycle wind turbine blades?* <https://www.livingcircular.veolia.com/fr/industrie/comment-recycler-les-pales-des-eoliennes>, accessed July 23, 2020.

the environmental code<sup>56</sup> requires operators to dismantle installations and restore the site at the end of operation; to ensure that they will be able to carry out these operations, they are required to provide financial guarantees for this purpose. In 2020, there are no wind farms in France that are not in operation<sup>57</sup>.

- *Physical security around wind turbines*

Wind turbines present accident risks: strong winds can break wind turbine structures. In 2000, a propeller failure at the Burgos wind farm in Spain sent debris spinning several hundred meters away<sup>58</sup>. One of the 62 m wind turbines at the Bouin wind farm in Vendée crashed to the ground during the passage of storm Carmen on January 1, 2018<sup>59</sup>.

The majority of known accidents are related to the use of second-hand equipment or lack of experience, a risk inherent in any emerging technology. Today's wind turbines are certified by independent organizations and are built under strict quality control, significantly reducing the risk of material failure. However, certified wind turbines are not always subjected to long-term tests in operating conditions. As with engineering structures, this raises the issue of inspection and maintenance of wind turbine installations, which are not always

### Impact on natural land dynamics

Wind turbines exploit kinetic energy produced by pressure differences in the atmosphere under the influence of the sun. These gas flows contribute to global climate dynamics. A study published by researchers from the Max-Planck Society in the journal *Earth System Dynamics*<sup>60</sup> shows that the potentially extractable energy (18 to 68 Terawatts (TW) depending on the method of evaluation) is of the same order of magnitude or more than that of the global energy demand (17 TW), but that some of the climatic consequences (on wind flows and their speed) of an extraction at this maximum level would be comparable to those of a doubling of the CO2 rate.

The study only takes into account onshore wind power; if we add offshore wind power, the potential is almost doubled.

In 2018, the average capacity produced by wind is 0.27 TWn 21, just 1.5% of the bottom of the range cited above, and a growth factor of 3.5 in eight years. All indications are that installed capacity will continue to grow strongly in the coming years, although a clear slowdown is observed in Europe. The margin is therefore narrowing, but remains more than comfortable.

In any case, the report states that the widespread use of wind energy would cause a change in precipitation, in heat dissipation by convection, as well as an increase in solar radiation at the Earth's surface. In conclusion, it recommends launching complex modeling studies to accompany and limit the development of the use of wind energy, while confirming that there is a maximum level for the recovery of wind energy, with consequences on the climate of the planet.

---

<sup>56</sup> "Environment Code - Article L553-3".

<sup>57</sup> *Limoux. Eoliennes du Limousin : on les démonte*,

<sup>58</sup> "Federation Environnement Durable - Vent du Bocage", *op. cit.*

<sup>59</sup> Laura JARRY, *Carmen Storm. Bouin wind turbine on the ground: "It would be a mini-tornado,"*

<sup>60</sup> L. M. MILLER, F. GANS, and A. KLEIDON, "Estimating maximum global land surface wind power extractability and associated climatic consequences," *Earth System Dynamics*, 11 February 2011, vol. 2, no. °1, pp. 1-12-.

## A wind of protest blows on the wind turbines

The book "Eoliennes, La face noire de la transition écologique", by Fabien Bouclé<sup>61</sup> takes stock of the situation and lists all the constraints that now apply to the wind energy sector.

The book demonstrates in a methodical way, with the support of a large number of documents, the ecological impact of 30 years of green energy transition.

The ecological impact **of the extraction of rare earths**, for the parts that make up the wind turbines, the impossibility of recycling carbon blades, the harmful impact on biodiversity, especially birds and fish, the nuisance on humans, especially on the polluted winds of low-frequency vibrations which, with the stroboscopic effect of the blades, create real nuisances on humans, the visual pollution of the landscape and their impact on our territory. (Low frequency sounds (from 20Hz to 200 Hz) and infrasound (below 20Hz) emitted by wind turbine fields are the subject of contradictory studies on their health impact).

Hasn't this "green" energy that national and European institutions defend at all costs become obsolete and harmful to our environment?

But the most worrying aspect of this list is that the wind energy economy, pushed by strong industrial lobbies, is often the object of illegal interest of local elected officials who receive counter-parties to promote the implantation of these wind turbines in their territory, when they are not themselves the direct beneficiaries. Throughout Europe, "mafia" organizations or individuals, for pure personal interest, participate in the promotion of this wind energy.

On the other hand, urban wind power integrated on buildings allows a different control, because these territories and wind potential on the outskirts of buildings is not part of territories on which a group of local elected officials has the possibility of control.

It is the developer, investor or owner who has the right to install these wind turbines on a building under construction. On the other hand, the building serving as a support, this device has no additional impact on the environment than the building itself. The device offers reduced noise pollution and impact on biodiversity. The height of the wind turbines, their dangerous blades are replaced by vertical axis micro wind turbines whose blades are of greater safety.

These problems of deployment of wind energy on our territories, raise several working hypotheses to rethink this operation:

- Could we work on the landscape of our cities in order to propose a better integration of these devices in an urban panorama?
- Could we bring the places of energy production closer to the places of consumption?
- Can our buildings become energy collectors, and integrate a field of smaller grouped wind turbines rather than a few large ones?

In the next chapter, we study the energy sharing technologies that could have an impact on the functioning of energy production infrastructures and on their possible dissemination across our territories.

---

<sup>61</sup> Fabien BOUCLÉ, *Wind turbines: the dark side of the ecological transition*, Éditions du Rocher, 2019.

### 1.3. SCIENTIFIC STATE OF THE ART

A large number of researches (articles, books and theses) have made important contributions of knowledge on the use of wind and to define the framework of this thesis. They are quoted in the parts that constitute this thesis. I wished to gather here the most significant elements.

#### 1. Studies of traditional mills or old architecture

The ancient forms of using wind in the design of buildings have been the subject of two interesting theses of architects of the GSA laboratory: That of Reza Dehghan<sup>62</sup> on the Bagdir, these ancient forms of wind towers integrated into the palace of some cities such as Yazd. By creating a numerical model of these towers, he was able to calculate the speed of airflow in the cells of the tower and evaluate the climatic performance of these structures. This work shows that the proportions of these old towers are almost perfect to optimize the ventilation by air convection. The work of Kambiz Moshtaghe<sup>63</sup> focused on the traditional forms of windmills in Iran and the evaluation of their energy performance from, again, modeling their operation.

#### 2. Studies on numerical simulation of airflow

This subject is the subject of many works, but I present here some of those that have been able to advance the knowledge of numerical simulation methods of flow in the study of buildings: This is the case of the Italian researcher Margherita Ferrucci<sup>64</sup> who has developed by studying ancient Italian palaces a design model of natural ventilation according to the typology of the building, their height and proportions.

On the numerical simulation of airflow, the work of DC Wilcox Turbulence Modeling for CFD<sup>65</sup> was used as a reference to define the conditions and the parameterization of the airflow study in turbulent regime, the characteristic flow regime of cities. This study allowed to define the level of roughness of the boundary layer in an urban site and to give hypotheses for the implementation of urban devices in an urban site.

The thesis of Munif Jourieh<sup>66</sup>, studies the implementation of wind turbines in these wind farms and gives valuable insights into how to assess the turbulence generated by a wind farm and strategies for ground implementation to minimize this impact.

Concerning case studies of wind energy systems and their simulation, it is worth mentioning the work of R. Yang<sup>67</sup> from Quanzhou University "Wind Energy Utilization on the roof of High-

---

<sup>62</sup> DEHGHAN KAMARAGI GHOLAMREZA, *Ventilation and cooling systems in traditional Persian Gulf architecture: device history, modeling, performance evaluation - Drought*, Université Paris Est, 2012.

<sup>63</sup> Kambiz MOSHTAGHE GOHARI, *Morphogenesis of Iranian windmills, techniques of wind management in an architectural way*, *op. cit.*

<sup>64</sup> Margherita FERRUCCI, *Natural ventilation in architecture: methods, tools and design rules*, These de doctorat, Paris Est, 2017.

<sup>65</sup> David C. WILCOX, *Turbulence Modeling for CFD*, 2nd edition, La C nada, Calif, D C W Industries, 1998, 540 pp.

<sup>66</sup> Munif JOURIEH, *D veloppement d'un mod le repr sentatif d'une  olienne afin d' tudier l'implantation de plusieurs machines sur un parc  olien*, phdthesis, Arts et M tiers ParisTech, 2007.

<sup>67</sup> Yan Hong CHEN, Xing Qian PENG, and Rong YANG, "Wind Energy Utilization of High-Rise Buildings Roof Numerical Analysis," *Applied Mechanics and Materials*, 2012, vol. 137, pp. 87-94.

rise Building<sup>168</sup> which evaluated performance scenarios of wind turbines on building roofs based on an analysis in ANSYS Fluent. This work only considers the roof as a possible source of implementation and only studies isolated building typologies and not integrated in an urban block in dense site.

### 3. Studies on micro-wind turbines and their integration in urban areas

Mark Moriarty in his dissertation<sup>69</sup> at the University of Pittsburgh develops a feasibility for embedded wind turbines on simple building networks. This work evaluates the energy potential based on comparison of known equivalent systems without numerical simulation or wind tunnel testing of the proposed devices.

The thesis of Bao Wang<sup>70</sup> from the University of Toulouse studies several scenarios of wind flow in neighborhoods that use mostly the Chinese or American city model, a field of tall towers, depending on their height and orientation to the wind. This work evaluates the modes of implementation on these structures but does not discuss the problem of architectural integration of these devices.

Zeng<sup>71</sup> of the MIT Energy Laboratory is developing a model of hybrid energy production integrating photovoltaic and wind devices and their distribution in urban areas. The model identifies a method for installing these two types of devices, based on the orientation of the buildings.

The paper by John Dabiri<sup>72</sup> of the Caltech Field Laboratory for Optimized Wind Energy (FLOWE) in California studies the density of vertical axis wind turbines or micro wind turbines allowing to increase their clustering. Turbulence at the blade exit is much less important in this type of device than in large wind turbines, where spiral turbulence effects create air movements over several hundred meters that cannot be used.

These studies helped to define the scope of this research and to combine in a single study the issues of architectural integration, performance evaluation and behavior in dense urban sites.

### 4. Towards the Internet of Energy

The Internet of Energy (IoE) is an important paradigm for understanding the future context of decentralized energy producing devices. IoE is the implementation of Internet of Things (IoT) technology in distributed energy systems to **optimize energy infrastructure efficiency and reduce waste**<sup>73</sup>. This energy system is particularly suited to the integration of energy production

---

<sup>69</sup> Mark MORIARTY, *FEASIBILITY OF SMALL-SCALE URBAN WIND ENERGY GENERATION*, University of Pittsburgh ETD, University of Pittsburgh, 2010.

<sup>70</sup> Biao WANG, *The impacts of urban morphology on wind: wind energy performance at the neighborhood scale*, 2015.

<sup>71</sup> Heshuang ZENG, *Integration of renewable energy with urban design: based on the examples of the solar photovoltaics and micro wind turbines*, Thesis, Massachusetts Institute of Technology, 2011.

<sup>72</sup> Robert W. WHITTLESEY, Sebastian LISKA, and John O. DABIRI, "Fish schooling as a basis for vertical axis wind turbine farm design," *Bioinspiration & Biomimetics*, August 2010, vol. 5, no. 3, p. 035005.

<sup>73</sup> *What is the Internet of Energy?* <https://www.nesgt.com/blog/2019/05/what-is-the-internet-of-energy>, accessed July 15, 2020.

devices in dense urban areas and allows for continuous improvement of energy exchange and sharing protocols in this network. This chapter details how these systems work.

The Internet of Energy (IoE) refers to the modernization and automation of electrical infrastructure for energy producers. This allows energy production to move forward more efficiently and cleanly, with the least amount of waste. The term is derived from the growing market for Internet of Things technology, which has enabled the development of the distributed energy systems that comprise IoE. An example of IoE technology includes the use of smart sensors, common to other applications of IoT technology, that enable IoE-facilitated mechanisms such as power monitoring, distributed storage, and renewable energy integration. Updating electrical infrastructure allows energy to flow efficiently, maximizing its potential and reducing energy waste. When energy is transmitted over lines that cannot conduct it efficiently, much of that energy is lost along the way. The lines simply don't have the capacity to carry all the energy being sent.

As countries around the world invest more in green energy and renewable resources, the inefficiencies of the world's existing power infrastructure are often overlooked. This means that renewable energy cannot be delivered at its optimal efficiency level because the grid cannot fully support it. For example, China is one of the world's largest producers of renewable energy, but it still experiences energy shortages and crises because it cannot supply this energy at a level that can meet the needs of its population. This leads to power outages and interruptions. The energy exists but the infrastructure does not. Similarly, the country is producing a considerable number of electric vehicles, but does not have enough charging stations to keep the vehicles running. In 2014, energy losses in China due to infrastructure inefficiency were more than 25%. However, according to China's National Bureau of Statistics, the country's energy efficiency levels have improved over the past 5 years, with the amount of energy used to produce one unit of China's gross domestic product (GDP) falling by 5% in 2016, according to the most recent data available as of January 2018<sup>74</sup>.

## 5. The exponential development of the Internet of Energy (IOE)

One potential solution to the problem of energy inefficiency is ultra high voltage (UHV) transmission, a system that allows energy to be transmitted rapidly over long distances. UHV solves the problem of power generation too far from load centers. China first implemented UHV in 2009, and its development is steadily expanding to meet demand.

China is working to automate distribution and add more resources to meet demand, including more charging stations for electric cars. It is also building storage sites, especially in the cities that consume the most energy, to store excess energy efficiently and close to where it will be needed. This will have additional economic benefits for companies supplying renewable energy, such as solar and wind, as more energy will be retained and sold, in addition to relatively low storage costs.

In the coming years ( See Figure 64), as the world works to use and exploit renewable energy sources, the use of non-renewable resources is expected to decline, reducing the need for obsolete infrastructure managing resources such as coal and oil<sup>75</sup>.

---

<sup>74</sup> James CHEN, *Internet of Energy (IoE)*,

<sup>75</sup> *Ibid.*

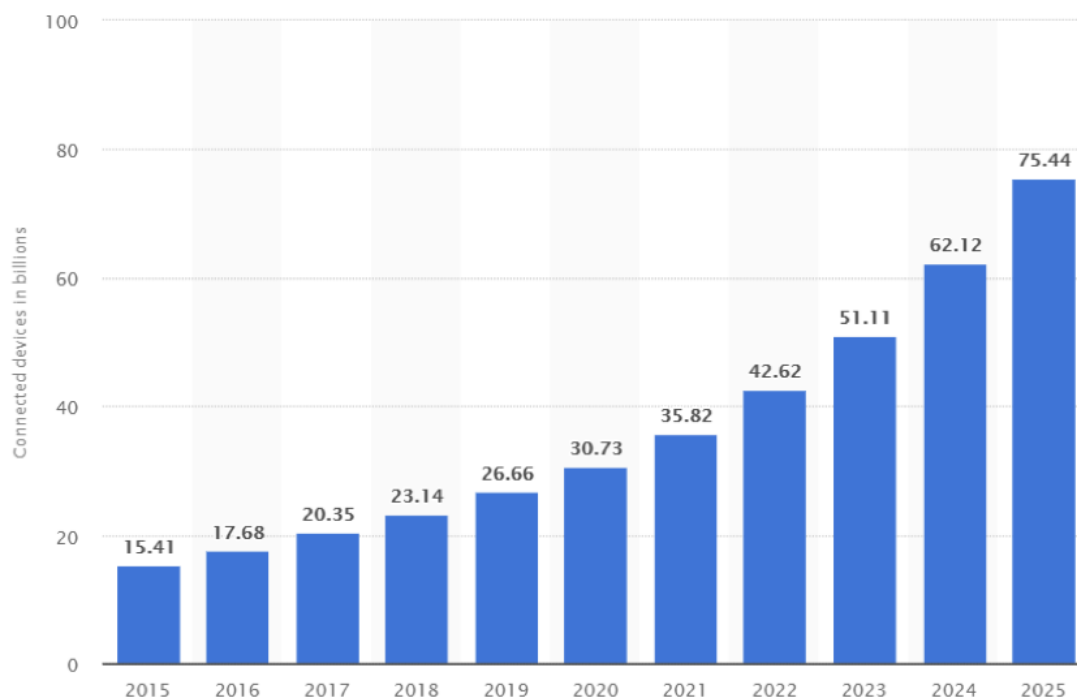


Figure 35. The Internet of Things (IoT) installed worldwide from 2015 to 2025 in billions

## 6. Example of IoE

Various companies have begun to implement IoT technology into the way they produce, transmit or consume energy.

General Electric combines Big Data, Machine Learning and IoT technologies to create an Internet of Energy. Sensors are used to collect data, which is then sent to an optimization algorithm for analysis. This allows for real-time monitoring of their equipment and has brought many benefits, including a 5% reduction in downtime and a 25% reduction in maintenance and operating costs. Marriott hotels have connected a switching unit to rooftop air conditioning chillers. When demand is about to increase, the system sends a message to Marriott asking if it is willing to suffer a power outage. If the hotel agrees, the chillers are remotely shut down. If the system were implemented across the entire hotel chain, the savings would be £700,000 per year, and guests wouldn't even notice the slight temperature rise due to the power down.

## 7. The impact of the Internet of Energy on production/consumption smoothing

Two technological revolutions form the dawn of the 21st century: the development of the Internet and the transition to a carbon-free global energy system (see Figure 65).

Decarbonization, decentralization and digitalization are transforming the energy sector. These three global trends are changing the way we produce, distribute and consume energy.

1. Global demand for clean energy soars
2. Centralized networks are no longer adequate
3. Smarter networks ensure more reliable supply
4. Dealing with mountains of data

## 5. Artificial intelligence and quantum computing are transforming the energy sector<sup>76</sup>.

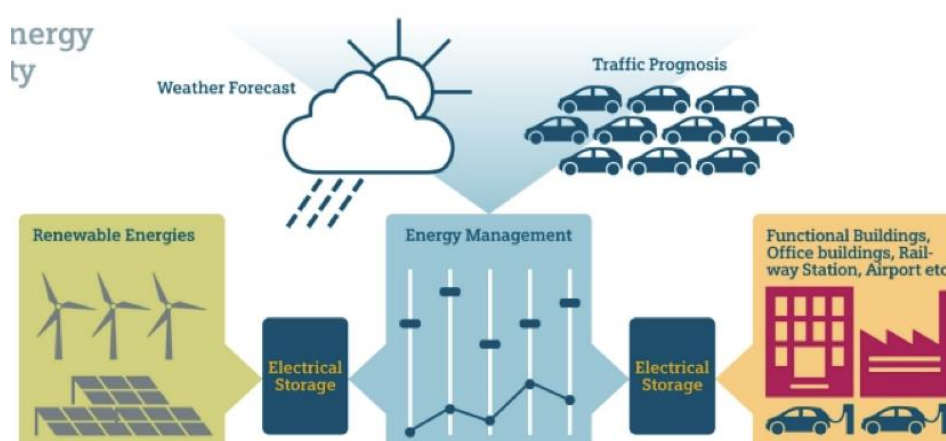


Figure 36. The example of the internet of energy for new urban mobility<sup>77</sup>

## 8. Towards the "SMART CITY"

A **smart city** is an urban area that uses various electronic data collection sensors to provide information to effectively manage resources and assets. This includes data collected from citizens, mechanical devices, assets, processed and analyzed to monitor and manage traffic and transportation systems, power plants, water supply systems, waste management, information systems, schools, libraries, and hospitals (See Figure 66).

The smart city concept integrates information and communication technologies (ICT) and various network-connected physical devices (the Internet of Things or IoT) to optimize the efficiency of urban operations and services and connect to citizens.

Smart city technology allows city officials to interact directly with community and urban infrastructure and to monitor the city and its evolution. Information and communication technologies (ICT) are used to improve the quality, performance and interactivity of city services, reduce costs and resource consumption, and increase contact between citizens and government.

The functions of smart cities are developed to manage urban flows and enable real-time responses. A smart city is therefore better prepared to respond to challenges than a city that has only a "transactional" relationship with its citizens. Yet the term itself remains unclear and open to many interpretations<sup>78</sup>.

<sup>76</sup> 5 problems the internet of energy can solve | Greenbiz, <https://www.greenbiz.com/article/5-problems-internet-energy-can-solve><https://www.greenbiz.com/article/5-problems-internet-energy-can-solve>, accessed July 15, 2020.

<sup>78</sup> MCLAREN, DUNCAN, AGYEMAN, and JULIAN, "Intelligent city," in *Sharing cities*.

The consulting group Frost & Sullivan uses 8 "smart" categories to define this entity: smart buildings, smart energy, smart information technology, smart mobility, smart city planning, smart business, smart governance, and smart citizenry<sup>79</sup>.

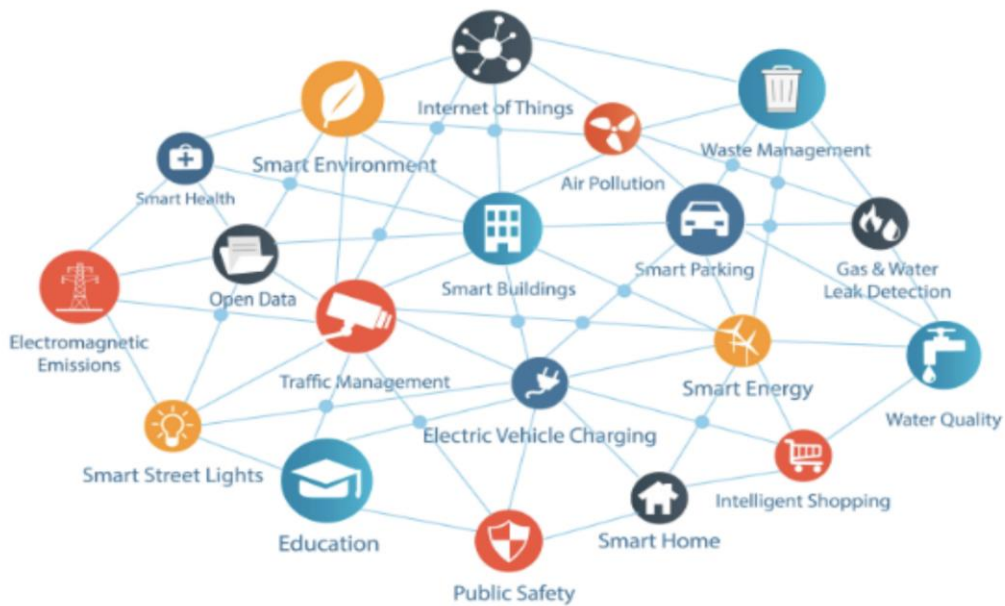


Figure 37. Example of a Smart city model, MIT Senseable City Lab, Carlo Rati

Digital networking generates a huge and ever-increasing volume of data that is collected and processed in "smart city data centers." Thousands of smart city sensors and data provide all kinds of information. These developments are improving public safety, as new communication technologies increasingly facilitate coordination between government and social agencies and individuals. For example, when a storm is forecast, all relevant data is collected, analyzed and evaluated. A predefined cascading chain of information transmits the findings to energy providers, hospitals, transportation operators and facility managers in real time, so they can take appropriate precautions. Networked services enable the creation of city management systems that optimally utilize resources and help minimize potential damage. This ability to respond is often called resilience. In other words, resilient cities<sup>80</sup> can flexibly manage potentially dangerous situations (see Figure 67).

Barcelona is also considered a pioneer city in this field. The city has created an administrative department to manage all urban resilience issues. A geographic information system combines data from the municipal infrastructure with information collected on areas such as public administration, the environment, public spaces and the population. The goal is to more

<sup>79</sup> Grid edge - where the energy system of the future takes off, <https://new.siemens.com/global/en/company/stories/infrastructure/grid-edge-where-the-energy-system-of-the-future-takes-off.html>, accessed July 15, 2020.

<sup>80</sup> In the context of land use planning or urbanism, a **city** is called **resilient** when it has the capacity to adapt to events in order to limit the effects of natural disasters and to return to normal functioning as quickly as possible.

effectively assess the impact of planned and unplanned events and improve the city's ability to respond<sup>81</sup>.

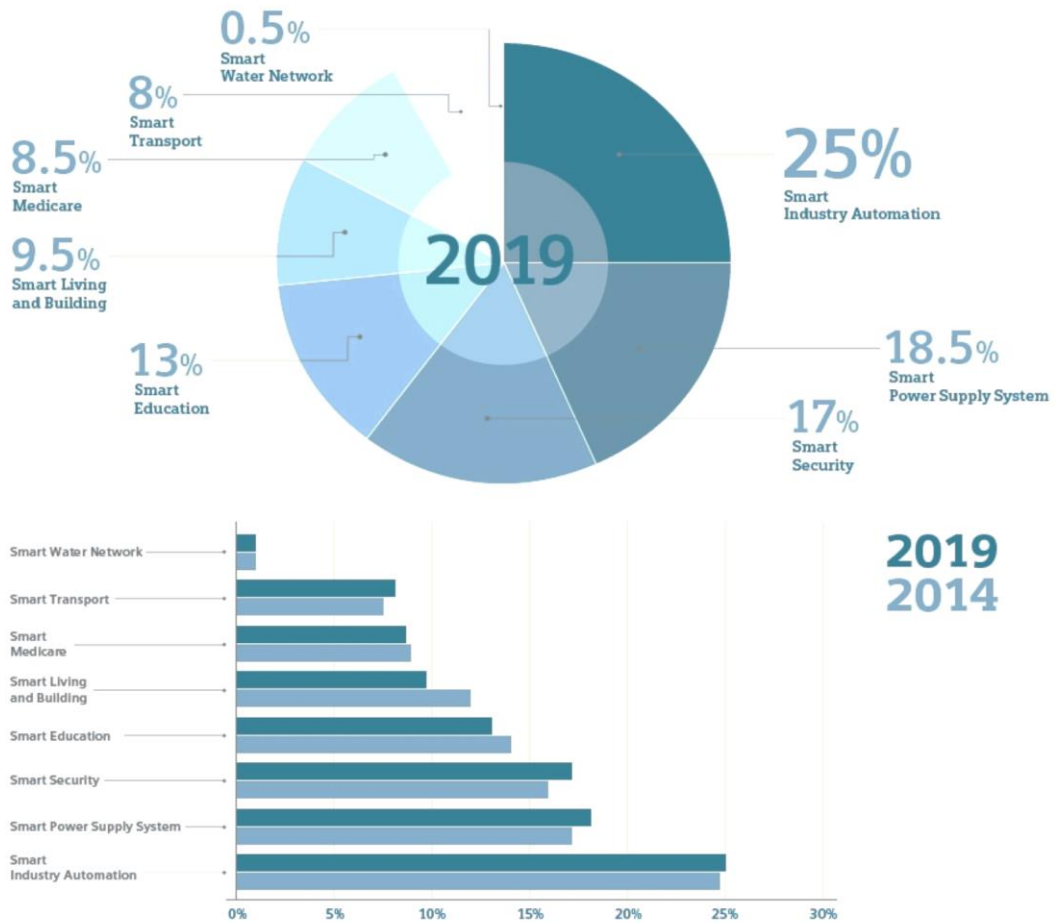


Figure 38. Global smart city market breakdown, 2014 - 2019, MIT Senseable City Lab, Carlo Ratti

## 9. Growing investments in smart city technologies

These examples illustrate how cities combining data from various infrastructures can improve efficiency, save money, reduce environmental pollution, and offer their residents a better quality of life. Such measures will lead to the creation of a complex information network spanning supply technologies, information and communication structures and social networks, paving the way for increasingly intelligent services at all levels. According to the OECD, the overall annual investment required for all infrastructure projects between 2010 and 2030 will be approximately \$1.8 trillion, and a large portion of this total will be invested in cities.

This vast investment is creating new business segments. A study by the German Association for Electrical, Electronic and Information Technology (VDE) indicates that the smart city technology segment is growing rapidly. Two-thirds of the association's 1,300 member companies expect to see an economically significant number of smart cities by 2030. Market research firm Technavio expects the global smart city market to grow by 16.6% annually between 2014 and 2019. North

<sup>81</sup> "Grid edge - where the energy system of the future takes off," *op. cit.*

and South America, have been ahead since 2014 on this topic, with North America clearly in the lead<sup>82</sup> ( See Figure 68).

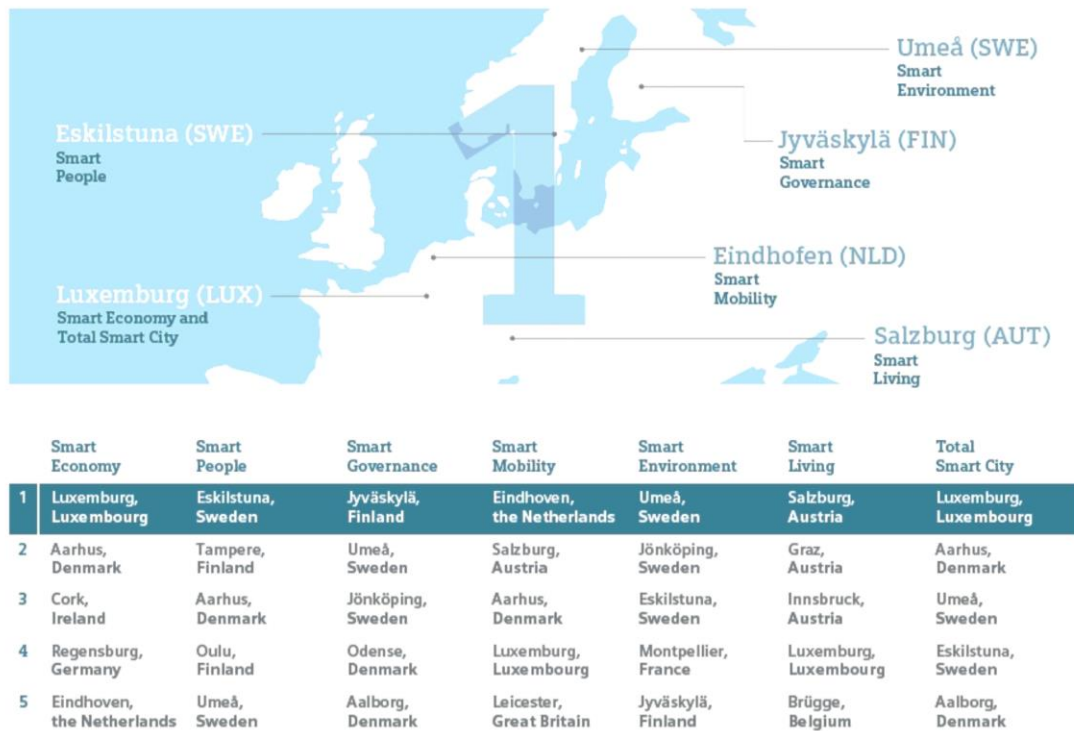


Figure 39. "Intelligence" ranking of mid-sized cities in Europe , based on IESE Cities in Motion Index, 2018

## 10. Transforming Singapore through technology

The digital revolution is underway and advances in digital technologies are transforming the way we live, work and communicate. Singapore is an island country, a smart nation with digital innovation and a world-class city with a government that provides its citizens with the best possible home and meets their diverse and changing needs.

At the broadest level, the economy is the biggest driver of Singapore's growth and competitiveness. It is supported by the government's efforts to catalyze growth and innovation in all areas, including the public sector. The focus of these efforts is to ensure that all segments of society can harness and benefit from digital technologies.

## 11. National Strategic Projects

To drive the widespread adoption of digital and smart technologies across Singapore, the city has identified key strategic national projects that are catalysts for Smart Nation action. ( See Figure 69).

<sup>82</sup> *Ibid.*

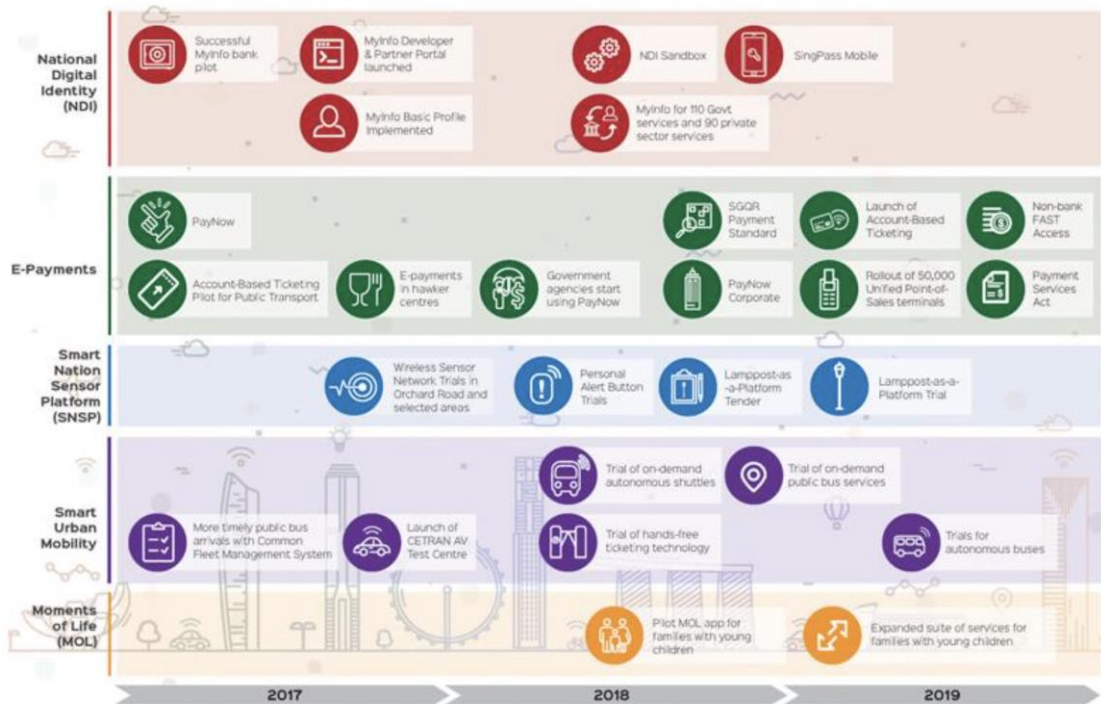


Figure 40. Strategic national projects for Singapore by Institute Smart Nation, an organization transforming the relationship between citizens and governance.

- **Open Data:** Datasets collected by public agencies are now available and accessible to the public via online portals so that anyone can participate and co-create citizen-centric solutions.
- **Living Lab:** Singapore remains committed to investing in research and innovation to catalyze emerging breakthroughs and drive new areas of economic growth. These initiatives include the Research, Innovation and Enterprise 2020 (RIE2020) and AI Singapore projects.
- **Industry and start-up ecosystem:** Start-up gas pedals, such as JTC Launchpad, a strong presence of venture capital and multinationals, and the establishment of SGInnovate, support Singapore's start-up ecosystem by connecting technopreneurs and industry mentors, while providing a bridge between innovation and enterprise.

The Punggol Digital District (PDD) is an example of an environment developed to attract the best talent and companies in the technology sector and foster their growth. By clustering growth sectors, the Singapore government has brought together high-value digital services in the PDD and created an ecosystem with testbed environments conducive to our companies and community thriving in a digital economy.

- **Computational Capabilities and Digital Inclusion:** Smart Nation efforts are highlighted by retraining and promoting coding and computational thinking skills so that all

segments of the population benefit, regardless of age or digital literacy. Resources are also in place to help businesses and SMEs pursue opportunities in the digital economy.

- **Cross-border collaboration:** It is important for cities to come together to share good ideas and best practices. Explore collaborations and test smart people-centered solutions. Singapore remains open to sharing new ideas and learning from others. This will enable us to adopt ideas and best practices that can benefit not only Singapore, but also the region and the world<sup>83</sup>.

In the following chapter, we study the typologies of the Parisian blocks in order to understand how urban forms generate surfaces that are conducive to energy capture and to the integration of active elements on the roof or façade.

## 4. ANALYSIS OF BUILDING TYPOLOGIES IN URBAN AREAS: THE EXAMPLE OF PARIS

### 4.1. Introduction

Our research raises the question of the relationship between buildings and wind. The city, because of its density, constitutes an interesting and complex subject of study. We have therefore studied the typologies of urban blocks in order to understand their cumulative impact on the movement of wind in the city.

We chose to develop a case study of the city of Paris for 2 reasons:

1. The first is related to the proximity and ease of access between the work and educational facilities and the city of Paris
2. The second reason is that, the historical and urban stratification of this city, constitutes a good example of the diversity of urban situations that we can meet in a city.

In parallel to the work we have done on wind measurements in Paris, we have studied the urban typologies of old and modern buildings in this city. Construction technologies, materials used, roof types, access aediculae, different heights and open courtyards in the urban blocks are all artifacts not visible from the street.

To approach this analysis, we have identified different typologies of buildings based on their construction periods. The APUR<sup>84</sup> offers an interesting source to identify the families of buildings built in Paris. This approach allows us to identify the shapes, the heights of the buildings, the differences of alignments in the urban block, allowing to anticipate the potential acceleration or slowing down of the wind in the city.

---

<sup>83</sup> *Transforming Singapore,*

<sup>84</sup> The Parisian Urban Planning Workshop

#### 4.2. Before 1800<sup>85</sup> :

Today, it is estimated that 6% of Parisian housing was built before 1800 (see figure 35). All the buildings built before 1800, constitute a relatively heterogeneous patchwork from the architectural point of view.

Collective housing buildings dating from this period are mainly found in the central arrondissements (1<sup>er</sup> to XI<sup>ème</sup> arrondissement), along the old N/S and E/W roads of the capital, along some radial extensions in the old suburbs (Saint-Antoine, Mouffetard), in housing estates (Odéon, île Saint-Louis, Palais-Royal, place des Vosges) as well as in some old village cores (La Villette, Vaugirard, Saint Blaise...). Their distribution also shows a dissymmetry between the left bank and the right bank, with a strong concentration of buildings dating before 1800 in the Marais district.

From the beginning of the 17th century, road regulations prohibited all corbelled construction above the tracks, imposed the common ownership and forced the alignment on the street. The facades of Parisian buildings remained flat until the middle of the 19th century.

The urban fabric inherited from the Ancien Régime is dense, with a network of narrow, irregularly laid out streets, rarely exceeding 10 meters in width. The blocks are small, except for the districts that were redeveloped after their creation. The plots are generally narrow and deep, from 4 to 6 meters wide and between 10 and 20 meters deep, but can be larger and more regular in the subdivisions (for example Place Dauphine). (See figure 36)

The establishment of buildings in line with the street is the general rule, but the desire to widen the roads has made the limits of the street move, except in the subdivisions, where they are straight. The open spaces in the heart of the block are often very fragmented, irregular in shape and very small in size. For the densest parcels, they are limited to simple light wells.



Figure 41: Collective housing buildings built in Paris before 1800 , source : Apur

---

<sup>85</sup> Dominique ALBA, *Analysis of the thermal performance of Parisian housing*,

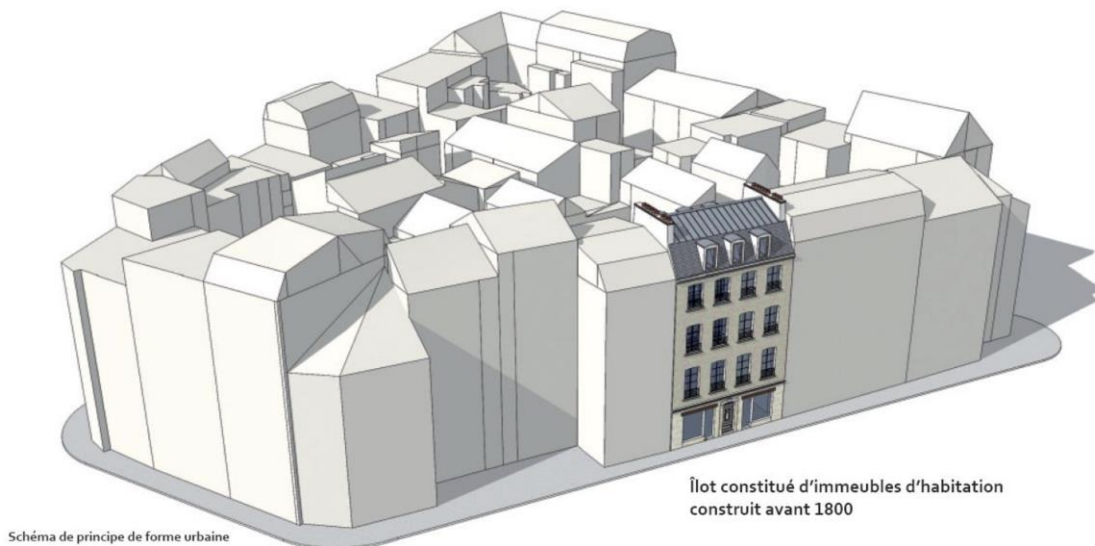


Figure 42. Block consisting of residential buildings built before 1800 , model D. Serero



Figure 43. Buildings built before 1800, rue Saint-Martin, 1st district , source : Apur

#### 4.3. Between 1801 - 1850 :

Most of the multi-family housing buildings dating from this period are located on the right bank (9% of Parisian housing). They are mainly found in an east-west crescent that bypasses the Marais district and passes between the Grands Boulevards and the former Fermiers Généraux enclosure. This is the case of the Chaussée d'Antin or "New Athens" housing estates. They are also located in the old suburbs of northern Paris, around the gates (Batignolles district), or in a few more selective operations within the Grands Boulevards (rue Rambuteau).

The urban form inherited from the first half of the 19th century is mainly the result of numerous subdivisions, often juxtaposed (see figure 38). The network of streets is relatively wide and rectilinear, distributing a regular plot of land. It should be noted that since 1783, it has been forbidden to open streets in Paris that are less than 10 m wide. The blocks are

geometrically shaped and cut into a regular plot. The series of relatively wide parcels can reach 18 meters, especially in the operations of subdivision.

On the scale of the block, the buildings form a generally very compact and mineral ensemble. The volumes are homogeneous and continuous along the street, from R + 4 + C to R + 5 + C. In subdivisions, the buildings are set up in a rational manner, with one building on the street, another at the bottom of the plot, and often courtyards and courtyards generally shared from one plot to the other. The establishment of the buildings in alignment and in common ownership limits the energy losses, by multiplying the leanings. Solar gain for courtyard facades is low, especially for the most densely built blocks<sup>86</sup> (see figure 39).

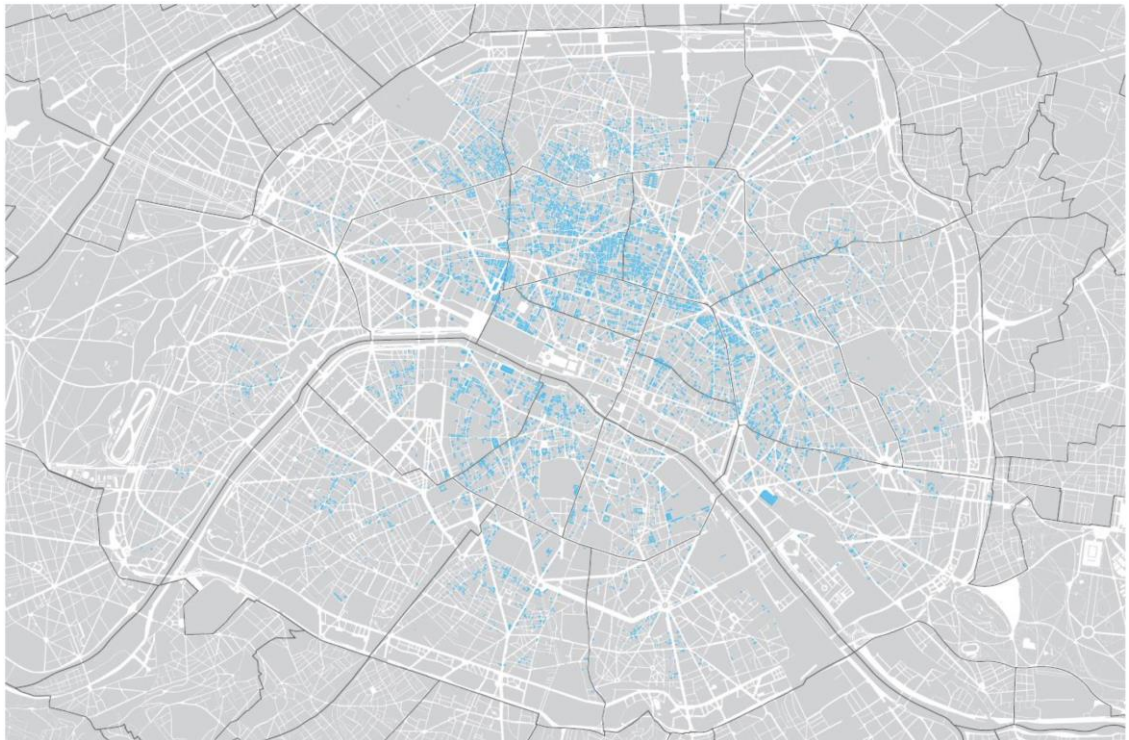


Figure 44: Collective housing buildings built in Paris between 1801 and 1850 ( <https://www.apur.org/fr> )

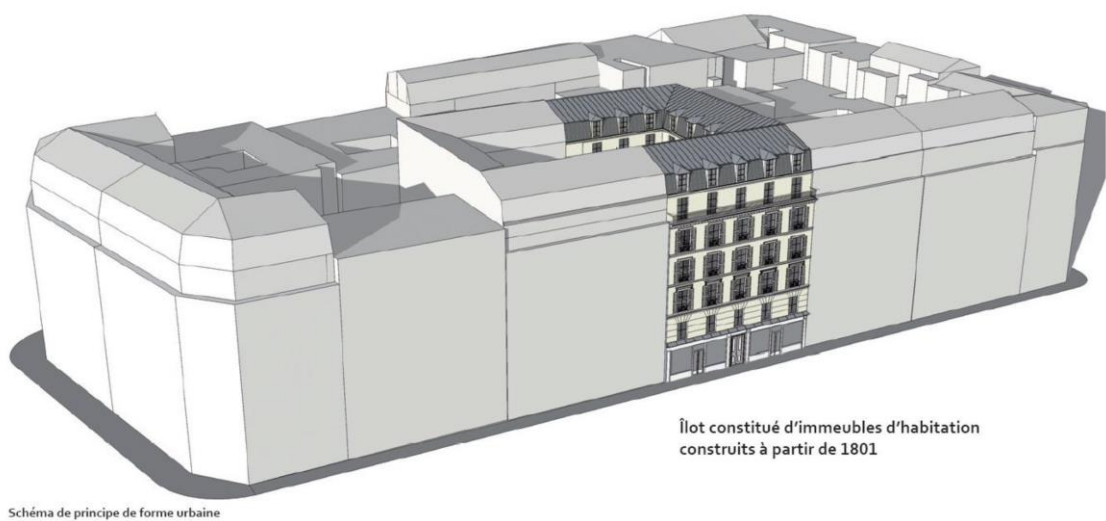


Schéma de principe de forme urbaine

86

Dominique ALBA, *Analysis of the thermal performance of Parisian housing built between 1801 and 1850*, 2011.

Figure 45. Block consisting of apartment buildings built from 1801 , modeling D. Serero



Figure 46. Buildings constructed between 1801 and 1850, rue de Trévis, Paris, 9th Arrondissement , Source : Apur

#### 4.4. Between 1851 - 1914 :

Today, an estimated 29% of Parisian housing was built between 1851 and 1914. Collective housing buildings dating from this period can be found both in the central districts and in the peripheral sectors of Paris, with a strong presence in the west. °They are located mainly along the large avenues built during this period (Sébastopol or Saint-Michel boulevards, etc.), around the three large train stations in the north of Paris, in the housing estates whose construction began during the first half of the 19th century (the western neighborhoods of Parc Monceau, Europe, Champ de Mars-Invalides, etc.), and along the new main thoroughfares opened up in the annexed territories (see figure 41).

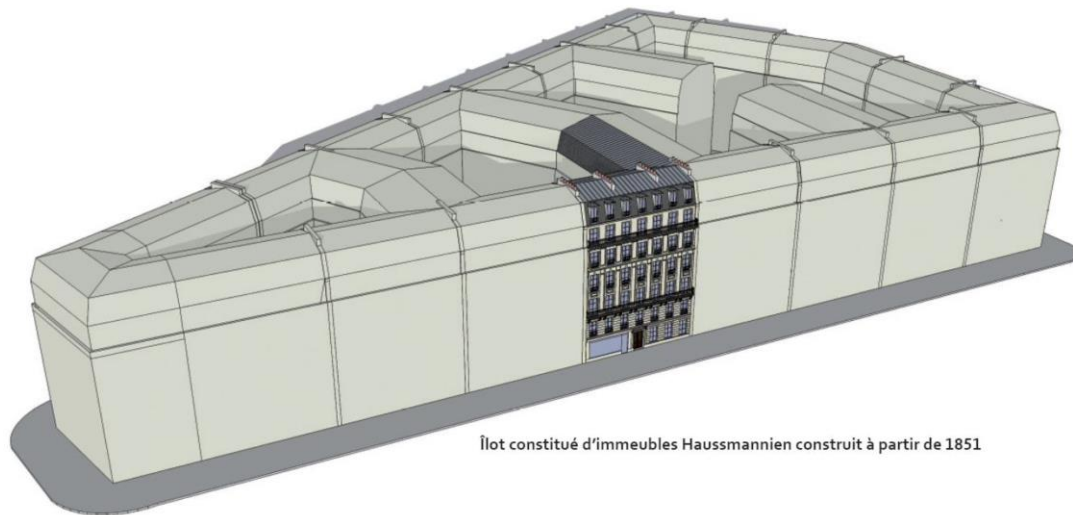
The urban form of the second half of the 19th century represents a considerable part of the landscape of Paris. It is the result of a global vision of the development of Paris, with a particular interest in the development of public roads.

In the breakthroughs as in the subdivisions, the lanes are wide (rarely less than 5 meters) and straight, and are part of a hierarchical network. The geometric form of the blocks is subject to the layout of the roads.

The parcel division is very well studied to offer a maximum and homogeneous occupation of the ground. The plots are generally regular in shape, with a minimum width of 5 meters on the street. At the scale of the block, the buildings form a generally very compact, mineral and dense whole. The volumes are homogeneous: from R+5+C for buildings built before 1902 and up to R+6+2C or +3C for those built after 1902, when the regulations became more permissive and allowed for a greater density of construction. The buildings are systematically located on the street alignment (see figures 41, 42, 43 and 44).



Figure 47. Collective housing buildings built in Paris between 1851 and 1914<sup>87</sup>



Îlot constitué d'immeubles Haussmannien construit à partir de 1851

Figure 48. Block consisting of apartment buildings built from 1851, modeling D. Serero



Figure 49. tenement buildings, built between 1851 and 1914, rue de Châteaudun, 9e, photo D. Serero.

<sup>87</sup> Dominique ALBA, *Analysis of the thermal performance of Parisian housing built between 1851 and 1914*, 2011.



Figure 50. Rue de Dunkerque and rue de Guérande, 9th district. Apartment buildings, subdivision operation, Source: Geoportail.

#### 4.5. Between 1918 - 1939<sup>88</sup> :

Approximately 17% of Parisian multi-family buildings were built between 1918 and 1939. The multi-family housing buildings dating from this period are relatively scattered throughout Paris.

The residential buildings of the inter-war period, housing luxury homes, are generally located in the central districts. Subdivisions of single-family homes (Hameau Boileau in the XVI<sup>ème</sup> arrondissement) are found more in the peripheral neighborhoods. Finally, social housing buildings of the HBM type are present in the peripheral neighborhoods, particularly in the area of the former military fortifications, decommissioned in 1919. This "belt" of public housing surrounds Paris, with a few interruptions in the southwest, in the west (Porte Dauphine), and in the railroad and industrial areas of the east and north.

Buildings of the HBM type: whether in the existing fabric or along the Maréchaux boulevards, the construction of collective housing buildings of the HBM type applied the hygienic principles of the time (guaranteeing ventilation and maximum sunlight for the dwellings), with a desire to break with the urban form of the Haussmannian city without yet freeing itself from the notion of the block, which would happen at the end of the 1950s.

Between Boulevard des Maréchaux and the "green belt", these housing complexes create a very well-defined urban fabric. The blocks are irrigated by wide and hierarchical local service roads (between 14 and 20 meters wide), either perpendicular or diagonal to the existing roads. The height of these buildings generally reaches 20 m at the cornice, divided into five or six levels topped by an attic roof. The buildings are located perpendicular or parallel to the public road, but, as far as possible, separated from each other. They respect the classic alignment on

<sup>88</sup> Dominique ALBA, *Analysis of the thermal performance of Parisian housing built between 1918 and 1939*, 2011.

the street, but the built front is discontinuous, punctuated by courtyards opening onto the public roads.

These were initially mineral, but have been progressively vegetated and, at present, can constitute public squares. The buildings are not very thick.

In the existing fabric, multi-family housing buildings may occupy several parcels grouped together as a result of consolidation, but they rarely result in the creation of new public roads. When the parcels are large enough, they have large interior courtyards. The volume of the buildings and the organization of the blocks are similar to the HBM of the boulevards des maréchaux, composed of buildings aligned with the street and giving onto courtyards that open onto the public roads, thus freeing up large linear facades.

Luxury residential buildings from the interwar period: these are present more occasionally. They present a more traditional urban form (compact blocks, buildings systematically aligned with the streets and in common), despite a slightly larger volume (R + 8 to R + 9) and width of facade. When the plots are large enough, they are occupied by green spaces of quality<sup>89</sup> (See figures 45, 46, 47 and 48).



Figure 51. Collective housing buildings built in Paris between 1918 and 1939 (<https://www.apur.org/fr>)

---

89

Dominique ALBA, *Analyse de la performance thermique des logements parisiens construits entre 1851 et 1914*, *op. cit.*



îlot constitué d'immeubles d'habitation  
de type H.B.M. construits à partir de 1920

Figure 52. Block of residential buildings built from 1920 , Modeling D.Serero



Figure 53. 1924-1930 H.B.M. housing building, C. Heubès architect, Avenue Simon Bolivar, 19th arrondissement ,  
photo: D. Serero



Figure 54. Housing building of the I.L.M. type, 1924-1926 boulevard Jourdan, 14th arrondissement. (<https://www.apur.org/fr>)

#### 4.6. Between 1945 - 1974<sup>90</sup> :

Approximately 21% of Parisian multi-family housing buildings were built between 1945 and 1967. Buildings constructed between 1945 and 1967 are few and far between in the central districts of Paris, with the exception of large facilities (Jussieu university campus, UNESCO headquarters). On the other hand, apartment buildings were widely scattered throughout the outlying districts, particularly in the south and east, and with the exception of the northwest. Large housing complexes were built at the time of the start of several emblematic operations ("Italie-XIII" in the 13th arrondissement, "Plaisance" in the 14th<sup>e</sup> arrondissement, the "Front de Seine" sector in the 14th<sup>e</sup> arrondissement) and were accompanied by the renovation of certain insalubrious blocks. In the central districts, housing operations are more selective. There were also new operations starting in 1968, for example in the Hauts de Belleville/Place des fêtes sector (XIX<sup>e</sup> arrondissement) as well as in more specific operations (Porte de la Chapelle).

Until the beginning of the 1960s, the collective housing buildings constructed after the Second World War generated an urban form that was a continuation of that of the previous period: construction in line with the street, discontinuous built frontage with open courtyards on the street, low volumetry (from R + 5 to R + 6).

On the other hand, the application by anticipation of the PUD, from 1962, favors the break with the traditional urban form. The building is no longer dependent on its relationship to the road, but on other more functional elements (orientation, prospect...). In small parcels, the buildings are systematically set back from the alignment. In the large parcels, they are implanted according to free massing plans.

The mass plans of the blocks are often open, with small bars of R + 5 to R + 7 or towers of R + 10 to R + 12. The gradual increase in building heights allows for the creation of open spaces at the foot of the buildings, which are often heavily planted<sup>91</sup> (See figures 49, 50, 51 and 52).

---

<sup>90</sup> Dominique ALBA, *Analysis of the thermal performance of Parisian housing built between 1945 and 1974*, 2011.

<sup>91</sup> *Ibid.*



Figure 55. Multi-family housing buildings built in Paris between 1945 and 1974 (<https://www.apur.org/fr>)

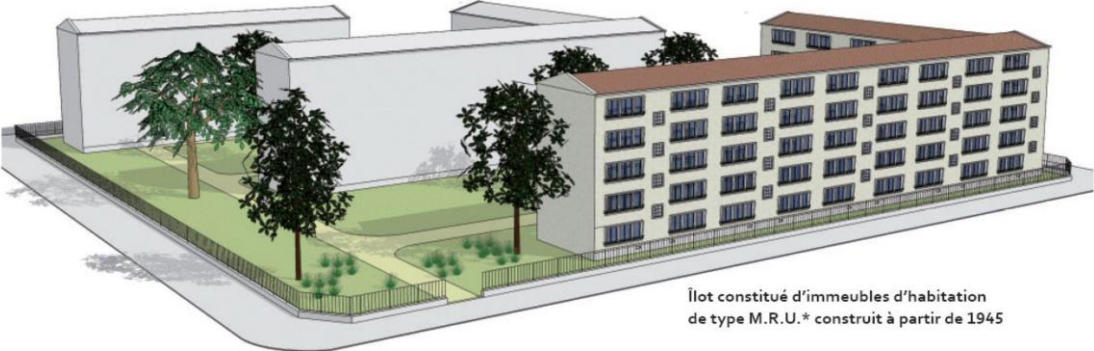


Figure 56. Block consisting of M.R.U.\* type apartment buildings built from 1945 , Modeling D. Serero



Figure 57. Apartment building, rue Dunois and boulevard Vincent Auriol, 13th district.



Figure 58. Place des Fêtes (XIXth arrondissement): large complex under construction, erasing the existing urban grid, 1971 (<https://www.apur.org/fr>)

#### 4.7. Between 1975 - 2000<sup>92</sup> :

Approximately 16% of Parisian multi-family housing buildings were built between 1975 and 2000. The majority of multi-family housing buildings dating from this period are located :

- or in a concentrated manner in large operations (Front de Seine, Place des Fêtes) or large ZACs (Amandiers in the 20th arrondissement, Guilleminot-Vercingétorix in the 14th

---

<sup>92</sup> Dominique ALBA, *Analysis of the thermal performance of Parisian housing built between 1975 and 2000*, 2011.

arrondissement<sup>e</sup> , Citroën-Cévennes in the 15th arrondissement, Bercy in the 12th arrondissement, Manin-Jaurès in the 19th arrondissement)

- or scattered in smaller-scale operations in the outlying districts forming a large eastern and southern crescent (as part of the continuation of the "Eastern Program Plan").

In the center, their presence is limited to a few emblematic operations (Horloge district). Finally, they are not very present in the western part of Paris. This period marks the end of towers and vertical constructions in Paris. This return to "urban architecture" in continuity with the existing fabric is characterized by the systematic establishment of buildings in line and in common on the street, which multiplies the back-to-back and limits energy losses. The blocks are generally closed. In the depth of the lots, the buildings are often not located at the edge of the parcel, which makes it possible to free up lateral open spaces that are shared from one parcel to the next.

Some major ZACs (Reuilly or Bercy, in the 12th arrondissement) involve several blocks. The programs give rise to new neighborhoods combining facilities, creation of public spaces and construction of housing.

The volume of the buildings varies from R + 4 to R + 8. In large development operations, particular attention is paid to the landscape unity of all the projects of the same operation. This search for homogeneity is articulated with varied architectural writing on the scale of the blocks or buildings<sup>93</sup> (See figures 53, 54, 55 and 56).



Figure 59. Multi-family housing buildings built in Paris between 1975 and 2000 (<https://www.apur.org/fr>)

<sup>93</sup> *Ibid.*



Îlot constitué d'immeubles d'habitation  
construit à partir de 1975

Figure 60. Block of apartment buildings built from 1975



Figure 61. Apartment building, 1982, Labro and Orzoni architects, rue des Écluses-Saint-Martin, 10th arrondissement.  
(<https://www.apur.org/fr>)



Figure 62. Citroën-Cévennes Joint Development Zone, 15th arrondissement, 1989-2006, Source: SEMEA 15, aerial mission 2004.

#### 4.8. Summary of identified urban typologies

The city of Paris, due to its long history, constitutes a patchwork of rich and varied urban typologies (see figure 57).



Figure 63. Mapping of buildings in Paris based on their typology and date of construction (<https://www.apur.org/fr>)

They are characterized by:

- Homogeneous blocks with a coherent and homogeneous urban profile

- More fragmented blocks with notably strong changes in scale, height and building openings that offer pronounced differences in volume in the city.

We will study in Part 4, the impact that these typologies have on the airflow in an urban site. Their height, their profile and their implantation in relation to masking or guiding elements of the city or its surroundings, constitute devices of increase or slowing down of the air movements.

In these different types of construction in urban areas, energy consumption is largely dependent on the thermal insulation and ventilation factors of the dwelling, as well as on the uses made of it. But in the context of old cities like Paris, thermal performance is often low. To reach the objective of a zero carbon emission, and that of a passive housing, we need to increase the energy performance, by correcting the problems encountered on the roofs, the external walls, the windows in direct contact with the outside.



Figure 64. Puissance de chauffage nécessaire par unité de surface d'un logement, source Ademe

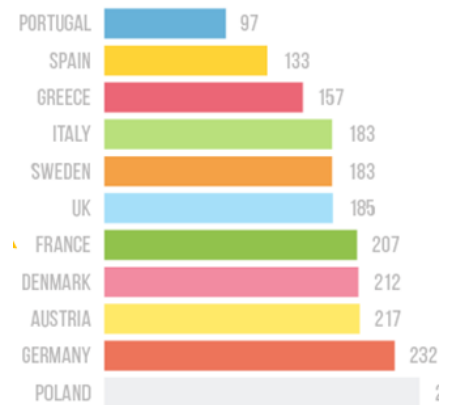


Figure 65. Puissance de chauffage nécessaire par unité de surface d'un logement en Europe en kWh/m<sup>2</sup>, Source Ademe

The following two diagrams (Figures 58 and 59) show the average energy consumption of a dwelling, and the comparison between the consumption per unit of space between the different European countries. France is in 7th position.

## 5. Conclusion

At the end of this first part, we have seen that, derived from the ancient forms of windmills, the modern wind turbine has emerged during the 20th century under the impulse of alternative energy production researches. But this development was done in a race to the large scale and with implantations in isolated sites, disfiguring sometimes our landscape heritage and generating numerous forms of pollution.

Then we saw how the paradigm of the energy internet or smart-grid allows us to envisage a change in the production and consumption of energy. It allows millions of users to be connected to each other, making it easier to manage intermittency and variations in the amount of energy produced.

We then studied the typologies of buildings and urban blocks in a city like Paris. These typologies, in spite of the will of the cities to want to unify their profile, always constitute a "collage" of different architectures, which adapted to the modern uses and the new modes of construction.

Could we bring the energy production sites closer to the consumption sites? Can our buildings become energy collector supports, and integrate grouped micro-wind turbines rather than a few large ones?

In Part 2, we will discuss how to map the winds, and the method we have proposed for surveying buildings.

In Part 3, we will recall the main principles of fluid mechanics and present the modes of analysis and simulation of wind behavior around buildings.

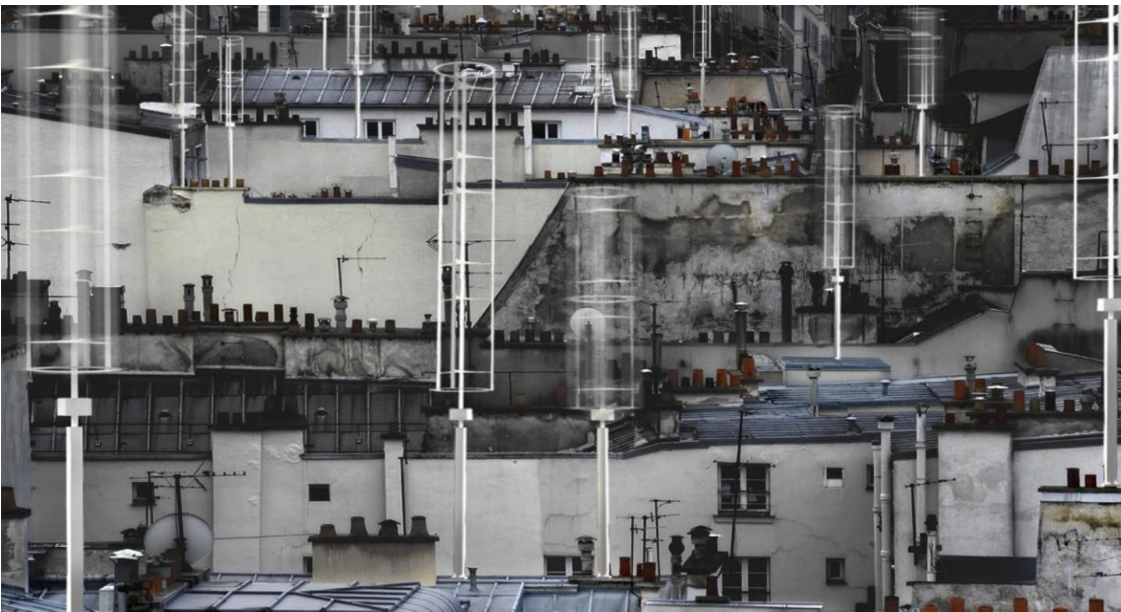
In Part 4, we will perform a large number of numerical simulations of these flows on buildings in order to understand the potential of architecture and cities to amplify the force of the wind.

In Part 5, we will present architectural integration modes of wind devices, as well as a design aid tool for architects, to facilitate the design of these devices in the sketch phase of the architectural project.



## PART 2

### METHODOLOGY OF ANALYSIS AND WIND SURVEYS IN URBAN AREAS



#### Contents:

- Renewable energy wind and energy internet
- Wind mapping and geographical potential analysis
- Method for collecting anemometric data in urban areas
- Typologies of wind devices and analysis of their potential and constraints (vertical axis, horizontal axis, vibration, ...)



## PART 2

2. INTRODUCTION.....	87
2.1.WIND MAPPING AND GEOGRAPHICAL POTENTIAL ANALYSIS .....	89
2.1.1. Get real-time wind data .....	91
2.1.2. Wind visualization and mapping .....	93
2.1.3. Moving particles on the GPU.....	96
2.1.4. Implementation of a method to measure urban winds.....	96
2.2.METHODOLOGY OF ANEMOMETRIC DATA COLLECTION IN URBAN AREAS .....	97
2.2.1. Analysis of wind behavior in urban areas.....	97
• Description of Netatmo connected anemometers .....	97
2.2.2. Map of connected weather stations in Paris.....	100
2.2.3. Map of wind measurement anemometers .....	100
2.2.4. Presentation of the study sites.....	101
2.2.5. Installation method of connected anemometers on an example of Haussmannian apartment building 136 avenue Parmentier, Paris XIème.....	102
2.2.6. Anemometer readings of a house in the Paris region (Arcueil 94).....	105
2.2.7. Anemometric measurements on an urban island building: Ecole d'Architecture Paris Val-de-Seine (75013).....	108
2.3. COMPARATIVE ANALYSIS OF WIND ENERGY SYSTEMS .....	110
2.3.1. Type of integration of the devices to the buildings and facades .....	110
2.3.2. Profiling of the wind speed increase device around a building .....	113
2.3.3. Typology of vertical axis micro-turbines implemented in research .....	114
2.4.CONCLUSION .....	117



## 2. INTRODUCTION

How to measure wind speeds on a territory or at the periphery of a building? Can a local energy source be distributed and shared locally?

This section presents the state of the art of wind analysis and mapping methods on a territory, as well as the bibliographic and technical research that fed this research. Due to the extremely variable and fluctuating nature of wind, many geographical areas, and in particular cities, are not subject to accurate wind surveys or synthetic wind maps. However, climate sciences, weather records and weather model simulations allow to extrapolate and model the global wind behavior.

In order to establish accurate information for our study, we used connected ultrasonic anemometers that were located at 3 study sites. The continuously provided wind data at each of these points is then compared with the data from the numerical wind tunnel we set up.

In this way, we can categorize the different types of wind in urban areas. These elements, and in particular the identification of the minimum and maximum wind spectrum, allow us to define the choice and the performance of the energy collection devices. The method of fixation on the roof or on the facade of the building, the type of wind, the altimetry of the device in relation to the roof levels, the potential nuisances around. We have also linked this information with technical specifications of wind turbines, their price and energy performance (see Appendix 1). This defines the characteristics of wind turbines to maximize their performance in an urban site and in a turbulent wind regime.

This method precisely allows to calibrate the simulation from precise and real points on site, then to develop the complete volumetric model of the wind behavior on a roof area, or an urban block in its entirety.

First, we will present an overview of the ratio of energy produced to energy consumed on a large scale, in comparison with other countries.

Then, it seemed important in the context of this research to introduce the notion of *the Internet of energy*, which sets up a paradigm shift in the collection and distribution of energy. The intermittent production of energy sources can be shared by a peer-to-peer network, without the need for centralized energy networks. This emerging technology is based on the principle of the Smart City, which is defined as a set of systems and objects interconnected to each other. This network improves the resilience of cities and their ability to adapt to sudden or unexpected changes.

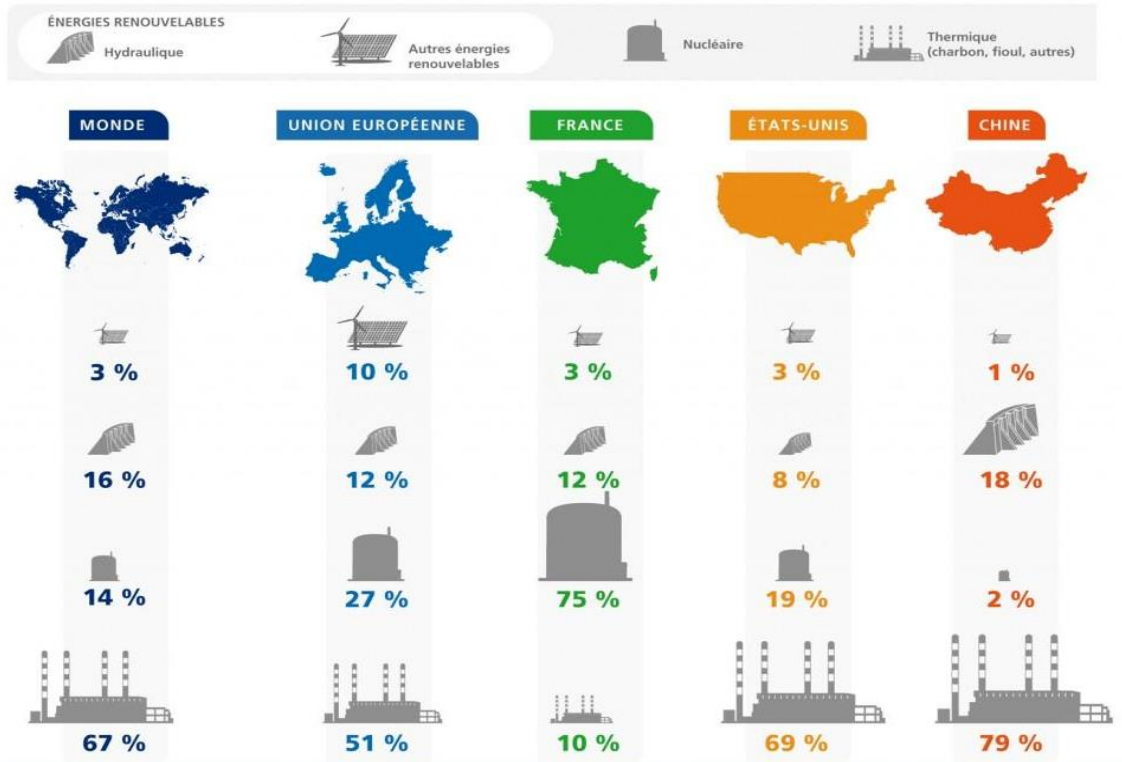


Figure 66. Summary of electricity generation in the world (source: EDF/IEA 2013)

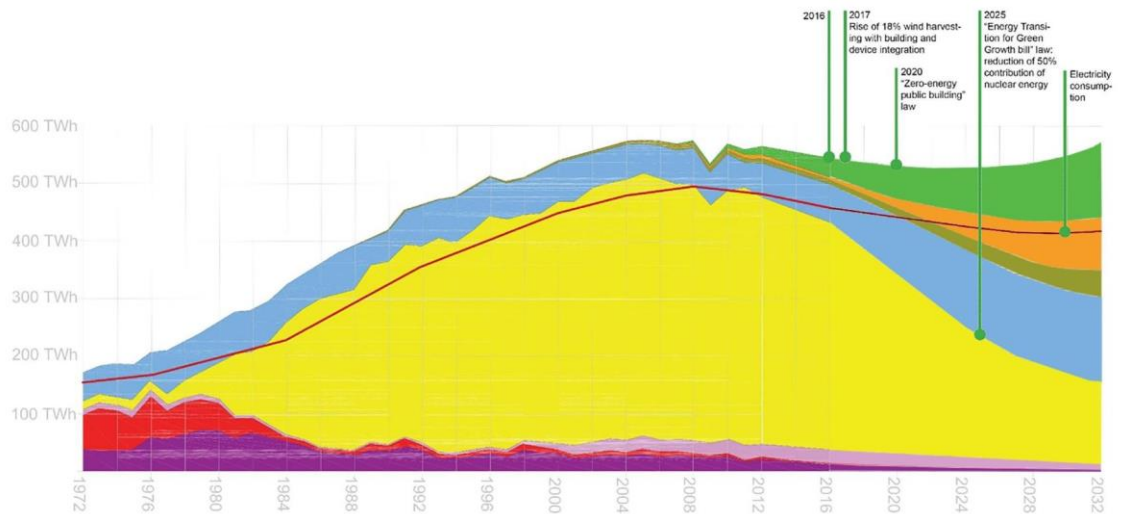


Figure 67. Sources de génération électrique en France et projection jusqu'à 2050 ( source : OECD/IEA 2014)

Figure 60 shows the amount of energy produced by type of source in France. In Figure 61, we have the evolution of production sources from 1972 to 2016 with the projection of the estimated energy production by sector based on government decisions, from 2018 to 2032. We also have on the diagram annotations that specify the plan to reduce carbon emissions and the targets for reducing non-renewable energy used for electricity production. We note that France is 75% dependent on nuclear energy in its overall balance, and that the sources of production using renewable energy are quite marginal (about 3%), while several countries of the European Community have largely begun their energy transition.

***What are the levers we can activate to accelerate this transformation? Wouldn't the implementation of energy capture devices on support buildings allow us to bring the energy production sites closer to the consumption sites?***

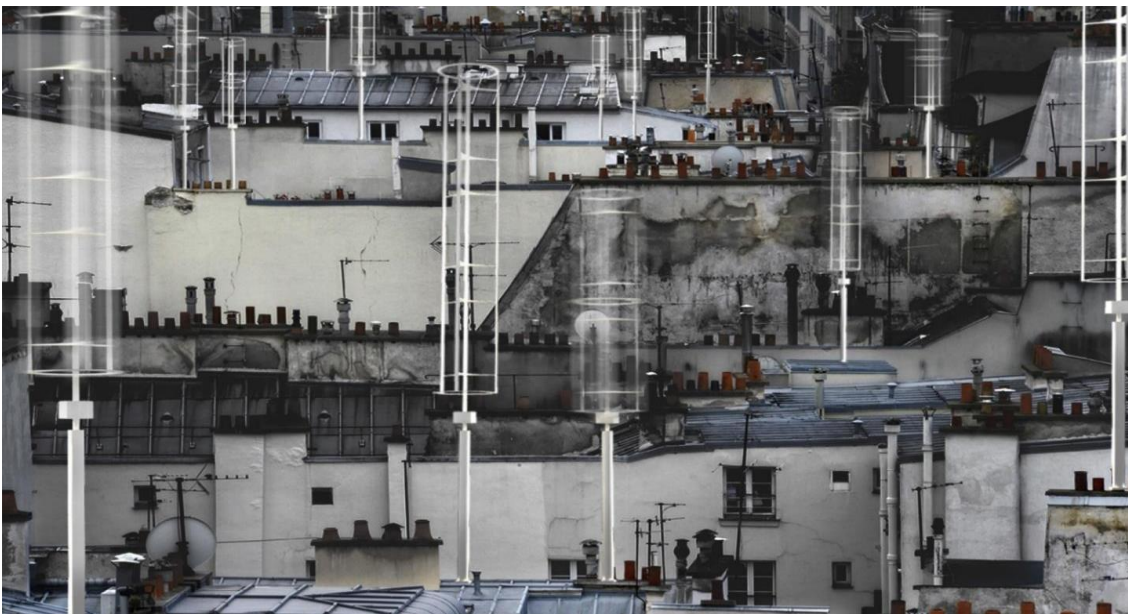


Figure 68. Visualization of a possible reappropriation of Parisian roofs with micro-generators , Photomontage: D. Serero

In order to compare the energy produced by the city and the energy consumed, we could compare the total surface of the Parisian roofs exposed to the wind and the possible yield of wind energy (see calculation in chapter 5.4). This estimation shows us that grafting energy capture devices on one building out of 4 in a city like Paris would allow to produce the energy consumed by the whole city.

## 2.1. WIND MAPPING AND GEOGRAPHICAL POTENTIAL ANALYSIS

The Figure 70 map is an exceptionally rare example of one of the earliest and most significant aerograph or wind rose maps that appeared in the 17th century<sup>ème</sup>. This unusual chart represents a transition point in the perception of direction or, more precisely, the transition from the wind rose to the wind map. The first sailors in the Mediterranean defined direction by the names of the different winds and the points from which they blew. This idea has its roots in ancient Greece. Homer identified four cardinal winds, but as navigation and cartography developed, more and more were added. This chart shows thirty-two named winds

and a multitude of different wind systems. Each of the winds is identified by several different names in Greek, Latin, French and Dutch.

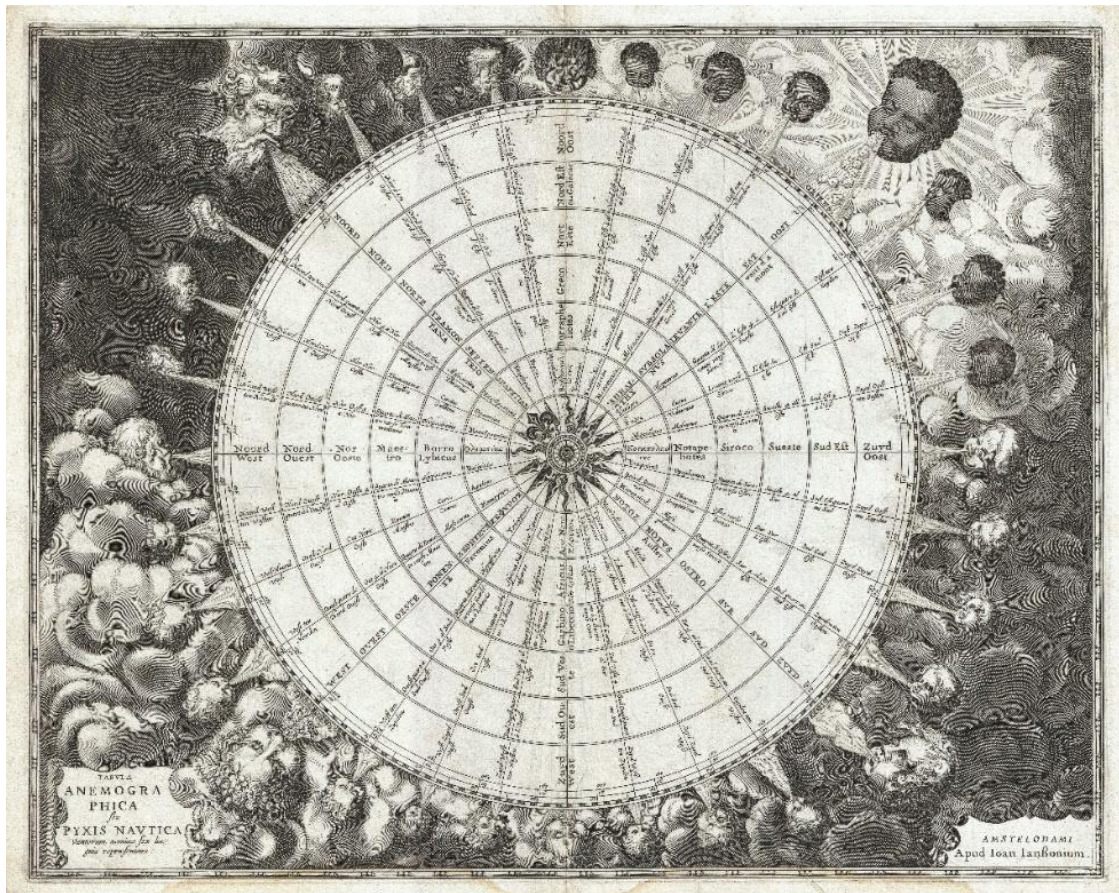


Figure 69 . Cette carte des vents a été publiée en 1650 dans l'Atlas Maritime, ou le volume 5 de l'Atlantis Majoris, de Janssonius, source : Geographicus.com

In the areas surrounding the sphere, each wind is personified by a figure bearing the racial characteristics associated with the region or direction represented. The upper left quadrant, representing the north, depicts bearded Germans or Scandinavians. The upper right, representing the east, shows dark-skinned faces without beards. The beardless, pale-skinned figures in the lower left and right, representing the west and south, are less distinguishable, but may be intended to represent Native Americans and Greeks. Anemometer charts, like this one, were functional objects and valuable reference tools.

Early navigators, referring to directions as winds, could sail with the north wind. This was especially convenient when trade winds dictated ocean trade. A warm southerly wind, for example, might suggest that certain routes, closed for part of the year, were now open. A navigator would have used this chart to compare different names for directions. For example, he might have used a chart made in Greece that identified the winds under the names of Greek gods, but he himself was trained to use a different nomenclature, for example Catalan or English.

With this chart, he could understand what various navigation logs and journals were referring to. Even though nautical charts existed in the 1600s, navigation was mainly done with the help of "Pilot Books", which asked the guy to follow the south wind for 3 days before turning with

the east wind, etc. This map was published as Plate 1 of 1650 Atlas Maritimus by Janssonius or in Volume 5 of his Atlantis Majoris<sup>94</sup>.

### 2.1.1. Get real-time wind data

Several sets of wind data exist on a local or global scale. They are consolidated either by national meteorological organizations, or by local networks, or by wind enthusiasts. More and more devices allow real time access to these data or to archives.

These data are in the vast majority of cases extrapolated from measurements made at ground level or in the atmosphere. Large areas of territory are thus globally described. However, in the framework of our research we need data in urban areas at a finer granularity. A part of this work aimed at creating even more local data, with a minimum of extrapolation in order to obtain information that takes into account the urban and architectural specificities of the context of each study. We present here some of these datasets.

Every 6 hours, the U.S. **National Weather Service** publishes weather data for the entire globe, known as GFS, in the form of a latitude/longitude grid with associated values (including wind speed). It is encoded in a special binary format called **GRIB**, which can be parsed into human-readable **JSON** with a special set of tools ( See Figure 78).

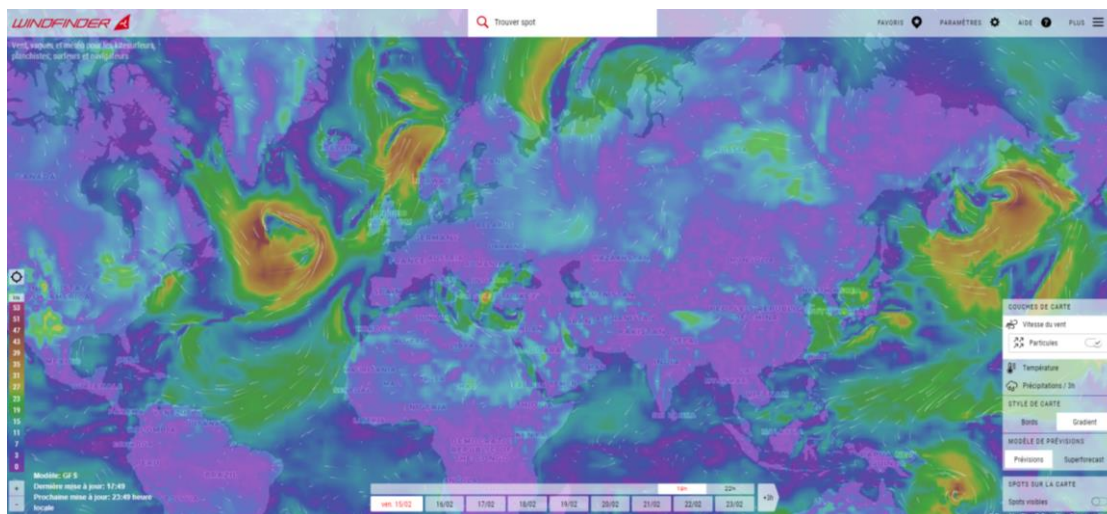


Figure 70. Le site internet *Windfinder.com* présente une cartographie en temps réel de la Vitesse du vent sur l'entièreté du globe

Windfinder provides wind and weather forecasts for more than 45,000 locations ("spots") around the world, which are relevant for kite surfers, windsurfers, sailors and paragliders. Most of these places are practice sites for these sports, as well as marinas or take-off and landing sites. They offer a unique global network of weather stations. Current wind speed and direction, air temperature and pressure, and other values at these sites can be viewed in real time<sup>95</sup> (See Figure 74).

<sup>94</sup> 1650 Jansson Wind Rose, Anemographic Chart, or Map of the Winds,

<sup>95</sup> WINDFINDER.COM, *Windfinder - wind, wave & weather reports, forecasts & statistics worldwide*,



Figure 71. The Windfinder site is multiplatform, Source: windfinder.com



Figure 72. The site is dedicated to the visualization and the prediction of wind in real time for the aficionados of the board sports

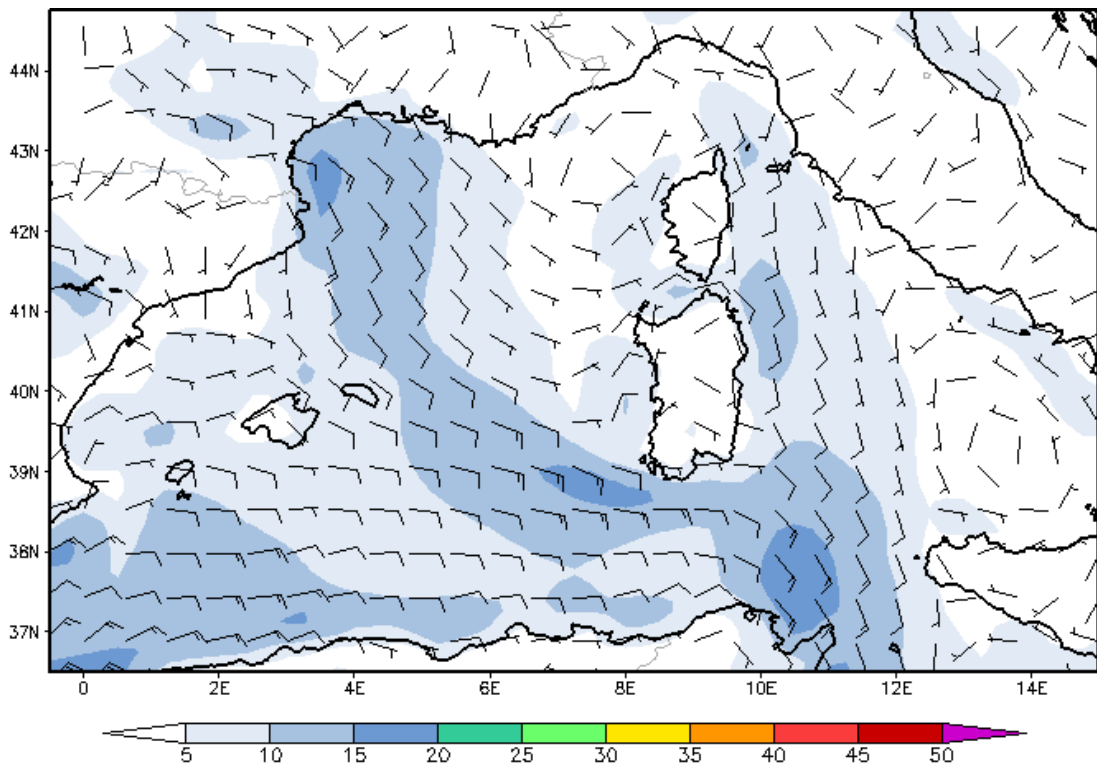


Figure 73. Surface wind per 18 hours in February 18, 2019, Source: Météo France

A network of EPW data (EnergyPlus Weather Data) exists and can be used by architects and engineers. These data are not very available in France and should be shared more widely. On the other hand, the EPW files used by Ladybug or Dynamo contain wind information extrapolated from readings on reference points, the list of which is given. Our attempts to import EPW files into Dynamo have shown a lot of instability.

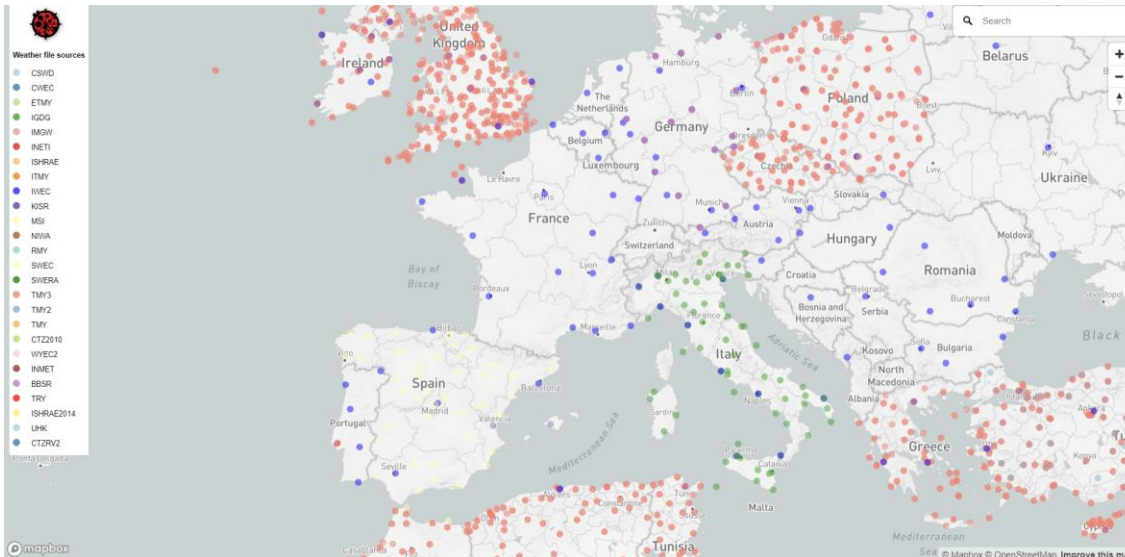


Figure 74 Maps of climate data available in Ladybug

It should be noted that it is difficult to use this hyperlocal information because of the very different wind directions and strengths recorded, which shows that there is too much variation in wind directions and strengths in urban areas.

This is discussed in **2.3.4 Presentation of the study sites** and refers to the need to create one's own dataset in order to analyze local specificities.

The readings taken on these buildings were compared to the reference weather stations in Paris, namely :

- Charles de Gaulle airport ( CDG)
- Orly airport
- The Montsouris Park weather station
- The Zamansky tower of the University of Paris Jussieu

We will present in chapter 2.2.1 a remarkable network of amateur weather stations to obtain accurate wind readings around buildings running on wifi from connected anemometers.

### 2.1.2. Wind visualization and mapping

There are many examples of online wind energy visualization, but one project that has set the standard in this area is **earth.nullschool.net**, a project created and driven by Cameron Beccario

(See Figure 75). It is not open source, but an older open source version on which most other implementations have based their code. Esri Wind-JS is an interesting open source derivation. Popular weather services that use this technique include Windy and VentuSky (See Figure 76).

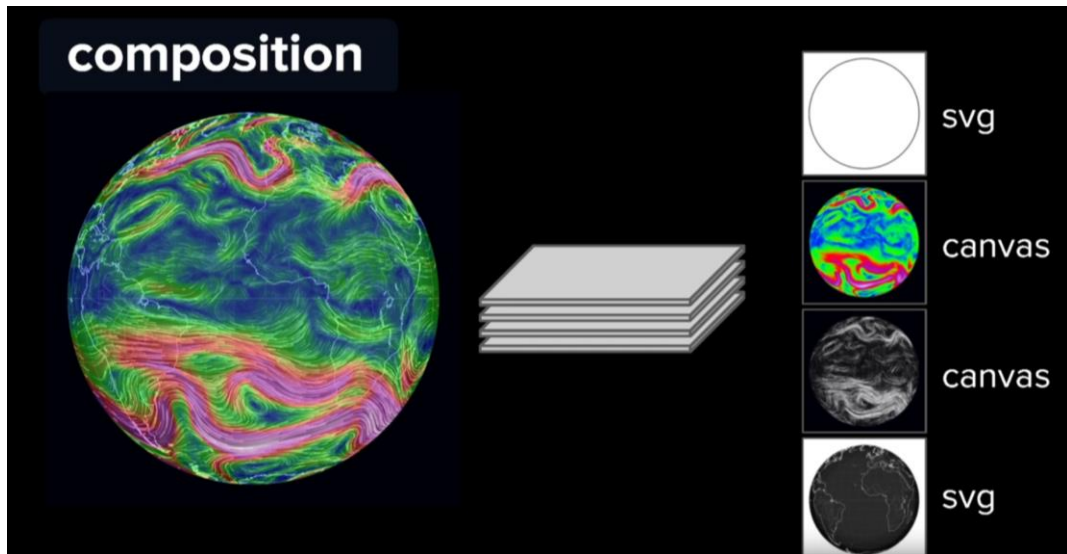


Figure 75. Extraction des couches constituées par les données météo, les supports de projection d'une cartographie en temps réel

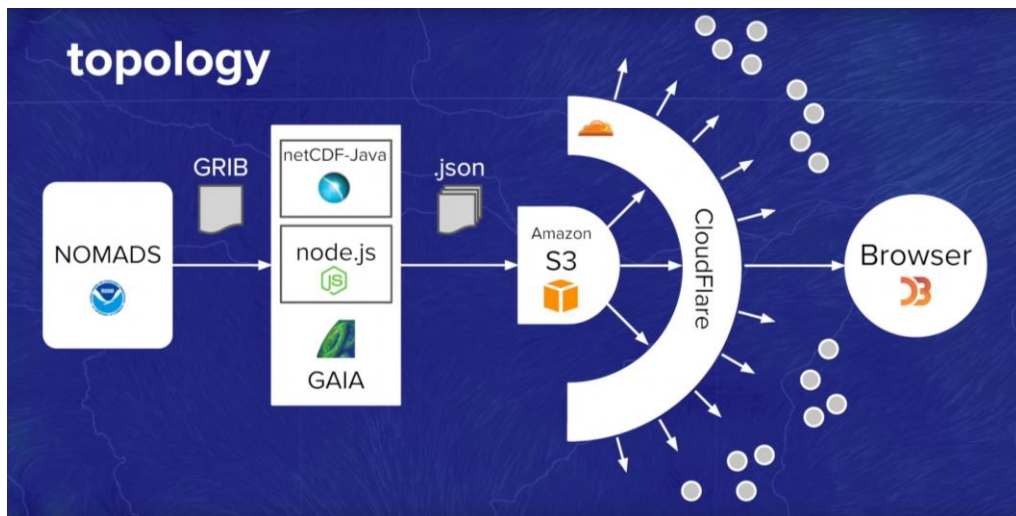


Figure 76. Modèle de liaison des données entre la cartographie des vents et les données satellites.

In general, such a visualization in a web browser is based on the 2D Canvas API and works as follows:

1. Generate an array of random particle positions on the screen and draw the particles.
2. For each particle, extract the wind data to obtain the velocity of the particle at its current location and move the particle accordingly.
3. Resetting a small portion of the particles to a random position. This ensures that the downwind areas never become completely empty.
4. Deletion on the current screen and drawing of the newly positioned particles.

This poses problems of performance limitations such as:

- Each time you update the data or the view (about 2 seconds for the Earth, for example), the processing time is long, because the data processing is expensive and is produced by the processor ( See figure 77).

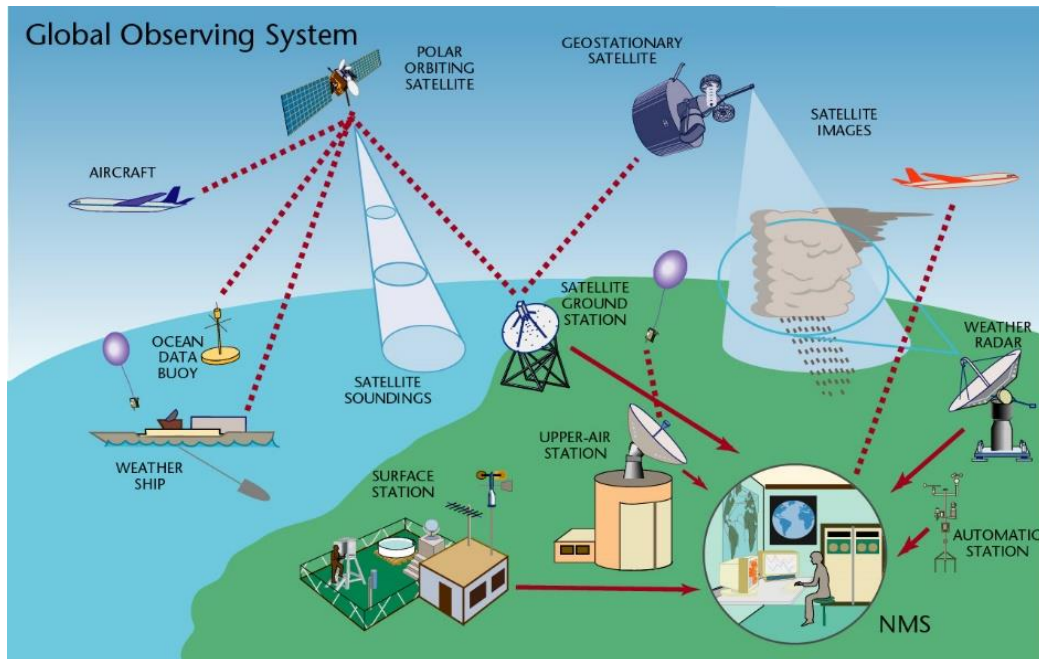


Figure 77: Global weather and anemometer observation system, source: World Meteorological Organisation, 2019

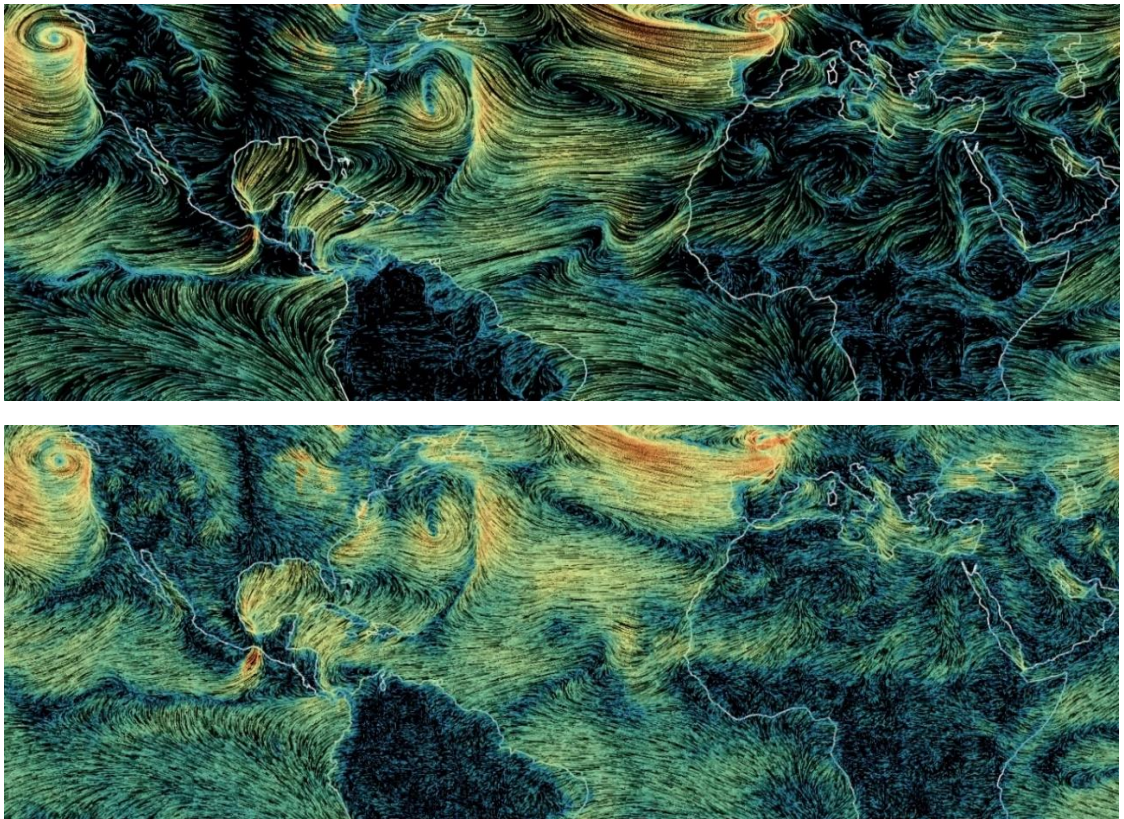


Figure 78. Two resolutions of interactive global wind mapping (source: mapbox.com)

### 2.1.3. Moving particles on the GPU

Existing wind visualizations store the state of the particles in arrays. How is this data stored and manipulated by the computer graphics processor? A new GL feature, called shader computation (in OpenGL ES 3.1 and equivalent WebGL 2.0 specifications), allows researchers to run "**shader code**" on arbitrary (non-rendering) data. Unfortunately, support for the new specification on browsers and mobile devices still remains poor. The display mode is therefore simplified by the use of "**textures**".

OpenGL allows to draw not only on the screen, but also to generate textures (via a concept called framebuffer). Thus, particle positions can be encoded as RGBA colors of an image, loaded into the GPU, calculated new positions according to the wind speed in the **fragment shader**, recoded into RGBA colors and drawn in a new image<sup>96</sup>.

### 2.1.4. Implementation of a method to measure urban winds

Our research has allowed us to hijack an anemometer from an amateur weather station to create a precise device for measuring the wind around buildings. These NETATMO anemometers communicate by wifi with a central equipment that shares the data acquired by various devices such as indoor and outdoor temperature, rainfall, sunshine, wind speed. All these devices are wireless, with a range of 20 to 50 meters, allowing devices to be installed on the roof, on the facade, on top of a mast and to move their location if necessary.

---

<sup>96</sup> Vladimir AGAFONKIN, *How I built a wind map with WebGL*, <https://blog.mapbox.com/how-i-built-a-wind-map-with-webgl-b63022b5537f>,

## 2.2.METHODOLOGY OF ANEMOMETRIC DATA COLLECTION IN URBAN AREAS

### 2.2.1. Analysis of wind behavior in urban areas

- *Description of Netatmo connected anemometers*

During the course of the study, it appeared essential to compare the results of the numerical simulations with real measurements taken on existing buildings. These comparisons were used to calibrate the numerical simulation devices. Wind speed and direction are measured using connected ultrasonic anemometers.



Figure 79. Station météo connectée utilisée par D. SERERO



Figure 80. Anémomètre à ultrasons et tablette ou smartphone d'interface de présentation des données en temps réel, source : [netatmo.com](https://www.netatmo.com)

The anemometer measures the time between sending a signal and receiving it in two perpendicular directions. The velocities on the N-S and W-E axes are then combined using trigonometric functions to obtain the actual velocity and direction.

#### **Measures posted<sup>97</sup> :**

1- Average speed and direction over the last 5 minutes. The arrow indicates the wind direction and its size is proportional to the speed. Light grey lines around the icon indicate the dominant wind directions during the last hour. An arrow pointing downward indicates a north wind (N=0°). An arrow pointing to the left indicates an East wind (E=90°).

2- Speed and direction of gust over the last 5 minutes.

3- Maximum burst (speed and direction) during the day (since midnight).

Picto no wind: this pictogram corresponds to an absence of wind.

Circular arrow pictogram: this pictogram means that the wind is rotating, i.e. it has no defined direction. The curves allow you to navigate through the historical data of wind averages (speed and direction) and gusts (speed and direction)<sup>98</sup> .

<sup>97</sup> *Features of the Smart Weather Station*, <https://www.netatmo.com/fr-fr/weather/weatherstation/specifications><https://www.netatmo.com/fr-fr/weather/weatherstation/specifications>, accessed July 17, 2020. [2]

<sup>98</sup> *Smart Weather Station and Accessories - How does wind measurement work? | Netatmo Helpcenter*, <https://helpcenter.netatmo.com/fr/station-meteo-intelligente-et-ses-accessoires/mesures-et-calibrations/la-mesure-du-vent-comment-ca-marche>,



Figure 83. Operating diagram of the connected ultrasonic anemometer by Netatmo site

We present here several views of the data retrieval interface and of the maps we can make with this element. Today the data of a large urban space can be shared with other users of the application to create collaborative maps.

Figure 84. Diagrams of wind speeds measured at the site 136 avenue Parmentier, 75011 Paris in 2018, Vertical axis: speed in M/s. The black curve represents the wind speed and the blue line the minimum winds recorded over the same period.



Figure 85. Plan, elevation, cross section of the anemometer used

Caractéristiques de l'anémomètre	
DIMENSIONS	Hauteur : 110 mm, Diamètre : 85 mm
CAPTEURS ET MESURES	Vitesse du vent : Range : 0 à 45 m/s (160 km/h) Précision : 0,5 m/s (1,8 km/h) Direction du vent : Précision : 5°
UNITÉS DE MESURE	m/s, km/h, mph, noeuds, Beaufort.
CARACTÉRISTIQUES SANS-FIL	Connexion sans fil entre les modules : Longue portée 100 m.
MATÉRIAUX ET DESIGN	Plastique haute qualité. Résistant aux UV, la grêle et les forts vents.

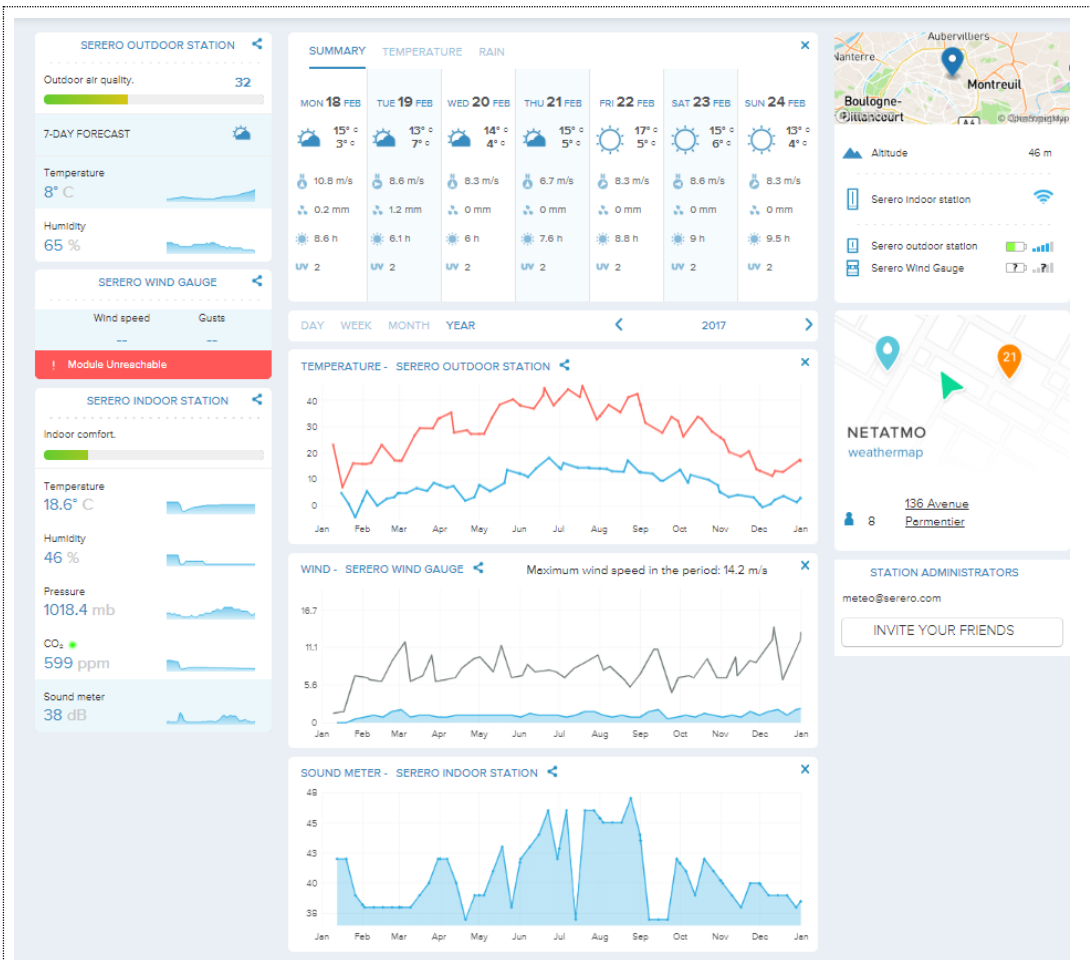


Figure 86. Interface générale de visualisation des données , application Netatmo, station météo

### 2.2.2. Map of connected weather stations in Paris

Figure 86 shows the NETATMO type weather stations that share their measurements and data on this collaborative platform. The density of the mesh in urban areas makes it easy to compare local differences in measurements related to the immediate context of the station.

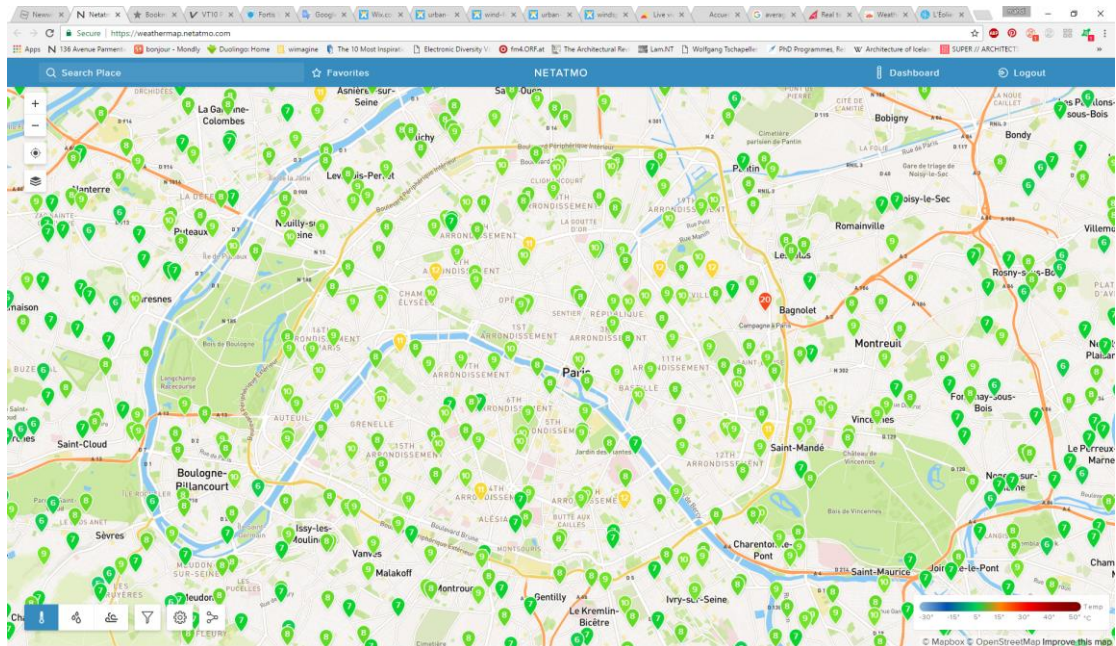


Figure 87. Cartographie des stations météo connectées de type Netatmo à Paris ( données en temps réel sur le site NETATMO)

### 2.2.3. Map of wind measurement anemometers

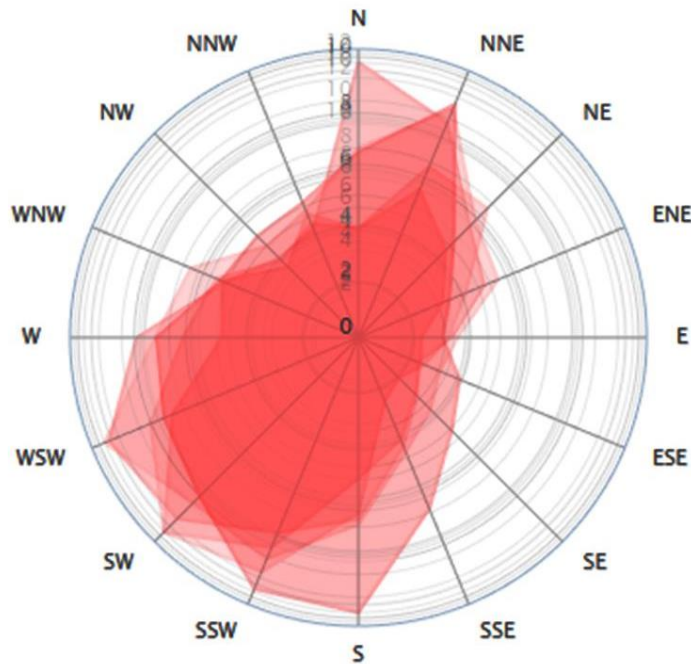


Figure 88 Wind measurement stations show the main directions in the City of Paris, by the Windfinder site.

Figure 87 shows the main directions recorded by the traditional weather stations in the urban area of Paris.

Figure 88 shows the NETATMO connected anemometers accessible on this collaborative platform. The orientation of the arrows shows the wind direction at each of these stations at a time  $t$ . The omnidirectional orientation shows the impact of the complexity of turbulence in urban areas.

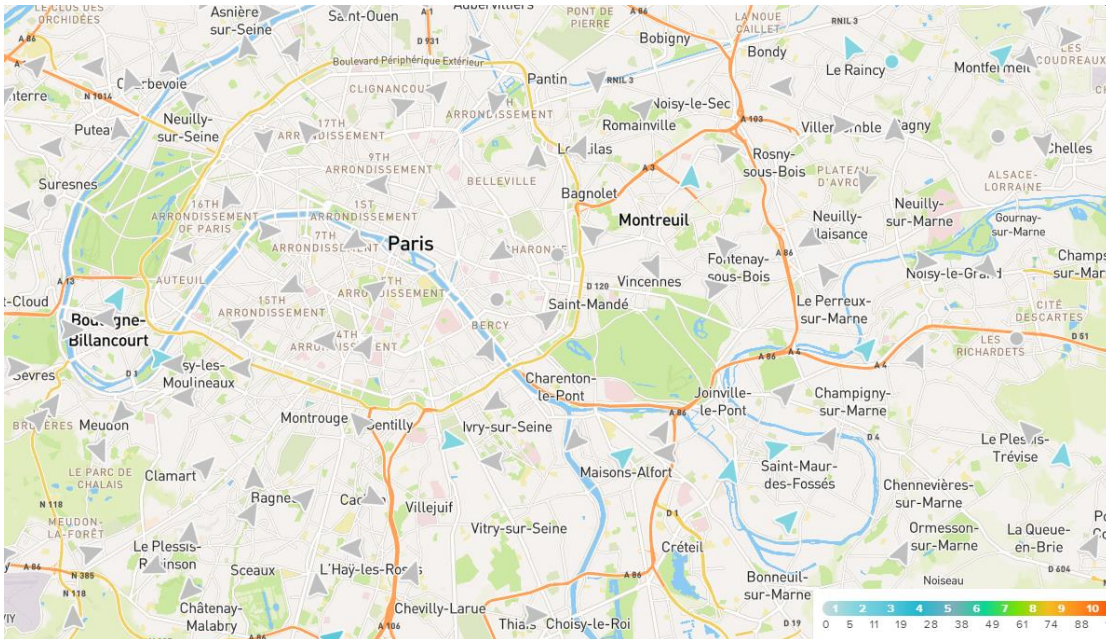


Figure 89 Geolocation of connected anemometers on 1/12/2017 in Paris on the Netatmo website

#### 2.2.4. Presentation of the study sites

As part of this research, since 2016, we have asked the owners of our current projects to install wind measurement elements on buildings under construction or at the end of their construction.

We received many refusals, often with little justification, but 7 buildings were able to have their impact on local winds monitored over a longer or shorter period. The wind data of a building, without being public to date, have a confidentiality character, because they are an indicator of the environmental impact of a building in its context.

We have therefore selected the following sites with the installation of measurement devices in several places in these buildings (see figure 88):

- A house in Arcueil ( 94 )
- A building in a suburb ( 75011 )
- An island building, the Paris Val-de-Seine School of Architecture

The readings taken on these buildings were compared to the reference weather stations in Paris, namely :

- Charles de Gaulle airport ( CDG )
- Orly airport
- The Montsouris Park weather station
- The Zamansky tower of the University of Paris Jussieu



Figure 90. Location of the wind recording weather stations installed by Serero that are compared daily, 2016-2020

The data will be used to calibrate the numerical simulations for each of the sites that are presented in Part 4, ( Chapter 4.1.1 to 4.6.8).

for wind speed readings from February 2017 to December 2018, the information can be downloaded at this link:

<https://drive.google.com/file/d/1aZmkhh1U-4wqAllfeilwOmJd4BaXo7p/view>

#### 2.2.5. Installation method of connected anemometers on an example of Haussmannian apartment building 136 avenue Parmentier, Paris XI<sup>ème</sup>

The first weather station was installed at 136 avenue Parmentier, Paris 11<sup>ème</sup>, on the roof of the building on January 24th 2016. Since that date, the daily wind speed has been recorded every 5 minutes and we have a monthly record of this information.

In addition to the Serero wind station, this research collects 4 other data sources in Paris from [www.windfinder.com](http://www.windfinder.com) and [www.infoclimat.fr](http://www.infoclimat.fr); including the Paris CDG airport weather station, Paris Orly airport, Parc Montsouris and on top of the Zamansky tower on the Jussieu Campus, Paris 5th. All these surveys and observations, give a solid experimental analysis on strategic points of the city of Paris.



Figure 91. Installation of the anemometer on the roof of the building 136 avenue Parmentier, Paris 11ème. A TV antenna was used to support the device.

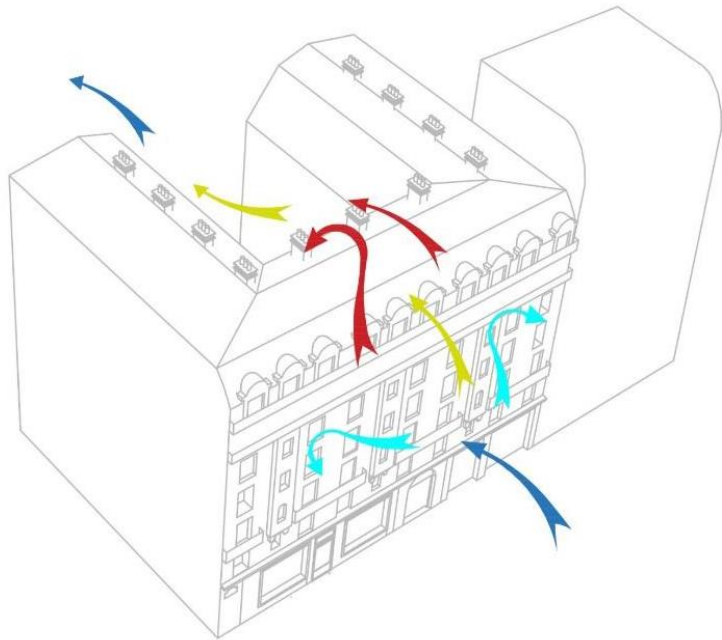
The measuring device was installed 1 meter back from the street façade at precisely 2 m above the roof by fixing a galvanized steel type in extension of an existing TV antenna. This installation is based on the numerical wind simulation presented in chapter 4.5 in figure 197.



Figure 92. Location of the wind survey station - 136 avenue Parmentier - Paris, D. Serero



Figure 93. 3D model of the Parmentier building showing schematic wind flows and the position of the measuring



anemometer, 3D model D. Serero

Here you will find a summary table of the data from these 4 wind survey stations compared as shown for the month of **December 2018**.

LOCATION	136. AVE PARAMENTIER				CDG AIRPORT			
	00:00	06:00	12:00	18:00	00:00	06:00	12:00	18:00
DATE								
01.09.2017	1,1/S	1,4/SSW	3,1/S	5/SW	1/NW	1/WNW	2	5/NE
02.09.2017	2,5/W	2,2/NW	3,6/SW	5/NE	2/NW	2/NW	3/NW	5/N
03.09.2017	1,1/ENE	1,4/SSE	3,6/S	3,3/S	1	2/ESE	3/S	4/SSE
04.09.2017	1,1/SSW	4,7/S	4,7/S	4,7/SW	1/N	2/S	6/SSW	2/W
05.09.2017	3,6/SW	2,5/S	5,3/SSW	5,8/S	3/SW	4/S	6/SW	5/SW
06.09.2017	5,6/SW	5,3/SW	5,3/SW	6,9/SW	6/W	5/W	7/W	7/W
07.09.2017	4,4/SSW	3,6/SW	3,9/SSW	6,9/SSW	2/W	3/S	5/WSSW	5/W
08.09.2017	3,6/S	5,3/S	6,9/S	5,8/S	5/WSSW	6/SSW	8/SW	6/SW
09.09.2017	3,6/S	5,3/SW	5,3/SW	6/SW	5/SSW	5/WSSW	7/WSSW	5/WNW
10.09.2017	ND	2,2/SSW	2,8/SW	6,9/S	3/SW	4/WSSW	5/SW	9/SW
11.09.2017	10,8/S	5,3/SW	8,1/SW	8,9/SW	9/SW	7/WSSW	10/WSSW	10/WSSW

Figure 94. Comparison of wind speed in the Paris area measured at national weather stations (Roissy, Orly), and anemometers connected at 22 m above ground level on the roof of a "Faubourg" type building . (in m/s, compared over 4 daily time slots).

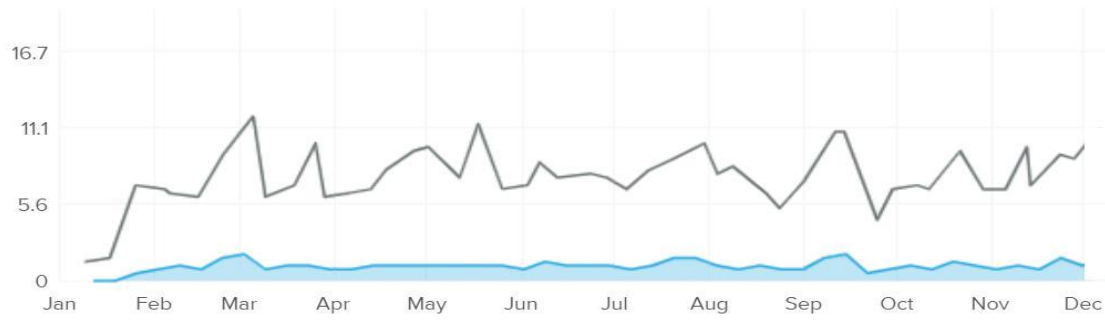


Figure 95. Parmentier weather station reading (monthly average winds in 2018) at 22m height from the street in a dense urban "Faubourg" environment.

### 2.2.6. Anemometer readings of a house in the Paris region (Arcueil 94)

The second weather station was installed at 39 rue de Chinon in Arcueil, on the roof of a house at 9 meters high in a clear residential area, P30 March 2017. Since that date, daily wind speed has been recorded every 5 minutes and we have a monthly record of this information. Figures 95-97 show the background of this installation.

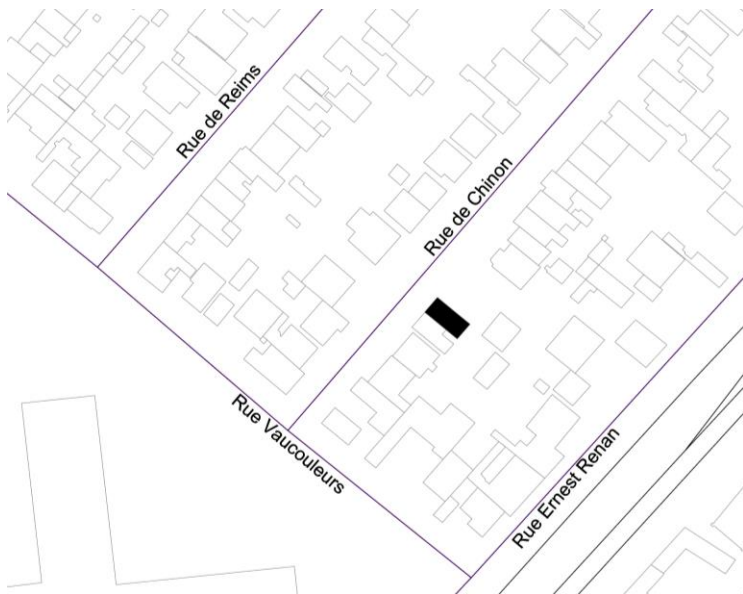


Figure 96. Location plan of the house in the Maison des examens neighborhood in Arcueil, D. Serero

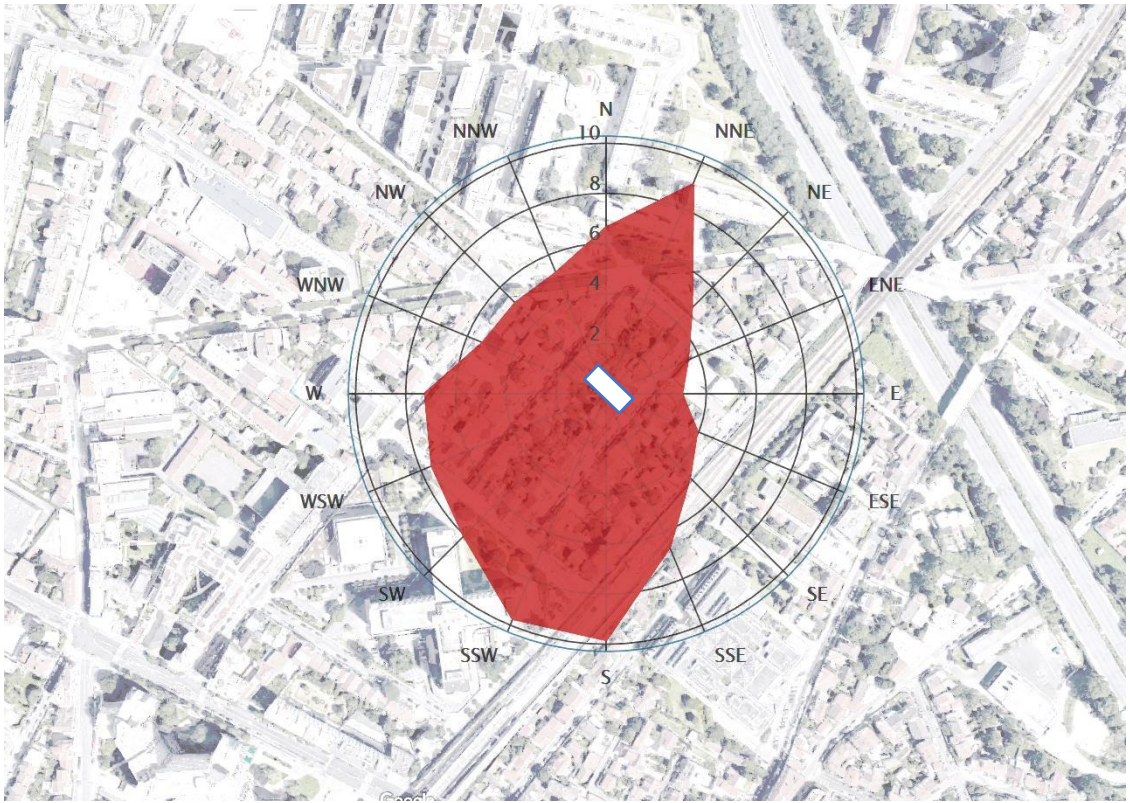


Figure 97. Wind direction distribution in annual percentage, site 39 rue de Chinon, Arcueil 94110



Figure 98. View of the new anemometer at a height of 8 meters above the ground of the Roméra house in Arcueil

LOCATION	RUE DE CHINON, ARCUEIL				CDG AIRPORT			
	00:00	06:00	12:00	18:00	00:00	06:00	12:00	18:00
DATE								
01.05.2018	3,9/SSE	4,7/S	6,7/SW	3,3/SSW	5/W	2/SW	3/S	5/SSE
02.05.2018	3,6/S	1,7/S	1,9/NNE	4,7/NNE	6/W	5/WSW	4/WSW	7/W
03.05.2018	3,6/NW	2,5/NW	1,7/NE	3,1/NE	3/SW	3/SW	5/SSW	4/W
04.05.2018	1,7/NE	2,2/NNE	2,8/NE	4,7/NNE	3/S	2/ESE	3/ENE	5/E
05.05.2018	2,5/NNE	3,1/NE	3,6/NNE	3,9/ENE	3/ENE	2/E	4/ESE	2/W
06.05.2018	3,9/NE	4,2/NE	1,4/ENE	2,2/SSW	1/WSW	5/WNW	5/NNW	5/NW
07.05.2018	3,3/SW	4,7/WNW	4,2/NW	3,9/W	1/N	2/WNW	2/N	4/NNE
08.05.2018	3,1/NW	2,2/NW	5/N	4,7/NNW	3/N	2/NE	5/ENE	6/ENE
09.05.2018	3,1/N	4,4/NE	5/NE	4,4/NE	4/NE	3/ENE	9/ESE	6/ESE
10.05.2018	3,1/ENE	2,2/NNE	4,2/NE	3,6/ENE	5/ESE	3/E	2/SSW	3/NNW
11.05.2018	1,4/ENE	1,7/S	3,3/SSW	3,9/S	5/NNE	3/NNE	3/ENE	4/NE
12.05.2018	1,7/SSE	2,5/S	4,4/S	4,2/S	4/S	5/S	5/SSW	3/NE
13.05.2018	3,1/S	3,3/SSE	4,2/SW	4,7/S	4/SSW	4/S	6/WSW	3/WSW
14.05.2018	2,8/SSE	ND	5,3/S	6,4/SW	3/SSW	3/SSW	4/SW	5/WNW

Figure 99: Extract from a sheet of wind speed data in the Paris region measured at national weather stations (Roissy, Orly), and anemometers connected at 8 m above ground level on the roof of a single-family building, D. Serero (in m/s, compared over 4 daily time slots).

The comparison of wind measurements at the two airports CDG and Orly show a large variation in wind direction at the same time in urban areas. The density of the urban environment generates disturbances in the airflow and this can explain the increases in speed and changes in direction with respect to the prevailing winds.



The data measured on these different sites show a great variation of speed and direction in urban areas. In the Paris area, the main wind direction is SSW and NNE, which gives us a first information for the implementation of energy capture devices on the roofs and facades of buildings. We present here an extract of the survey on the ENSAPVS site in comparison with the CDG and Orly weather stations.

LOCATION	ENSAPVS				CDG AIRPORT			
HOURLY	00:00	06:00	12:00	18:00	00:00	06:00	12:00	18:00
DATE								
30.01.2018	4.1/SSW	5.9/S	4.2/SSW	4.8/SSW	5/S	6/SSW	1/N	2/SSW
31.01.2018	4.5/SSE	2.8/SSW	3.4/WSW	3.1/ENE	1/N	1/NNE	2/NNW	1/N
01.02.2018	3.1/E	4.5/SSE	5.3/S	ND	1/N	3/SSE	4/S	6/SSW
02.02.2018	2/N	1.9/SSW	4/S	1.9/S	1/N	1/N	5/SSE	1/N
03.02.2018	4.9/S	3.2/S	4/SE	7/SE	6/SW	6/SW	7/S	9/SSE
04.02.2018	4.8/S	4.5/ENE	3.4/WNW	ND	8/SSW	5/SE	1/N	5/WSW
05.02.2018	4.7/WNW	ND	5.5/S	4.5/S	1/SE	1/N	1/NNE	1/ESE
06.02.2018	6.1/N	3.1/NW	3.1/NNE	1.9/WSW	8/NNW	3/NW	4/NNW	0
07.02.2018	ND	3.9/E	2.2/S	4.3/WNW	4/S	4/S	1/N	1/N
08.02.2018	ND	4.2/NW	ND	5.5/NW	2/W	3/WNW	1/N	1/NNE
09.02.2018	4.8/NE	3.6/NE	4.2/NE	1.9/ENE	1/N	1/N	1/NNE	1/N
10.02.2018	2.5/NE	3.1/NNE	5.3/N	4.7/NE	3/NE	4/NE	1/N	3/N
11.02.2018	2.5/NNE	2.8/NW	2.2/NNE	2.2/NNE	1/NNE	1/N	1/N	1/N
12.02.2018	1.9/NE	4.2/NE	3.6/ENE	1.9/NE	1/NNE	1/NNE	1/N	1/N
13.02.2018	4.2/ENE	3.6/ENE	3.6/ENE	1.9/ENE	5/E	6/E	8/E	1/N

Figure 103. Comparison of wind speed in the Paris area measured at national weather stations (Roissy, Orly), and anemometers connected 30 m above ground on the roof of a building . Each reading indicates wind speed and wind direction (in m/s, compared over 4 daily time slots).

## 2.3. COMPARATIVE ANALYSIS OF WIND ENERGY SYSTEMS

### 2.3.1. Type of integration of the devices to the buildings and facades

Now that we have identified the wind speed, and the typologies of buildings adapted for the integration of these devices, our research aims at identifying where and how to place these devices in order to maximize the wind speed on micro-turbines. As specified by the wind surveys: the average wind speed in Paris is 5 m/s, with days at more than 20m/s and days at less than 1m/s. But what we are looking for is an implementation, and an implantation of the wind turbine which allows to limit the impact of turbulences of the urban winds and to smooth the constancy of the velocity of the wind between 5 and 12 m/s in order to optimize its maximum capacity of energy production.

The table in figure 103 shows some of the micro-wind turbines currently available on the market, as well as their dimensions and maximum power output.

This table shows that the typologies of devices are very varied and potentially adapted to specific installations in a building or a place. We could not, within the framework of this research, study all these typologies in simulations, but they show their wide variety.

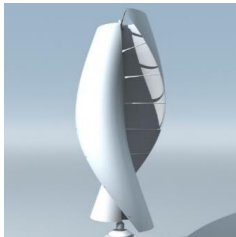
	MICRO TYPE	DROIT	HELICOIDAL	CLUSTER / AGGREGATION
DARRIEUS QR5				
A GODET				
WINDSPIRE				
SAVONNIUS				
WIND LENS				

Figure 104. Comparison chart of the wide variety of wind devices that exist to date.



### 2.3.2. Profiling of the wind speed increase device around a building

By analyzing the wind distribution maps around the building, we will see in Part 4 (chapter 4.2) that red-orange "hotspots" appear on points along the edges of the building volume. This locates "hot spots" in space where the air speed is faster than in the area around the building. The implementation of wind devices in this area would allow an increase in wind speed of 2 to 2.5 times, or according to the Betz limit, a power gain of more than 8 times the power of the air without building.

One way to improve this increase in wind speed would be to "compress" the air stream in the vicinity of the building and therefore to propose blades, holes, structure allowing punctually to add an effect of amplification of the air stream (Figures 104, 105 and 106).

According to the volume of the building, its historical typology, our research led us to propose by successive stages of type "test and learn" of the devices of increase of the air speed. We show conceptual and schematic views of these devices in a typical Parisian building. We propose here a provocative "vision" of an air velocity augmentation device that could be installed on the roof of an old building. This proposal does not constitute an architectural project, but simply a working hypothesis.

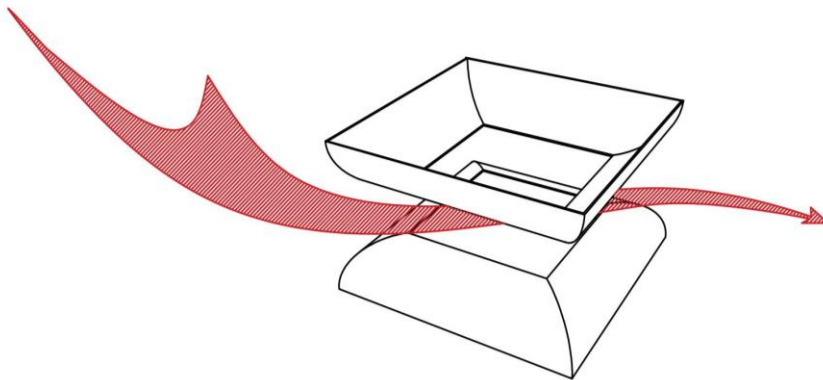
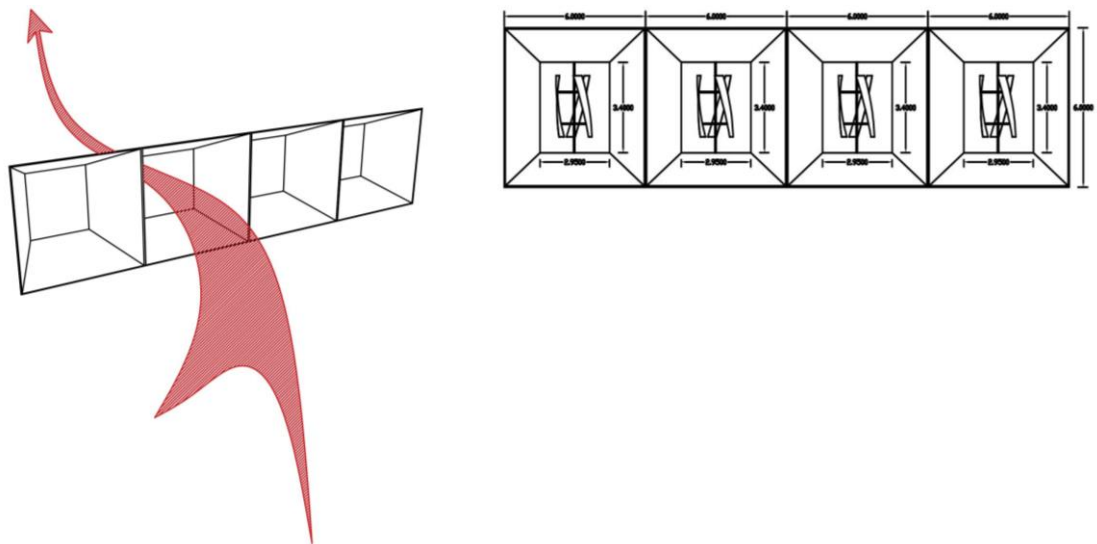


Figure 105. Integration of wind devices in roof wings (roof turning) to accelerate the airflow.



Figure 106. Preliminary vision for an old Parisian building, renovated with different devices studied



107. Integration of wind devices in these funnel type cells to accelerate the airflow.

This type of device makes it possible to consider local energy production for both the housing and the offices of this building. These devices are included in the technical volume authorized by the city of Paris for renewable energy production or for urban agricultural greenhouses.

### 2.3.3. Typology of vertical axis micro-turbines implemented in research

Within the framework of this initial study, we worked on 4 types of wind turbines with vertical or horizontal axis (See figure 107 to 110). The development of these wind turbines is carried out in part 4 and 54, but the size of these devices, their aesthetics, and their mode of fixation was studied in order to project a first vision of capture devices integrated into the building.

These micro-turbines (small volumes) limit especially the turbulences associated with the passage of the air in the turbine, reduce the noise of friction of a blade and offer a lower speed of engagement.

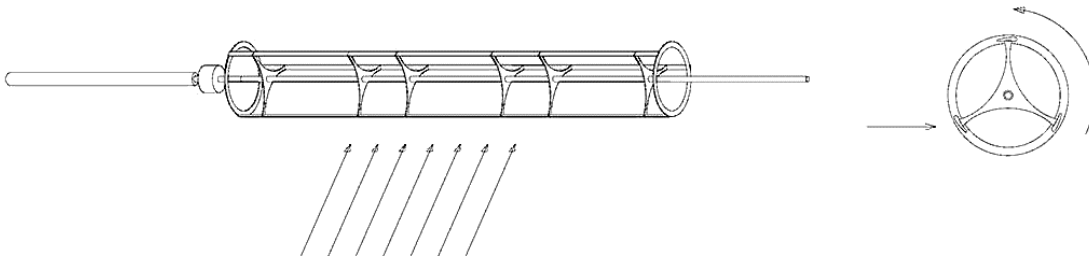


Figure 108. Electricity generation by "wind arrow" with horizontal axis (Windspire)  $L= 3m$ ,  $0.6m$  diameter , drawings D. Serero

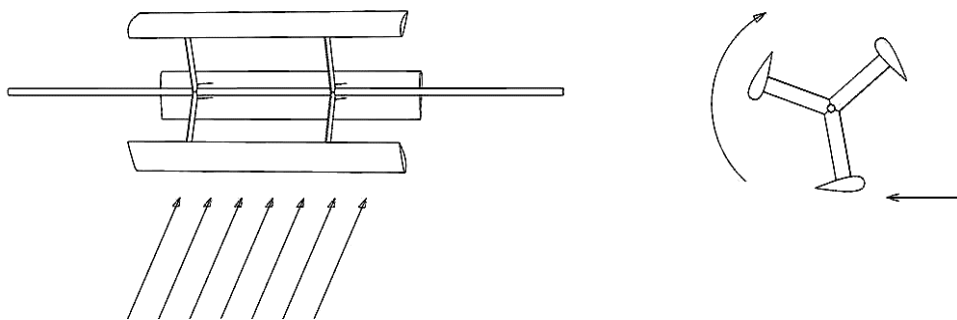


Figure 109. Electricity generation by "wind arrow" with horizontal axis (Windspire)  $L= 2m$ ,  $0.6m$  diameter , drawings D. Serero

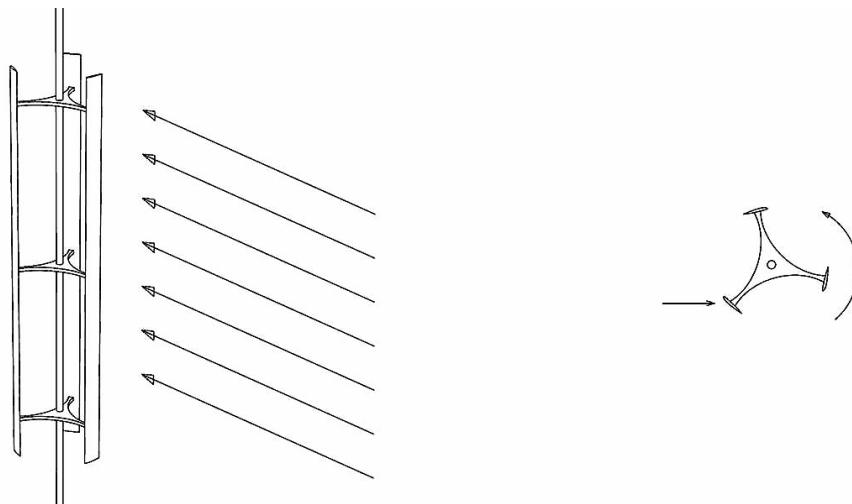


Figure 110. Electricity generation by "wind arrow" with vertical axis ( Windspire)  $H= 3m$ ,  $0.6m$  diameter , drawings D. Serero

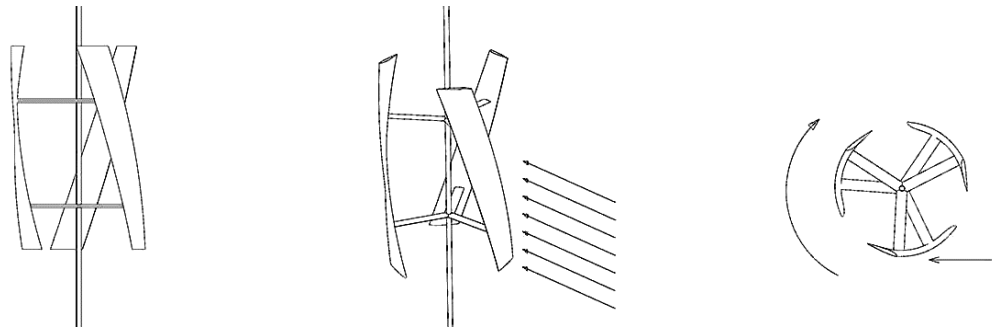


Figure 111. Micro-wind turbine electricity generation with vertical axis  $H=1m$ ,  $0.7m$  diameter , drawings D. Serero

The collection of energy on architectural surfaces requires limiting the visual impact of these devices on the architecture. It seemed important to us to work on devices that are not visible or largely integrated into the architecture of the building. For these reasons, many of the devices that we will propose use rather the edge effects and the distribution of the devices on linear surfaces of the building rather than on points punctually placed in the center of the building.

These devices are concentrated and dressed with an amplifier/stabilizer that we will call "foil" as defined in chapter 5.1.1. The effect of air intake on long building surfaces allows to increase the performance of the systems and to propose a "series" connection of the energy collection elements. It seems to us that the interest of this research is to prove that wind turbines integrated into an architecture can be a vector of interesting performance and elegantly integrated into a building facade or roof.

Could we develop low-profile wind systems here that are close to architecture? Devices without apparent movement, or whose movement is not visible? Or devices that participate in the architectural writing of the building. We plan to give the name of "aerofoil" to the wind energy capture device.

Vertical axis turbine devices reveal several interests in our study.

1. They easily allow energy capture on turbulent winds or winds changing direction. The vertical axis adapts to any change in wind, no matter how turbulent, and allows for limited movement on one axis of the turbine.
2. On the other hand, the vertical axis turbines allow a capture on a lower profile and closer to the building
3. Thirdly the turbines installed in "cluster" limit the disturbances of the air stream behind it and allow to combine elements of energy capture in series by bringing them closer to each other (3 to 5 meters). The study of the University of Stanford shows that a cluster of wind turbines type Spire, or Darrieus, shows that the energy extracted from vertical axis wind turbines can be multiplied by assemblies of 10 to 25 elements spaced every 2 meters without losing more than 10% of the wind energy.

## 2.4. CONCLUSION

Wind speed measurements on several buildings with anemometers show that buildings increase the wind speed at their periphery and in the urban environment. They are generators by their mere presence of a real wind energy source.

The installation of micro-turbines on the points of increase of the air speed in roof or in front of the buildings constitute a clear improvement of the performances of the wind turbines.

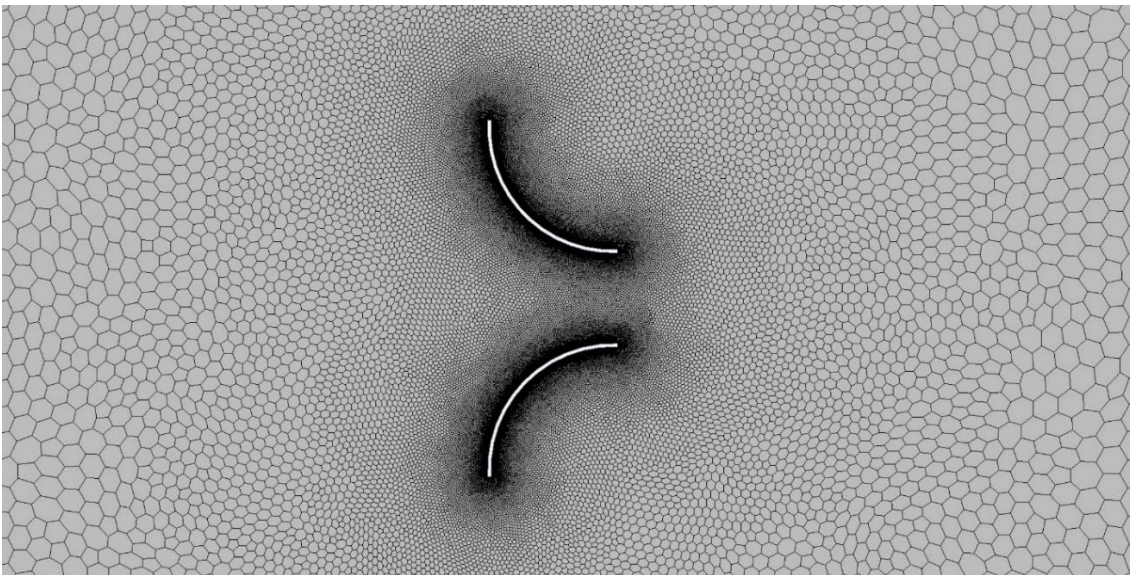
The objective of the rest of this research is to analyze the historical and modern architectural typologies of the building and to study in each case, the location and type of wind device to be installed. The numerical wind tunnel simulation, which will be presented in part 4, shows that micro-turbine devices help to stabilize the compressed air flow near their location.

We will see that by calculating the energy generated by optimizing the implementation of these devices on the roof, we could reduce the electricity consumption of a family home by 20 to 25%. Beyond the constraints related to the regulation on the maximum height of the devices, the wind conditions can be the object of numerical simulations allowing to improve the orientation, the height and the choice of the device to produce energy in an efficient way from an available and ubiquitous energy source.



# PART 3

## MODELING AND PERFORMANCE EVALUATION OF DEVICES



Contents:

- Presentation of the physical principles of fluid mechanics
- Modeling method and definition of initial conditions
- Calibration of numerical simulation results on an experimental physical wind tunnel
- Numerical simulation of a building roof device with 3 types of initial conditions



INTRODUCTION.....	123
1. PRINCIPLES OF AIR MOVEMENT IN URBAN AREAS.....	123
1. Wind and buildings, location of maximum wind speed .....	123
• Wind characteristics in the urban canopy layer:.....	124
• Wind characteristics in open areas (rivers, seaside, ...) .....	124
• Urban Turbulence Assessment.....	124
• Calculation of the wind power density.....	125
1. PHYSICAL PRINCIPLES OF FLUID MECHANICS .....	126
1.1. Equations of fluid mechanics.....	126
1.2. Continuity equation.....	126
1.3. Steady state or unsteady state.....	127
• Mesh convergence .....	128
1.4. The similarity factor for the downscaled study: the Reynolds number .....	128
1.5. Classification of flows .....	130
1.6. Computational fluid dynamics (CFD).....	132
1.7. Methodology of work in numerical fluid mechanics.....	133
1.8. Choice of the numerical tool for the numerical simulation of airflow	133
1.9. Notion of mesh for numerical study.....	134
• The volume.....	134
• Deformation angle .....	135
• Polyhedral mesh.....	135
• Hexahedral mesh (Trimmer) .....	135
2. METHOD OF MODELING AND DEFINITION OF INITIAL CONDITIONS OF THE SIMULATION .....	135
2.1. Definition and modeling of geometry .....	136
• Geometry .....	137
• Choice of mesh size.....	137
2.2. Definition of the calculation parameters .....	139
• Gradients.....	140
• Turbulent.....	140
• K-Epsilon Turbulence & Realizable K-Epsilon Two Layer ..	140
• Reynolds-Averaged Navier Stokes .....	140
• Two-Layer All y+ Wall Treatment.....	140
• Implicit Unsteady .....	141
• Two dimensional .....	141

•	Choice of boundary and initial conditions.....	141
-	Boundary conditions .....	141
2.3.	Initial Conditions .....	141
•	Properties of the solver .....	141
•	Air speed profile .....	141
2.4.	Results and analysis .....	142
•	Definition of boundary conditions.....	143
•	Launching the calculations .....	143
3.	NUMERICAL SIMULATION OF A BUILDING ROOFING SYSTEM WITH 3 TYPES OF INITIAL CONDITIONS.....	144
3.1.	Definitions of the initial conditions of the simulation .....	144
•	The geometry.....	145
•	Making the mesh .....	145
3.2.	Simulation N°1 of a wind amplification device .....	147
•	Choice of physical conditions .....	148
3.3.	Simulation N°2 of a wind amplification device .....	149
3.4.	Simulation N°3 of a wind amplification device .....	152
4.	Conclusion .....	154

### 3. INTRODUCTION

In this section, we present a synthesis of the physics of fluid mechanics used in this research and how they are used to understand the aerodynamic phenomena in urban sites. For the airflow simulation on buildings, we will briefly present the simulation tool and its parameterizations, explain the relationship and calibration (specified in chapter 4.0) of these tools with a physical wind tunnel and the on-site wind surveys.

The study of 3 cases will allow to show the method of experimental analysis, and the results on simple profiles of roofs.

#### 1. PRINCIPLES OF AIR MOVEMENT IN URBAN AREAS

##### 1. Wind and buildings, location of maximum wind speed

Wind is the movement of air relative to the Earth created by the difference in atmospheric pressure and caused by the temperature difference due to the intensity of solar radiation reaching the Earth's surface<sup>99</sup>. The main characteristics of wind, such as surface resistance, turbulence scales and intensity, wind speed, and wind profile in urban areas are strongly affected (Figure 111) by the roughness properties of urban areas<sup>100</sup>.

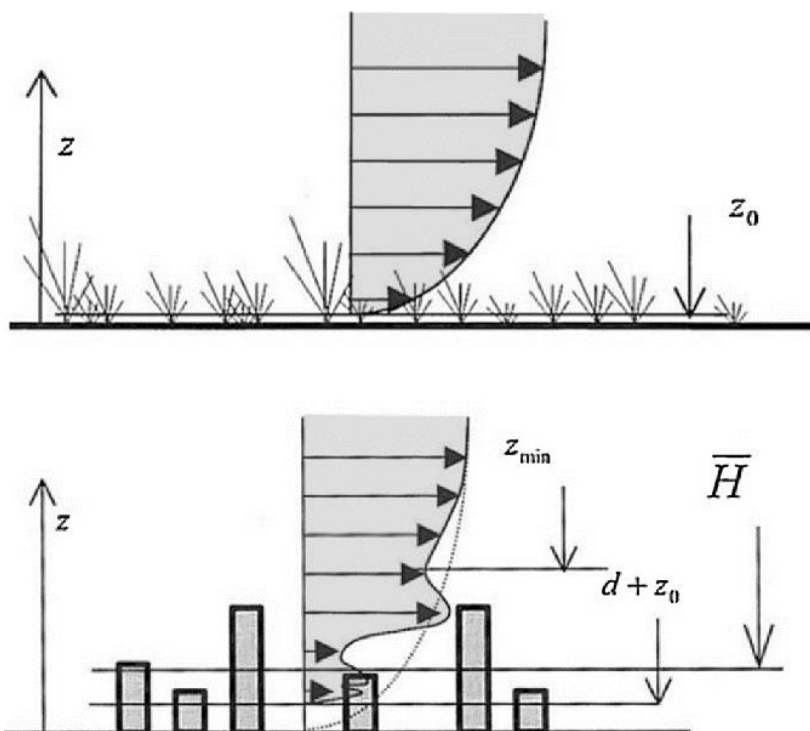


Figure 112. Changes in urban wind flow related to architectural volumes

<sup>99</sup> Ibrahim AL-BAHADLY, "Building a wind turbine for rural home," Energy for sustainable development 13.3, 2009.

<sup>100</sup> NG EDWARD, "Improving the wind environment in high-density cities by understanding urban morphology and surface roughness: a study in Hong Kong," 2011.

The roughness of the surface, which results in an area of high turbulence, as shown in Figures 112 and 113, significantly influences the wind speed and direction, hence its extractable power<sup>101</sup>.

When air strikes buildings and other obstacles in the urban environment, a complex air swirl or wave pattern is formed, as shown in Figure 114. The combination of shape, height, and distance from buildings affects the direction and intensity of the wind and can affect the amount of energy produced in the urban environment<sup>102</sup>.

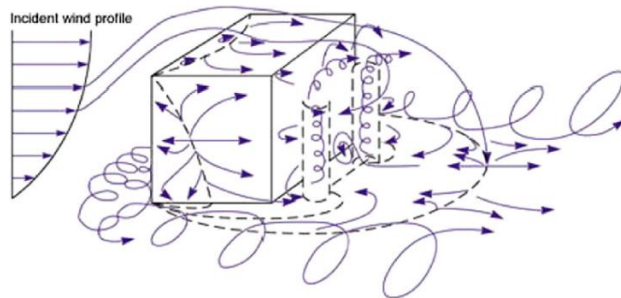


Figure 113. Différentes typologies de turbulence dans l'écoulement du vent

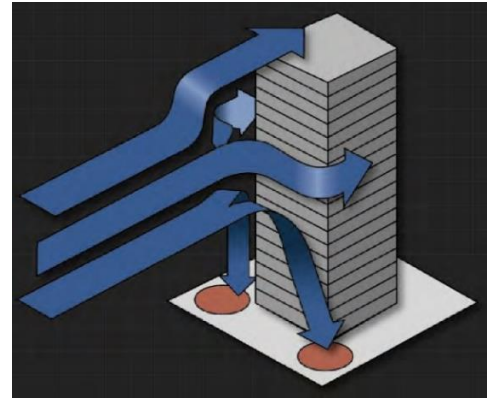


Figure 114. Effets du vent sur des bâtiments de grande hauteur

- *Wind characteristics in the urban canopy layer:*

In the urban canopy layer, flow is almost entirely governed by the geometry of the street or canyons (length ratio and length/depth ratio) and by the height distribution of buildings, especially in urban areas where buildings are closely spaced and grazing flow occurs.<sup>103</sup>

- *Wind characteristics in open areas (rivers, seaside, ...)*

In urban areas, wind speeds are generally highest when the wind is parallel to the river. However, lower relative wind speeds can be found when the approach airflow is perpendicular to the river due to the change in aerodynamic drag. The air crossing the river generally becomes less turbulent after passing through the building.<sup>104</sup>

- *Urban Turbulence Assessment*

Since wind profiles in urban areas tend to be more turbulent due to the presence of buildings, trees along streets, and other obstacles<sup>105</sup>, computational wind technology (CWE) has recently been developed to evaluate the interaction between wind and buildings. A number of different

<sup>101</sup> RICCIAR DELLI F, POLIMENO S. JWIND ENG IND AERODYN, "Some characteristics of the wind flow in the lower urban boundary layer," 2006.

<sup>102</sup> ROY DENOON, BRAD COCHRAN, DAVID BANKS, GRAEME WOOD, *Harvesting Wind Power from Tall Buildings*, 2008.

<sup>103</sup> ABD RAZAK, HAGISHIMA, and TANIMOTO, "Analysis of airflow over building arrays for assessment of urban wind environment," *Building and Environment*, 2013.

<sup>104</sup> Curtis R WOOD, "Wind observations above an urban river using a new lidar technique, scintillometry and anemometry," *The Science of the total environment*, 2013.

<sup>105</sup> ELIASSON and OFFERLE, "Wind fields and turbulence statistics in an urban street canyon," *Atmospheric Environment*, 2006, vol. 40, n°1, pp. 1-16-

techniques have been used in CFD simulations with various turbulence models. The choice is usually made based on the details of the flow to be obtained and the available computational resources<sup>106</sup>. CFD modeling is used in our research to determine building effects at locations where a turbine could be incorporated.

- *Calculation of the wind power density*

The energy produced by a building integrated device (BID) is important information for research development. The extractable power from the wind is estimated using the following equation:

$$PUISSANCE = \frac{1}{2} \times \rho \times A \times v^3 \times cp$$

Where the variables are defined by :

$$\rho(\text{densité de l'air}) = 1.23 \left[ \frac{kg}{m^3} \right]$$

$$A = \pi \times r^2 = \frac{1}{4} \pi \times d^2 \text{ (operating area of the wind turbine)}$$

**D** [m<sup>2</sup>] = Diameter of the wind turbine

**V** = Air speed

**cp<sub>max</sub>** = 0.59 (a coefficient of performance of the wind without unit / Betz limit)

We generally use the Betz limit to evaluate the power extractable by the wind from a specific set of conditions. For a horizontal axis wind turbine, it is defined by the following equation:

$$PUISSANCE = 0.12 \times d^2 \times v^3$$

Since the device for producing energy from wind is identical (constant turbine diameter), the extractable power from the wind is only determined by the input wind speed.

The study in fluid dynamics simulation of a building section shows that its location and profile have an immediate impact on the wind speed around the building. An animation showing the evolution of the wind speed over time shows that the hot spots where the wind speed can be 2 to 3 times higher than the air inlet speed fluctuate towards specific areas around the edge and the skin of the building.

How can we, as architects, take advantage of this situation to propose specific harvesting devices and uses for the building?

Figure 114 is a cross-sectional simulation of a 3-story building on pilings that shows the multiplier effect of a building on extractable wind energy production using the Betz limit calculation.

---

<sup>106</sup> UCHIDA and OHYA, "Micro-siting technique for wind turbine generators by using large-eddy simulation," *Wind Engineering and Industrial Aerodynamics*, 2008, pp. 2121-2138-.

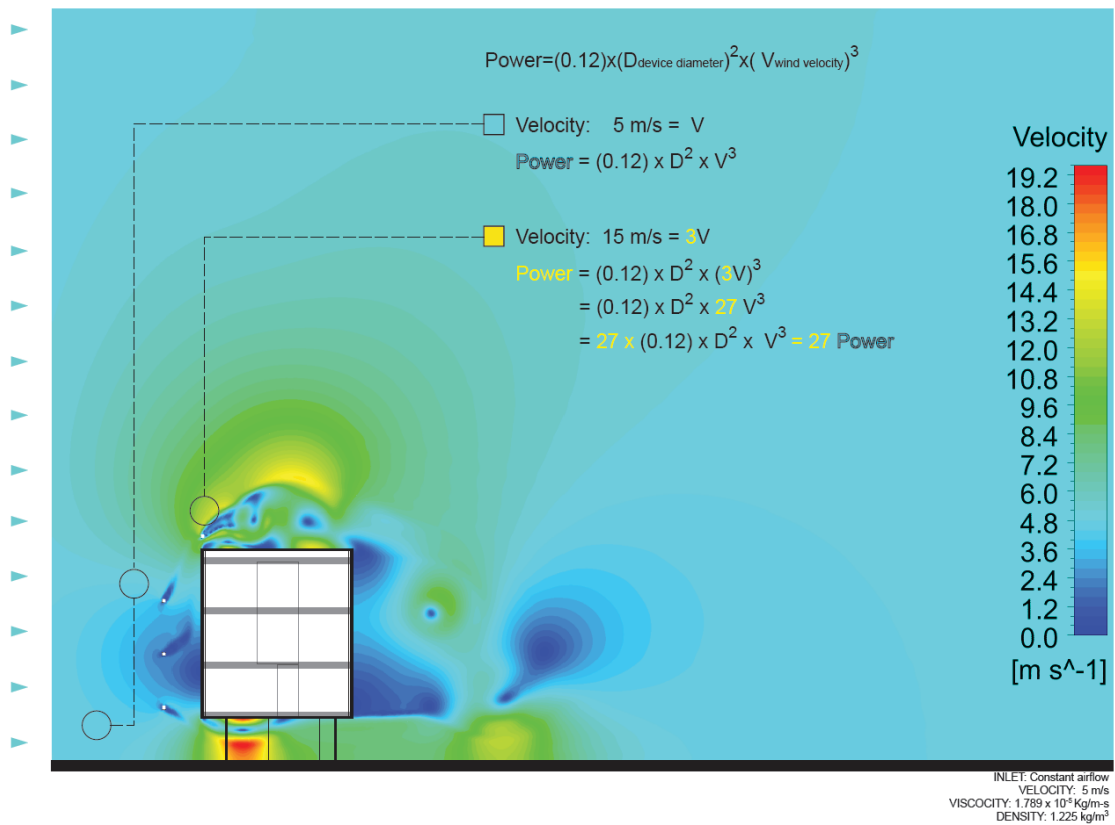


Figure 115. Dynamic wind aerodynamic simulation on a cross-section of a building on piles. Simulation by D. Serero

## 1. PHYSICAL PRINCIPLES OF FLUID MECHANICS

### 1.1. Equations of fluid mechanics

Fluid mechanics is a field of physics devoted to the study of the behavior of fluids (liquids, gases and plasmas) and the associated internal forces. It is a branch of continuum mechanics that models matter using particles that are small enough for mathematical analysis but large enough relative to molecules to be described by continuous functions.

It is divided into two parts: fluid statics, which is the study of fluids at rest, and fluid dynamics, which is the study of fluids in motion.

### 1.2. Continuity equation

In fluid mechanics, the principle of conservation of mass can be described by the **continuity equation** in several different forms: local conservative (normal time derivative), local non-conservative (the time derivative follows the particle in its motion), or integral. Depending on the problem, one or the other of these equations can be used, all being equivalent.

We note here:

$\rho = \rho(\vec{x}, t)$ : the density of the fluid at the point marked by the vector  $\vec{x}$  at time  $t$

$\vec{V} = \vec{V}(\vec{x}, t)$ : the velocity of a fluid particle at the point marked by the vector  $\vec{x}$  at time  $t$

Taking  $\phi = 1$ , we find

$$\frac{\partial \rho}{\partial t} + \vec{\nabla} \cdot (\rho \vec{V}) = 0$$

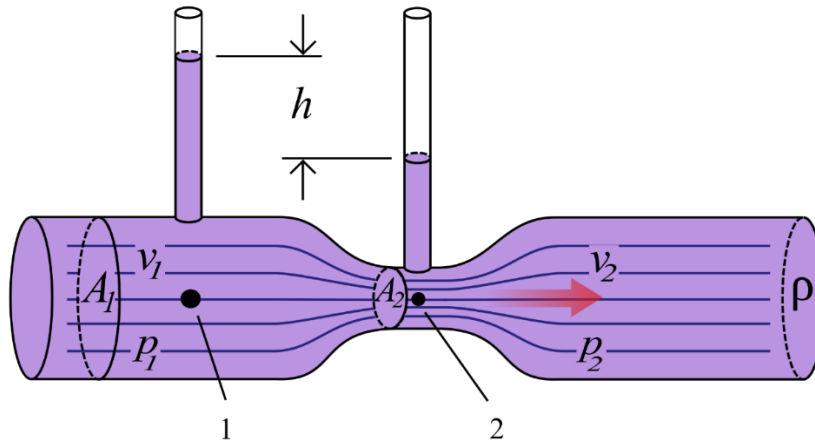


Figure 116. The Venturi effect

The Venturi effect illustrates this principle of conservation of mass (Figure 115). A certain amount of material passes through an orifice in a unit of time (e.g. in 1 s). If the orifice is reduced in size and the amount of material flowing through it is both constant in time and space (flow rate), then the velocity of passage through the orifice increases to allow the entire amount of material to flow through it in the same unit of time.

This effect is encountered in many situations in the territory: increase of the wind speed at the passage of a mountain pass, in an alley. In all these situations, the air fluid is not compressible, and evolves in forced circulation in an inextensible pipe. They are therefore subject to the Venturi effect.

### 1.3. Steady state or unsteady state

The objective is to understand the principles and major trend.

A steady state is a situation for which the transient term is zero; therefore, the first term in the above equations is neglected, so :

$$\frac{\partial y}{\partial x} \frac{\partial \rho \phi}{\partial t} = 0$$

This is a steady state, an operating state "long" after the system has been started (valve opening, turbine starting); the result is independent of time, there is no time discretization. This situation greatly simplifies the calculations.

However, this does not allow to take into account fluctuations of the inlet or outlet conditions, or the description of a filling. In these cases, it is necessary to make a transient calculation ("unsteady"), i.e. at several successive times.

If the time step is too large, numerical errors are introduced and propagated. Moreover, it can make the convergence at each step complicated. But the smaller the time step,

the longer and more resource-intensive the calculation. In order to find a compromise, we generally try to ensure that a fluid particle travels through less than one mesh between each calculation step, i.e. to have a **number of Courant**, called in the CFL environment (Courant, Friedrichs and Lewy condition):

$$\text{nombredeCourant} = \frac{\text{vélodité} \times \text{pasdetemps}}{\text{tailled'éléments}}$$

However, we have carried out some of these calculations in stationary mode because it is a faster mode of calculation at the beginning of the research. P

Once the assumptions were clarified, we subsequently performed several calculations in unsteady mode closer to a non-laminar airflow.

The stationary regime can be considered as a time average of the unsteady flow. But this calculation is very long on the hardware available for this research (4 core processors) and this was not possible in the means granted to this thesis.

However, this type of calculation has an impact on the calculation of the drag force at the distance of the building. However, this area is not our main object of study, because we seek rather to evaluate the increases in speed at the "edges" of the building.

We are interested in areas of air separation or compression in the immediate vicinity of the building, where the stationary model is close to the unsteady aerodynamic behavior.

- *Mesh convergence*

In finite element simulations, a denser mesh provides more accurate results.

On the other hand, the larger the mesh, the longer the computation time. The choice of the mesh allows to have a good compromise between the computation time and a satisfactory accuracy, this through a study of mesh convergence.

Here are the main steps we are talking about here in order to propose a manual mesh convergence:

- Create a mesh using a reasonable number of elements, then analyze the model.
- Recreate the mesh by increasing the mesh density, recalculate it, compare the results with the first calculation.
- Continue to increase the mesh density, reanalyze the model; then verify that the results converge satisfactorily.

This type of mesh convergence study allows us to have an accurate solution, with a sufficiently dense mesh, without requiring too much computing resources.

#### 1.4. The similarity factor for the downscaled study: the Reynolds number<sup>107</sup>

In 1883, the experiments carried out by the engineer and physicist Osborne Reynolds made it possible to show the existence of two flow regimes: the laminar regime and the turbulent regime. In his experiments, O. Reynolds injected dye upstream of a transparent straight cylindrical pipe in which a liquid was flowing with a flow rate controlled by a valve located downstream, which allowed him to visualize the formation of a fluid colored. He looked at various parameters such as the viscosity of the fluid, the flow rate, and the diameter of the pipe

---

<sup>107</sup> Glenn ELERT, *Flow Regimes*,

(See Figure 116) . By varying these quantities, he was able to observe three main behaviors of the file of fluid:

$$Re = \frac{\text{résistance initiale}}{\text{résistance visqueuse}} = \frac{\rho v \ell}{\eta}$$

- $Re =$  Reynolds number
- $\rho =$  Density of the fluid
- $v =$  Relative speed of the fluid
- $\ell =$  Characteristic length of the system
- $\eta =$  Mechanical viscosity of the fluid

- Behavior A: the colored fluid stream adopts a regular motion: the lines formed are approximately parallel and diffuse very slowly. This is the laminar regime.
- Behavior B: the colored fluid stream has a chaotic and unstable shape: the lines intermingle and diffuse throughout the pipe section, which constitutes the turbulent regime.

The transition from behavior A to behavior B is achieved through another state, behavior C, during which the colored lines show oscillations. This is the transient regime.

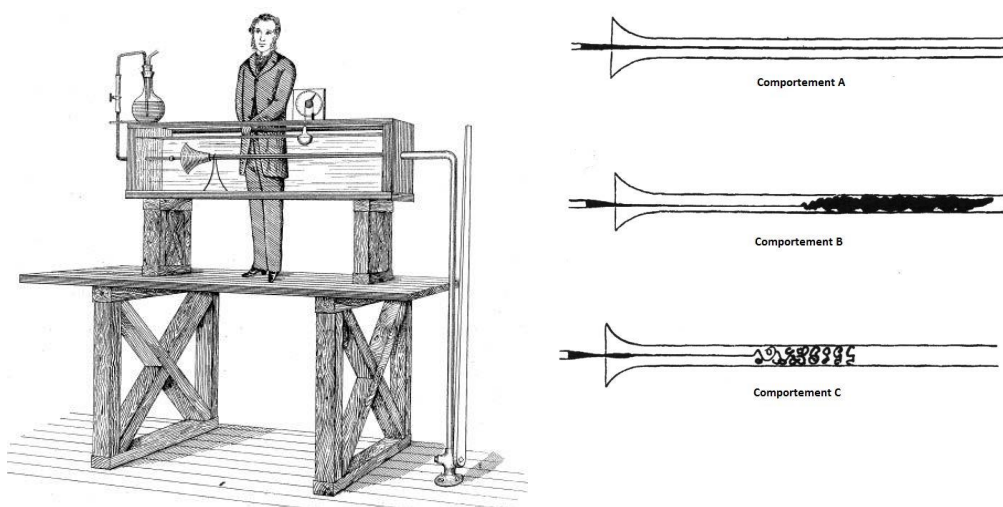


Figure 117. Experiment of O. Reynolds: presentation of the device (left) and representation of the main behaviors A, B and C of the colored fluid nets obtained.

In architectural or industrial design, when a ship, airplane or building is to be manufactured, a scale model is built and tested so that the performance of the realized object can be calculated from the test results of the scale model. Lord Rayleigh showed that the tests of the scaled model gave comparable results only when the non-dimensional factor of the model was equal to that of the realized object when working under design conditions. By equating the non-dimensional factor of the realized object to that of the model, we obtain the test speed of the model. This is called **the corresponding speed and the comparison of the two conditions between the real object and the results of the test of a model reduced to its corresponding speed is known as the principle of dynamic similarity.**

By 1921, more than twenty wind tunnels had been built around the world. However, all those of substantial size were operating at normal atmospheric pressures. This meant that the experimental results obtained using scale models in the tunnels were questionable, because a special parameter called the Reynolds number did not correspond to those encountered in real large-scale aircraft flights. In other words, the Reynolds number of 1/20 scale models tested at operational flight speeds would be too low by a factor of 20. Classical Reynolds experiments had shown that airflow conditions could be radically different for scale models and large-scale aircraft. Since the Reynolds number is also proportional to the air density, an obvious solution to the problem of scale effects would be to test 1 / 20 scale models at a pressure of 20 atmospheres. The Reynolds number would then be the same in wind tunnel tests and real large-scale flights<sup>108</sup>.

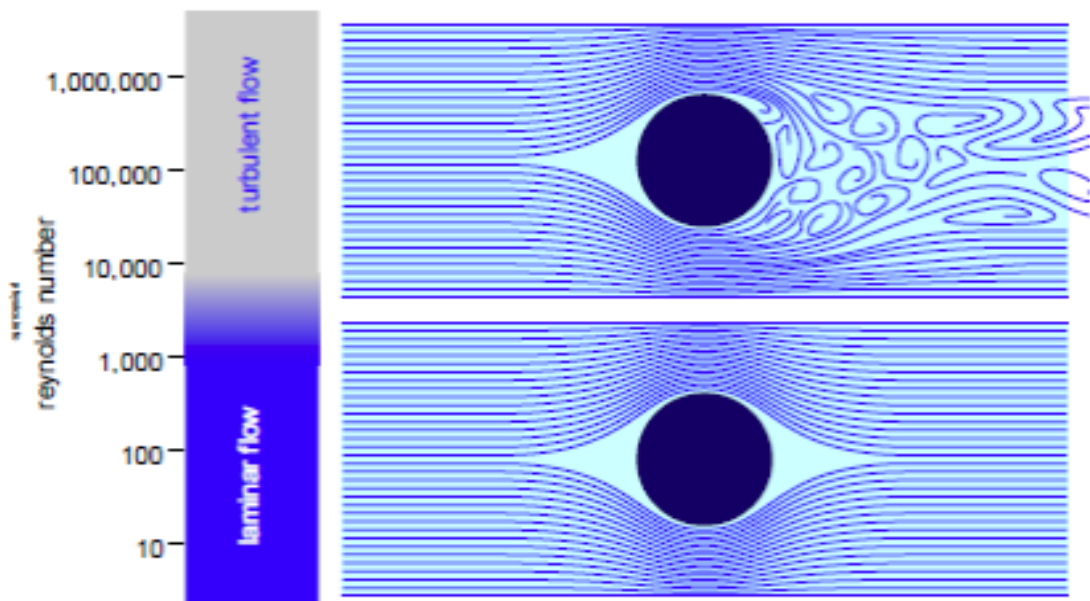


Figure 118. Flow regimes

### 1.5. Classification of flows<sup>109</sup>

<sup>108</sup> *ibid.*

<sup>109</sup> Ms. HELOISE, Mr. ALAIN, Mr. BRUNO, Ms. VANESSA, Mr. BONIFACE, Mr. STEPHEN, and INRIA SOPHIA-ANTIPOLIS, "Numerical simulation of 'flows around non-profiled bodies éby éhybrid turbulence models and a émulti-rate scheme," p. 210.

The flow regimes of a fluid can be classified according to the Reynolds number of the experiment (Figure 117). We can recall here, the flow regimes around the smooth-walled circular cylinder observed by B. Mutlu Sumer and J. Fredsoe :

For  $Re < 0.5$  (Figure 118), the streamlines are symmetrical between upstream and downstream of the cylinder. The flow is said to be **laminar** and the forces on the cylinder are mainly viscous. Boundary layer separation occurs when the Reynolds number is greater than 5.

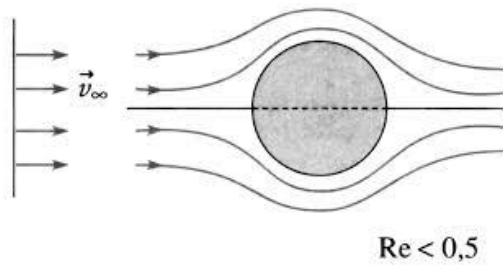


Figure 119.  $Re < 0,5$ : Pas de séparation, écoulement rampant

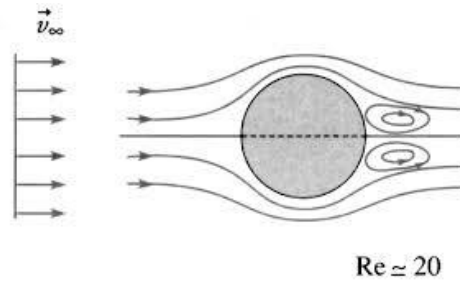


Figure 120.  $5 < Re < 40$  : Paire de tourbillons de recirculation symétriques

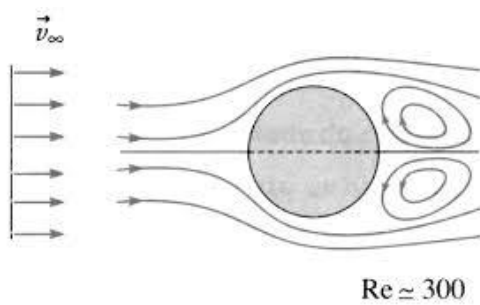


Figure 121.  $40 < Re < 180$  : Transition vers la turbulence dans le sillage

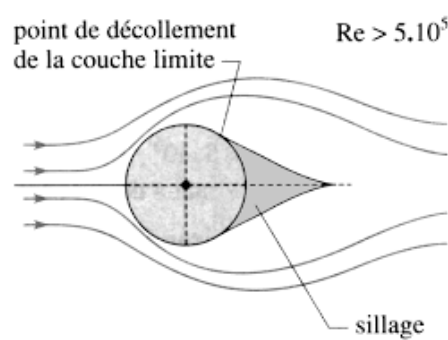


Figure 122. Régime sous-critique :  $300 < Re < 3 \times 10^5$

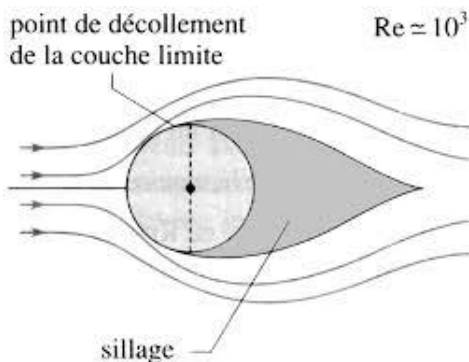


Figure 123. La moyenne du coefficient de portance est non nulle dans le régime critique  $3 \times 10^5 < Re < 3.5 \times 10^5$

For  $5 < Re < 40$  (Figure 119), the inertia forces increase which causes a detachment of the boundary layer behind the obstacle. Thus a stable recirculation zone forms

downstream of the cylinder and its size increases with the Reynolds number accompanied by a displacement upstream of the detachment point. This zone consists of a fixed pair of vortices, symmetrical with respect to the longitudinal axis and attached to the cylinder. The flow is said to be **stationary detached**.

For  $40 < Re < 180$  (Figure 120), the flow wake becomes asymmetric and unstable. This gives rise to the phenomenon of **vortex detachment**: vortices form on either side of the cylinder and are alternately convective in the wake forming a laminar vortex alley, called the Von Karman alley<sup>110</sup>. This detachment is periodic and two-dimensional, i.e. the detachment does not take place in the transverse direction.

For  $300 < Re < 3 \times 10^5$  (Figure 121), the flow downstream of the cylinder becomes fully turbulent, the vortices detach from the cylinder beyond the boundary layer and behave chaotically in the wake. The boundary layer upstream of the detachment point always remains laminar. This Reynolds range corresponds to the subcritical regime.

For  $3 \times 10^5 < Re < 3.5 \times 10^5$  (Figure 122), the critical regime is reached. The boundary layer remains laminar on one side of the cylinder. On the other side, it is partly turbulent and breaks away further downstream of the obstacle, which reduces the recirculation area and results in a sharp decrease in the drag coefficient. The average lift of the cylinder is no longer zero over this Reynolds number range due to the asymmetric nature of the flow. Downstream of the cylinder, the flow is turbulent and **the Strouhal number**<sup>111</sup> until then equal to 0.2, undergoes an abrupt change for  $Re = 3.5 \times 10^5$ , its value reaching 0.45.

For  $3.5 \times 10^5 < Re < 1.5 \times 10^6$ , we speak of the supercritical regime. The boundary layer is turbulent at the breakaway on both sides of the cylinder and the transition is localized between the stagnation point and the separation point.

For  $1.5 \times 10^6 < Re < 4 \times 10^6$ , this is the high transition. The boundary layer is completely turbulent on one side of the cylinder and partially laminar and turbulent on the other side.

## 1.6. Computational fluid dynamics (CFD)

Computational Fluid Dynamics (CFD) is the study of the motion of a fluid, or its effects, by numerically solving the equations governing the fluid. Depending on the approximations chosen, which are, in general, the result of a compromise in terms of

---

<sup>110</sup> The phenomenon of vortex detachment was first studied experimentally by Henri Bénard in France, then theoretically by Theodor Von Karman in Germany. It is created within the boundary layer and depends on the Reynolds number. When the Reynolds number is between 48 and 300, the vortices created for a  $Re$  lower than 48 become unstable.

<sup>111</sup> The Strouhal number ( $St$ ) is a dimensionless number describing oscillating circulation mechanisms. This number is named after Vincent Strouhal, a Czech physicist. Physically, it represents the ratio of the advection time and the characteristic time of instationnarity. If  $St < 1$ , the flow is said to be quasi stationary.

physical representation needs versus available computational or modeling resources, the equations solved can be the Euler equations, the Navier-Stokes equations, etc.

CFD has recently become an essential tool in virtually all branches of fluid dynamics, from aerospace propulsion to weather prediction to ship hull design. In the research field, this approach is the object of a major effort, as it allows access to all instantaneous information (velocity, pressure, concentration) for each point of the computational domain, for a global cost generally modest compared to the corresponding experimental manipulations.

### 1.7. Methodology of work in numerical fluid mechanics

In general, the numerical solution of a fluid mechanics problem goes through three main phases:

1. The preparation of the problem: this involves the definition of a geometry, a mesh discretizing the computational domain, the choice of models and numerical methods used;
2. The numerical solution of the problem through the execution of a computer program. Many problems of minimal interest require computers with very large capacities;
3. The exploitation of the results: first their coherence is checked, then they are examined in order to bring answers to the questions posed by the initial MFN problem.

The exploitation of the results is most often done by scientific post-processing software used in many branches of physics, or by the post-processing modules available in some fluid dynamics simulation software.

### 1.8. Choice of the numerical tool for the numerical simulation of airflow

A number of software packages exist and have proven their worth in airflow simulation at the urban and architectural scale. At the beginning of this thesis, we have tested several tools such as: ANSYS Fluent, Flow Design, STAR-CCM+, Simscale.

The calculation code is specific to each tool but the simulation results can be relatively similar. Their differences are in the import and export modes of the calculation data, in their capacity to adapt the model and the numerical environment to the type of simulation, in their level of precision, in their calculation speed, and especially in their mode of optimization of the data to be extracted at the end of the experimentation (to limit the calculation times)

We ultimately chose STAR-CCM+ as the CFD (Computational Fluid Dynamic) software used for the calculations in this thesis. This tool has been owned by the Siemens group since 2016. The strong point of this computational code is that it allows to solve simultaneously the flow and heat exchange problems, unlike other codes where these elements are dissociated. On the other hand, given the accuracy of the tool and its ability to parameterize, it is a relatively fast tool for the calculation.

It should be noted, however, that some calculations took several weeks to complete and were sometimes simplified (e.g. from unsteady to stationary mode or from a 3D to a 2D model) in order to limit the calculation time to less than 1 week on the computer equipment available for this thesis.

STAR-CCM+ is not a simple CFD solver. In fact, it provides a suite of **integrated components for modeling purposes**. These components include:

- 3D-CAD and CAD modeler
- Surface preparation tool
- Automatic meshing technology
- A variety of physical models (turbulence, combustion, etc.)

STAR CCM+ was chosen for this thesis work because it is provided by the co-director of this thesis, Jean Denis Parisse, and it has **proven itself on large scale building calculations** such as the Shard building in London, and the World Trade Center in New York.

### 1.9. Notion of mesh for numerical study<sup>112</sup>

Several elements characterize the mesh for the study of airflow in a zone: the orientation of the cell, its shape, its volume, its type of deformation, and its tessellation mode of a surface. Let us specify here the important criteria and the coherence between them to generate an optimal mesh of a study area.

- *The volume*

The volume change ratio describes the ratio of a cell's volume to that of its largest neighbor ( Figure 123) . A value of 1.0 indicates that the cell has equal or greater volume than its neighbors. As the cell volume decreases relative to its neighbors (such as a ribbon or flat cell), then the volume variation ration can be used to categorize that cell. A large volume change from one cell to another can lead to potential inaccuracies and instability in the solvers. Cells with a volume change of 0.01 or less are considered unsuitable cells for calculation.

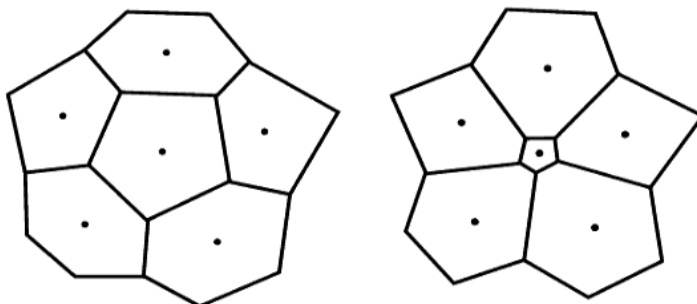


Figure 124. The diagram on the left shows a better distribution of cell volume changes

---

<sup>112</sup> Mesh concept in Star-CCM+, <http://hmf.enseeiht.fr/travaux/beiepe/book/export/html/1108>,

- *Deformation angle*

This asymmetry measure is designed to identify whether the cells on either side of a mesh are formed in such a way as to allow the diffusion of quantities without these quantities becoming unbounded.

Deformation angles equal to or greater than  $90^\circ$  typically result in solver convergence problems. The problems result from the fact that the formulation of the diffusion term for the transported scalar variables contains the dot product  $a \cdot ds$  in the denominator and this dot product is zero when the angle is  $90^\circ$  ( Figure 124) . Although STAR-CCM+ is careful to avoid such a division-by-zero error, the accuracy of the diffusion calculation is reduced and there is a loss of robustness in such cases.

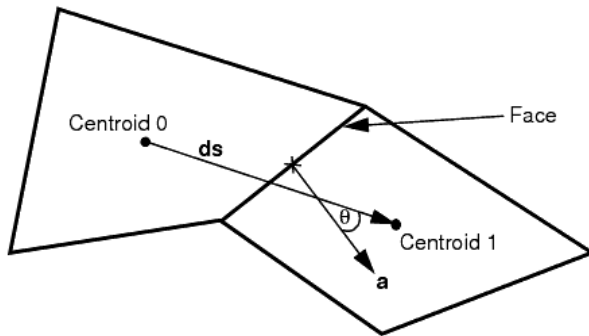


Figure 125. The deformation angle of the cell

- *Polyhedral mesh*

Polyhedral meshes provide a balanced solution for complex geometry problems. They are relatively easy and efficient to construct, requiring no more surface preparation than the tetrahedral mesh. They also contain approximately five times fewer cells than a tetrahedral mesh for a given starting surface. Multi-region meshes with a conformal mesh interface are allowed.

- Because of the good growth behavior, polyhedra are generally preferred when aerodynamic coefficients are of paramount importance.
- Due to the pseudo-random orientation of the faces, polyhedra also generally perform better than cut meshes when using large sweeps in the direction of flow (such as angle of attack or slip).
- Typical polyhedral meshes contain from 2 to 20 million cells, depending on the complexity of the geometry and flow field, and the treatment near the wall.

- *Hexahedral mesh (Trimmer)*

By default, the "trimmer" mesh model, a feature of STAR CCM+, uses a mesh constructed from hexahedral cells, from which the base mesh can be subdivided.

- In a simulation with one direction of flow, or only a small variation in flow, the mesh with the grid lines aligned with the flow often provides the most adequate approach to obtain good answers.
- Typical meshes created contain from 4 to 40 million cells, depending on the geometry and flow field, and the treatment near the wall.

*gffghgfjjsg5434345nom*

## 2. METHOD OF MODELING AND DEFINITION OF INITIAL CONDITIONS OF THE SIMULATION

Our wind flow simulation is mainly based on 2D simulations, rather than 3D simulations, in order to have a more accurate reading of the phenomena in progress. They will be based on sections of a 3D model of a building or a site. We will identify here the following steps to define the hypotheses from the analysis, the calculation model and the conclusions of each analysis

1. Definition and modeling of geometry
2. Choice of mesh type and generation
3. Choice of calculation models
4. Definition of initial and boundary conditions
5. Results and analysis

### 2.1. Definition and modeling of geometry

As an architect, we have a very wide range of tools for 3D or 2D geometry modeling. The scale of the building, the level of detail, the type of lines and curves (straight lines, splines), the definition of surfaces (Nurbs, polygonal), the type of tessellation (triangulations...) are a universe that architects define for each project according to the research results, simple modeling for visualization, collaborative modeling for interoperability type BIM, parametric, modeling for digital fabrication of the project, are all criteria that enter into the choice of a type of geometry, a software, and a generative function

We tried, through studies and simulations, to find the clearest method to compare the flows and their impact around the buildings, and to visualize these rather complex flows. The choice, very quickly, was to leave room for simple cross-sections that show an air movement in an air section rather than in all its spatial complexity. This method clarifies the results and their comparison, reduces the calculation time, and impacts the complexity of the flows on a surface.

We therefore worked on building a **2-dimensional** mesh by choosing a **polygonal mesh rather than a square one in order to optimize the number of meshes in the model.**

For analysis, our buildings or urban environments, we have been particularly attentive to the following elements:

- The relationship to the ground and the boundary conditions of the geometry
- The treatment of the façade and its return to the roof
- The wind direction and the impact of the context on this air inlet.
- The study area

The airflow on a geometry is very much impacted by these different criteria which must be adjusted as precisely as possible (Figure 125).

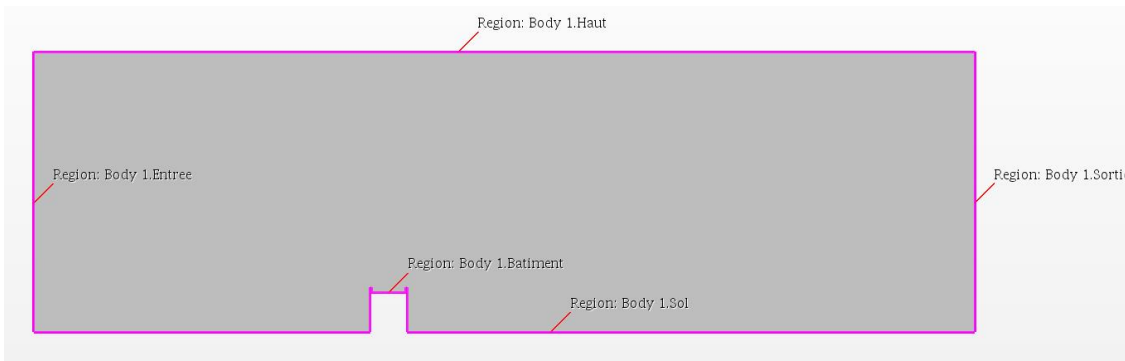


Figure 126. Definition of the analysis domain and domain boundary conditions

- *Geometry*

1. We have created a rectangle in 3D-CAD with an additional point on the "inlet" side. In our study, the square will be 100 m long and the air height 25 m.

2. Then his sketch and extruded on a small depth (we will work in 2D). Then we renamed the different faces as follows:

- **Air Inlet**
- **Bottom:** center of symmetry of the enclosure
- **Top:** high limit of the enclosure for analysis (according to Y)
- **Outlet:** limit according to X of the enclosure for analysis

The conversion to 2 dimensions will be done once the mesh is generated. At this stage we have a 3D geometry with 7 different faces.

- *Choice of mesh size*

After creating the geometry, it is very important to choose a suitable mesh for a short and accurate calculation.

To illustrate the importance of the mesh we tested three meshes of different resolutions.

The first mesh ( figure 126) created is an unrefined hexagonal mesh, on the whole domain. The meshes are of length 0.0015m for the most refined and 0.003m for the coarsest. This gives a total of 5200 meshes on our domain. We have created a volume shapes block on the whole length of the mesh as explained.

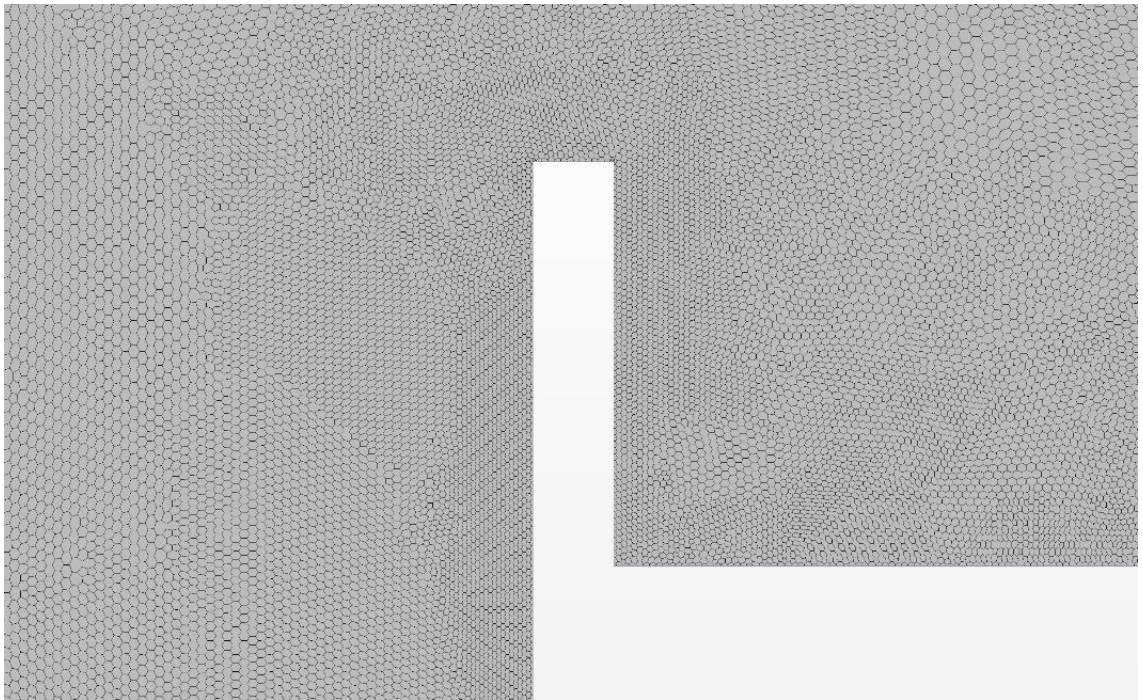


*Figure 127 Detail on a mesh generated around the building under study*

The second mesh created is a refined hexagonal mesh, on the whole length of the volume. The meshes are 0.00015m long for the most refined ones, i.e. 10 times smaller than before. We have **572,414 cells**; **1,706,838 faces** and **1,138,034 greens**. On our domain. This mesh is less refined on the top of the central wall. To create this mesh, we created a second volume Shape on half of the square of the volume.

If we zoom in on the intersection of the two block rectangles of the mesh, we can see a little more of the refinement of this second mesh.

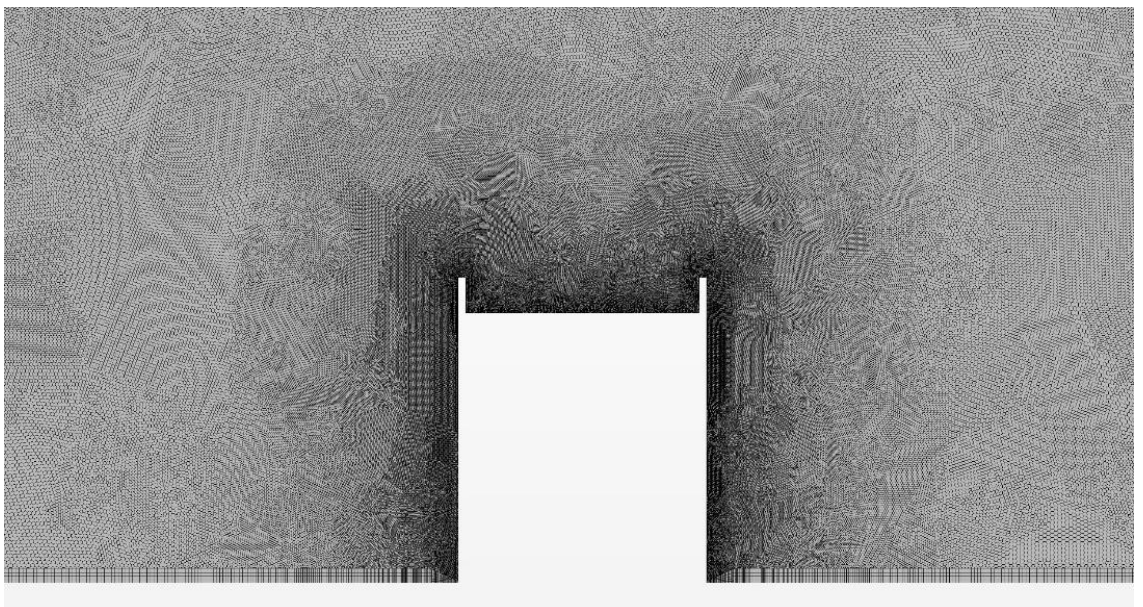


*Figure 128 Detail of the mesh in the area around the building*

The last mesh was created after having been confronted with calculation divergences due to the too coarse output mesh. It is thus essential for our problem to have a very refined mesh on the whole continuity of the acroteria (a few centimeters above to not see the calculation diverge). The refinement close to the "top" surface is useless for our calculation, it saves calculation time to associate a coarse mesh.

To create this mesh, it is necessary to have a third block of refinements (or a single block of different parameters). The third block must thus take the whole length of the geometry.

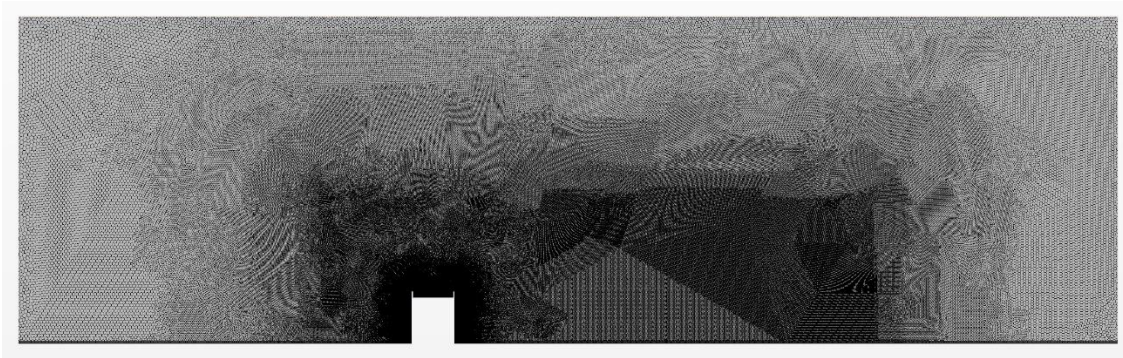


Figure 129 Detail of a general mesh of the domain

The computation times of the 3 meshes are very different ( Figures 126, 127 and 128 ). It is obvious that the very refined mesh will take much more resources, memory and CPU time for the calculation. Nevertheless, in our situation, it is essential to have this precision in order to visualize the phenomenon. It will therefore be necessary to choose the mesh models carefully at a later stage in order to save computing time.

Convergence problems can occur when choosing a coarse mesh. We have used the refined mesh for the modeling.

After defining the mesh, to generate it, we used the **Mesh>badge for 2D meshing** function. It is important to save this file to be able to modify this mesh later if necessary, once it is switched to 2D all the options will no longer be available.

Once saved we can increase the mesh with **Mesh> automated mesh(2D)**. Choose polygonal mesher and add Prism layer Mesher on the bottom (ground) with the value of 5

The mesh is now in 2 dimensions.

## 2.2. Definition of the calculation parameters

We will now detail the possible model choices to model this building.

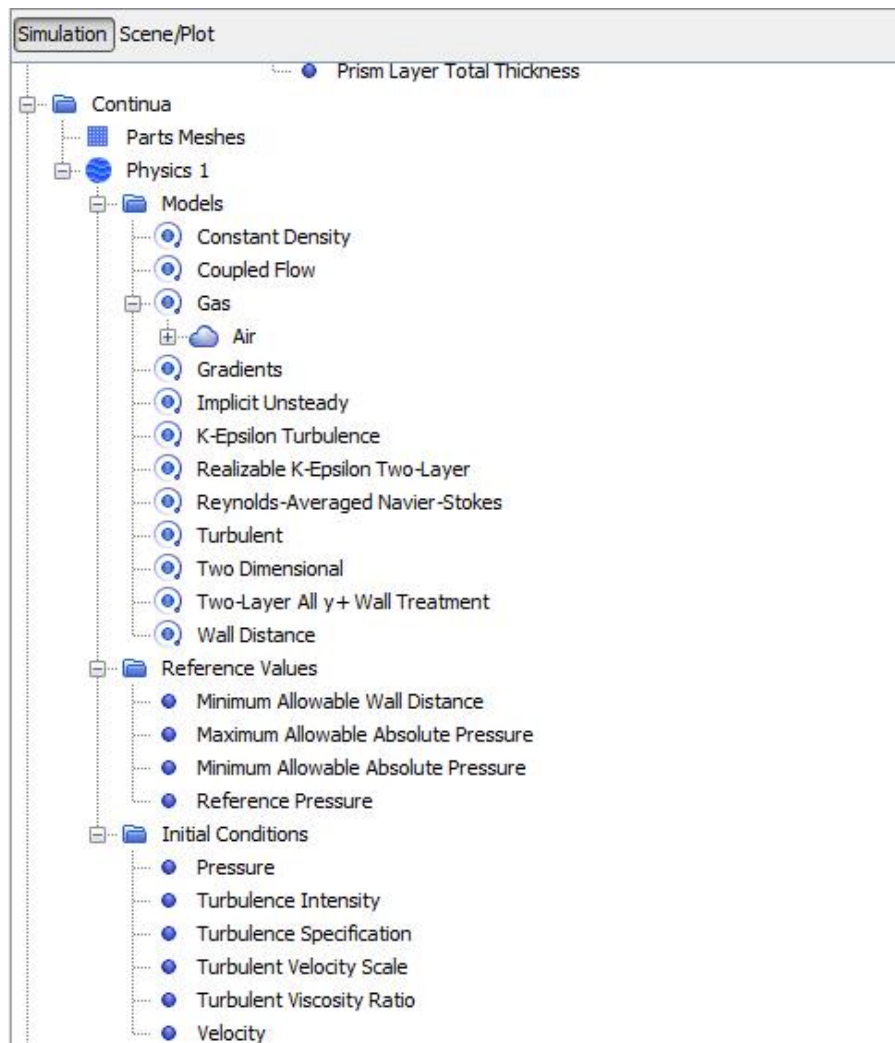


Figure 130 Extract from the simulation programming window

- *Gradients*

Gradients are used in several terms in the solution of the transport equation.

- Reconstruction of the field values in the cell faces.
- Diffusive terms.
- The pressure gradient for the coupled Flow model.
- Strain rate and rotation rate for turbulent models.

This option is automatically checked.

- *Turbulent*

Turbulent flow model as desired.

- *K-Epsilon Turbulence & Realizable K-Epsilon Two Layer*

The k-epsilon model is selected in the turbulent flow resolution.

- *Reynolds-Averaged Navier Stokes*

The Navier-Stokes equations are averaged, which is essential for any turbulence analysis.

- *Two-Layer All y+ Wall Treatment*

The Two-Layer all y+ Treatment is the intermediate treatment between the high-wall treatment and the low y+ treatment. In fact, it tries to use the high wall treatment for coarse meshes and the low y+ treatment for more refined meshes. It is also possible to solve intermediate meshes

with this option. Since our mesh contains some coarse and some fine blocks, this is the option to choose.

- *Implicit Unsteady*

By choosing the Coupled Flow model, the Implicit Unsteady solver model is the alternative to the permanent mode.

- *Two dimensional*

Our problem is in 2 dimensions, so this option must be checked.

- *Choice of boundary and initial conditions*

We have now defined the geometry and the mesh of our building. It is now time for us to choose our boundary and initial conditions that will close our problem.

- *Boundary conditions*

The 2D geometry consists of 5 surfaces that each require a boundary condition. To set a boundary condition, we used: **Region > Region 2D > Boundaries**

The surfaces subject to boundary conditions are as follows for our study:

*Air Inlet* : Select a "Velocity Inlet" condition for this surface. For our case, let's enter a Velocity of 5.0m/s. In the studies, this value is based on insitu anemometric readings.

*Bottom*: Selection of the "wall" option and no-slip wall for shear stress specification and wall surface specification is smooth. With the value of constant Von Karman which is 0.42.

*Top*: Selection of the "Pressure Outlet" option, the air around the enclosure is at atmospheric pressure; the default value (0 Pa) should therefore be left, since STARCCM+ works here in relative pressure values compared to atmospheric pressure.

*Outlet*: Like Bottom, the outlet of the enclosure is also composed of air, selection of the option "Pressure Outlet" with 0 Pa.

### 2.3. Initial Conditions

To initialize our problem, we need to create 3 "*Fields functions*".

In **Region > Region 2D > Initial Conditions > Species Mass Fraction**, select the "**Composite**" option.

In the **Tools > Fields functions** tab, right-click on **new**.

- *Properties of the solver*

The solver is the tool for calculating the equations of the simulation. Here the velocity according to x in the small mesh :  $u=1\text{m/s}$

Number of currents: 50

Length of a small mesh : 0.00015m

This implies a time step of at most 0.0015s to be stable. We will choose a time step of 0.001s in **Solvers > Implicit Unsteady** to observe a convergence of our calculations fast enough.

- *Air speed profile*

The Fields functions, allows to define the air velocity profile. When meshing, it is important to finely mesh the boundary layer area because it is an area where the velocity gradient is important.

The variation of the average air speed is dependent on complex interactions such as: stratification in the lower layers, thermal turbulence, the nature of roughness encountered by the wind and its distribution. The growth of the air speed also varies with the height above the ground.

When the winds are blowing, the stability conditions of the atmosphere are generally neutral, and the thermal phenomena can be neglected in front of the dynamic wind phenomena. The growth of the mean velocity with height  $z$  can be represented by

In our case, the velocity profile of the simulations is defined by the wind measured on site affected by a coefficient  $K$  which corresponds to the roughness of the environment.

$$\vec{U}_z = \vec{U}_M \chi k$$

With :

**Error! Bookmark not defined.**  $\vec{U}_z$  The average wind speed at height  $z$ ,

$K$  : The registration coefficient depending on the roughness of the context (from 0.5 (open urban spaces) to 1.2 (large city with high buildings))

$\vec{U}_M$  speed measured by the anemometer connected on site at a specific height ( $h$ ).

However, in most of the simulations we did, we did not capture a logarithmic wind speed profile related to the ground layer. The studies were done on specific areas around buildings, where the boundary layer does not have a significant impact. On the other hand, the air velocities used in the simulations are chosen in relation to measurements taken by connected anemometers when the buildings are existing. This method provides a higher accuracy than the use of a coefficient  $K$  of roughness of the context which can only be approximate in a dense urban context. This method is similar to the calculation performed in a physical wind tunnel where the velocity profile is uniform at the experimental input.

## 2.4. Results and analysis

Testing the mesh and the chosen models:

- First, it is necessary to test the mesh and the different models. For this, we launch a first simulation

In our case  $Ri = 2.5 \cdot 10^{-4}$  Typically for  $Ri < 0.1$  the flow is turbulent, for  $Ri < 0.25$  the flow is unstable and can give rise to a Kelvin-Helmholtz instability.

Because of viscosity, the velocity of the fluids at the interface tends to equalize, which induces a velocity gradient in each fluid. This results in a dynamic of rotation and vortices in each fluid.

The results obtained using STARCCM+ are as follows:

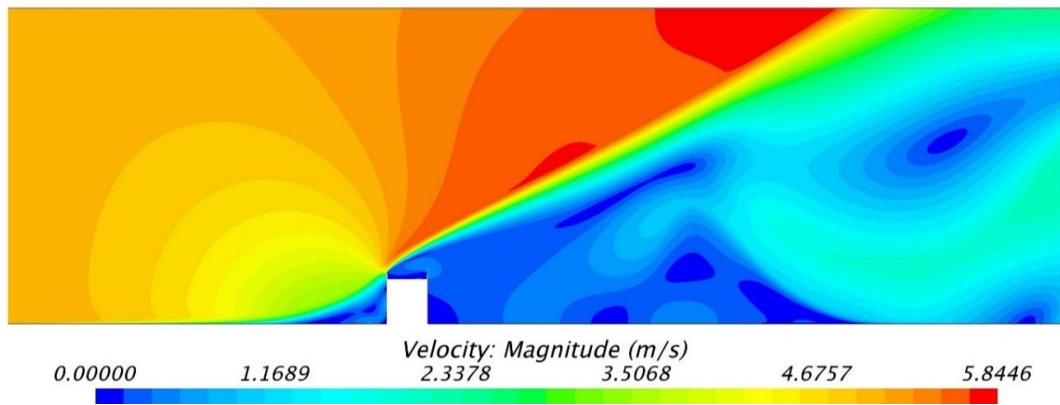


Figure 131. Air velocity distribution in the model

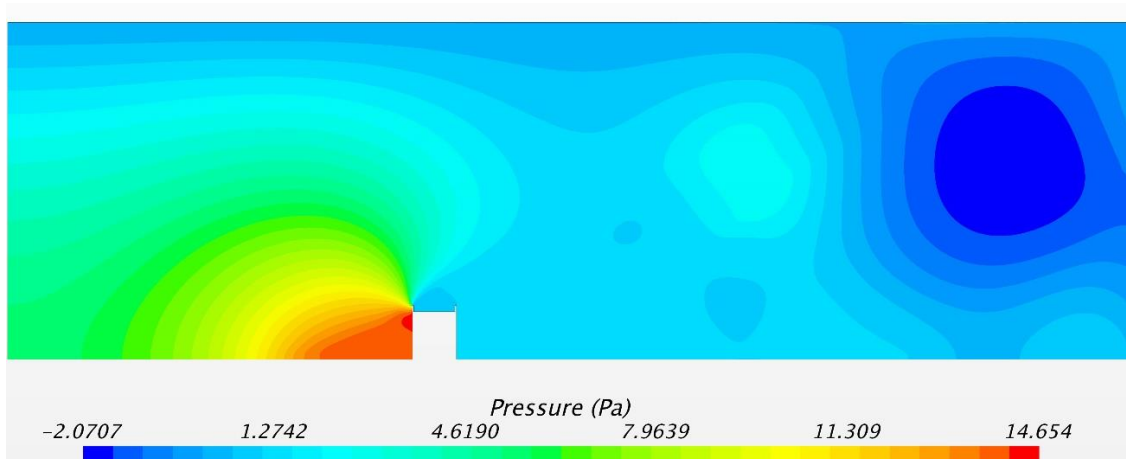


Figure 132. Pressure distribution in the numerical model

We obtain this type of instability with our simulation, the periodicity and the vortex character prove that it is most likely the Kelvin-Helmholtz instability. We will have to avoid this phenomenon for the rest of our study.

- *Definition of boundary conditions*

Now that the initial conditions are defined, we will now define the boundary conditions of our building.

- *Launching the calculations*

Now that all the parameters are set, we can start the calculations. But first we have to set the time step of each iteration and the physical time of the simulation (or the number of iterations)

For the time step of each iteration, we must first estimate the characteristic times of all the physical phenomena likely to occur. The time step of the simulation must be smaller than all these characteristic times.

Taking as characteristic size the size of the smallest mesh (2 mm). The characteristic velocity is 1m/s. The diffusivity of H<sub>2</sub> in air is 61 mm<sup>2</sup> /s.

In **Solver => Implicit unsteady** enter the value of 0.001s in **Time-step**.

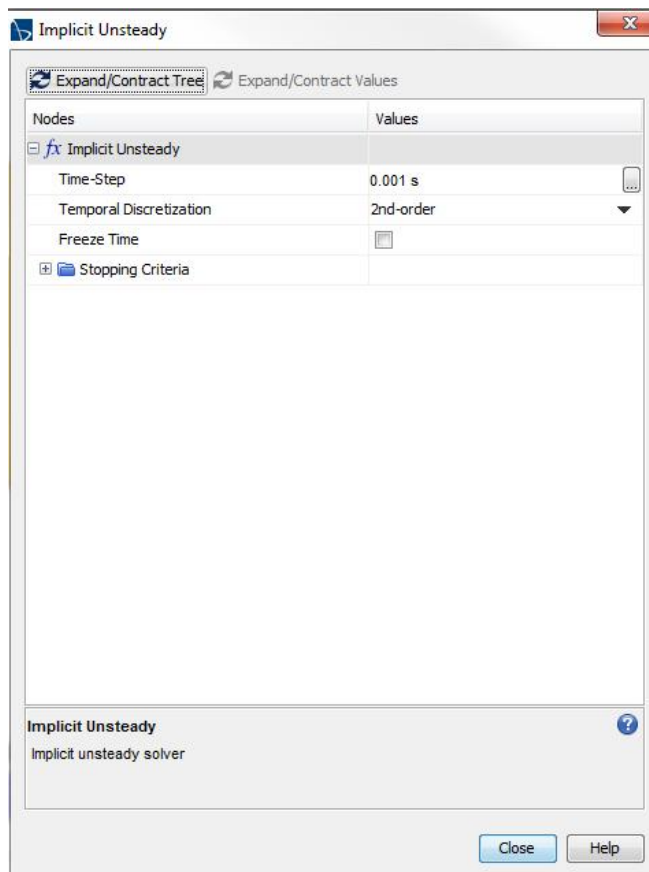


Figure 133 Extract from the STAR CCM+ window for the definition of the Solver

In **Stopping criteria** => **Maximum Physical Time** enter the simulation time value. (We have chosen 2s for our simulation)

These different configurations of the STARCCM+ environment allow us to adjust our virtual wind tunnel to our study objects: the buildings, with their scale, their volumetry, their frontality to the wind. How to improve the calibration of our tool? This is the point we will see in the next part.

### 3. NUMERICAL SIMULATION OF A BUILDING ROOFING SYSTEM WITH 3 TYPES OF INITIAL CONDITIONS

#### 3.1. Definitions of the initial conditions of the simulation

This experiment uses the STAR CCM+ software to simulate the wind behavior of a wind device on the roof of a building in order to find the best scale, orientation, and positioning of the device on the roof. The objective of the research is twofold: to locate a generator at the point of maximum wind speed increase and on the other hand to limit turbulences in the device and in its periphery.

In the following study, we have modeled the wind behavior on 3 different experiments where only the initial conditions and the calculation parameters vary, in order to identify their impact on the results produced.

The implementation of this calculation is done on a 2D profile drawn directly in the STARCCM+ modeling tool. The following elements describe the sequence of commands (in English) of the STARCCM+ interface used to prepare and launch the simulation.

- *The geometry*

### 1) Modeling of the wing to be studied

- Modeling the wing in the 3D CAD MODEL of Star CCM+.
- Close surface (option available when importing to STAR-CCM+)
- *Data: the curvature of the wing is 2 meters radius actual size.*

### 2) Definition of the study area called "Domain"

- Create the box (rectangle called "domain") of dimension :

**L= 0.30m** (along the x axis)

**l = 0.20 m** (along the y axis)

C

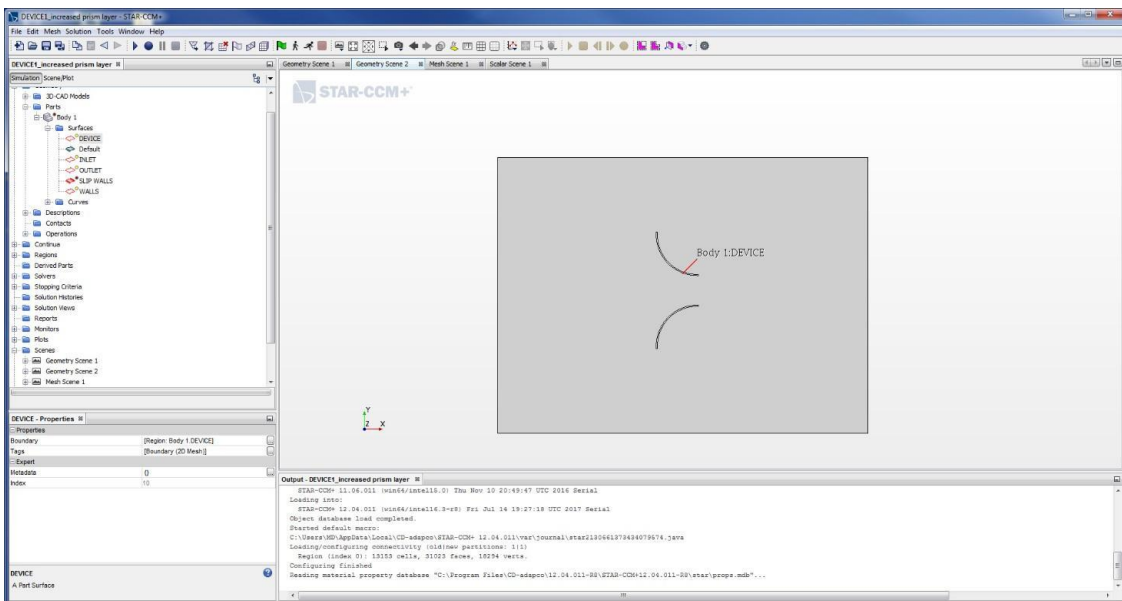


Figure 134. Star CCM+ Screenshot of the modeling of the profile to be studied

### Positioning of the wing in the field

- *Faces: bottom=bottom, top=top, left = outlet, right =inlet*
- Extrusion on any depth (allows to do the "subtract" operation with the domain as "target part")
- Only one body remains, renamed domain.

- *Making the mesh*

### 1) Parameterization of the mesh elements

- Geometry > operation > new > badge for 2D meshing (Input part= domain)

- Run the **Badge for 2D meshing** (projects the extrusion on the z=0 plane).
- Geometry > operation > new > **automated mesh (2D)** (Input part= domain)
- Meshers > Triangular mesher, Prism layer mesher
- Base size **0,01m**

	Relative to base size	Absolute
Target surface size	<b>1 %</b>	<b>1E - 4 m</b>
Minimum surface size	<b>1 %</b>	<b>1E - 4 m</b>
Surface curvature		<b>36</b>
Surface growth rate		<b>1,05</b>
Number of prism layers		<b>20</b>
Prism layer stretching		<b>1,2</b>
Prism layer total thickness	<b>20 %</b>	

## 2) Parameterization of the specific elements of the mesh

### a) definition of edges and their effects

- Part surfaces: top, bottom, inlet, outlet.
- **Target surface size** > custom

Value: 300 % of base size (0,03m)

*NB: the other options are left in "parent" mode*

### b) device

- Wake refinement: "specify wake refinement options" is not necessary in our study

Distance	<b>0,15 m</b>
Direction	<b>(0.97 , 0.26 , 0.0 )</b>
Spread Angle	<b>0.3 rad</b>
Relative size	<b>100 % of base size (0,01m)</b>
Wake refinement > growth rate	<b>1.05</b>

*NB: The direction of the wake refinement corresponds to an angle of 15° with the direction defined by the x axis.*

### 3.2. Simulation N°1 of a wind amplification device

Once the geometry of the wing is modeled, the initial conditions entered and the mesh made, we obtain this view of the profile and the study area. We studied a double funnel-shaped curve, on a reduced study area. The "spread angle" allows the use of the mesh at angles between 0° and about twenty degrees. This first study is launched with a dense mesh of 327 000 meshes and an unsteady regime stopped at 3:30min. The computation time of this simulation is about 2 hours, despite the relatively small domain of the study (50cmX30cm)

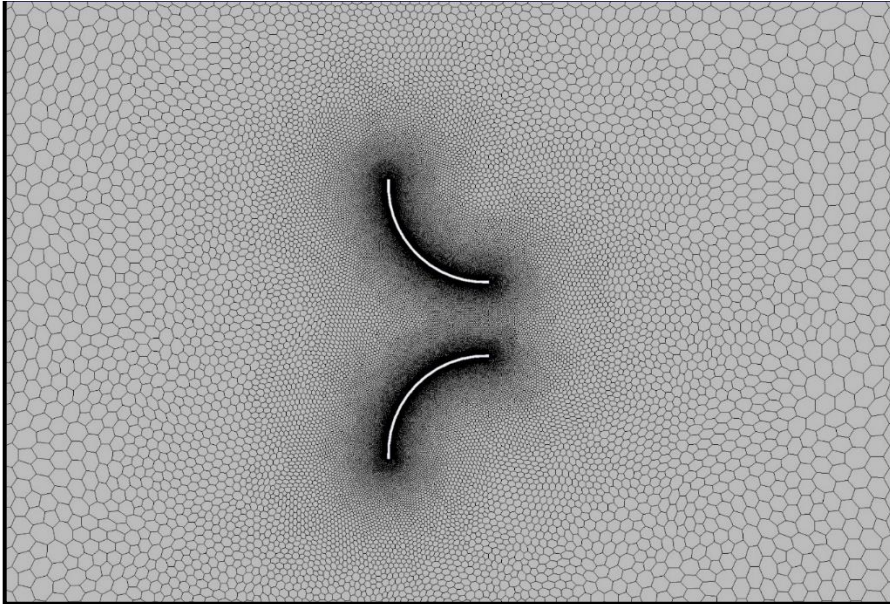


Figure 135. Star CCM+ - Profile and 2D mesh view

Number of meshes: 327,057, Calculation time: at 3'30"- unstable

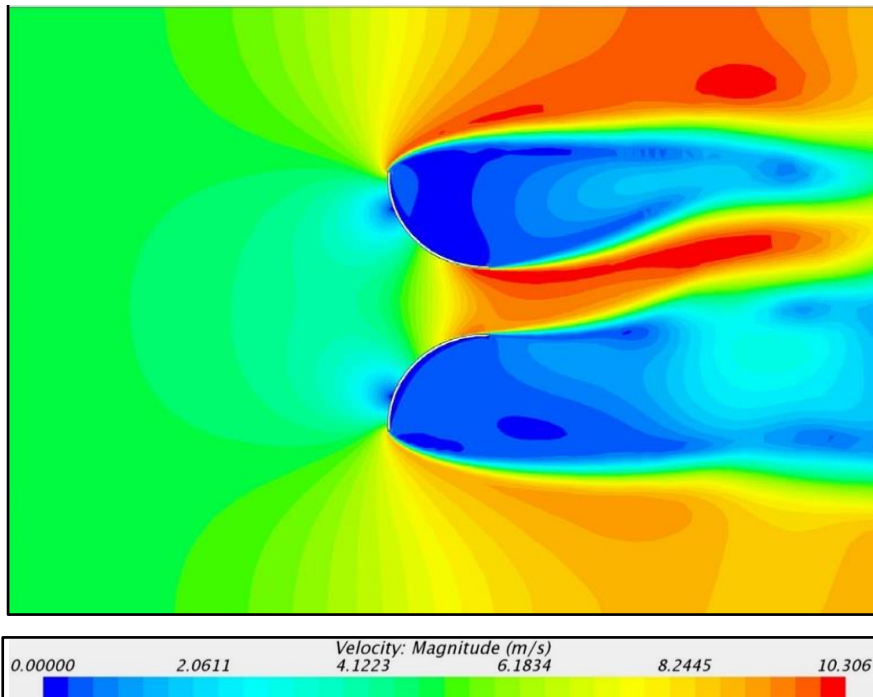


Figure 136. Star CCM+ - Magnitude of velocities following the launch of the simulation

- *Choice of physical conditions*

## 1- Initial conditions

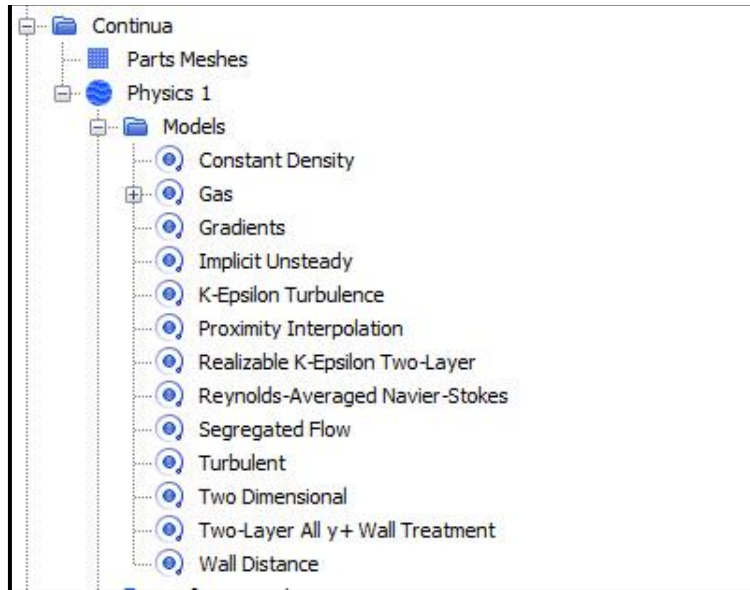


Figure 137. Fig. 86: Star CCM+ - Initial conditions

- Speed taken equal at any point to the entry speed (*standard of 28.5 m/s for the calculations carried out*).

## 2- Model used

- Continua > physics1

Definition of the steady state simulation.

The physical models selected for multiphase simulations differ from those for steady-state simulations. This allows the user to select which methods and solution models to use for the calculation. The implicit unsteady model is the only transient solver available with the segregated and turbulent flow models. The model allows the user to specify the time step to be used in the simulation, among other parameters.

## 3- Solvers

### 1) Time

- Implicit steady > temporal discretization: second order
- stopping criteria > **Maximum inner iterations: 20**

### 2) Space

- 3rd order

## 4- Residues

At each of these simulations, we analyze the residuals of the calculation, i.e. the degree of convergence of the Navier-Stokes equations. This graph, made up of 5 to 6 parameters of the equation, allows us to verify if, in an order of 1,000 to 10,000 iterations, the simulation performed leads to a relevant and qualitative result. At each calculation, a large number of

winds are evaluated in order to progressively improve the simulation and the accuracy of the calculation (Residuals ideally below 0.001 for 1000 to 10 000 iterations).

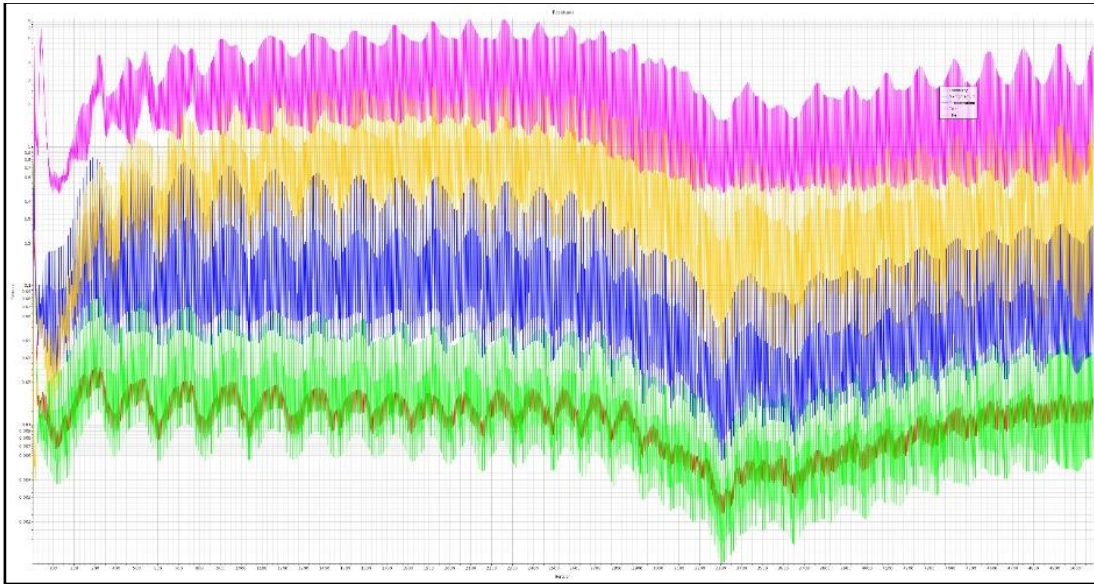


Figure 138. Star CCM+, the residue curves of the equation not converged during the first calculations

*The TDR (turbulence dissipation ratio) offers 10,000 times more residue than the other parameters*

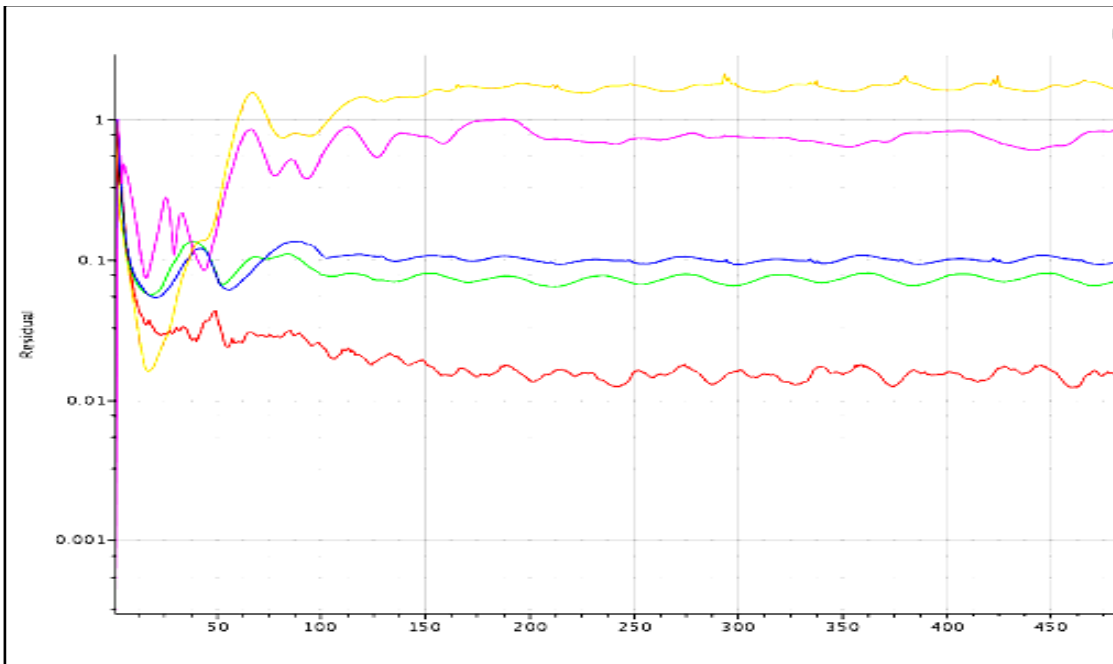


Figure 139. Analysis of the computational "Residues" on the first 500 iterations. The calculation was not extended to 10,000 iterations because of the computation times exceeding several weeks.

### 3.3. Simulation N°2 of a wind amplification device

This second study is launched with a less dense mesh of 11,000 meshes and a stationary regime. The magnitude of the area velocities measured is not the average of the velocities over time, but the constant air velocity, if the air flow is indeed stationary.

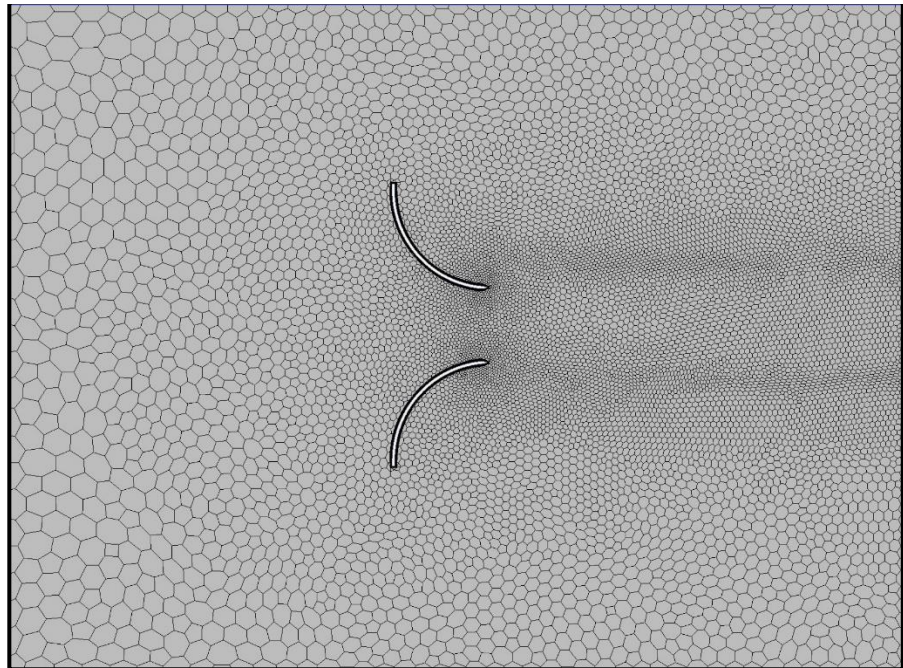


Figure 140. 2D mesh shape

Number of meshes : 11 327

Time : steady state

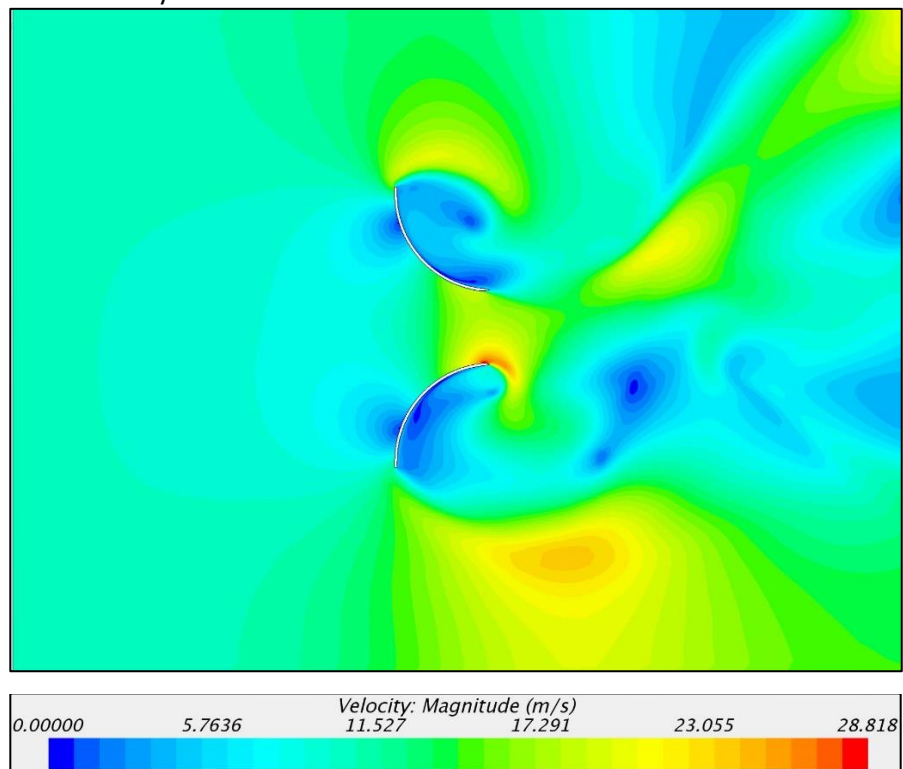


Figure 141. Velocity Magnitude

### 1- Initial conditions

- speed taken equal at all points to the entry speed (Standard of 28.5m/s)

for the calculations carried out).

## 2- Models - continua > physics1

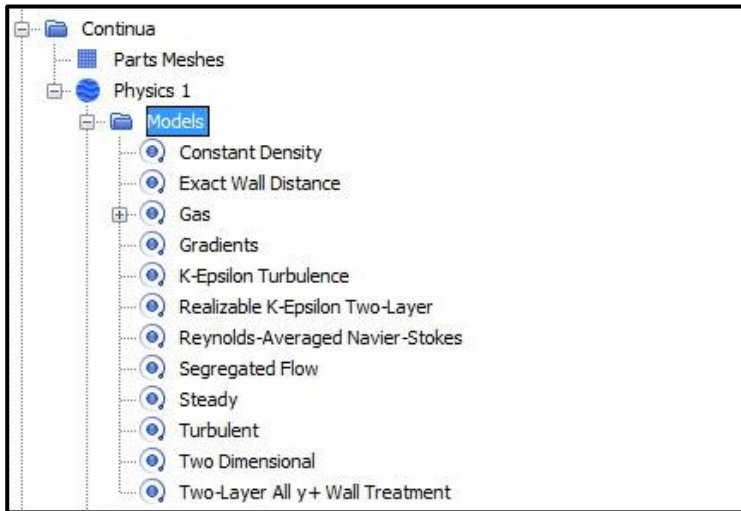


Figure 142. STAR CCM+ -Initial conditions

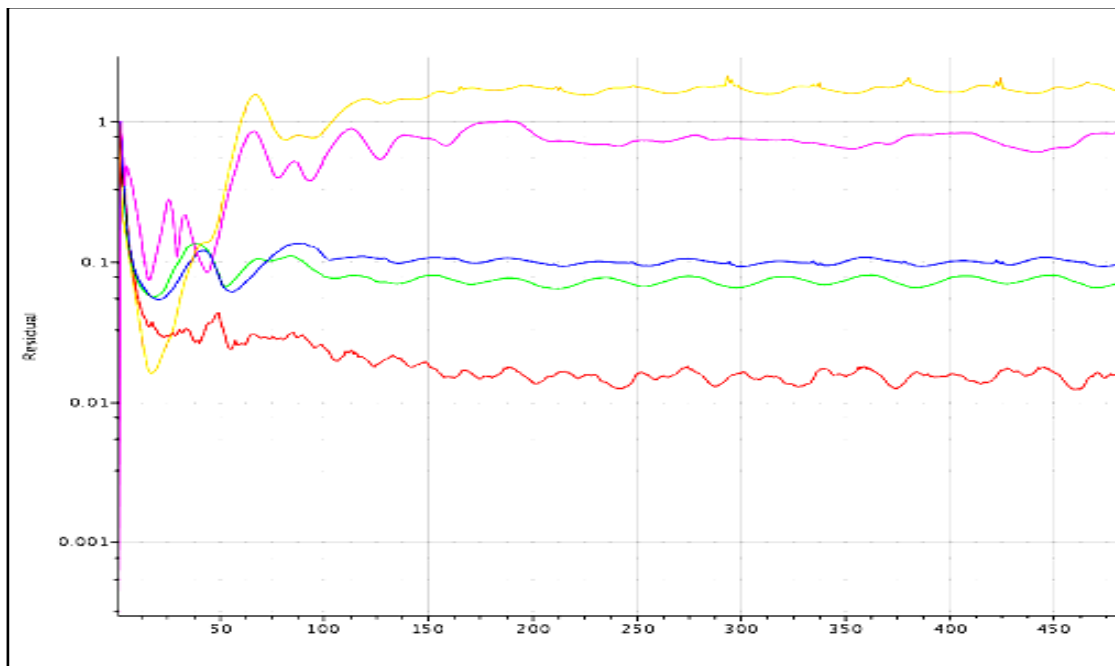


Figure 143 . Analysis of the "Residues" of calculation.

### 3.4. Simulation N°3 of a wind amplification device

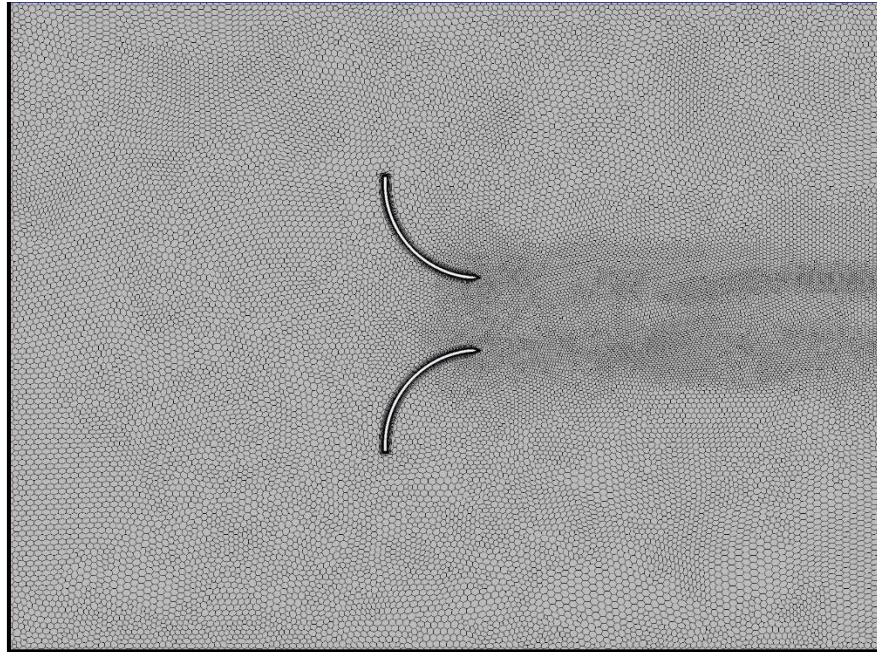


Figure 144. 2D mesh shape

Number of meshes: 26,093

Time: steady state

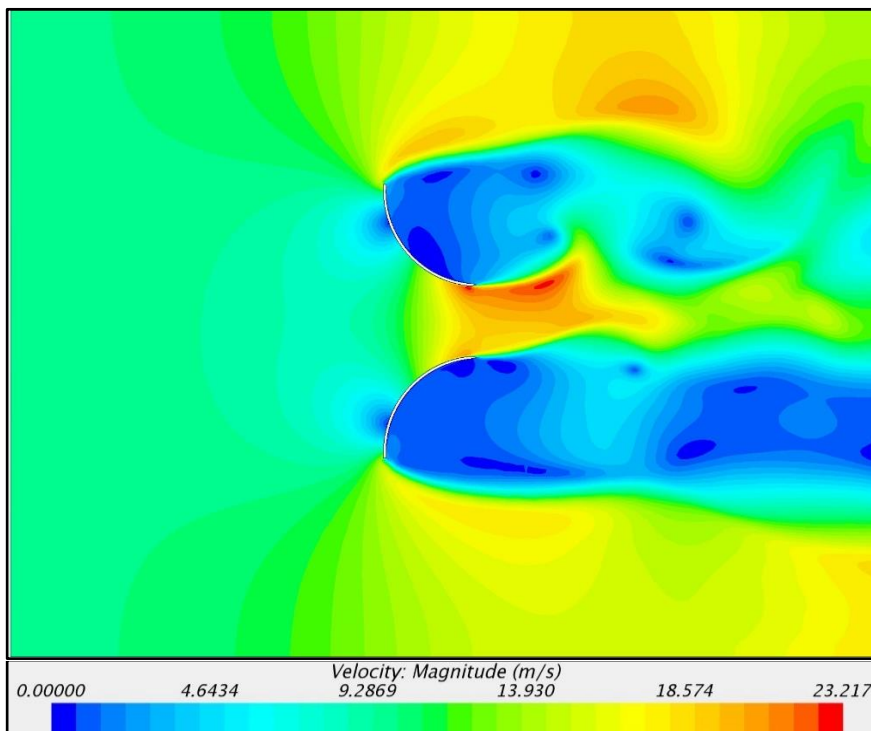


Figure 145. Magnitude of the velocities

This third study is launched with a medium dense mesh of 27,000 meshes and a stationary regime. The magnitude of the area velocities recorded is not the average of

the velocities in time, but the constant air velocity, if the air flow is indeed stationary. We observe that the definition of the speeds is more continuous and more homogeneous. This can be explained by the increase in the density of the meshes which captures a better precision the behavior of the air.

### 1- Initial conditions

- velocity taken equal at any point to the entry velocity (standard of 28.5m/s for the calculations carried out).

### 2- Models - continua > physics1

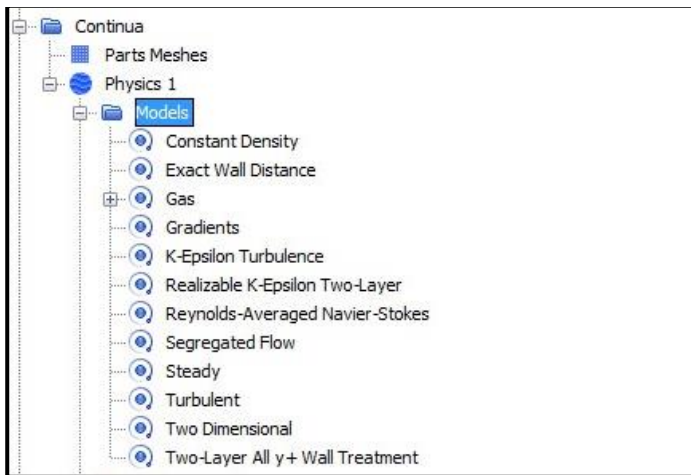


Figure 146. STAR CCM+, Condition Setting Window: " PHYSICS "

We have studied 2 choices of turbulence model in our simulations. K-EPSILON TURBULENCE

In the selection of the physical model, select Steady in the tab calculation of time, gas in the material, separated flow in the flow, constant density in the equation of state and laminar under the viscous regime.

### 3- Solvers

#### 1) Time

- implicit steady > temporal discretization: 2nd order
- stopping criteria > maximum inner iterations: 20

#### 2) Space

- 3rd order

The TDR offers 10,000 times more residue than other parameters (see point - 4, chapter 3.4.2)

## 4. Conclusion

Numerical simulation tools such as STAR-CCM+ allow the creation of a virtual wind tunnel that can be precisely tailored and configured to the type of study being conducted.

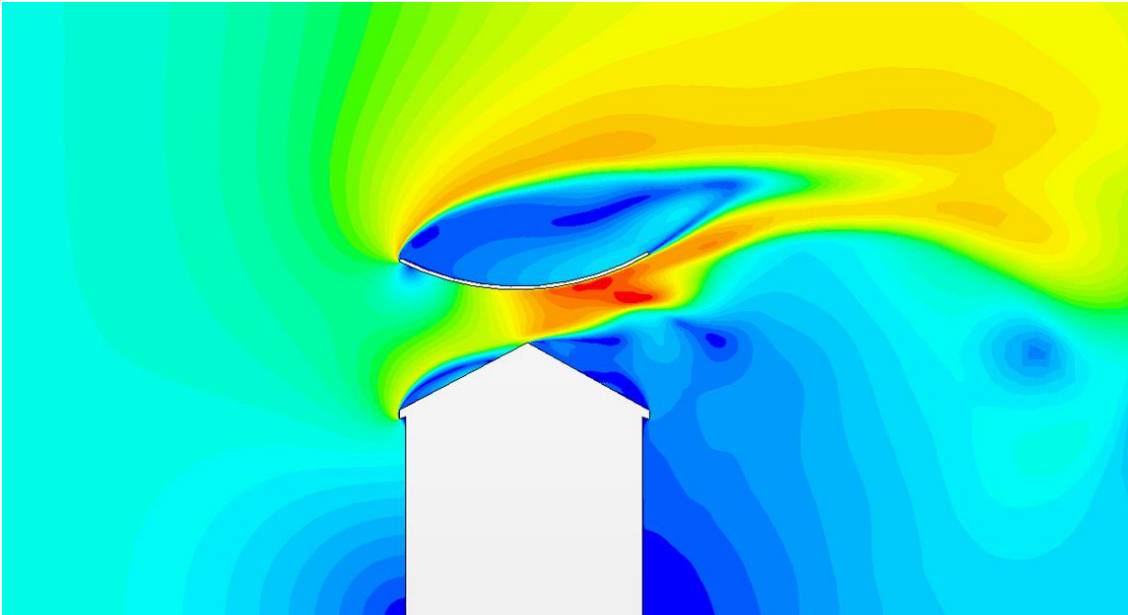
The dimensioning of the test chamber, the wind speed, the precise experimental characteristics can be adjusted according to the necessary experiments and this without the complexity of a physical wind tunnel manipulation. On the other hand, the speed reading by color mapping facilitates the identification of areas of increased air speed or turbulence. This method of analysis does not generate difficulties of measurement related, as it is often the case, to a handling in physical wind tunnel (slowing down of the air at the level of the measurement probe).

On the other hand, the choice of initial and boundary conditions is decisive to obtain accurate results consistent with the case studied. The calibration of the numerical wind tunnel with measurements made on site, ensures that the calculation assumptions are close to or even identical to those of the wind measured at this location. In this chapter, we have learned how to configure and observe air flows in laminar and turbulent regime and to adapt the simulation conditions to the measurements taken on site thanks to the connected anemometers.

In the fourth part, we will apply this parameterization of the numerical wind tunnel on 3 scales of buildings in urban site. This approach will allow us to specify the geometries of concrete models of buildings and wind speed amplification devices, in order to adjust the calculation model to this scale and this type of context. Calculation after calculation, we will be able to refine the profiling of the building and the implantation mode of the energy collection device.

# PART 4

## METHODOLOGY FOR INTEGRATING DEVICES INTO ARCHITECTURAL ENVELOPES



### Contents:

- Analysis of wind behaviour in urban areas and surveys
- Numerical wind modeling in urban areas
- Study of wind gas pedals
- Case Study 1: A low volume in an open area
- Case Study 2: A residential building in a suburb-type site
- Case study 3: A building-island (IGH) in a windy site
- Realization of CNC prototypes of these devices (scale 1)



4.0 INTRODUCTION.....	159
1. PRESENTATION OF THE METHODOLOGY .....	159
1.1. Wind behaviour surveys in urban areas .....	160
1.2. Wind data extraction with a connected anemometer .....	163
1.3. Calibration of the numerical simulation with respect to the insitu surveys .....	163
2. NUMERICAL MODELLING - THEORETICAL STUDY 1 : A LOW VOLUME IN AN OPEN AREA.....	164
2.1. Initial study without foil in vertical section .....	165
2.2. Studies of horizontal gas pedals of the Aerofoil type.....	166
• Foil type H1 .....	166
• Foil type H4 .....	172
• Foil type H5 .....	173
• Conclusion.....	174
3. THEORETICAL STUDY 2 : VERTICAL ACCELERATORS - BUILDING PLAN WITH FOIL TYPE V1 .....	174
• Introduction .....	174
3.1. Theoretical study 2: without foil in horizontal section.....	176
3.1. Study with vertical foil V1 at 45° .....	177
3.2. Study with foil V2 and quarter-circle building angle cut .....	178
3.3. Study with V3 foil at 90° to the façade.....	179
3.4. Study with foil V4 and rounded building angle .....	180
3.5. Study with foil V5 and 45° building angle cutting .....	181
• Conclusion.....	182
4. THEORETICAL STUDY 3 : ACROTHERIAL DEVICES.....	182
• Initial wind study on acroterion.....	182
• Wind study on acroterion with device A1 .....	183
5. THEORETICAL STUDY 4: A HOUSING BUILDING IN AN URBAN SUBURB - BUILDING AT 136 AVENUE PARMENTIER, 75011 PARIS.....	184
• Wind surveys on the apartment building .....	184
• Initial study of wind on the roof of the Mansard .....	188
• Wind study with M1 foil on the roof of the Mansard.....	189
6. THEORETICAL STUDY 4 : AN IGH BUILDING IN A SALES SITE .....	190
6.1. Presentation of the context of the Paris Val-de-Seine School of Architecture (75013) .....	190
6.2. Method of wind surveys around this island building .....	191
6.3. School of Architecture Paris Val-de-Seine (75013).....	192
6.4. Method of aeraulic simulation in urban area of the ENSAPVS site.....	194

6.5.	Airflow study in vertical sections of the building.....	196
6.6.	Study of the building-island in horizontal sections at different altimetries .....	198
	• Building study at 12m.....	198
	• Building study at 25m.....	199
	• Conclusion .....	199
6.7.	Study of an area in detail at the level of the 2 towers.....	200
6.8.	Study of a building zone with the addition of wind speed foil mplification .....	201
6.9.	Other analysis with profiled foils to create a stabilized airflow zone.....	202
	• Conclusion .....	202
7.	ASSESSMENT OF THESE 4 STUDIES .....	203
8.	STUDY OF WIND TURBINES ADAPTED TO ARCHITECTURAL INTEGRATION .....	203

## 4.0 INTRODUCTION

This section discusses the method adopted for the analysis of wind flow at the periphery of several typologies of architectural volumes. In order to understand the complexity of the role of the urban environment on wind flow in the city, we have chosen to study 3 sites of different scales.

**The objective of this approach is to categorize the different types of wind in urban areas. This characteristic, and in particular the identification of the spectrum of minimum and maximum winds, makes it possible to define the choice and the performance of the devices of energy capture, the mode of fixing in roof of building, the type of wind, the altimetry of the device compared to the levels of the roofs, the potential nuisances around.**

We wish to develop a method to identify **the optimal location for wind turbines** on the periphery of a building and to achieve an improvement of the extracted energy performance by studying the positioning of a wind amplification wing on the building. This type of analysis has also been developed by Baskaran and Kashef<sup>113</sup> of the Institute for Research in Construction (Canada), or that of Tominaga and Akabayashi<sup>114</sup> of the Niigata Institute of Technology by implementing flow simulation techniques around buildings and their roofs.

But in our case, we have established wind measurements with in situ anemometers, and modeled a localized mapping of urban winds. On-site experimental measurements are therefore used as a mode of calibration and verification of numerical simulations without wind devices. Instead of a theoretical wind study on a building, we combined numerical wind simulations using the STAR CCM+ software with wind surveys, over long periods of time (more than 1 year). By combining this information with a numerical wind tunnel analysis, we hope to define the rules for the implementation of wind turbines and air control devices on the building's surroundings.

### 1. PRESENTATION OF THE METHODOLOGY

For this research, we used connected ultrasonic anemometers of the type Netatmo<sup>115</sup> which were implemented on 3 study sites (Figure 146). These anemometers, intended for use in consumer weather stations, are remarkably reliable for a moderate price and transmit wind data in real time via a wifi terminal near the anemometer. The wind data, provided continuously at each of these points, are then fed into the digital wind tunnel that we have set up on STAR CCM+.

---

<sup>113</sup> Appupillai BASKARAN and Ahmed KASHEF, "Investigation of air flow around buildings using computational fluid dynamics techniques," *Engineering Structures*, November 1, 1996, vol. 18, n°11, pp. 861-875.

<sup>114</sup> Yoshihide TOMINAGA, Shin-ichi AKABAYASHI, Takuya KITAHARA, and Yuki ARINAMI, "Air flow around isolated gable-roof buildings with different roof pitches: Wind tunnel experiments and CFD simulations," *Building and Environment*, January 1, 2015, vol. 84, pp. 204-213.

<sup>115</sup> Ultrasonic anemometers connected to a wireless network like Netatmo. See the readings over one year on the meteo application : meteo@serero.com, mp :Concours1

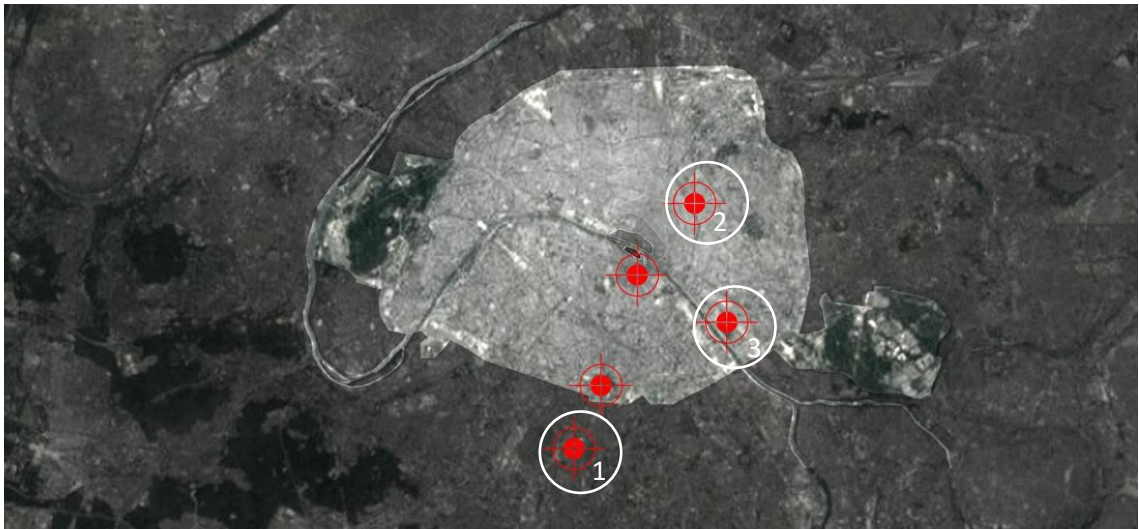


Figure 147 Location of the 3 study sites with wind monitoring stations installed by Serero from 2016 to 2020

The use of this type of Netatmo connected weather station has already been made to generate externalized data by several researchers such as for example Chapman and Bell<sup>116</sup> who revealed in 2017, thanks to this system, under the effect of solar radiation, temperature differences in real time of 1 to 6°C in the streets of the city of London.

More precisely, this method allows to calibrate the numerical simulation from precise and real wind surveys on site, and then to develop the complete volumetric model of the wind behavior on a roof area, or an entire city block.

This study can only be done by retrieving a stream of geo-localized data, and relating this information to the technical specifications of wind turbines, their energy performance and their engagement speed<sup>117</sup>. **We can thus, thanks to this method, define the characteristics of wind turbines to maximize their performance in an urban site and in a turbulent airflow regime.**

### 1.1. Wind behaviour surveys in urban areas

---

<sup>116</sup> Lee CHAPMAN, Cassandra BELL, and Simon BELL, "Can the crowdsourcing data paradigm take atmospheric science to a new level? A case study of the urban heat island of London quantified using Netatmo weather stations," *International Journal of Climatology*, 2017, vol. 37, n°9, pp. 3597-3605.

<sup>117</sup> Switch-on speed: the rotor starts moving as soon as the wind reaches 2 m/s (up to 4 m/s, the production is null)



Figure 148 Etude d'un volume architectural bas pour l'intégration de micro-éoliennes et de foils. (H=9m)



Figure 149 Etude d'un immeuble de dans un îlot urbain d'échelle intermédiaire (H=35m)



Figure 150 Etude de bâtiment-îlot en bordure de Seine de grande échelle (H=75m)



Figure 151 Etude complémentaire d'un bâtiment de très grande échelle dans un espace dégagé (Esplanade La Défense) (H=110m)

We develop in this part three case studies of buildings from urban environment with multiple historical layers<sup>118</sup> whose diversity of typology and construction allows to consider different modes of wind energy capture. We also study in this part the implementation of a wind gas pedal associated with buildings. The aerofoils<sup>119</sup> (see chapter 5.1.7 on Aerofoils) which are integrated in this study, allow to control the air speed, to direct it on the generating turbine, but also to accelerate it. It also allows to hide, thanks to its profile, the device on the roof of the building. Wind behaviour in urban environment

The wind information collected by these connected anemometers allows us to obtain the following information: direction, (omnidirectional, unidirectional or bidirectional), speed and frequencies.

<sup>118</sup> See the historical study of Parisian blocks in chapter 2 of this research.

<sup>119</sup> Aerofoil, or airfoil: blade (lat: folia) which allows to control the movement of the air on a given surface, either by compressing the air stream to accelerate its speed, or to use its lift (aviation) or its support (car racing)



Figure 152 - Installation d'un anémomètre connecté sur une maison à Arcueil (92) par D. Serero



Figure 153 Vue toiture de l'anémomètre connecté sur une maison à Arcueil (92) par D. Serero

The measurement of these winds carried out precisely **at the level of the envelope (periphery) of the building**, and not by extrapolation from a remote meteorological station or in open space sites (not representative of the urban context), such as Charles De Gaulle and Orly airports, provides precise information on :

- the specific impact of the architecture on the wind at a given point.
- the presence of surrounding urban landscape elements such as gable walls, or the presence of wind corridors that punctually modify the movement and speed of the resulting wind.

A map of all the Netatmo anemometers<sup>120</sup> (Figure 153) located in Paris shows, at the same time, wind directions in the urban area almost at 360°, without any precise direction being defined or clearly identified.

In the following aeraulic studies, we compared **the control wind speed measurement in free space (no building) nearby, and the average wind speed measured at several locations on a building** (at the ends of the building, at the façade or at the roof).

For reasons of **calculation time**, but also simplicity and accuracy of reading, these simulations were made on vertical sections or horizontal sections of the building. This allows to limit the number of mesh points<sup>121</sup> of the aeraulic analysis, and to reduce the calculation time. On complex buildings where the analysis and the position of the turbines should be refined, **a complete study in a 3-dimensional calculation allowed to improve the accuracy of the analysis.**

<sup>120</sup> *Connected Anemometer*, <https://www.netatmo.com/fr-fr/weather/weatherstation/anemometer>,

<sup>121</sup> The number of meshes defines the accuracy and number of points for wind analysis in a numerical wind study

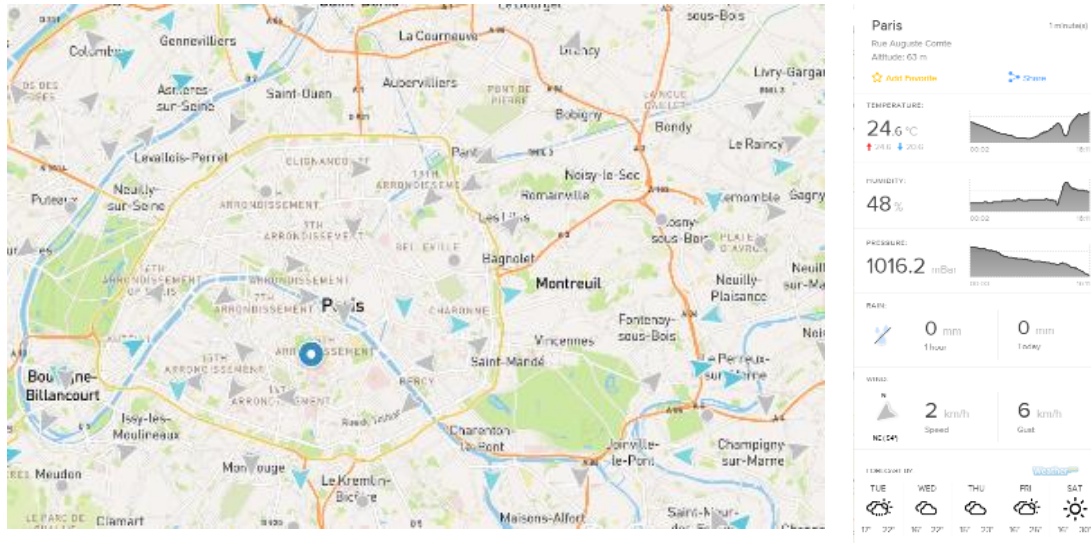


Figure 154 Wind map of Paris measured by Netatmo anemometers

## 1.2. Wind data extraction with a connected anemometer

These comparisons were used to calibrate the numerical simulation device. **The anemometer measures the time between sending and receiving a signal in two perpendicular directions.** The velocities on the N-S and W-E axes are then combined using trigonometric functions to obtain the actual velocity and direction.

The data realized by these devices (See figures 83 and 85) are the following:

- 1- Average speed and direction over the last 5 minutes. The arrow indicates the wind direction and its size is proportional to the speed. Light grey lines around the icon indicate the dominant wind directions during the last hour. An arrow pointing downward indicates a north wind ( $N=0^\circ$ ). An arrow pointing to the left indicates an East wind ( $E=90^\circ$ ).
- 2- Speed and direction of gust over the last 5 minutes.
- 3- Maximum burst (speed and direction) during the day (since midnight).

## 1.3. Calibration of the numerical simulation with respect to the insitu surveys

We sought to accurately calibrate the numerical simulation from accurate, real-world wind readings on site.

To achieve this, we followed the following method:

- Wind surveys with in situ anemometers, and modeling of localized and scaled urban wind mapping.
- Development of a 3D virtual model of the building and the neighborhood

- Numerical simulation of wind behavior on the same roof as the one surveyed with the same incident wind
- Comparison of wind speeds in the virtual model and in the surveyed area
- If the data are equivalent, within 3%, the numerical model is acceptable. If the differences are larger, model a larger urban area and adjust the boundary conditions and the roughness of the urban profile. Then another comparison.
- This method is repeated until a similarity of the virtual model/on-site survey behaviors is obtained.
- Instead of a theoretical wind study on a building, we have combined numerical wind simulations using the STAR CCM+ software with wind surveys, over long periods of time (more than 1 year). By combining this information with a numerical wind tunnel analysis, we hope to define the rules for the implementation of wind turbines and air control devices on the building's surroundings.

## 2. NUMERICAL MODELLING - THEORETICAL STUDY 1 : A LOW VOLUME IN AN OPEN AREA

The first case study that we carried out, is based on the wind flow on a simple volume on 2 or 3 levels of type individual house located at Arcueil with double slope roof. We realized a 3D model of this example and we studied the wind behavior on this volume before the installation of an IED<sup>122</sup> and then after the fixation of a wind speed increase device. The volume is studied in vertical section, and in a clear site in order to be able to more easily compare the evolution of wind speeds between each study.

---

<sup>122</sup> Building-integrated wind device

## 2.1. Initial study without foil in vertical section

This study concerns an architectural volume of 9 m high by 5 m wide of individual house type with a side wind.

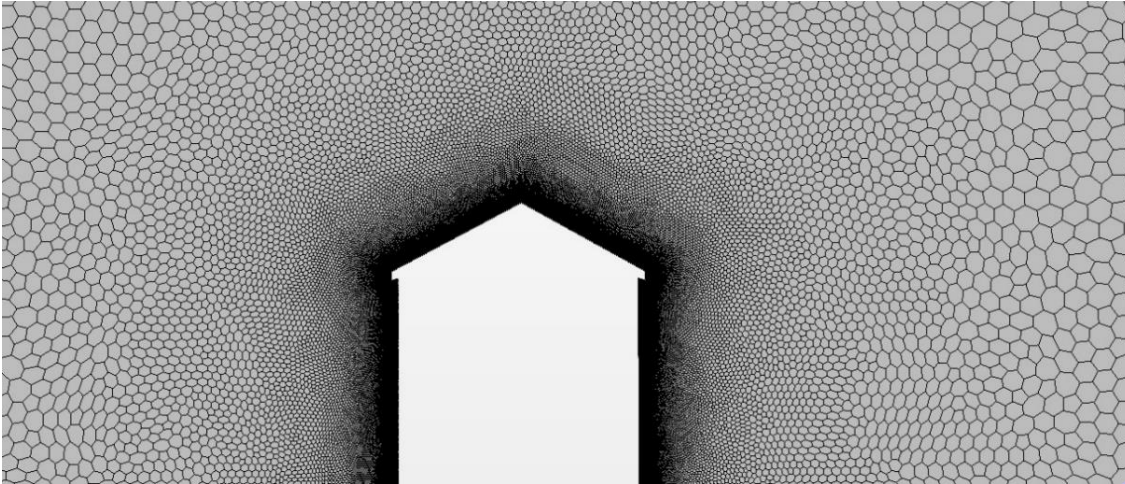


Figure 155. Mesh of the 2D model of the typical house

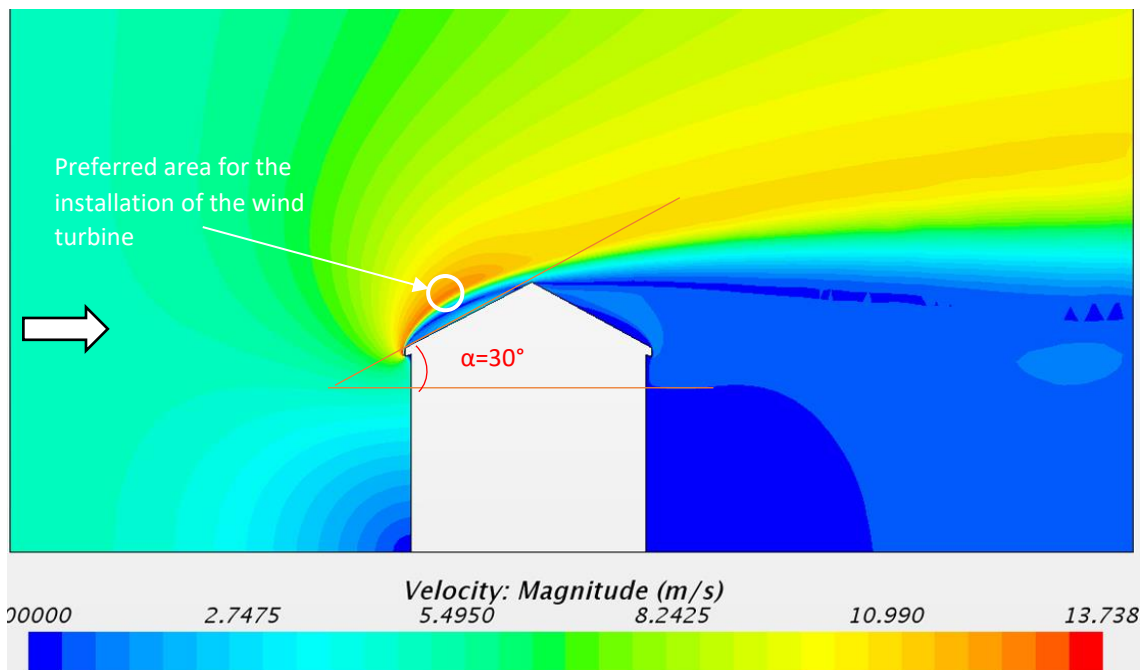


Figure 156. False color study of the wind speed around the house

This first wind study, without any added device to the building, shows that a double-sloped roof has the ability to accelerate an incoming wind of 10 m/seconds to a wind speed of 12 m/s at 1m above the ridge, i.e. a 20% increase in the air speed above the building by the simple profile of the double-sloped roof

## 2.2. Studies of horizontal gas pedals of the Aerofoil type

The following studies integrate an amplification wing profile called aerofoil implanted at 1.50 m above the ridge and fixed on the roof structure. These successive studies show that the air speed progressively increases from 10 to 16 meters per second, **i.e. an increase of 30% of the air speed by adding this device** (see figure 156). In this study, the supporting structures of the wing were not modeled but their mask represents 0.5% of the airflow area and we considered them as having a marginal impact on the calculation.

An analysis of the wind speed zones generated by this study, allows to **locate very precisely the hot spots (red zones) in plan and in section on the building** (Fig. 156 to 168).

- *Foil type H1*

The H1 foil type is a curved profile (approximately 45° of the circle perimeter, 5m radius of curvature) fixed above the roof at the ridge axis. This shape was chosen to compress the air stream evenly and progressively at the roof level of the building. The compression effect of the air stream is provided by the slope of the building roof and the curve of the foil. For an emergent wind of 5 m/s, the air speed at the back of the foil (approximately 1 m from the ridge axis) is 16 m/s, **i.e. an increase of 3.2 times the incoming air speed**. This flow is stationary.

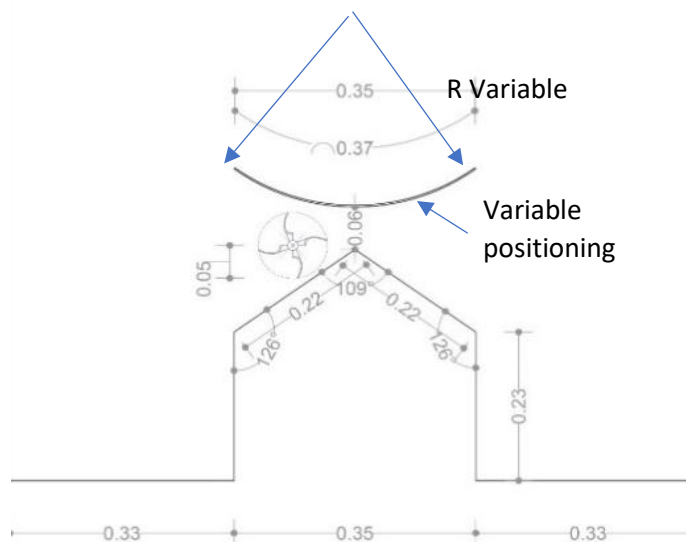


Figure 157. Dimensional study of the digital/physical model of the house with foil .

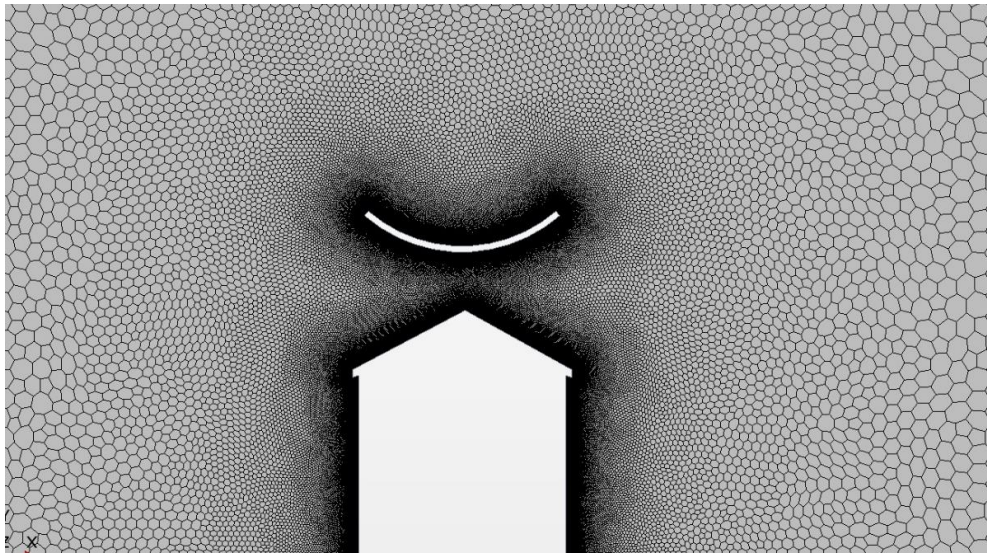


Figure 158. Mesh of the 2D model of the house with foil type 1

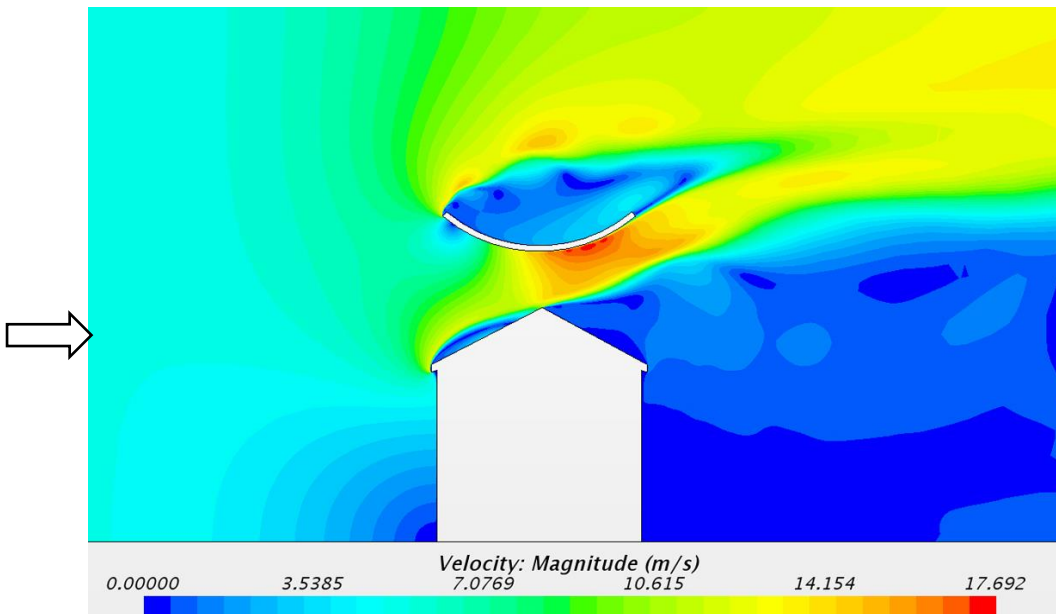


Figure 159. False color study of the wind speed around the house with foil type 1

- Foil type H2

The H2 foil type is a curved profile (approx. 35° of the circle perimeter, radius of curvature 9m) fixed above the roof at the ridge axis. The distance between the roof and the profile is 1.40 m and the radius of curvature is larger than that of the H1 foil. The compression effect of the air stream is provided by the slope of the roof and the curve of the foil. For an emergent wind of 5 m/s, the air speed at the back of the foil at approximately 1 m from the ridge axis is 14.5 m/s, i.e. an increase in wind speed of 2.9 times the incoming air speed.

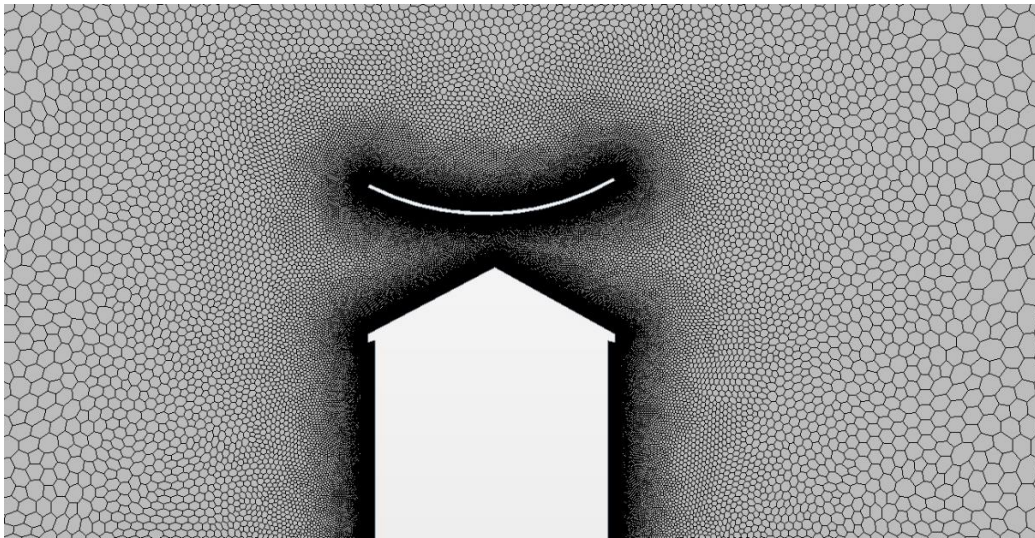


Figure 160. Mesh of the 2D model of the typical house with foil type 2

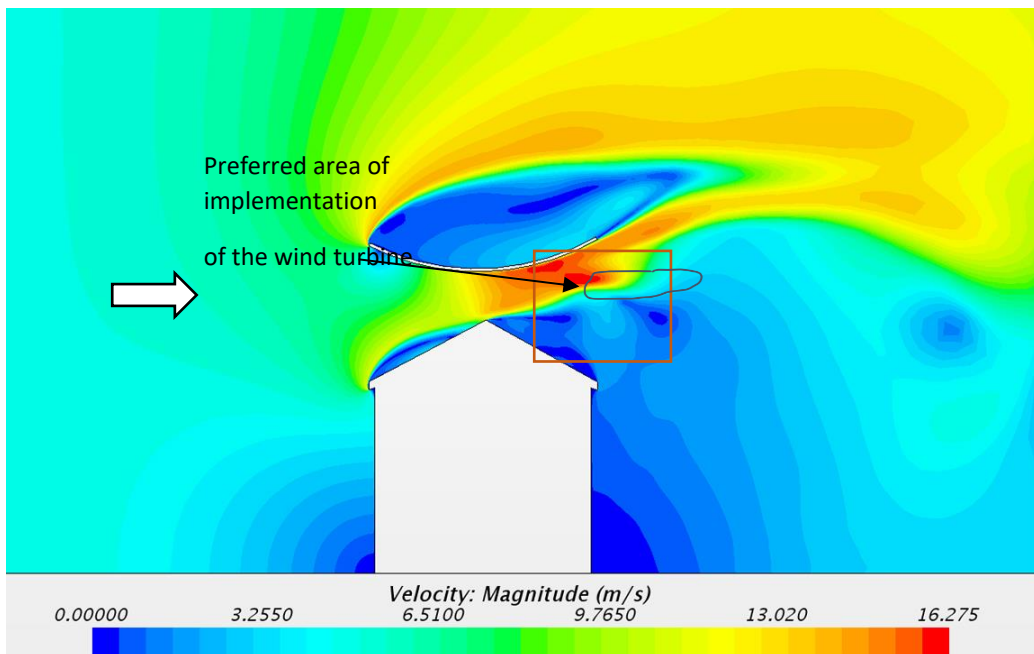


Figure 161. False color study of wind speed around the house with foil type 2 . The red rectangle shows the enlarged area in Figure 167.

Can we refine the analysis of the wind flow behavior in the area between the roof and the aerofoil, in order to specify the most interesting area for the implementation of an energy generating device?

To do this, we performed a detail of the numerical simulation on the part above the ridge to refine the areas of increased wind speed. Here we have gridded the cross-section through the volume of air above the roof in a square of 25cm high by 25cm wide. This grid allows us to refine the reading of the phenomenon of increasing air speed.

We note a zone of increased wind speed in the median axis between the foil and the roof ridge (13.2 to 14 m/s), as well as a zone under the foil of maximum wind speed. This zone 1 (see figure 159) in the shape of a triangle is difficult to use for a device with a diameter of 0.80 m to 1.20 m.



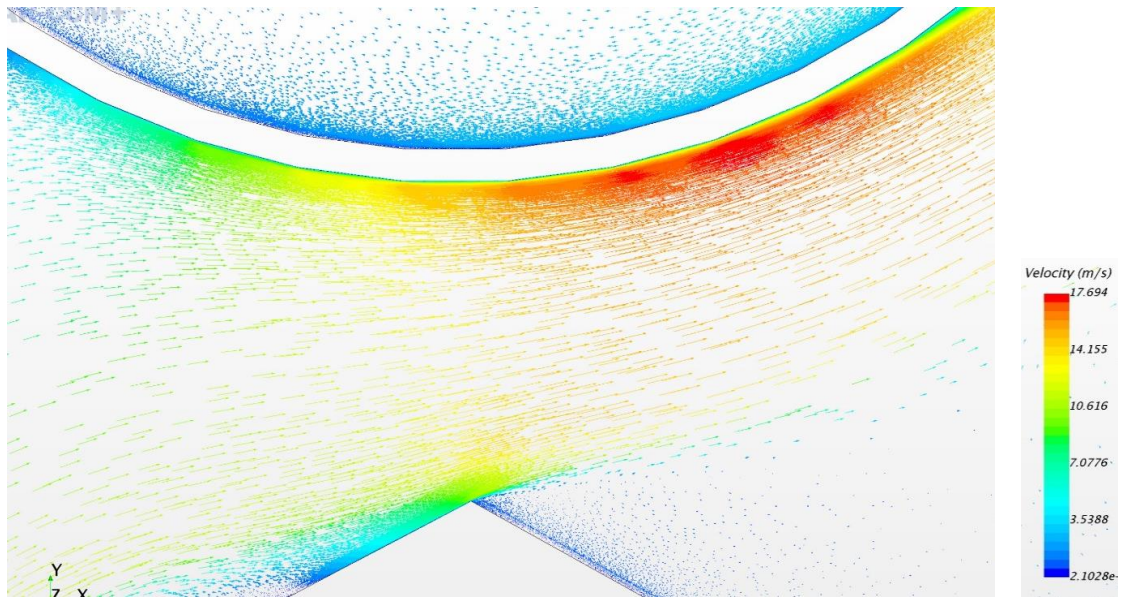


Figure 163 : Champ vectoriel du vent au dessus de la maison avec foil type 2

Figure 162 shows a vector field between the roof and the foil. This field allows to measure by the length of the vectors the wind speed, and by the orientation of the vector, the wind direction in each of these points. The direction of movement of the wind is oriented towards the reddest area. These vectors give information on the location and angle of the wind turbine to be positioned in this area.

- Foil type H3

The foil type H3 is an inverted circle profile fixed above the roof and offset by 1.5m from the ridge axis. The distance between the roof and the profile is 1.40 m. The compression effect of the air stream is ensured by the slope of the house roof and the curve of the foil. **For an emergent wind of 5 m/s, the wind speed at the back of the foil at approximately 1 m from the ridge axis is 11.5 m/s, i.e. an increase of 2.3 times the incoming air speed.**

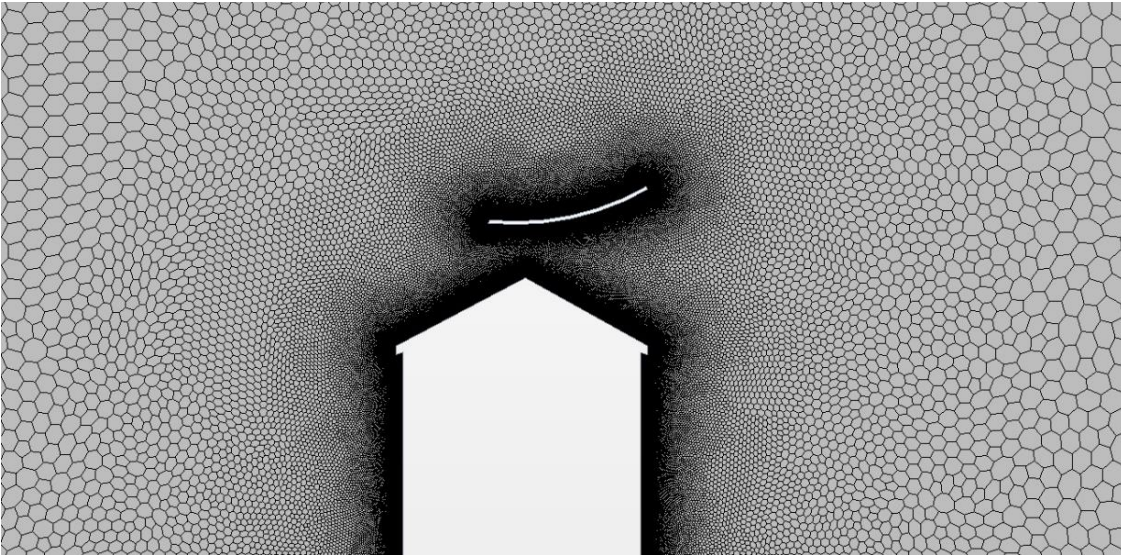


Figure 164. Mesh of the 2D model of the typical house with foil type 3

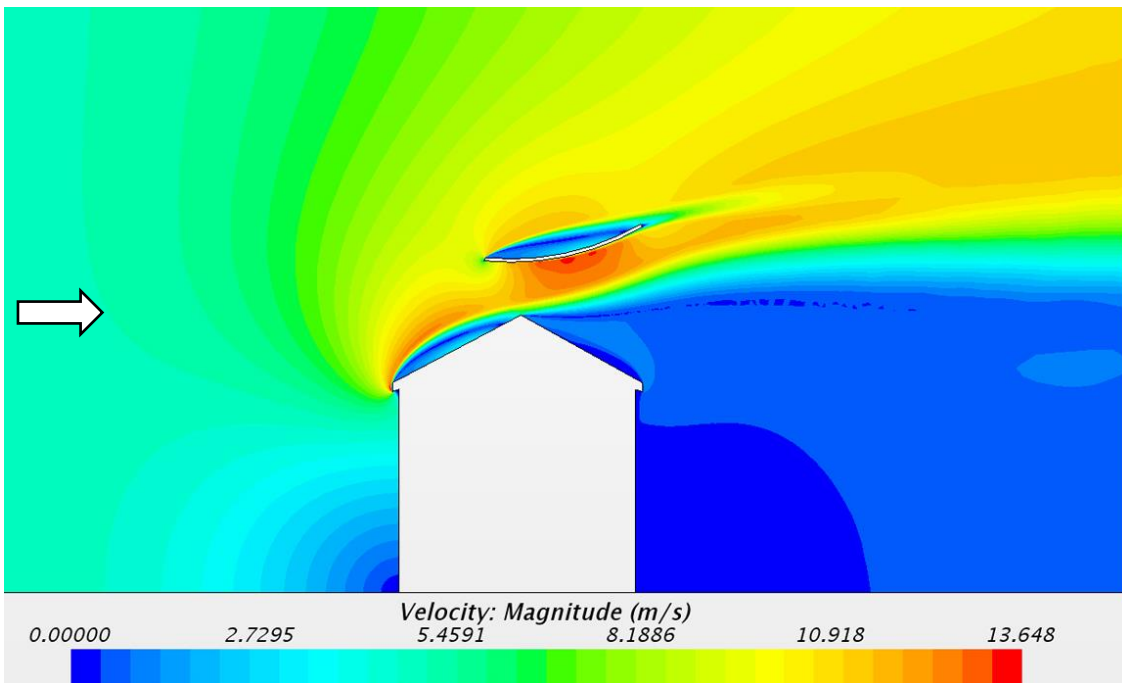


Figure 165. False color study of the wind speed around the house with foil type 3

- *Foil type H4*

The foil type H4 is an inverted circle profile fixed above the roof with an offset of 1.5m horizontally to the ridge axis. The distance between the roof and the profile is 1.40 m. The compression effect of the air stream is ensured by the slope of the house roof and the curve of the foil. **For an emergent wind of 5 m/s, the wind speed at the back of the foil at approximately 1 m from the ridge axis is 14.0 m/s, i.e. an increase in speed of 2.8 times the incoming air speed.**

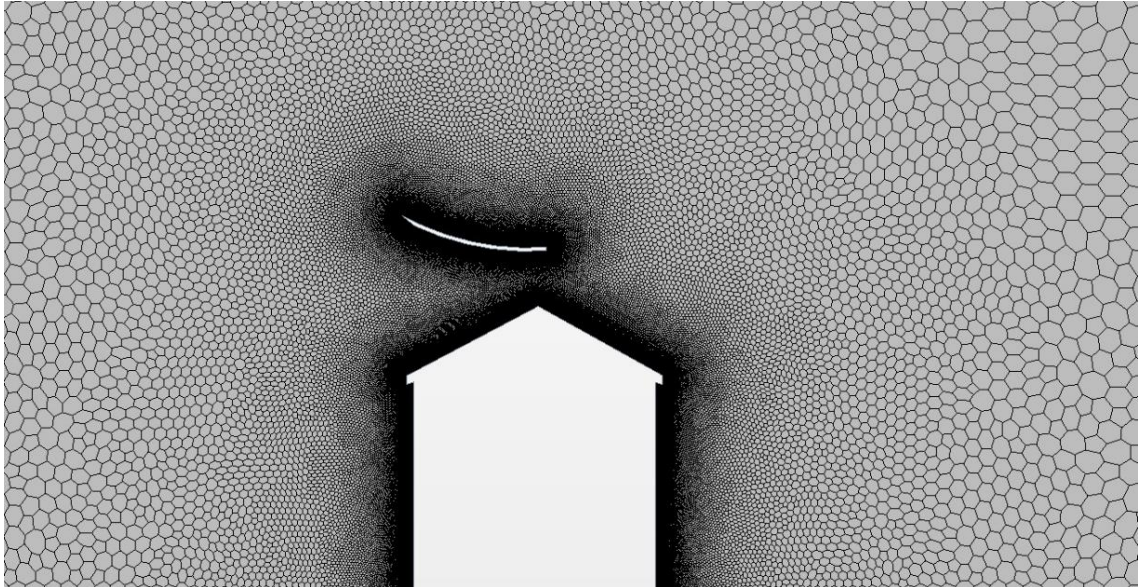


Figure 166. Mesh of the 2D model of the typical house with foil type 4

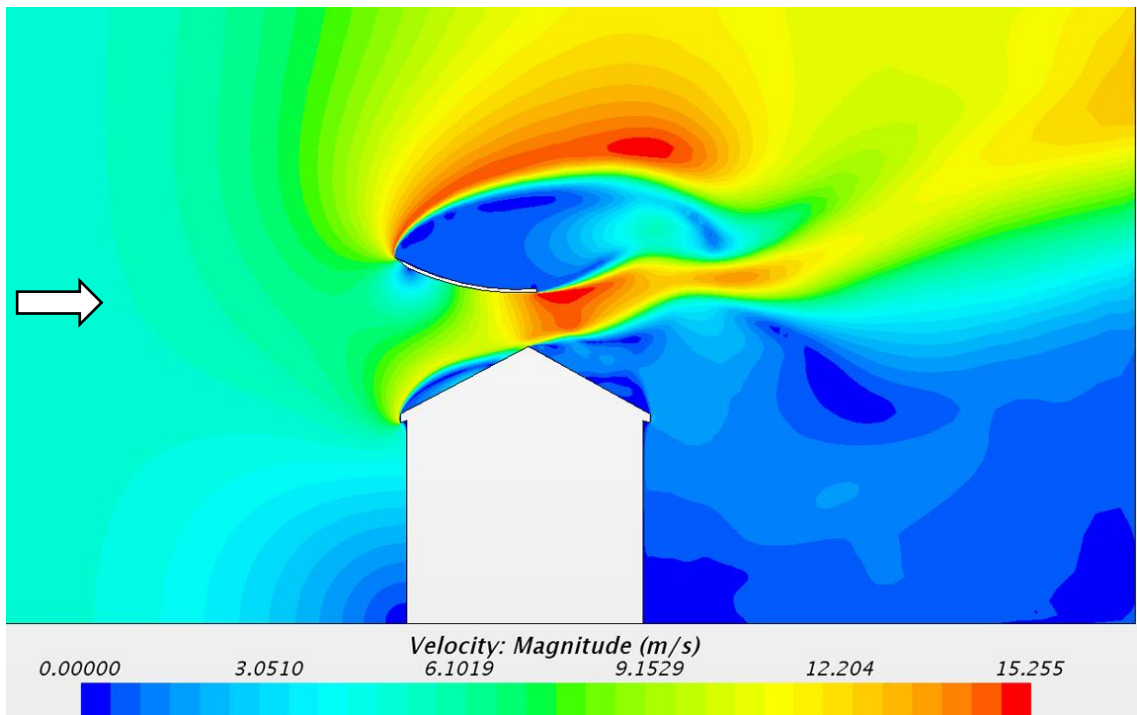


Figure 167. False color study of the wind speed around the house with foil type 4

- *Foil type H5*

We also studied the impact on the wind of a butterfly type V foil. The tip of the profile shape does not allow to progressively increase the air speed on its shape.

We note that in these studies the aerofoils studied are profiles without any camber, in order to limit the effects of lift or the effects of support created by the air movement on the architecture. The adjustment of these elements will be specific to each building.

The foil type 5 is an inverted V-profile (slopes symmetrical to the roof in relation to the horizontal) fixed above the roof at the ridge axis. The distance between the roof and the profile is 1.40m.

**For an emergent wind of 5 m/s, the wind speed at the back of the foil a, approximately 1 m from the ridge axis, is 13.0 m/s, an increase of 2.6 times the incoming air speed.**

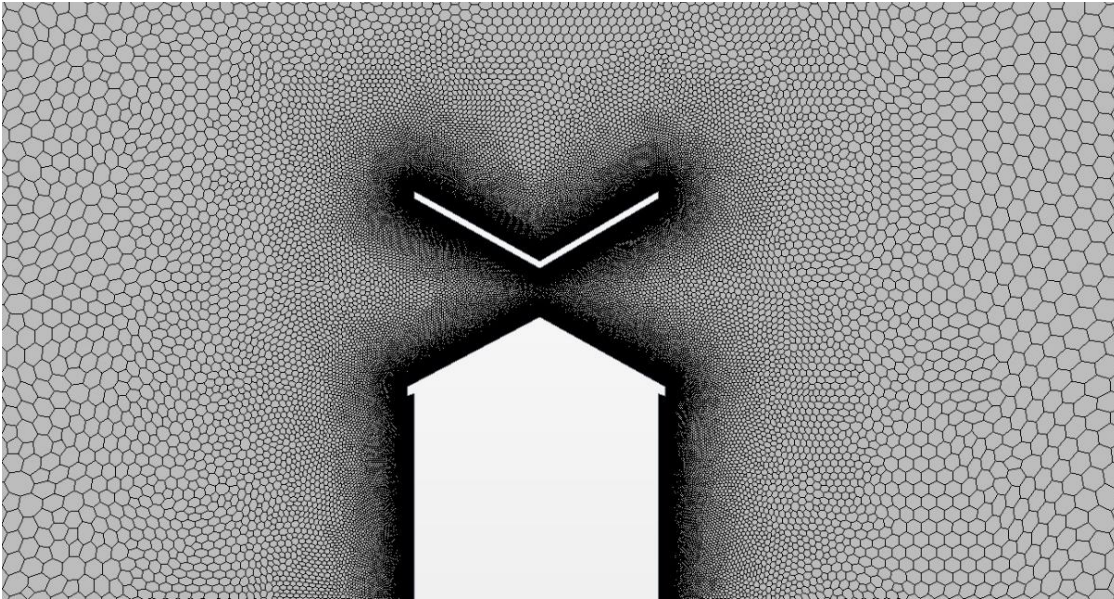


Figure 168. Mesh of the 2D model of the typical house with foil type 5

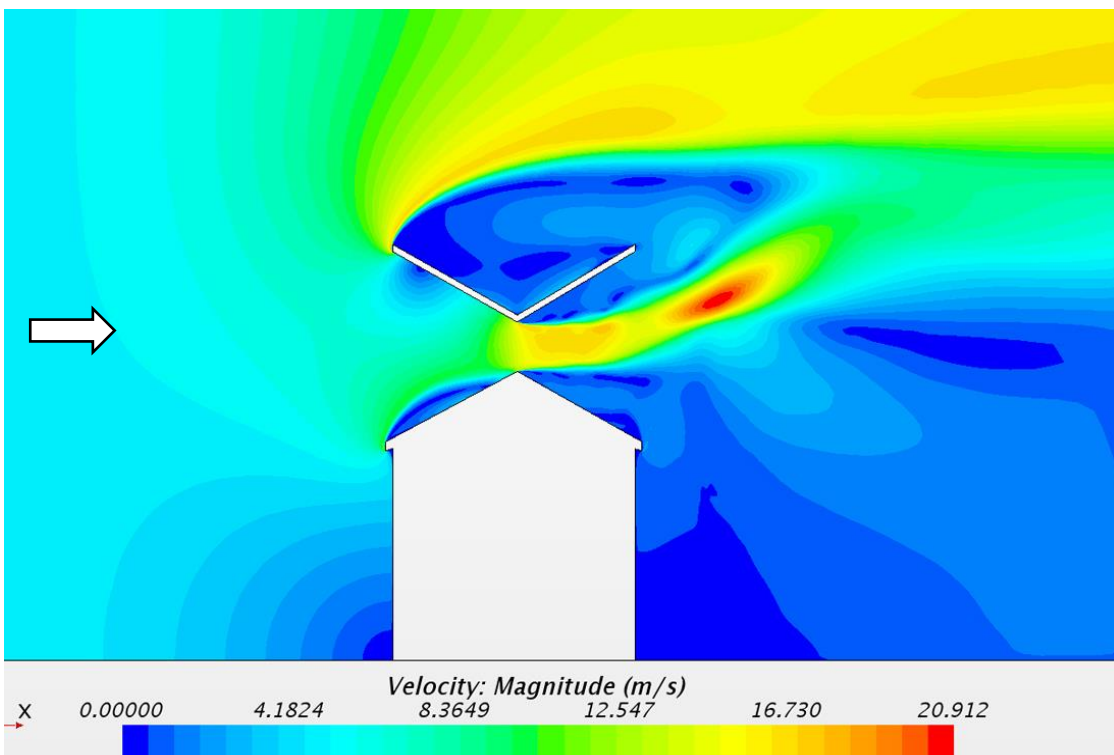


Figure 169. False color study of the wind speed around the house with foil type 5

- *Conclusion*

As a conclusion of this first study, we identify that an area of approximately 100% increase in wind speed is located at 1.50 m height and offset by 1.80m from the building's roof ridge axis. This analysis of the wind speed maps from the aerodynamic simulation identifies the areas of greatest increase in air speed. However, after several calculations and simulations, we could see that these areas are not always stable over time and can move towards the ridge axis. For these reasons, we have kept the implementation of the device at the axis of the roof rather than offset it from this line. These different case studies show that the angle of the foil with respect to the horizontal and the slope of the roof are key parameters to regulate and control the zones of strong wind gusts according to the Betz limit<sup>123</sup>. The red zone (of high wind speed) when larger on the simulation generates a more stable performance zone of the wind device. **The electrical power generated by a wind turbine in this zone of the simulations (see chapter 3.1.1) is in a ratio depending on the cube of the air speed, at a given location, so an increase in air speed of: 100% from 8 to 16 m/s corresponds to a power increase of coefficient 8.**

### 3. THEORETICAL STUDY 2 : VERTICAL ACCELERATORS - BUILDING PLAN WITH FOIL TYPE V1

- *Introduction*

In dense urban sites, the proximity of buildings and their verticality allows to favor vertical devices installed on the facade rather than on the roof. In these cases, the unfolding of the facades is superior to that of the roofs. The performance of these systems is amplified by the "wind corridor" effect of the streets. High-rise buildings, which exceed the average skyline of the city, are particularly exposed to the wind (and in particular because of the building's overhang of the urban "ground" boundary layer. Here we study several types of "foils" attached to the façade or corner of a building<sup>124</sup>. The distance of the foil from the building, its angle to the wind, and the relative position of the turbine are studied for an emergent wind of 5 m/s, the air speed at the rear of the foil approximately 1 m from the foil axis and 16.5 m/s, i.e., an increase of 3.3 times the incoming air speed. This flow is stationary<sup>125</sup>.

In the case of high-rise buildings, the facade surface is much larger than the roof surface. In these cases, the use of vertical aerofoils offers a larger surface area for energy collection.

This study was performed in plan, in a corner of the building with two types of wind speed and two types of wind arrival angles. We studied, in a first step, the relative position between the aerofoil angle and the building. We rounded and then chamfered the angle of the building facing the wind in order to guide the air over a greater length (see figures 169 and 170).

---

<sup>123</sup> Rupp CARRIVEAU, *Fundamental and Advanced Topics in Wind Power*, BoD - Books on Demand, 2011, 438 pp.

<sup>124</sup> ANNIE-CLAUDE BAYEUL-LAINÉ, "Three-dimensional modeling of the hydrofoil of Mr. Gérard WILLS using the Star CCM+ computational code", Study report, CNAM ParisTech, 2011.

<sup>125</sup> Dr. S. Srinivasa RAO, K. SHANMUKESH, M. K. NAIDU, and P. KALLA, "Design and Analysis of Archimedes Aero-Foil Wind Turbine Blade for Light and Moderate Wind Speeds," *International Journal on Recent Technologies in Mechanical and Electrical Engineering*, August 31, 2018, vol. 5, n°8, pp. 01 - 05-01 - 05.



Figure 170 3D studies of a 45° aerofoil on a rounded corner of a building

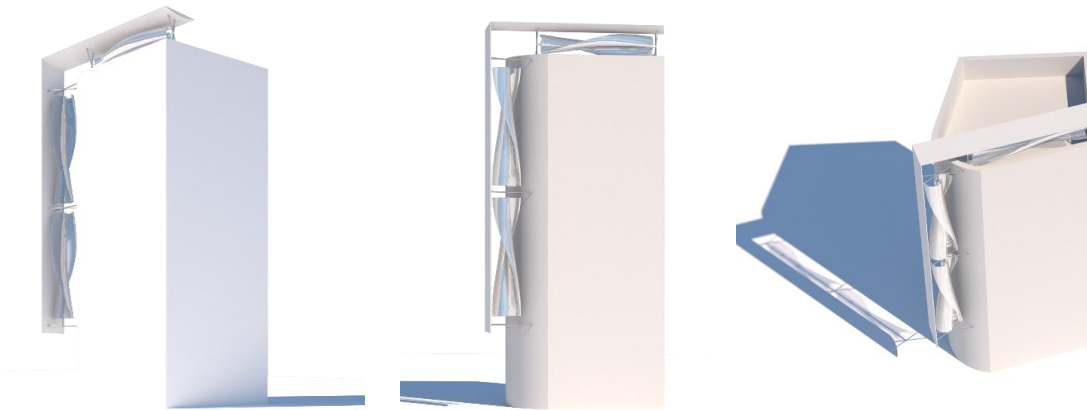


Figure 171 3D architectural studies of a 45° aerofoil installation on a pointed building

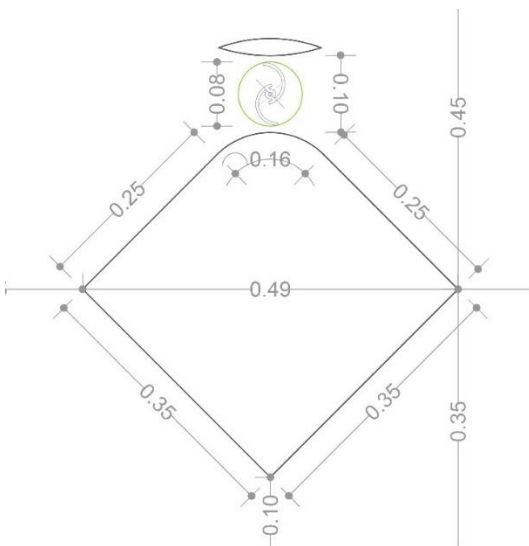


Figure 172. Etude dimensionnelle Foil vertical type H1, Echelle 1/20

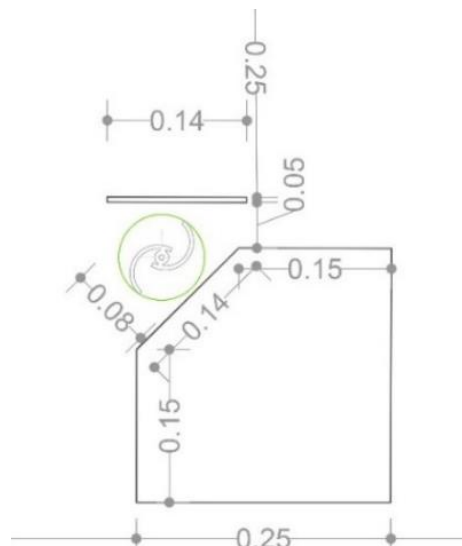


Figure 173. Etude dimensionnelle du foil vertical Type H2, Echelle 1/20

### 3.1. Theoretical study 2: without foil in horizontal section

This wind simulation, without any device added to the building, shows the airflow in plane on the rounded corner of a building (case of a building at the corner of 2 streets).

In the corner of the building, an increase in wind speed of 8 to 10 m/s can be observed with an incoming wind of 5 m/second due to the angle formed on the ground between the wind direction and the position of the building.

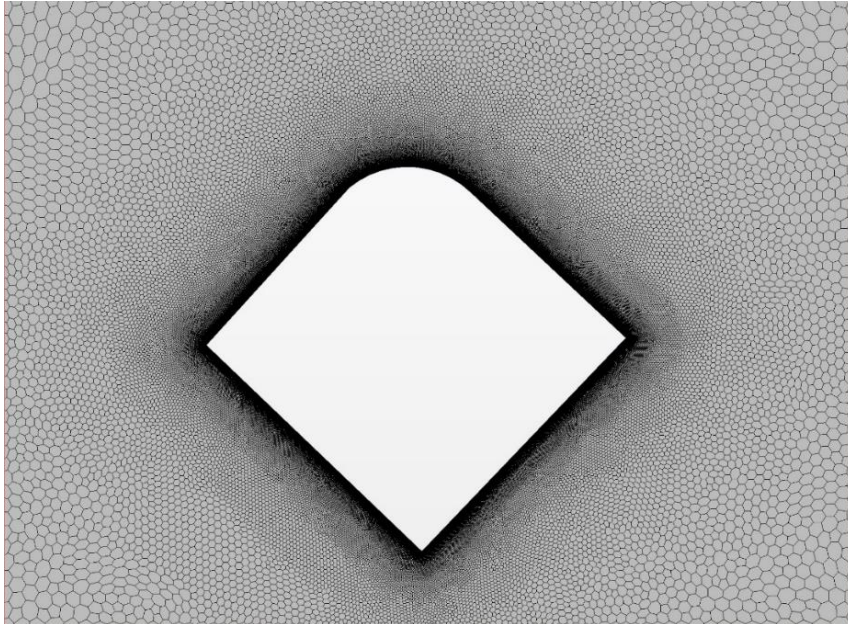


Figure 174. 2D model mesh of the building study area without foil

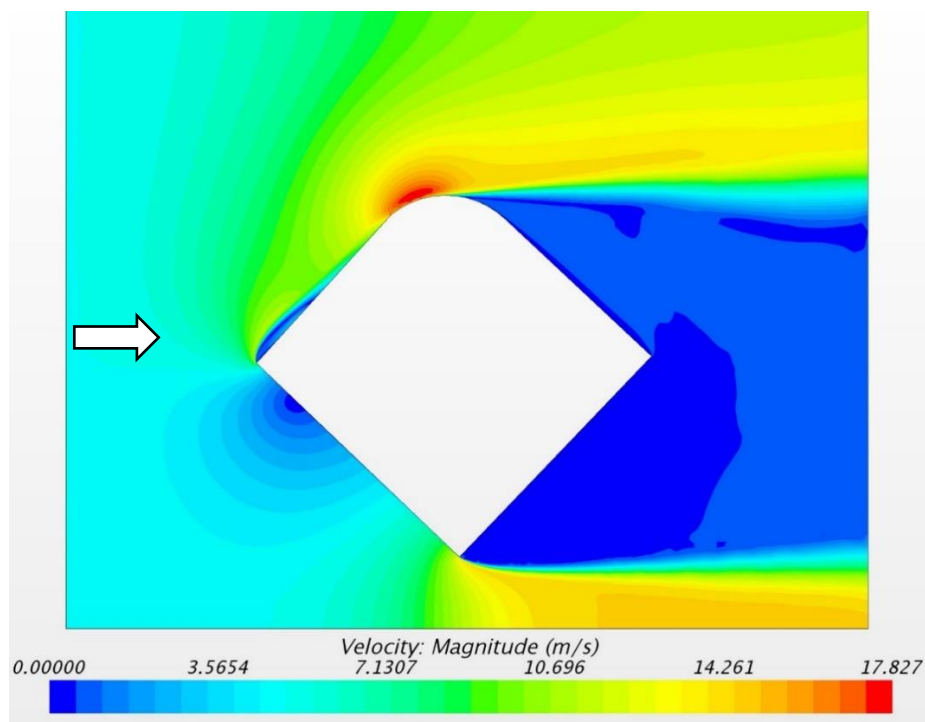


Figure 175. False color study of wind speed without foil

### 3.2. Study with vertical foil V1 at 45°.

The foil type V1 is an airfoil located in the corner of the building at 45°. The distance between the building and the profile is 1.00 m. The compression effect of the air stream is provided by the angle of the building and the curvature of the foil. For an emergent wind of 5 m/s, the increase in wind speed between the building and the foil is approximately 14 m/s, i.e. an increase of 2.8 times the incoming air speed.

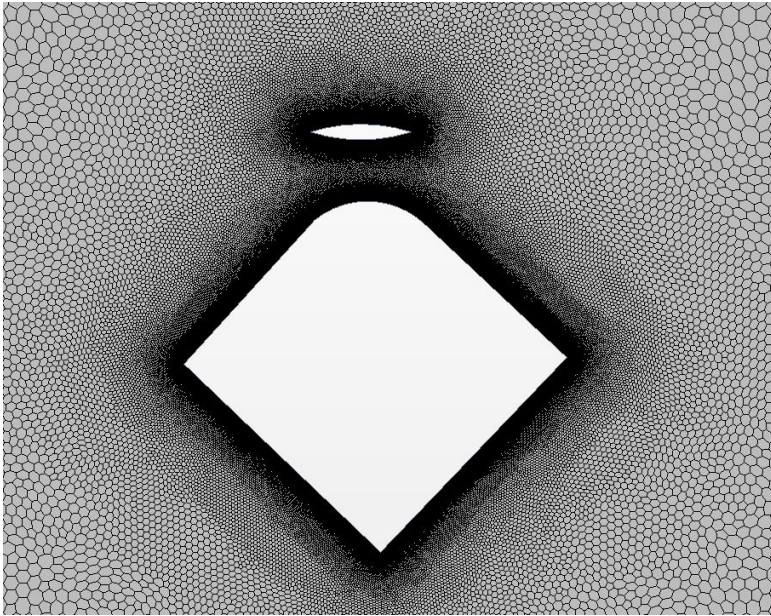


Figure 176. 2D model mesh of the building study area with integrated V1 foil type.

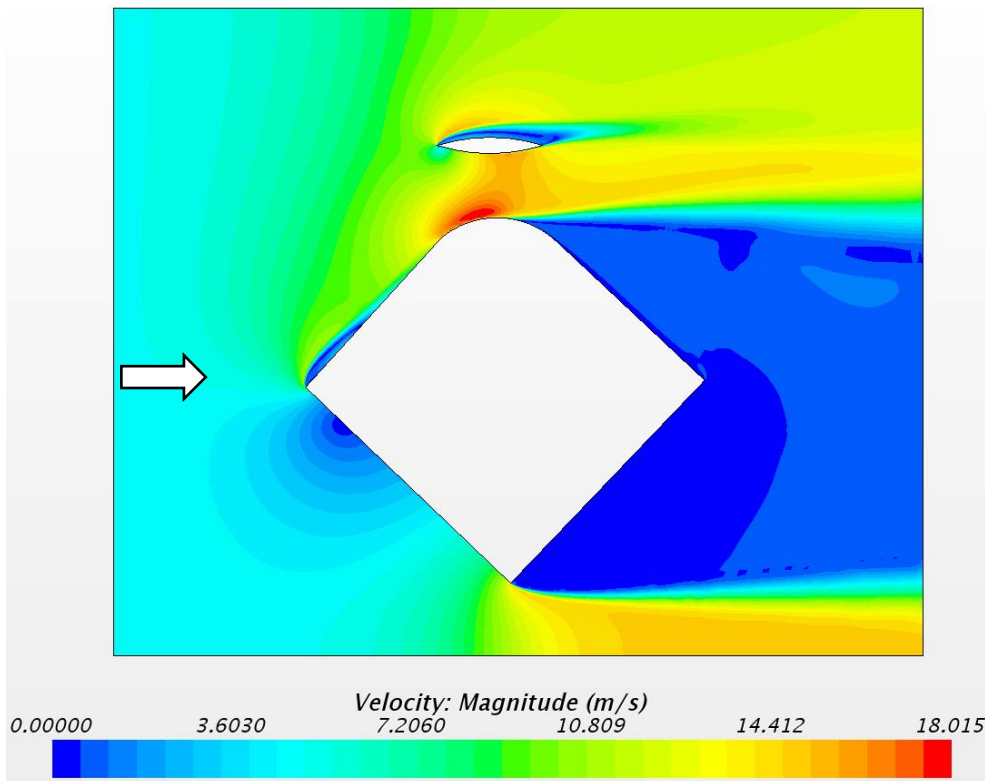


Figure 177. False color study of the wind acceleration around the integrated vertical foil type V1

### 3.3. Study with foil V2 and quarter-circle building angle cut

The foil type V2 is an airfoil positioned parallel to one of the building's facades. The distance between the building and the profile is 0.60 m. The hollow cut of the profile of the building allows the embedding of the wind turbine in the volume of the building to limit its visual impact. For an emergent wind of 5 m/s, the increase in wind speed between the building and the foil is approximately 9 m/s, an increase of 1.3 times the incoming air speed.

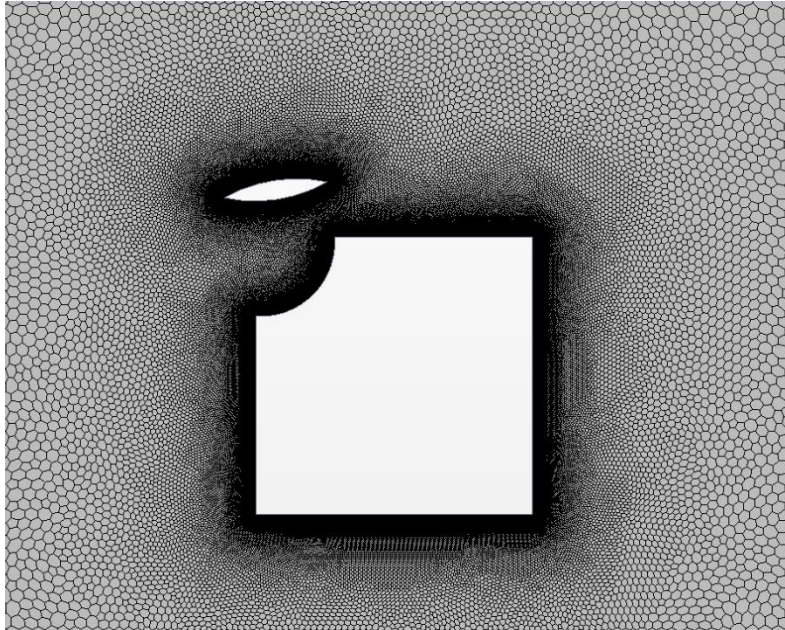


Figure 178. 2D model mesh of the building study area with integrated foil type 2

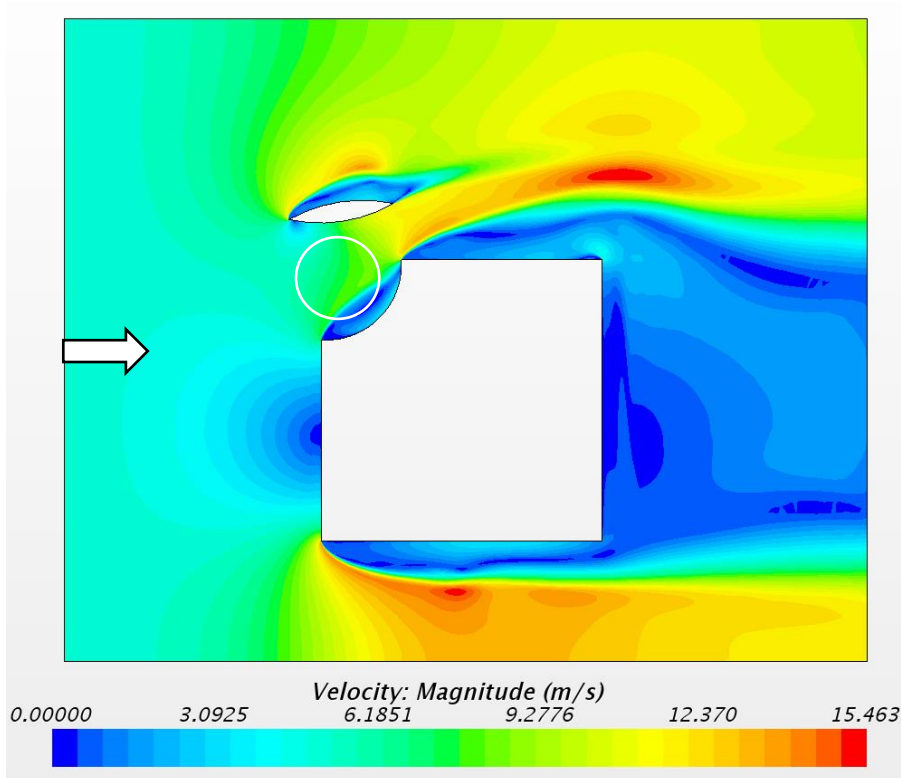


Figure 179. False color study of the wind speed around the integrated vertical foil type 2 . This simulation shows that this choice of hollow volume has no interest in accelerating the air in place

### 3.4. Study with V3 foil at 90° to the façade

The foil type V3 is an airfoil positioned parallel to one of the building's facades. The distance between the building and the profile is 1.10 m. The compression effect of the air stream is provided by the angle of the building and the curvature of the foil. **For an emergent wind of 5 m/s, the wind speed between the building and the foil is approximately 12 m/s, i.e. an increase of 2.2 times the incoming air speed.**

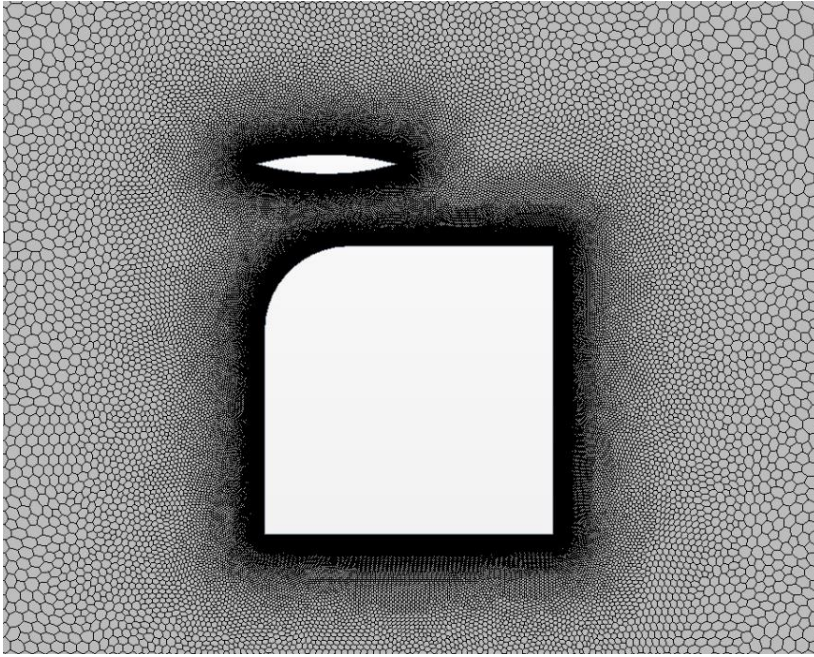


Figure 180. Mesh of the 2D model of the building study area with integrated V3 foil type

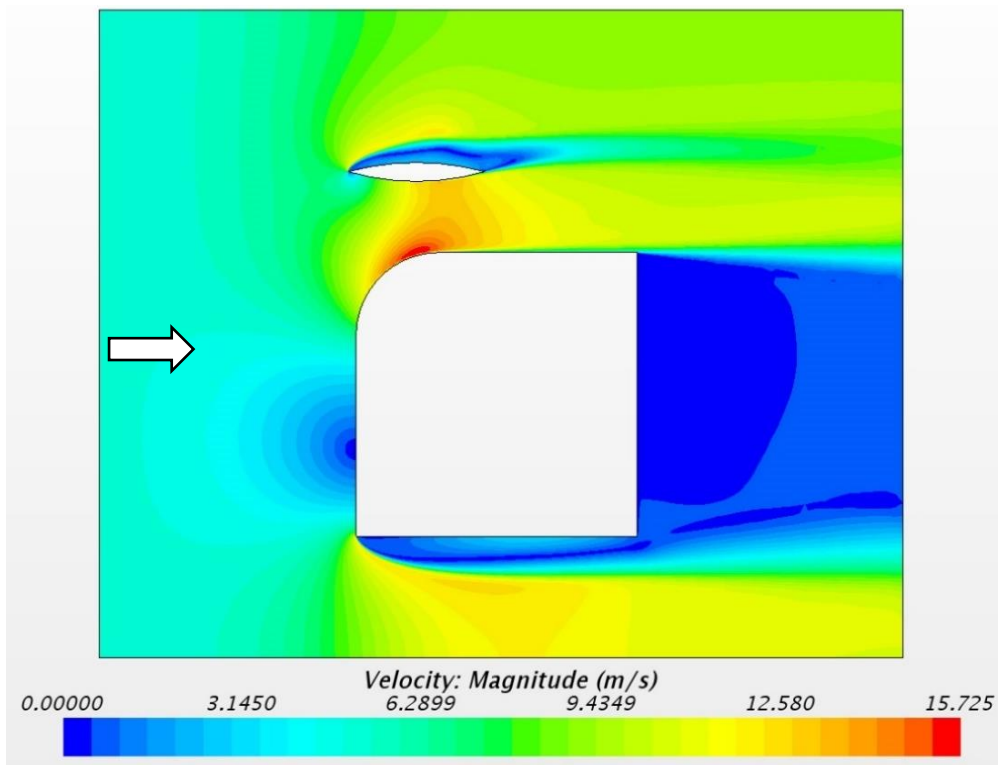


Figure 181. False color study of the wind speed around the integrated vertical foil type V3

### 3.5. Study with foil V4 and rounded building angle

The foil type V4 is an airfoil positioned at 45° to the building. The distance between the building and the profile is 1.10 m. The compression effect of the air stream is provided by the angle of the building and the curvature of the foil. **For an emergent wind of 5 m/s, the wind speed between the building and the foil is approximately 11 m/s, i.e. an increase of 2.1 times the incoming air speed.**

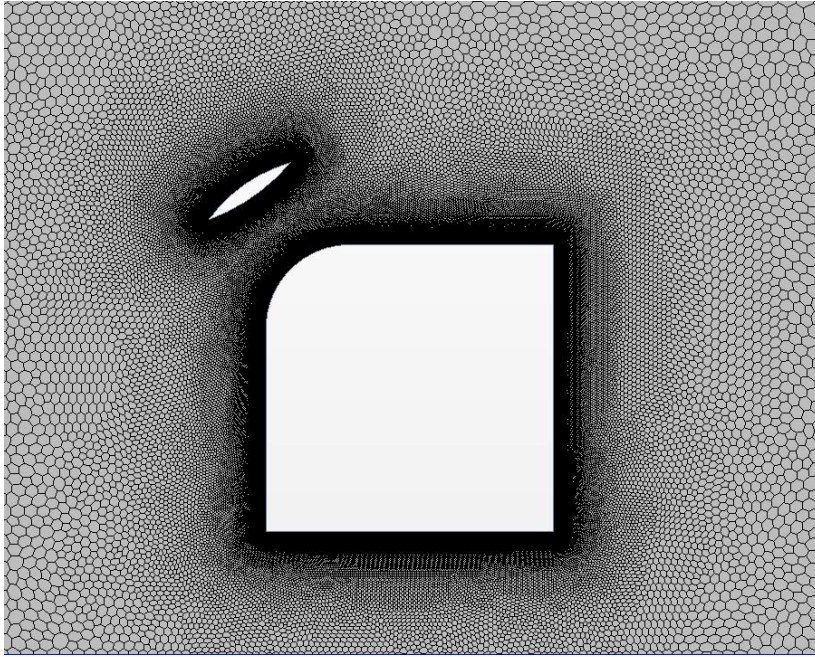


Figure 182. 2D model mesh of the building study area with integrated V4 foil type

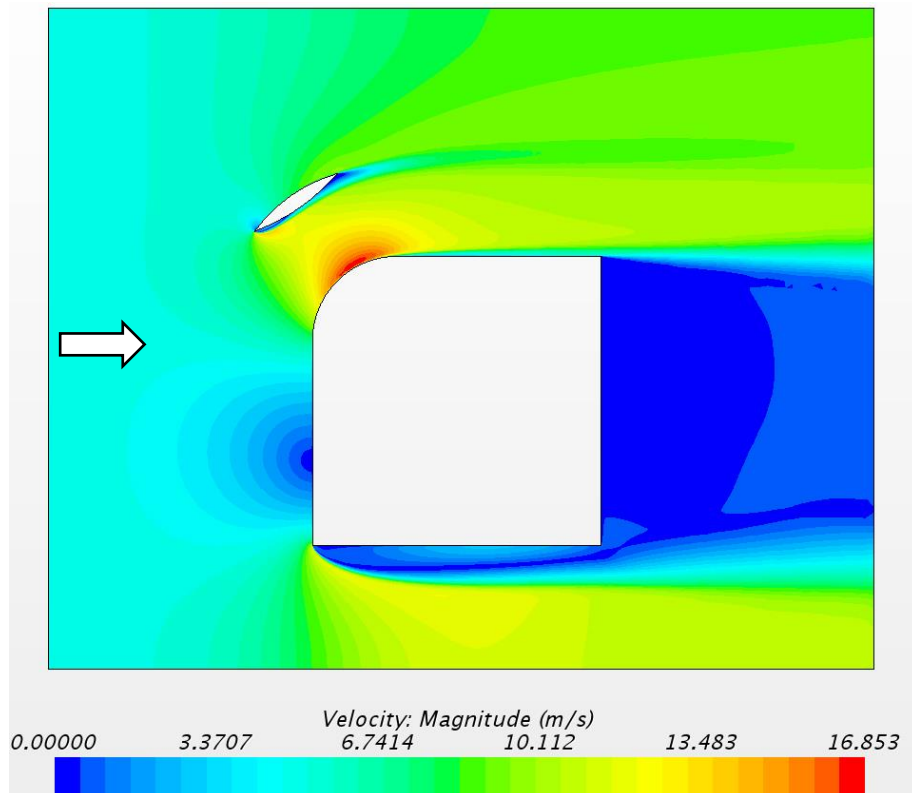


Figure 183. False color study of the wind speed around the integrated vertical foil type V4

### 3.6. Study with foil V5 and 45° building angle cutting

The foil type V5 is an airfoil positioned at 45° to the building. The distance between the building and the profile is 1.10 m. The compression effect of the air stream is provided by the chamfered angle of the building and the curvature of the foil. **For an emergent wind of 5 m/s, the wind speed between the building and the foil is approximately 10 m/s, i.e. an increase of 2 times the incoming air speed.**

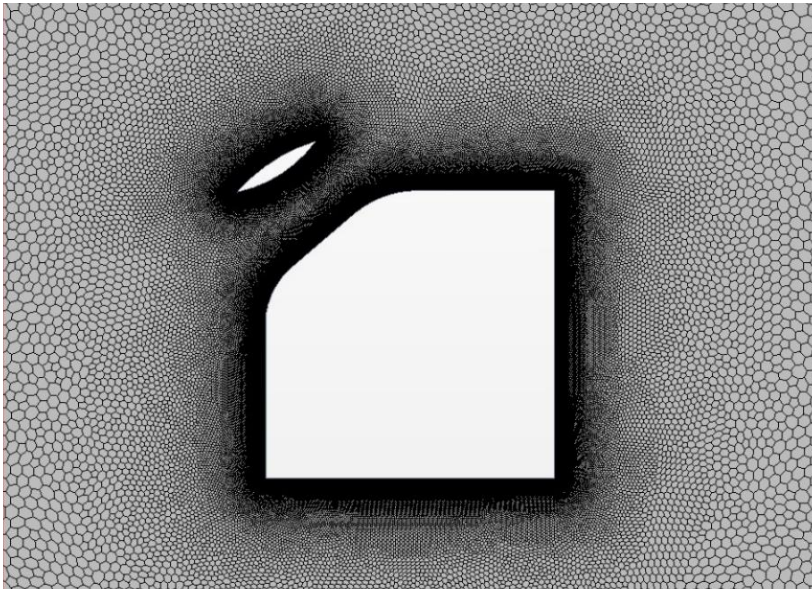


Figure 184. 2D model mesh of the building study area with integrated foil type 5

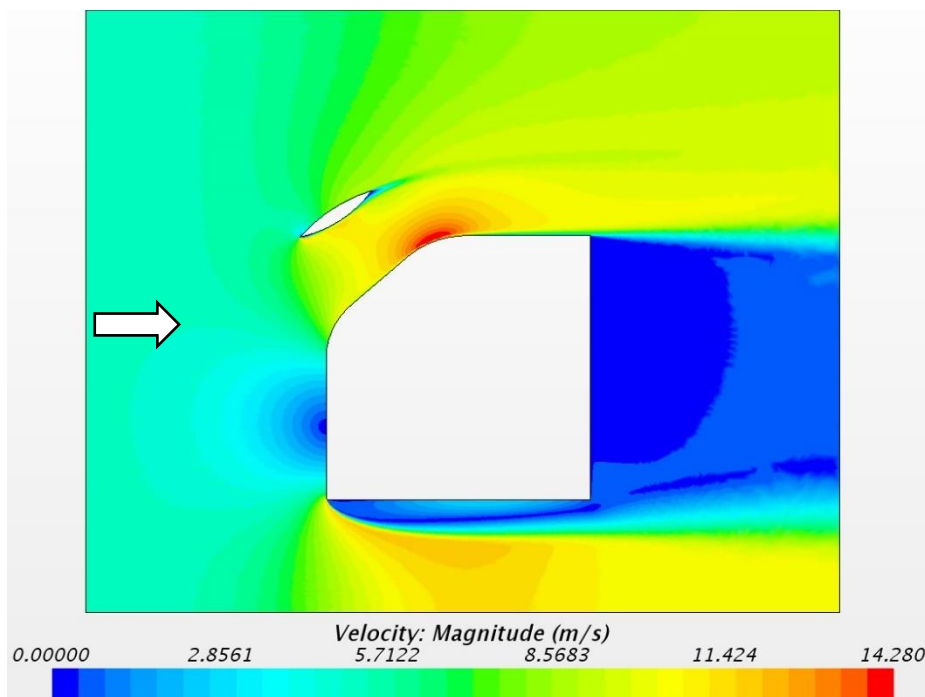


Figure 185. False color study of the wind speed around the integrated vertical foil type 5

- *Conclusion*

In conclusion, in the case of vertical aerofoil studies, the position of the blade at 45 degrees to the corner of the building is the one that generates the greatest increase in air velocity (see Figure 175). This result is quite constraining architecturally, as it prevents the creation of bays or windows in the 45° building corner, but it allows both air channeling and an increase in wind speed at 1 m from the building wall. The air speed between the building and the aerofoil is about 15M/s. With a base wind speed of 5 m/s, the air speed increases by a factor of 3.

**The electrical power generated by a wind turbine in this area (see figure 176) is in a ratio depending on the cube of the air speed, at a given location, so an increase in air speed of: 100% from 8 to 16 m/s corresponds to an increase in power of 2<sup>3</sup> or 8.**

#### 4. THEORETICAL STUDY 3 : ACROTHERIAL DEVICES

In the case of the integration of a device in the roof, we also studied an implementation in acroterion. The acroterion<sup>126</sup> protruding from the facade above the roof is an important point of increase of the wind speed above the building and of detachment of the layer. However, this study shows that the wind angle relative to the building is concentrated on a relatively thin surface and with some instability.

We have therefore studied a wind device fixed directly above the acroterion. This device allows an increase in speed which is much more punctual but which remains of the order of 80 to 100%.

- *Initial wind study on acroterion*

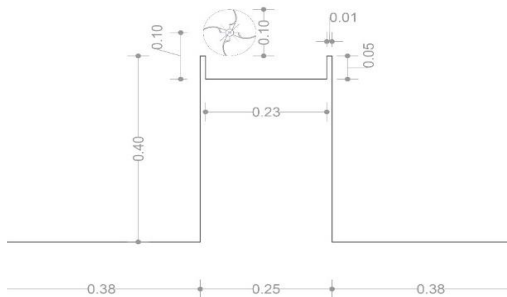


Figure 186. Etude dimensionnelle du bâtiment avec dispositif en en acrotère type 1

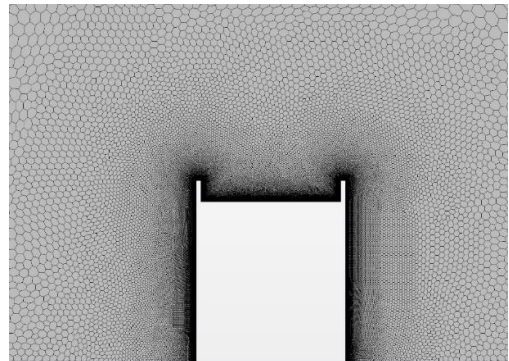


Figure 187. Maillage du modèle 2D de la zone d'étude du bâtiment avec dispositif acrotère type 1 intégré

<sup>126</sup> Extension of the facade masonry on the roof to allow for the waterproofing of the roof

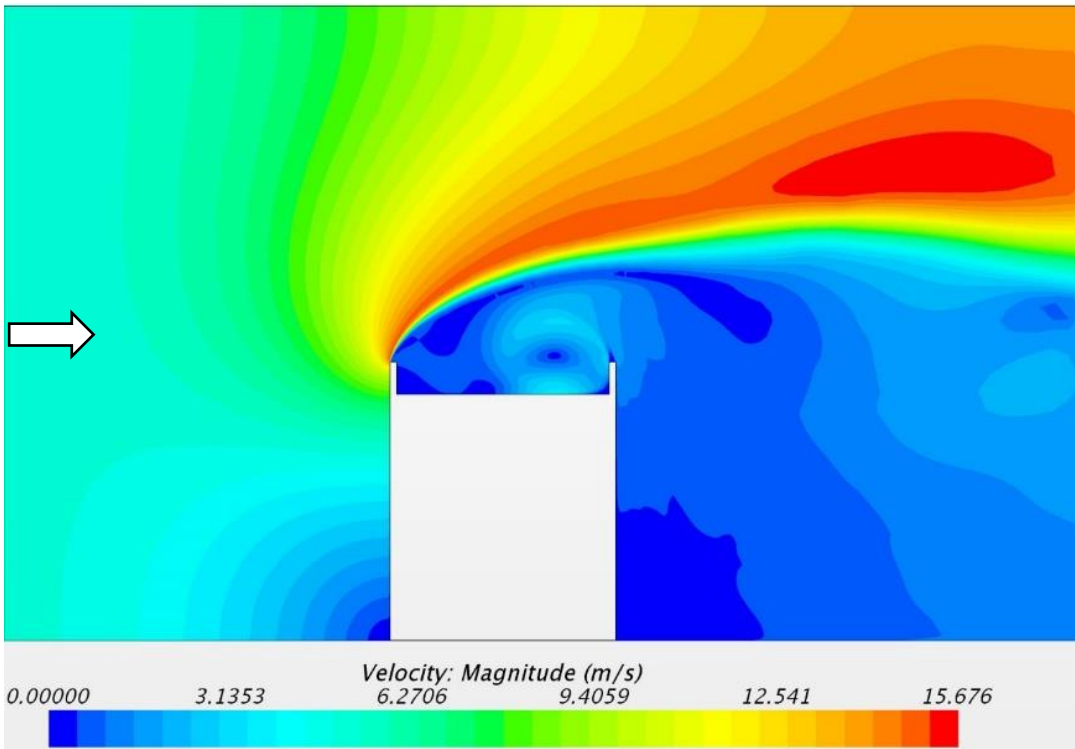


Figure 188. False color study of the wind speed around the acroterial device type 1

- Wind study on acroterion with device A1

This device shall be slightly set back from the acroterion<sup>127</sup> at 0.80 m from the edge of the roof.

This study shows that the wind speed, related to this device, is concentrated on a relatively thin surface and with some instability. For an emergent wind of 5 m/s, the wind speed between the building and the foil is approximately 10 m/s, which is twice the increase in incoming air speed.

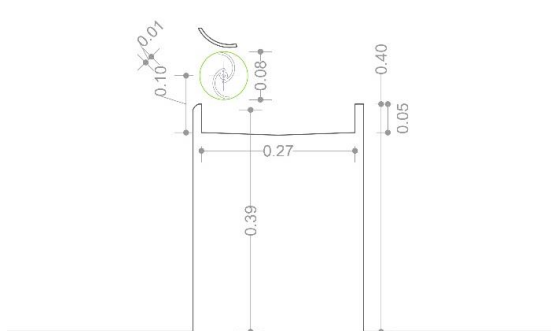


Figure 189. Etude dimensionnelle du bâtiment avec dispositif en acrotère type 1

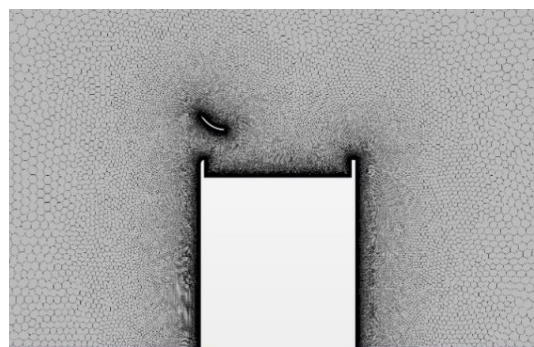


Figure 190. Maillage du modèle 3D de la zone d'étude du bâtiment avec dispositif acrotère type 1 intégré

<sup>127</sup> Extension of the facade masonry on the roof to allow for the waterproofing of the roof

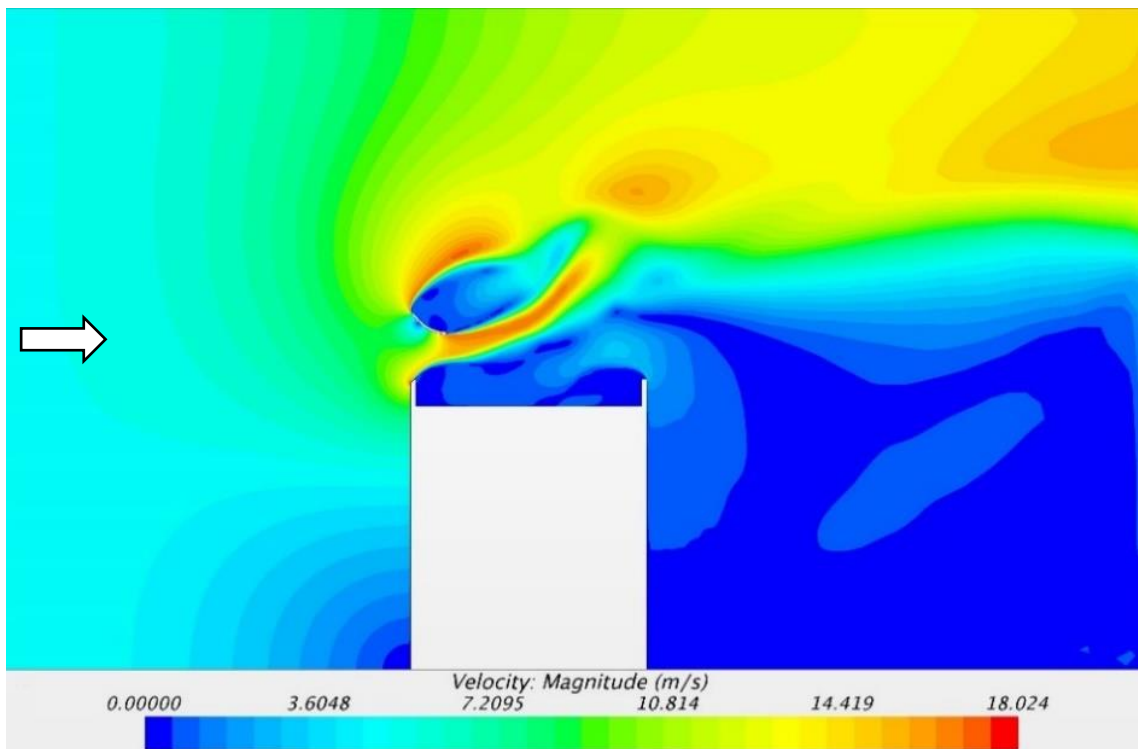


Figure 191. False color study of the wind speed increase around the acroterial device type 1

## 5. THEORETICAL STUDY 4: A HOUSING BUILDING IN AN URBAN SUBURB - BUILDING AT 136 AVENUE PARMENTIER, 75011 PARIS

- *Wind surveys on the apartment building*

In case studies 1 and 2, we studied a Haussmannian building with a Mansard-type roof. These roofs have a shape regulated by the urban template of the City of Paris, and they allow the facades to be set back in order to light the streets. This roof profile, with its rounded shape, already acts as a wind gas pedal system.

The simple implementation of a turbine in the upper part of this type of roof presents an increase in wind speed of 120 to 140% that reaches the energy collection device.

On this type of roof, wind turbines can be installed at chimney stacks, roof lights and roof accesses, but also at the location of flatter roof supports to position for example radio or TV receivers.

The emergence of fiber to connect and serve buildings with high-speed communication networks, has freed most Parisian buildings from television antennas by opening up space on their roofs while limiting the turbulence associated with these structures.



Figure 192 Figure 191: Installation of the anemometer on the roof of the building 136 avenue Parmentier, Paris 11ème. A TV antenna was used to support the device.



Figure 193. Localisation de la station de relevé de vent – 136 avenue Parmentier, Paris 11ème

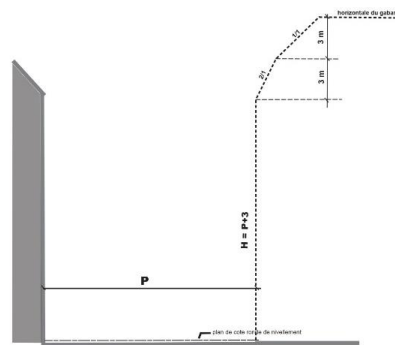


Figure 194 Gabarit - enveloppe en bordure d'une voie de largeur égale ou supérieure à 12 m et inférieure à 20 m non bordée pour installation d'aérofoil

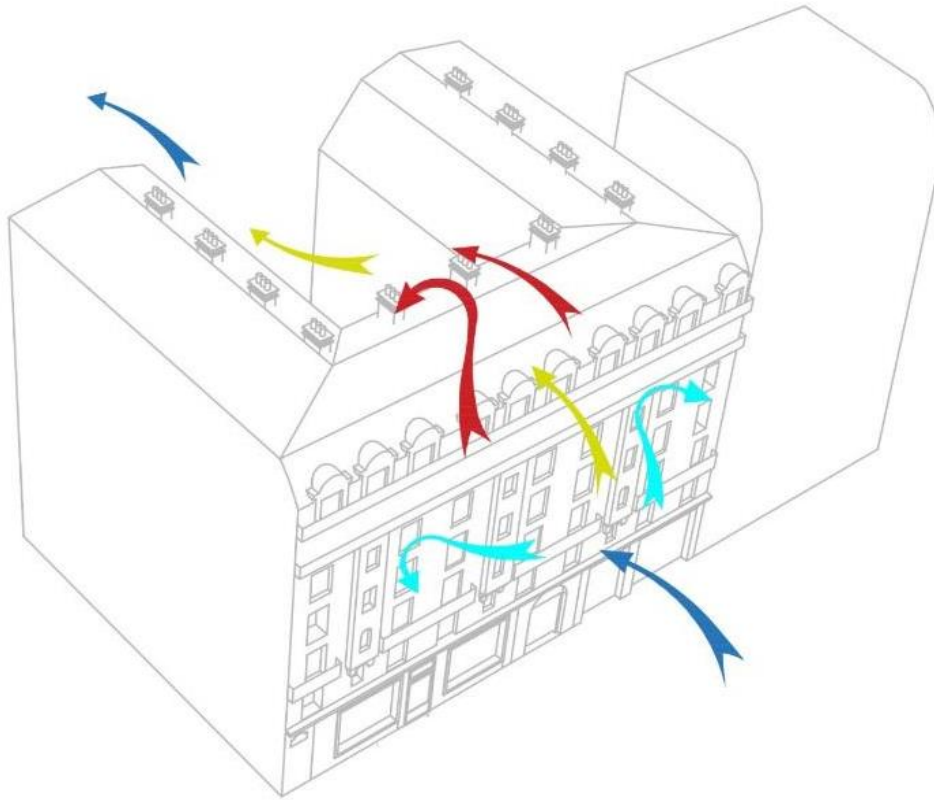


Figure 195. Comparison of wind speed measured at the site and at 22m above ground level and the wind measured in the CFD model.

The first weather station was installed at 136 avenue Parmentier, Paris 11ème, on the roof of the building on January 24th 2016. Since that date, the daily wind speed has been recorded every 10 minutes and we have a monthly record of this information.

In addition to the Serero wind station, this research collects 4 other data sources in Paris from [www.windfinder.com](http://www.windfinder.com) and [www.infoclimat.fr](http://www.infoclimat.fr); including the Paris CDG airport weather station, Paris Orly airport, Parc Montsouris and the top of the Zamansky tower on the Jussieu Campus, Paris 5th. All these surveys and observations, give a solid experimental analysis on strategic points of the city of Paris.

Here you will find a summary table of the data from these 4 wind survey stations compared as shown for the month of **December 2018**.

LOCATION	136. AVE PARAMENTIER				CDG AIRPORT				ORLY AIRPORT			
	00:00	06:00	12:00	18:00	00:00	06:00	12:00	18:00	00:00	06:00	12:00	18:00
DATE												
01.09.2017	1,1/S	1,4/SSW	3,1/S	5/SW	1/NW	1/WNW	2	5/NE	0	1	1/S	2/NNE
02.09.2017	2,5/W	2,2/NW	3,6/SW	5/NE	2/NW	2/NW	3/NW	5/N	2/NW	2/NNW	4/N	3/NW
03.09.2017	1,1/ENE	1,4/SSE	3,6/S	3,3/S	1	2/ESE	3/S	4/SSE	2/W	1/S	3/SSW	3/SSE
04.09.2017	1,1/SSW	4,7/S	4,7/S	4,7/SW	1/N	2/S	6/SSW	2/W	1/E	4/SW	4/SSW	4/W
05.09.2017	3,6/SW	2,5/S	5,3/SSW	5,8/S	3/SW	4/S	6/SW	5/SW	3/SSW	3/SSW	6/WSW	3/SSW
06.09.2017	5,6/SW	5,3/SW	5,3/SW	6,9/SW	6/W	5/W	7/W	7/W	5/WSW	4/W	5/W	5/W
07.09.2017	4,4/SSW	3,6/SW	3,9/SSW	6,9/SSW	2/W	3/S	5/WSW	5/W	4/W	3/WSW	3/WSW	4/WSW
08.09.2017	3,6/S	5,3/S	6,9/S	5,8/S	5/WSW	6/SSW	8/SW	6/SW	3/SW	5/SW	7/SW	5/SW
09.09.2017	3,6/S	5,3/SW	5,3/SW	6/SW	5/SSW	5/WSW	7/WSW	5/WNW	4/SW	4/SW	6/WSW	4/W
10.09.2017	ND	2,2/SSW	2,8/SW	6,9/S	3/SW	4/WSW	5/SW	9/SW	2/SW	2/WSW	3/SSW	7/SW
11.09.2017	10,8/S	5,3/SW	8,1/SW	8,9/SW	9/SW	7/WSW	10/WSW	10/WSW	9/SW	6/W	9/WSW	7/WSW
12.09.2017	4,7/SW	6,1/S	6,7/SW	6,4/SW	5/WSW	6/WSW	5/W	7/WNW	5/WSW	3/SW	5/WSW	6/WSW
13.09.2017	6,1/S	7,5/SSW	5,3/SSW	4,7/WSW	9/SSW	9/SW	9/W	7/W	7/SSW	8/SW	8/WSW	4/WNW
14.09.2017	10,8/SSE	5,6/SW	5,3/SW	3,6/WSW	4/W	6/WSW	10/W	6/WSW	4/WSW	7/WSW	8/W	6/W
15.09.2017	3,3/SW	3,9/SW	ND	ND	5/WSW	3/SW	3/WNW	3/W	3/SW	3/W	3/W	5/W
16.09.2017	ND	2,2/SSW	ND	ND	2	3/WSW	3/WSW	4/W	2/WSW	2/WSW	3/SSW	2/WSW
17.09.2017	ND	1,4/S	1,9/S	1,9/SW	2/SSE	3/SE	2/SW	2/WNW	2/SSE	3/SSW	2/SSW	3/NNW

Figure 196. Comparison of wind speed in the Paris region measured at national weather stations (Roissy, Orly, Montsouris), and anemometers connected at 22 m above ground level on the roof of a compressed air plant

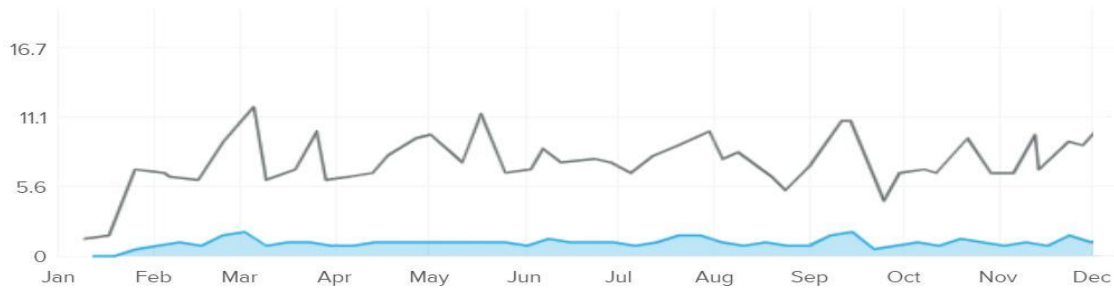


Figure 197. Wind speed reading from the Parmentier weather station (monthly average winds in 2018) at 22m height from the street in a dense urban "Faubourg." In m/s on the vertical ave.

The wind speeds were used to derive the average velocity. Wind directions were used to identify the main wind direction for the initial conditions of the numerical model.

- *Initial study of wind on the roof of the Mansard*

We study here the impact of the mansard roof of a Parisian building on the wind flow at its periphery.

This study shows that the increase in wind speed is strong and continuous on both sides of the mansard roof (the attic and the terrace). For an emergent wind of 5 m/s, the wind speed between the building and the foil is approximately 10 m/s, which is an increase of 2 times the incoming air speed.

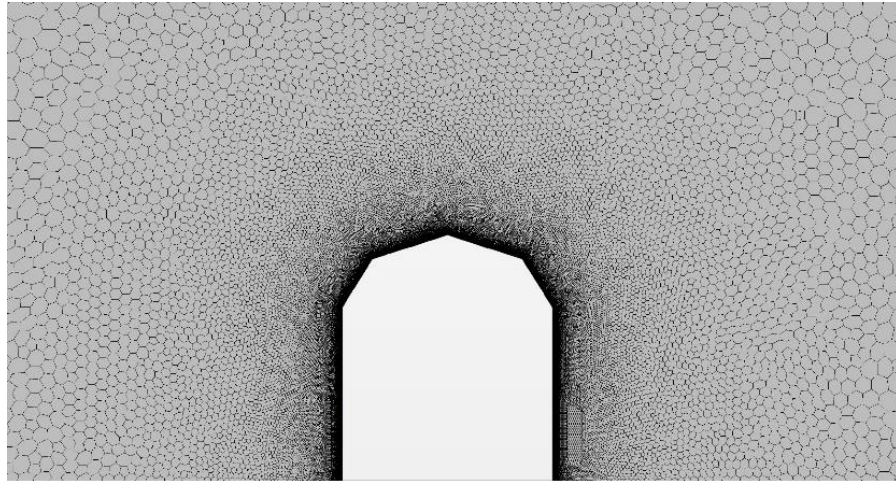


Figure 198. Mesh of the 3D model of the study area of the mansard roof without device

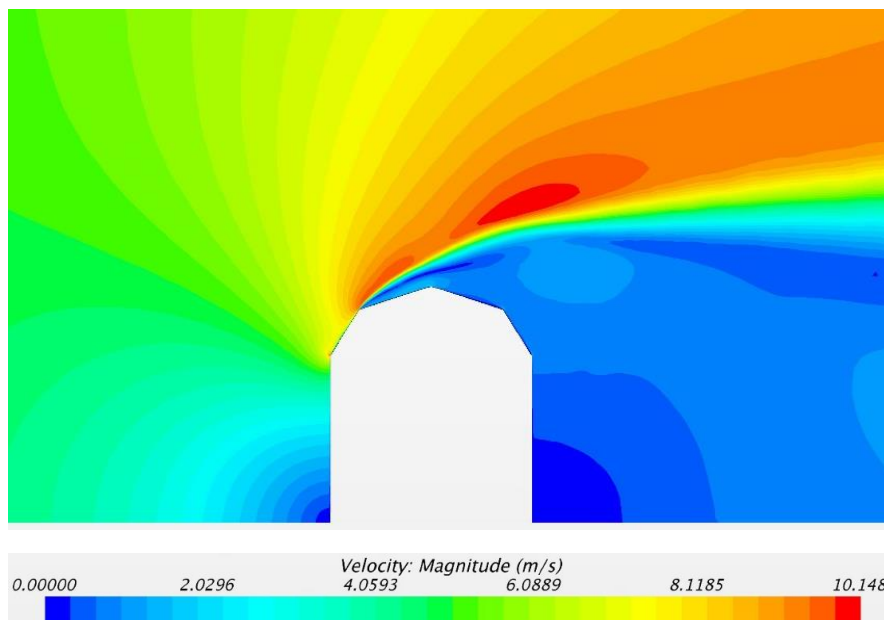


Figure 199. Simulation of wind speed around the roof of the building without a device

- *Wind study with M1 foil on the roof of the Mansard*

We study here the impact of the mansard roof of a Parisian building on the wind flow at its periphery.

This study shows that the increase in wind speed is strong and continuous on both sides of the mansard roof (the attic and the terrace). **For an emergent wind of 5 m/s, the wind speed between the building and the foil is approximately 10 m/s, which is an increase of 2 times the incoming air speed.**

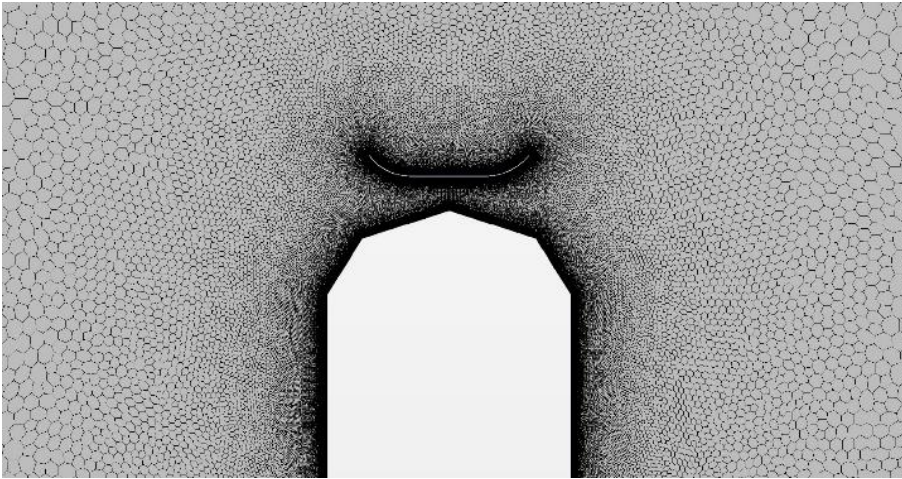


Figure 200. Mesh of the 3D model with device

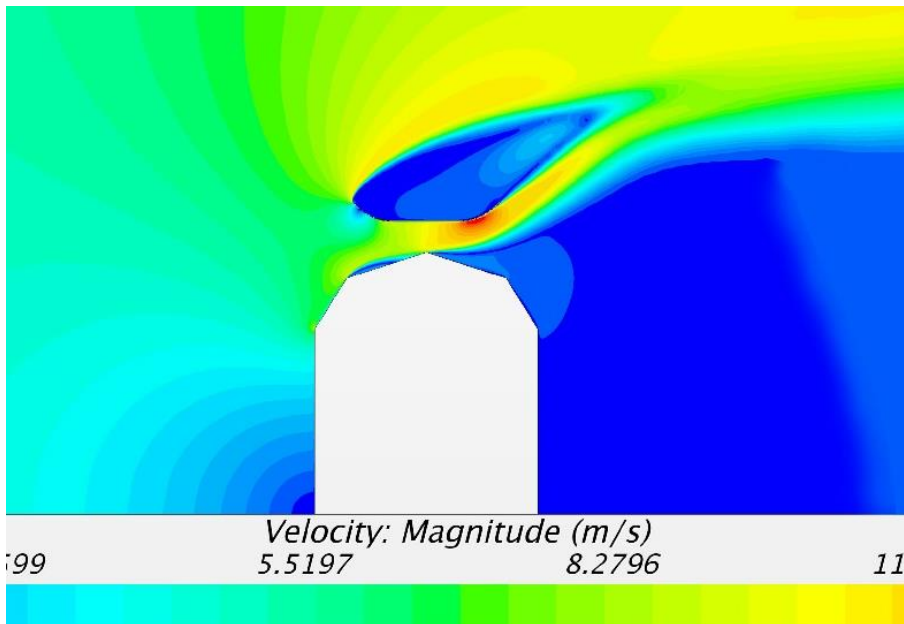


Figure 201. Simulation of the increase in wind speed around the Haussmannian building with the

## 6. THEORETICAL STUDY 4 : AN IGH BUILDING IN A SALES SITE

### 6.1. Presentation of the context of the Paris Val-de-Seine School of Architecture (75013)

The site studied is the Paris Val-de-Seine School of Architecture. The building is located at 3 quai Panhard Levassor in Paris 75013. Built by the architect Frédéric Borel in 2008, the building is composed of an old compressed air factory (the Sudac). A very high chimney (more than 50 meters high) and a new building of IGH type (high rise building) of 50 meters high. This group of buildings is particularly interesting for 3 reasons:

- This building is a building-island, that is to say that all these buildings constitute a complete Parisian island lined with streets.
- Secondly, the building is located in a windy area in two ways: it is located on the banks of the Seine and this location provides a particularly clear wind corridor at this point. It is also located near the ring road, a second important wind corridor in the northwest direction.
- Thirdly, this building is easily accessible from all points since it is a public building for which, after requesting authorization, the design department authorized us to launch a pilot experiment consisting of wind speed measurements around the periphery of this building. 9 singular points were identified as interesting<sup>128</sup> (See Figure 206). We therefore positioned 3 ultrasonic anemometers at different points on the site for several months. These points were used to take continuous wind measurements (the Netatmo software records a wind report at 5 minute intervals). They were compared with a reference wind measurement (Vref) taken by an anemometer positioned on a railing near the ring road adjacent to the School of Architecture. The comparison between the Vref reference measurement and the readings at several points on the building confirms the important impact of the scale of this structure on the winds. Because of its overall volumetry and its multiple recesses, which are part of Frédéric Borel's architecture, the building generates specific wind corridors and shows increases in its speed that our analysis was able to identify. We have compared the winds on 3 zones, particularly interesting of this building, which were identified during the wind surveys.
  4. Between the two towers, on the Seine side, there is a very strong wind corridor which has been the subject of the installation of windbreaks on a terrace in the upper part of the building.
  5. The side terraces at the top of the towers show that on the sides of the building, significant areas of increased wind speed exist.
  6. At the top of the building, at the level of the technical equipment of the air handling unit, the elevator kiosk also generates a very high wind speed of 2 to 3 meters above the roof level.

From this point of view, this building constitutes a significant case to compare emerging winds on a site and its architectural profile in order to evaluate the possible capture of wind energy. It seems that this situation suggests a strong potential of Frédéric Borel's architecture to integrate wind devices into his fragmented architecture, made of detachments and articulations of volumes in

---

<sup>128</sup> See diagram of the location of these anemometer devices in 4.7.3

relation to each other. This formal architectural language generates "**edge effects**", effects **of detachment** on the roof or **increases in air speed** at its periphery, the power and effectiveness of which are rarely identified at the time of its design.

## 6.2. Method of wind surveys around this island building



Figure 202. Location of the new anemometer at ENSAPVS

Because of its location at the crossroads of two major open urban corridors, the Seine River on one side and the ring road on the other, the Paris Val-de-Seine School of Architecture offers an open and windy site with a 270 degree view. The Paris Val-de-Seine school building is located on an urban university campus where each university department constitutes a real island in the city. The volumetric entities that define the architecture of this building are an urban island building, on the scale of the city.

We have proposed several anemometer installations on the roofs and overhangs of this building to verify wind flows around the building.



Figure 203. View of the device inserted on the roof of the building (Paris 75013)

### 6.3. School of Architecture Paris Val-de-Seine (75013)

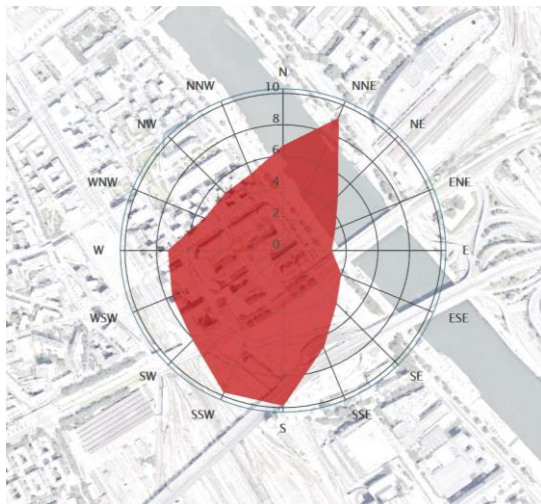


Figure 204. Distribution de la direction du vent en pourcentage annuel, Ecole d'Architecture Paris Val-de-Seine. Paris 75013

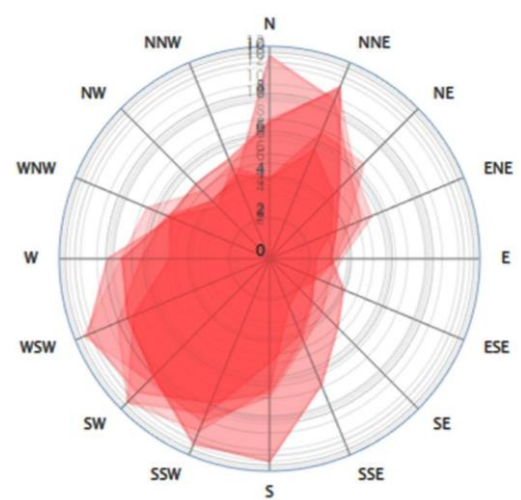


Figure 205. Etude des vents mesurés par la totalité des stations météo connectées montrant les directions de vent principales à Paris. Par Windfinder

The data measured at these different points are used to construct the wind rose (Figure 203). This traditional method of wind analysis does not reflect the complexity of the phenomena. It shows a south-west/north-east wind direction with a large variation in speed and direction in

urban areas. These elements are used to parameterize the numerical model. In the Paris area, the main wind direction is SSW and NNE. This information gives us a first hypothesis for the implementation of energy capture devices on the roofs and facades of buildings.

We then produced a very detailed 3D model of the buildings, as well as the entire context on a periphery of approximately one kilometer. This digital model allows us to study the impact of winds on the site, in horizontal and vertical section. It should be noted that the buildings at the back of the Paris Val-de-Seine school are raised 10 to 15 meters above the ground level of the building in order to pass over the railway tracks of the Austerlitz station. This **artificial topography** also participates in the raising of the wind emerging from the Seine around ENSAPVS.



Figure 206. Le bâtiment de l'ENSAPVS dans son grand contexte urbain (source : modélisation 3D par D. Serero)

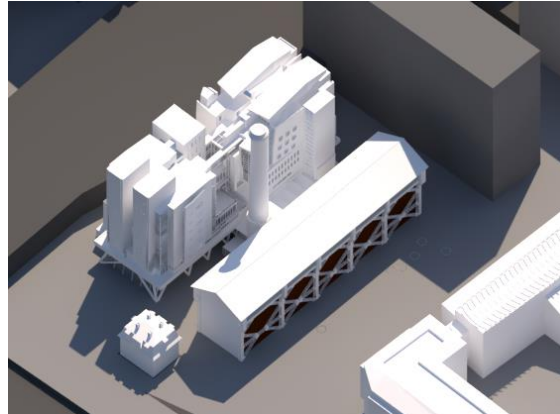


Figure 207. Vue aérienne des différents bâtiments qui constituent l'ENSAPVS (source idem)

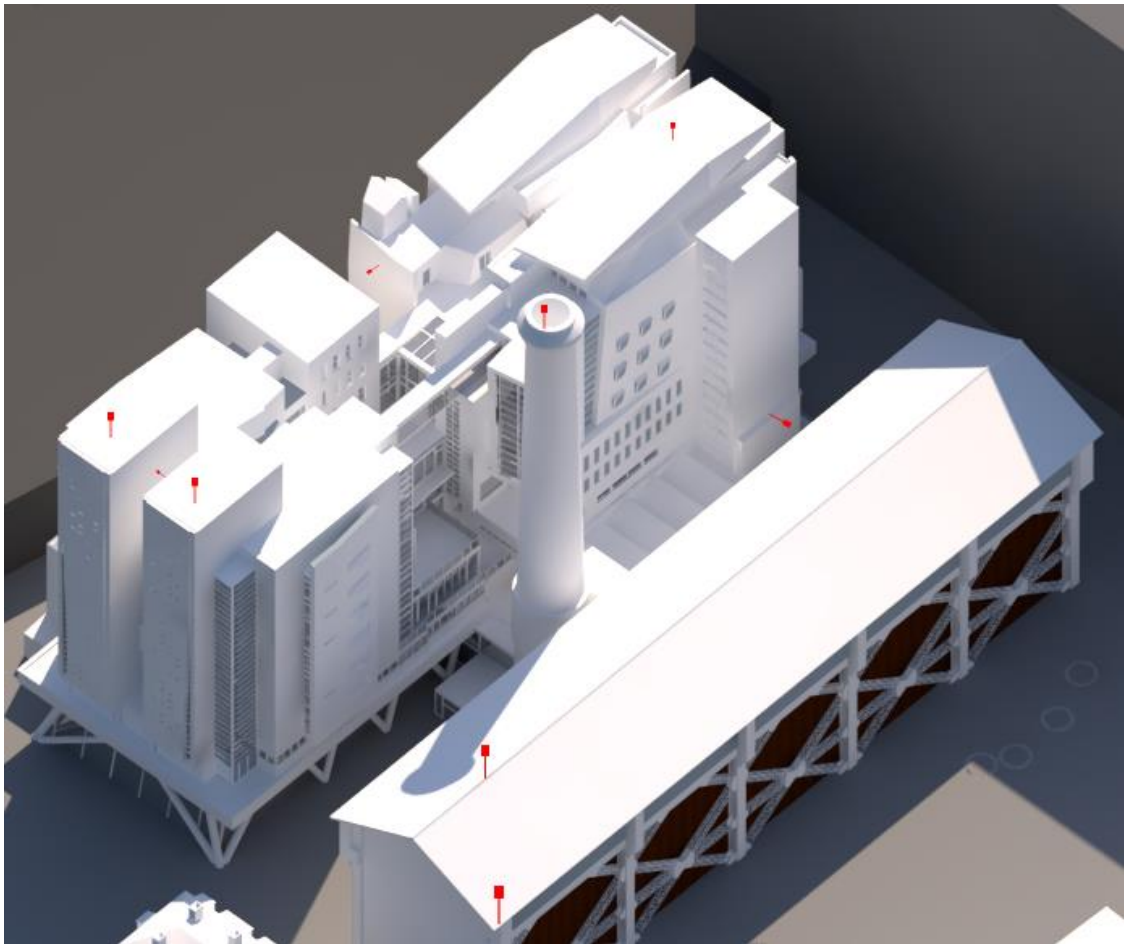


Figure 208. Position of the 9 zones identified for the survey by connected anemometers

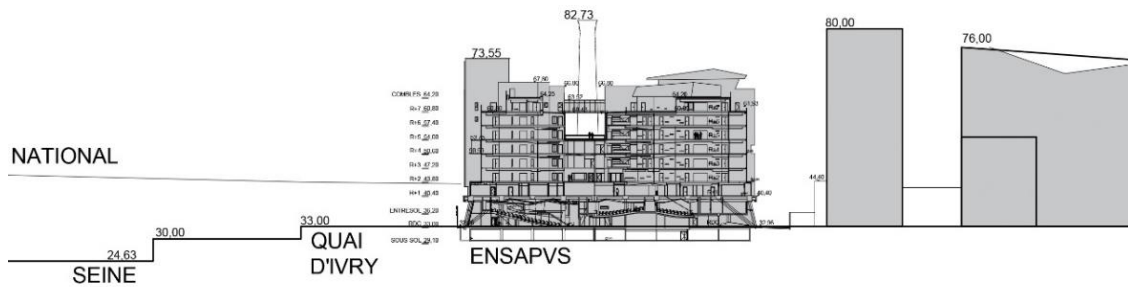


Figure 209. Urban section of ENSAPVS showing the relationship between the Seine and the Avenue de France at the top of the site. ( source : Section drawn by D. Serero)

#### 6.4. Method of aeraulic simulation in urban area of the ENSAPVS site

The plan of the Paris Val-de-Seine School of Architecture is conceived as the assembly of four towers connected by a central core<sup>129</sup>. This architectural principle, according to the architect Frédéric Borel<sup>130</sup>, develops the idea of having four schools and four pedagogies of the project cohabit within the same space. This strategy translates into an architecture of fractioning, of shearing, where narrow volumes truly behave like wind gas pedals. The presence of these large

<sup>129</sup> Richard SCOFFIER, *Ecole nationale supérieure d'architecture de Paris Val-de-Seine*, Archibooks, 148 p.

<sup>130</sup> Richard SCOFFIER, *Frédéric Borel*, 01 ed. in Paris, France, Norma, 2004, 224 p.

towers at an urban crossroads between the Seine and its quays and the open space constituted by the outer boulevard along the Masséna campus area that guides the winds in this district.

These increases in wind speed have required the reinforcement of curtain walls and railings, particularly in the rooms on the 7<sup>ème</sup> and 8<sup>ème</sup> floors which have terraces dedicated to teaching and which could never really be used due to the high winds and the lifting of objects on this terrace.

The method developed here aims to analyze the airflow around the building from a detailed 3D model of the existing site. We selected 2 vertical sections and 2 planes in this 3D volume that present the **singularity points of the geometry or topography of this site**. Using the Star CCM+ numerical simulation software, we performed several simulations of 3-dimensional airflow behavior. This calculation has a medium resolution (10,000 mesh facets) imposes 8 to 10 days of computation time (200 to 240 hours, Intel Core i7, 16 cores) making it difficult to interact and fine-tune the 3D model. Our limited resources during this research did not allow us access to a virtual computing machine to reduce the computation time and to increase the resolution of the full 3D simulation.

In order to minimize the calculation time to 2 days, we have proposed to perform calculations on reduced areas such as on precisely selected horizontal or vertical sections. This technique also allows to improve the readability of the wind behavior in the produced graphic documents.

However, it does not allow to identify in the spatial reference frame **the zones of air speed change**, nor to identify with an animation **the stationary state of the winds** outside this model.

The first step of this study is the realization of a **mesh** allowing to accentuate the definition of the calculation around the particular and singular points of the structure. The diagram below gives an example of a mesh for **about 25 000 meshes**. The whole numerical simulation is thus calculated and evaluated progressively from the calculation algorithm on these 25000 meshes in the model.

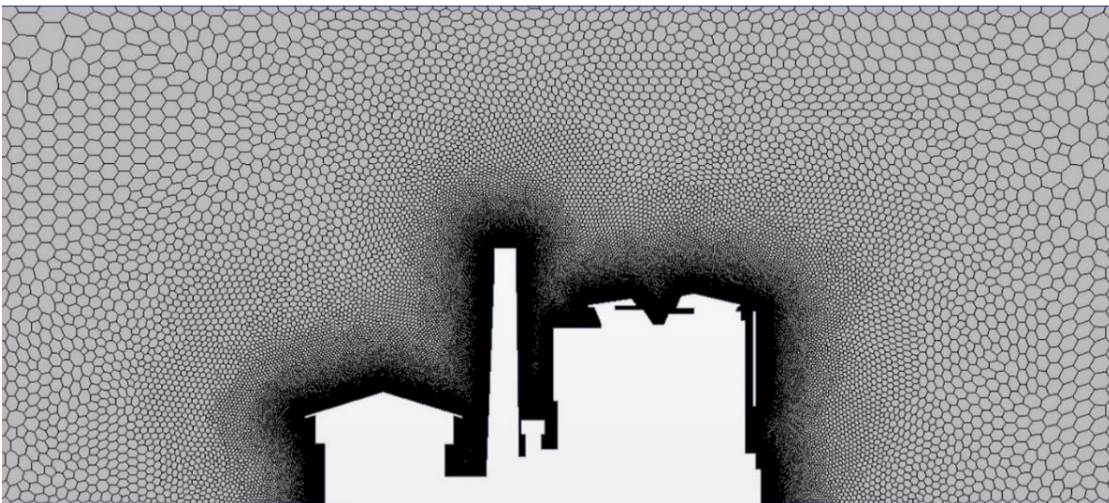


*Figure 210. Definition of the aeraulic analysis mesh on the 3D model of ENSAPVS, according to an East-West vertical section*

### 6.5. Airflow study in vertical sections of the building

We have, for that, realized an aeraulic simulation which shows the behavior of the wind, the increases or the slowing down of the speeds in a specific line<sup>131</sup> of the building. The choice of this first row reveals the great diversity and variation in the building. It should be noted, however, that the central stack has a punctual impact on the site due to its diameter at ground level of 5 meters (See figure 210).

Each of these slices allows us to estimate the increase in wind speeds for a given wind (5m/s emergent wind) in the high speed zones (dark red) as a function of the architectural profiling. In order to identify singular scenarios or behaviors, we dragged the analysis sections through the site. It should also be noted in these simulations the effects of air depression created by this volume on the rear part of the building, low pressure zones (identified in dark blue and light blue on the simulation).

As seen in chapter 3.4.2, at each of these simulations<sup>132</sup>, we analyze the residuals of the calculation, i.e. the degree of convergence of the Navier-Stokes equations. This graph, made up of 5 to 6 parameters of the equation, allows us to verify if, after 1,000 to 10,000 iterations, the simulation carried out leads to a relevant and qualitative result. At each calculation, a large number of winds are evaluated in order to progressively improve the simulation and the accuracy of the calculation (residuals ideally below 0.001 for 1000 to 10 000 iterations).

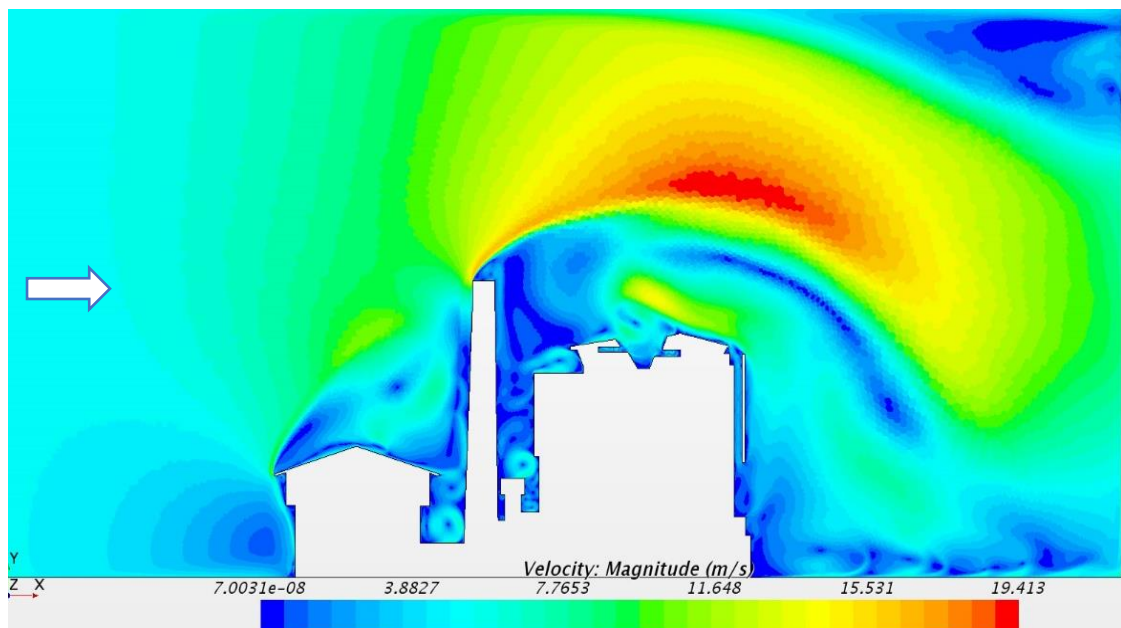


Figure 211. Aeraulic simulation with an average speed of 5m/s, on a North-South section of the ENSAPVS building (on a chimney) Calculation at 10 000 iterations

<sup>131</sup> A building line is a reference axis often used to identify the axes of structural elements.

<sup>132</sup> We present in chapter 3.4.2 the parameters used for the numerical simulation (definition of the type of physical model calculation by the epsilon K equation and turbulence model) and define the reference values and contextual initial conditions.

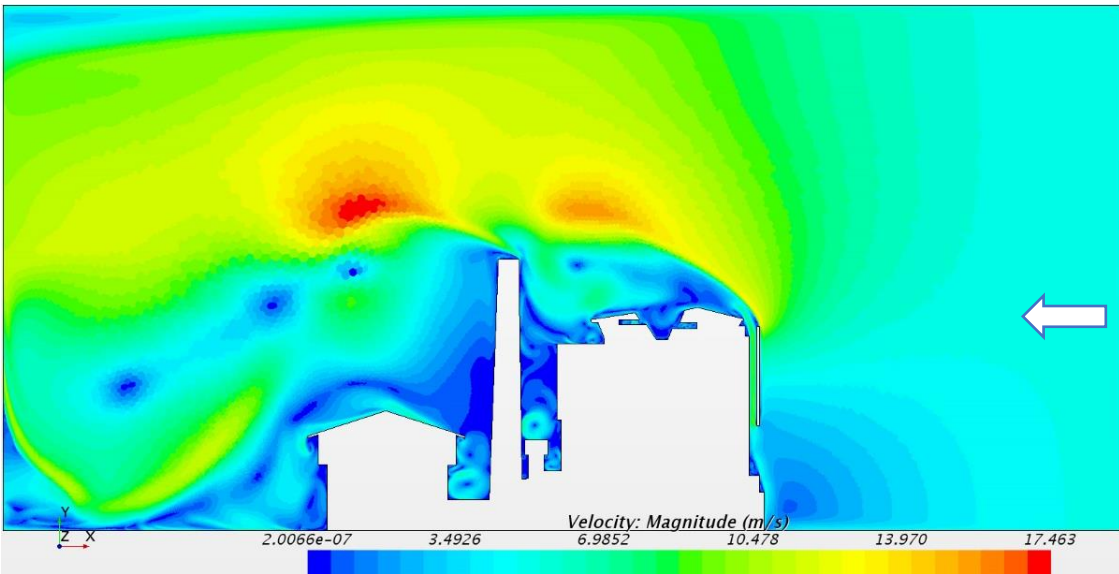


Figure 212. Aerodynamic simulation on a North-South section of the ENSAPVS building (with wind speed of 5 m/s, West-East wind direction)

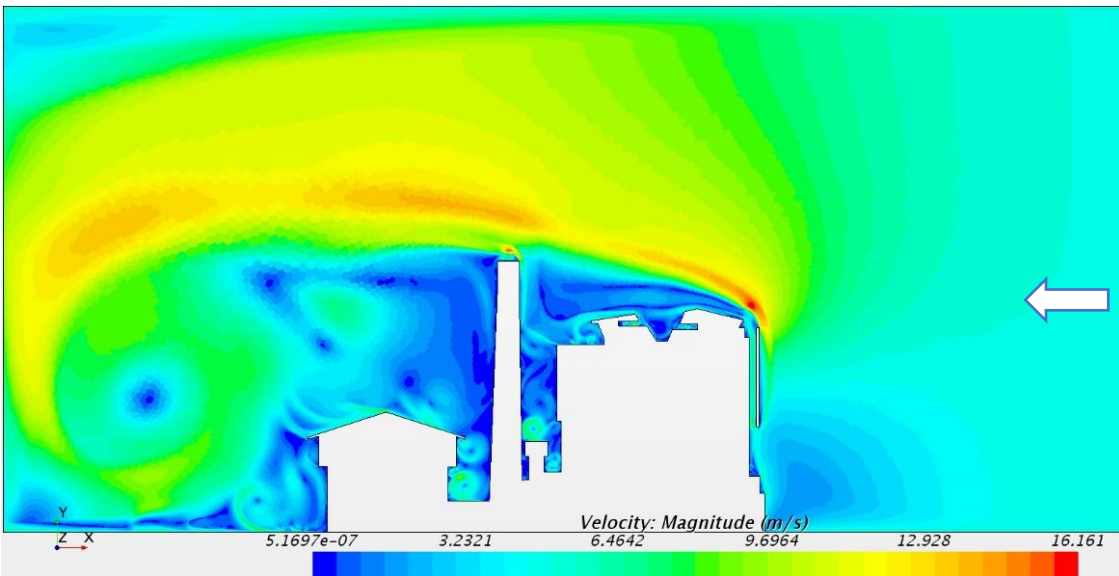


Figure 213 Aerodynamic simulation on a North-South section of the ENSAPVS building (with wind speed of 5 m/s, West-East wind direction)

## 6.6. Study of the building-island in horizontal sections at different altimetries

- *Building study at 12m*

The analysis method is similar to what has been shown previously with the production of a dense mesh around the building as well as the definition of the calculation assumptions in terms of context and geometry. For this study, we have enlarged the computational domain in order to limit the effects of boundary layers on the calculation. The interstitial spaces between the two buildings of ENSAPVS constitute wind channelling zones at different altimetries.

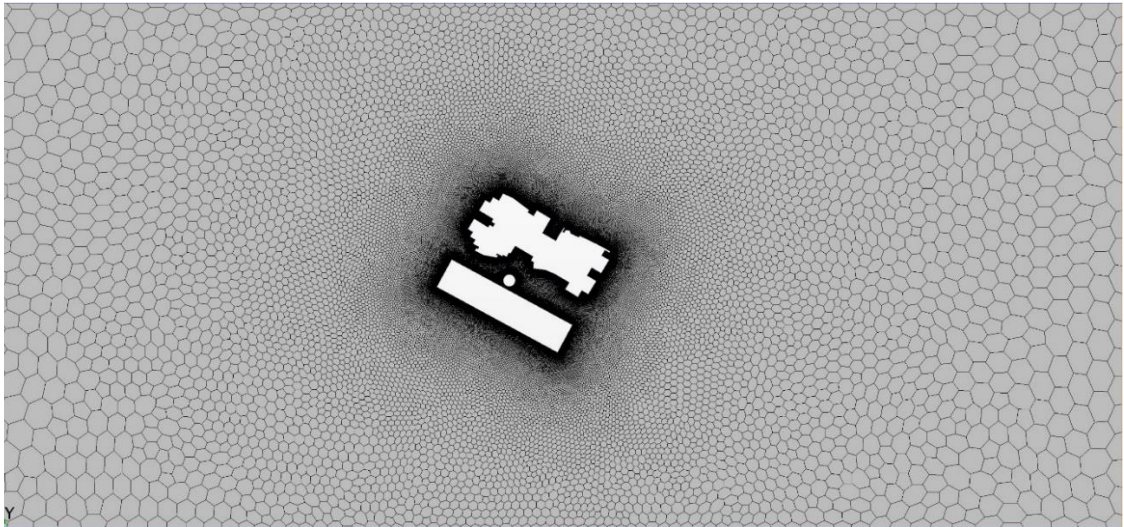


Figure 214. Analysis plane mesh of the ENSAPVS building with increased densities on the areas near the building at 12m

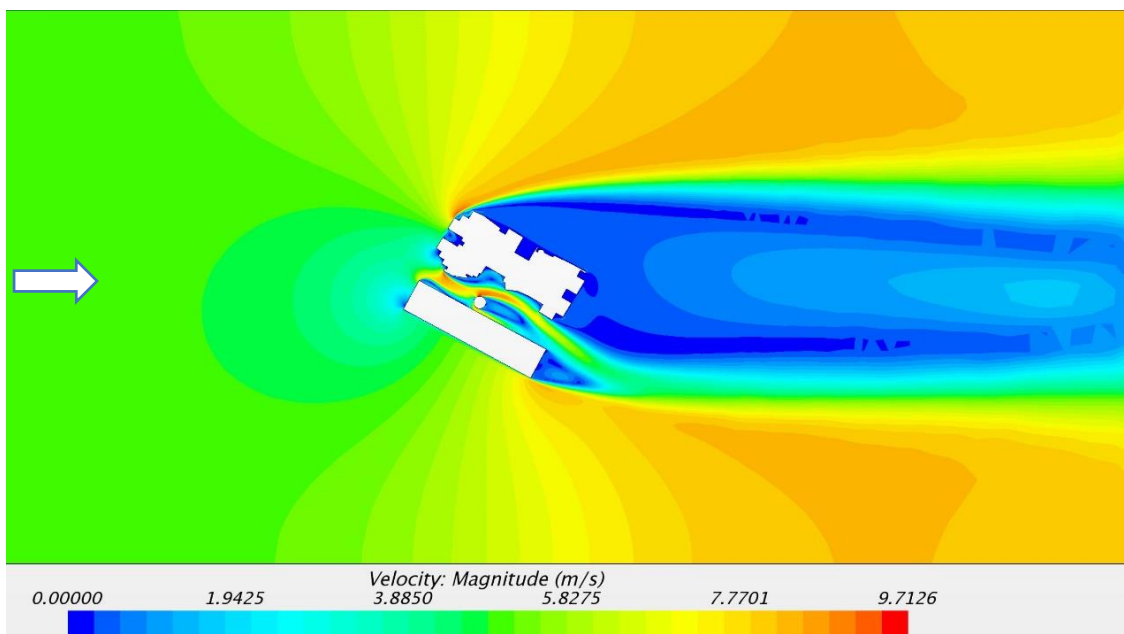


Figure 215. Aeraulic simulation on a horizontal section at 12 m altitude of the ENSAPVS building (with an air speed of 5 m/s, West-East wind direction)

- *Building study at 25m*

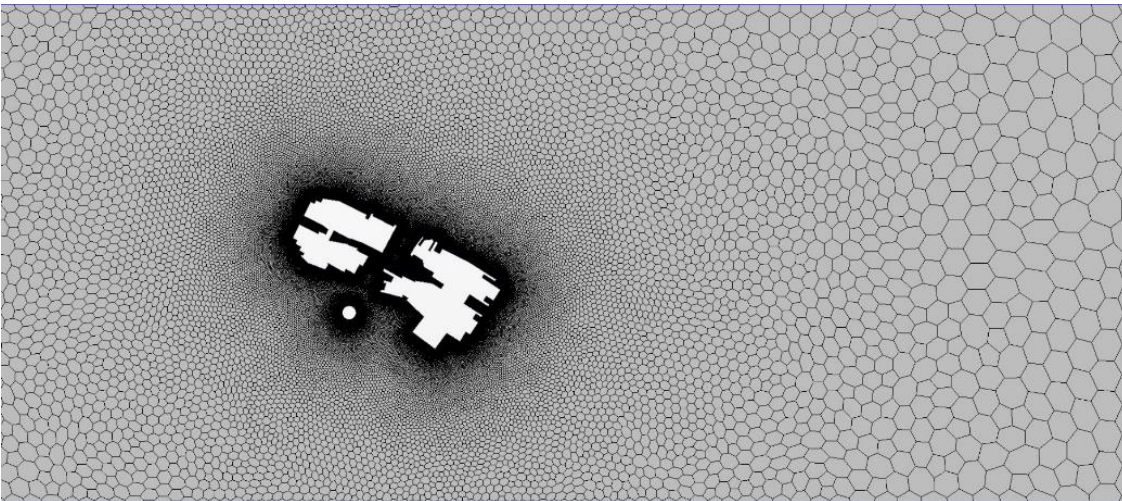


Figure 216. Analysis plane mesh of the ENSAPVS building with increased densities on areas near the building.

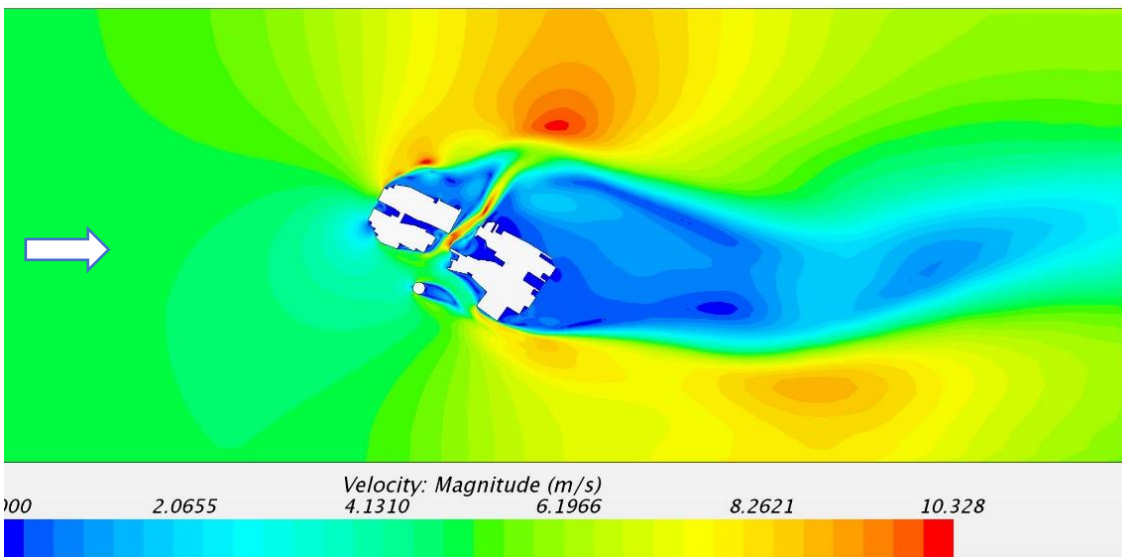


Figure 217. Aerodynamic simulation on a horizontal section at 12m elevation of the ENSAPVS building (with an air speed of 5 m/s, West-East wind direction)

- *Conclusion*

This study shows the impact of wind on the towers on the Seine side with strong increases in wind speed in this area. In such a complex building, we note both in plan and in section, masking effects of elements such as the chimney, the front towers and the rear towers. And that these hard points generate an increase in wind speed at their periphery.

The relative direction of the architectural volume elements and the prevailing wind direction is very important in identifying the best areas for energy capture and the impact of wind turbulence on the surrounding buildings.

This study shows that this island building also plays a real role of wind protection of the other buildings of the district smaller at its periphery (dark blue zone with less than 1m)

### 6.7. Study of an area in detail at the level of the 2 towers

Studies of the wind behavior at different levels of the 2 towers on the Seine side of ENSAPVS show a strong increase in wind speed between the 2 towers. We will study, in this section, a close detail of a zone at +70m above ground level, where 2 towers act as amplifiers of the wind forces on the site. With an emergent wind of 5 m/s, an increase in wind speed between the 2 towers is approximately 17 m/s (Fig. 217), i.e. an increase of 3.2 times its base speed. We also note an edge effect on the outer edge of the tower with an increase in speed to 11m/s, an increase of coefficient 2 in the wind speed on their outer side (Fig. 217).

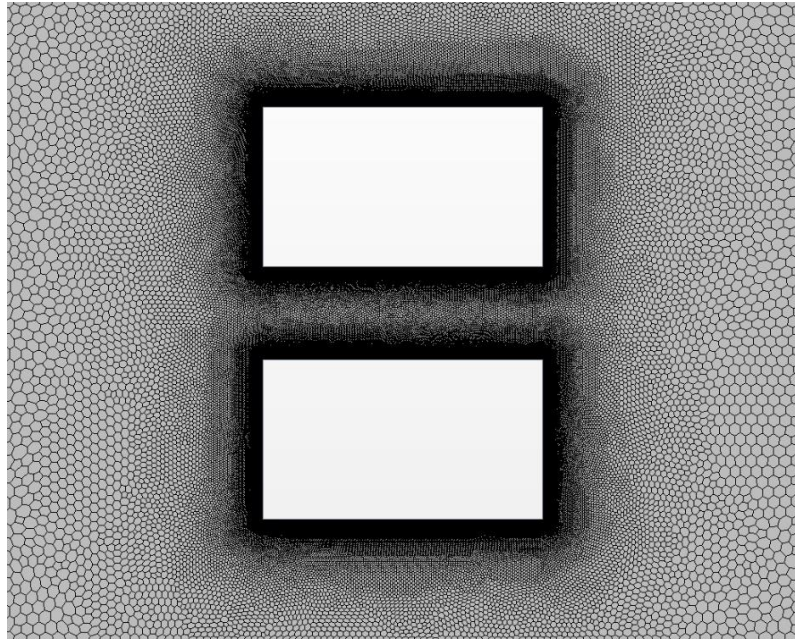


Figure 218. Study mesh on a horizontal section at +70m altimetry of the ENSAPVS building (dimensions tower: 25m wide X45m long, scale: 1 /1000th)

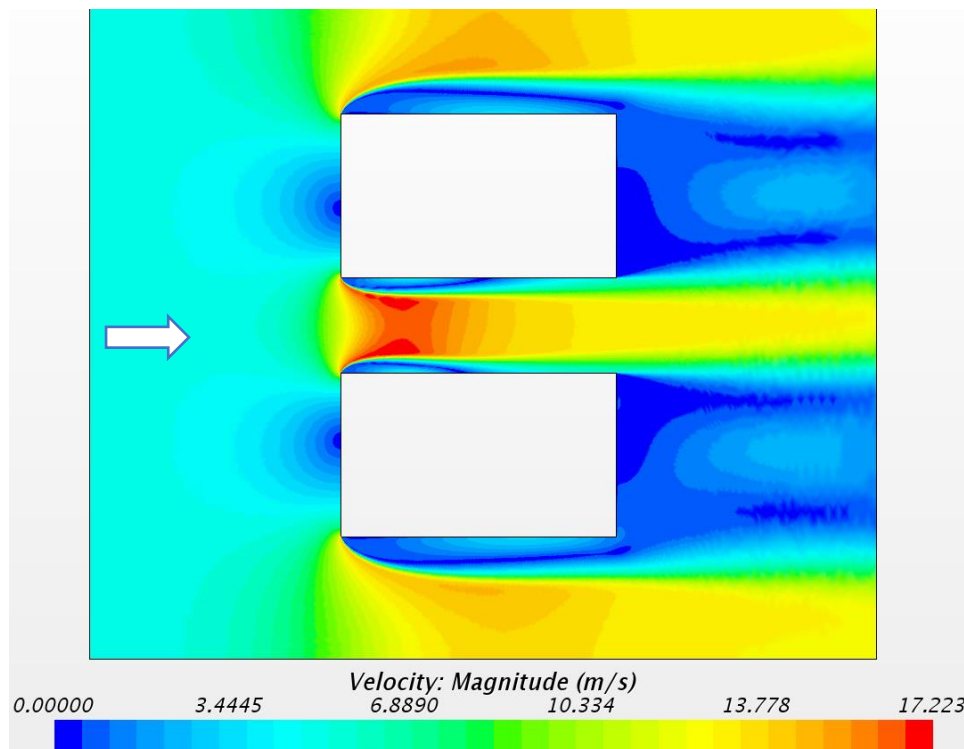


Figure 219. Aeraulic study of a detail of the space between the 2 towers (at altitude + 70m)

## 6.8. Study of a building zone with the addition of wind speed foil mplification

The space between the 2 towers, in spite of its right-angled edges, behaves like a natural wind amplifier. This space oriented towards the Seine is particularly active at the lowest wind speeds.

We propose to add in this study some punctual devices to reduce the wind and concentrate the flow in an identified area of the building. These elements are made of rigid shell panels (like an airplane wing) that we will call amplifiers or aerofoil aiming at concentrating and improving the stability of the wind speed around these 2 towers.

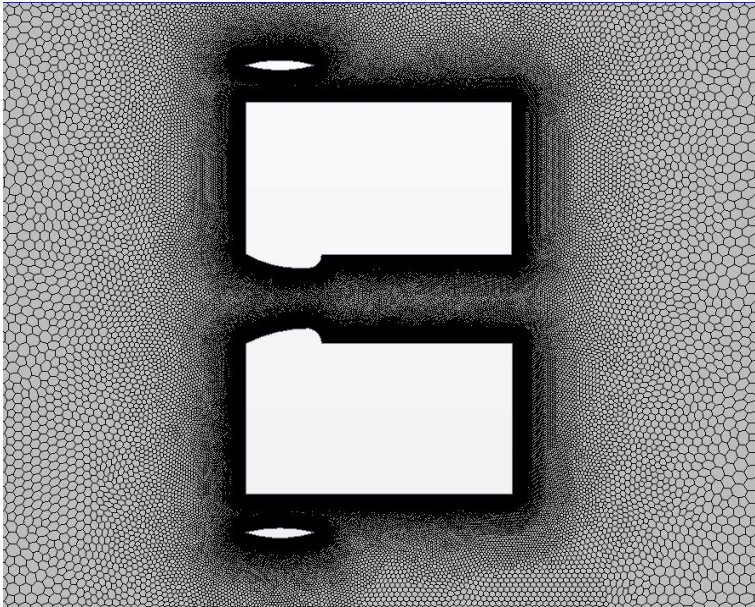


Figure 220. Study mesh on a horizontal section at +70m altimetry of the ENSAPVS building with 4 aerofoils

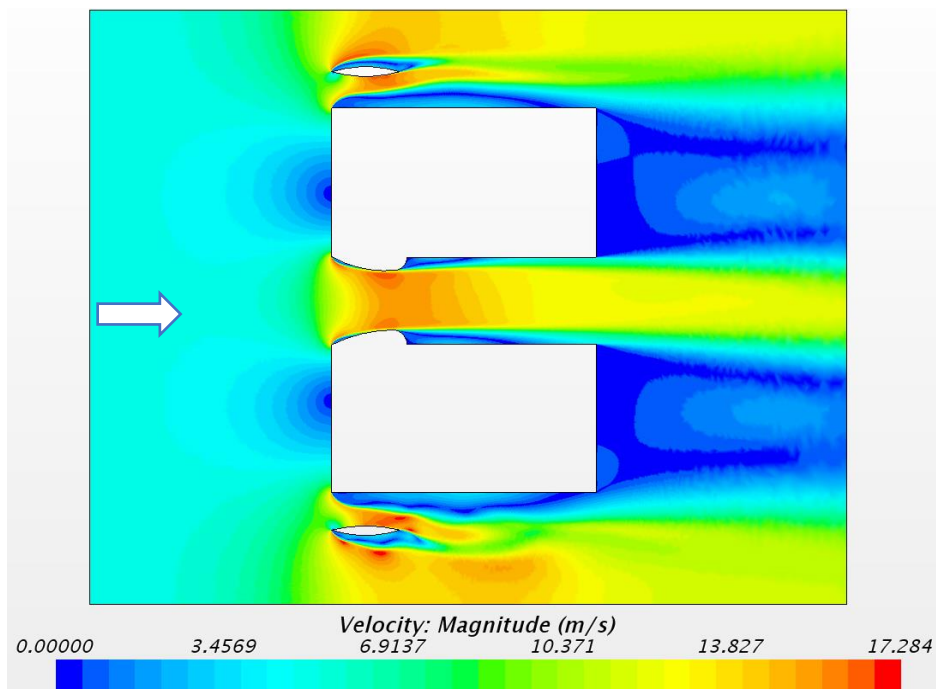


Figure 221. Airflow simulation at the 2 towers with the addition of aerofoils)

### 6.9. Other analysis with profiled foils to create a stabilized airflow zone

We then propose to modify the angle of the aerofoils along the towers to concentrate and improve the stability of the wind speed. **With an emergent wind speed of 5 m/s the wind speed between the 2 towers is approximately 16m/s or a 3-fold increase and 18m/s between the towers or 3.2 times the wind speed.**

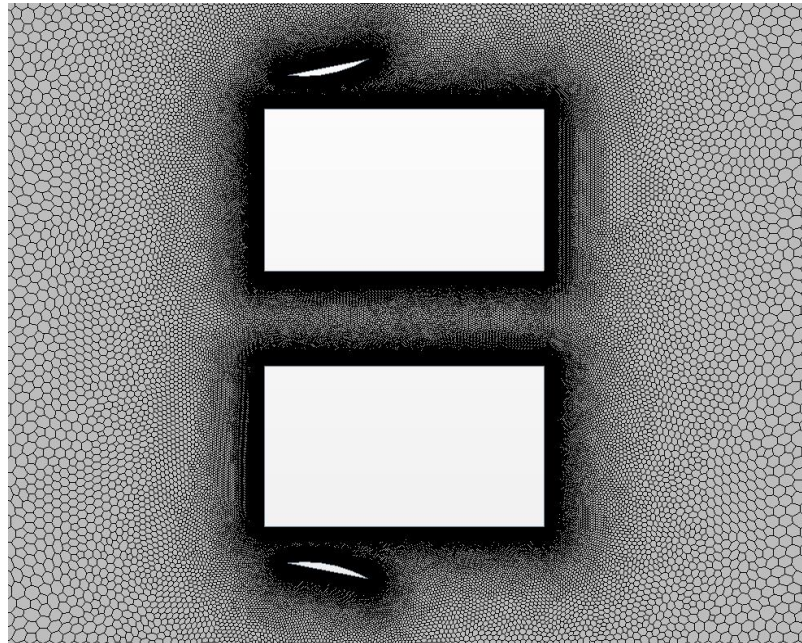


Figure 222. Study mesh on a horizontal section at +70m altimetry of the ENSAPVS building

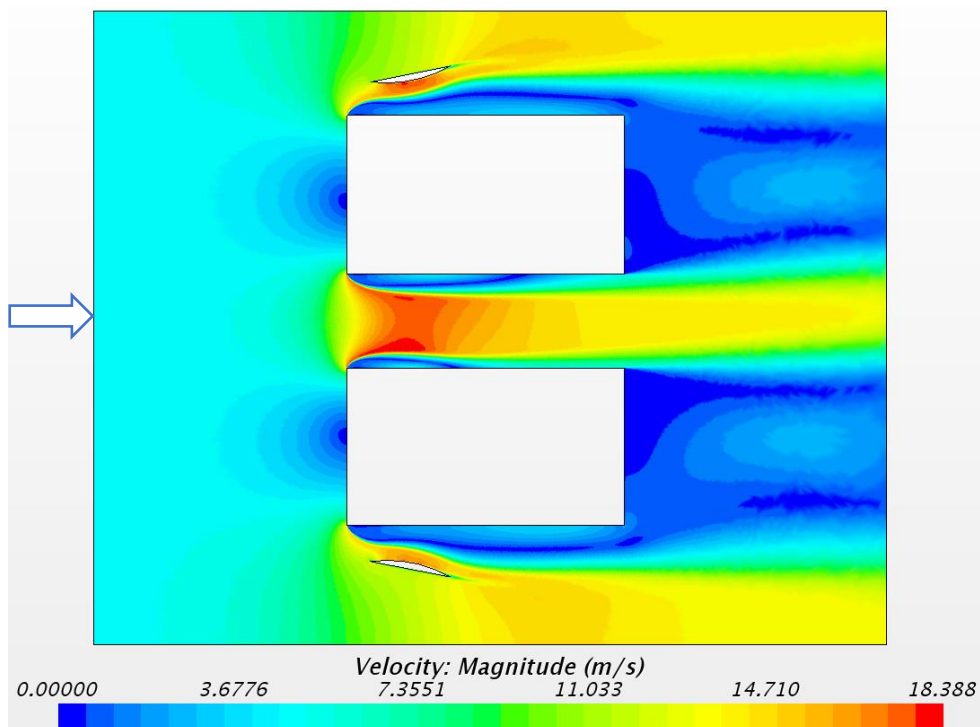


Figure 223. Aeraulic simulation at the 2 towers with the addition of a erofoil

- **Conclusion**

This study shows that in the case of twin towers, the space between the towers creates an important role in increasing the wind speed, on the order of a coefficient 3 ( Figure 221).

For the outer edges, slightly outwardly inclined aerofoils stabilize the airflow against the tower (Fig 222) and provide an acceleration zone of up to 14m/s.

For these reasons, we have kept the implementation of the main energy capture device at the axis between the 2 towers and secondary sensors along the aerofoils on the edges of the lateral sides . (See an example of integration in chapter 5.6.3)

**The electrical power generated by a wind turbine in this area (see chapter 3.1.1) is in a ratio depending on the cube of the air speed at a given location. By going from 5 to 13 m/s , the increase in air speed is of coefficient 2.5.**

## 7. ASSESSMENT OF THESE 4 STUDIES

In chapters 4.3 4.7, we were able to make an accurate simulation of the wind flow, when it comes into contact with different architectures: a 2-slope roof, an acroterion, a mansard roof and a complex building like ENSAPVS. Each of these profiles offers a type of wind acceleration around the building.

We also studied the addition of an acceleration and air speed control wing around the building.

These case studies on the impact of architectural volumes on airflow show us that the volumetry of buildings in an open urban environment, constitutes by its mere presence a surface of increase of the wind speed on site which can go from 150 to 200%.

The precise and careful integration of aerofoil profiles allows us to achieve an increase of 35 to 30% in the air speed at the periphery of the building. This allows us to increase the overall wind speed coefficient in precisely defined areas by 200 to 350%.

Comprehensive 3D simulations over the height or length of the building show that these wind speeds are not always continuous over time. However, the principle of an aggregation of wind turbines in a network or cluster<sup>133</sup> allows to multiply the zones of strong increase of energy production.

## 8. STUDY OF WIND TURBINES ADAPTED TO ARCHITECTURAL INTEGRATION

We will study, in the last part, the realization and the 3D modeling of several wind turbines. If the question of optimization and design of the turbine or electrical generator is not part of this research, it seems to us to be an important element for the architectural integration of the device.

We have studied very precisely the "design and conception" options of these elongated wind turbines in order to understand and evaluate their integration to the building. To do this, we made 3D prints of several models. These models were then tested in a wind tunnel to verify their operation and interaction with the building. We study in the following part in more detail, the mode of positioning and interaction between the architecture and the energy production turbine. Concerning the modeling, software such as Katia from Dassault Systèmes or SolidWorks

allow the integration of double curvature surface generation algorithms (helix type) in the design. We have, in a first step, modeled 3-blade turbines of needle type. The difficulty of operation of these turbines is related to the need to launch them at startup (because they do not start by themselves). Their starting speed is high. We also studied a Savonius type wind turbine. This Savonius type is more versatile and easier to integrate into a volume. However, depending on the study of the turbine rotation speed, the width of the blades, the depth of the bucket, and the height of the turbine must be adjusted (see figures 223 and 224).

We then proposed a Savonius-type turbine with a helical twist in its height to distribute and balance its rotation more easily. This is the device we used in most of the 3D simulations we performed<sup>134</sup>.

The 3D printing of these turbines is made by a hot filament printer. If this type does not allow a very great precision, as for the generation of the surface (precision of the impression lower than 0,1 millimeter) it was however economic to realize these prototypes.

We can envisage in the long run that the analysis or the precise numerical simulation will allow to customize the shape, the type or the length of the wind turbine according to the building.

Today, turbine systems can be printed or reinforced from carbon blades because the pressures on the wind turbines are high. Direct printing would only allow a life span of 2 or 3 years.

Another interest of 3D printing is the ability to test and multiply the profile of these aerofoils infinitely according to its shape and the attraction exerted by the wind on this turbine.

The use of a directly 3D printed (not molded) turbine has been tested for one of our prototypes. However, the foil must be skilfully braced and attached to the main structure while limiting the effects of vibration of the elements.

---

<sup>134</sup> The 3D prints for this study were made at the Fablab of the ENSAPVS school and at the independent Fablab VOLUMES with the help of Corentin Boiteau.



Figure 224 3D study of the wind devices integrated in the ENSAPVS building



Figure 225. Device study on the ENSAPVS building



# PART 5

## DESIGN AND ARCHITECTURAL INTEGRATION OF DEVICES



### Contents:

- Presentation of the architectural design method
- Typologies of integrated turbines and experimental study models
- Quantification of device performance
- Actional dendrograms for design support
- Case studies of architectural integration of wind power generation devices
- Creation of an open access library of wind device models on a collaborative BIM platform



DESIGN AND ARCHITECTURAL INTEGRATION OF DEVICES.....	207
1. INTRODUCTION.....	211
2. PRESENTATION OF THE ARCHITECTURAL DESIGN METHOD .....	211
2.1. The aerofoil, a wind gas pedal and stabilizer.....	212
2.2. Design of air intakes on a surface .....	212
2.3. Relative position of the turbine and the "aerofoil.....	213
2.4. The architectural volumes studied .....	214
2.5. Aggregation of wind devices Redundancy rather than optimization .....	215
2.6. The interest of using vertical axis micro wind turbines .....	216
2.7. Aerofoil based gas pedals .....	218
2.7.1. Hydrodynamic coefficients .....	220
• Rake is the angle between the chord of the airfoil (the line joining the leading edge to the trailing edge) and the position reference (usually the nominal operating attitude at cruising speed). The pitch can be adjusted to modify the lift. ....	220
• Angle of incidence of a foil.....	220
2.8. Aerofoil integration method .....	221
2.9. Study of the aeraulic systems on the racing cars.....	222
• Aerodynamic support .....	222
• Spoiler, lower body, DTM blades, .....	223
• Fins .....	223
• Spoilers and side skirts.....	224
• DTM blades .....	224
2.10. Wind turbines on measures profiled on the architecture and on the real site .....	225
• Variable angle aerofoils to accelerate and control the airflow .....	225
3. TYPES OF INTEGRATED TURBINES AND EXPERIMENTAL STUDY MODELS.....	226
3.1. Main types of wind turbines .....	227
• Nomenclature of the integrated wind turbines studied.....	228
3.2. Working method: M aquettes of physical studies as a source of design .....	229
3.3. 3D modeling of vertical axis turbines optimized for urban wind.....	230
3.4. 3D printing of optimized vertical axis turbines .....	230
3.5. Study models of integrated wind devices.....	233
3.6. Study in mock-up and profiling of devices.....	234
3.7. Physical wind tunnel study.....	234
3.8. Results and comparison with digital wind tunnel.....	234

3.9. The modes of integration of wind devices .....	235
4. QUANTIFICATION OF THE POWER OF THE DEVICES .....	236
5. PRINCIPLE ESTIMATION OF THE GLOBAL ENERGY PRODUCED IN A TYPICAL CITY	237
6. ACTIONABLE DENDROGRAMS FOR DESIGN SUPPORT.....	238
7. EXAMPLES OF ARCHITECTURAL INTEGRATION OF WIND POWER GENERATION DEVICES .....	241
7.1. Old or heritage buildings .....	243
7.2. Small scale building in isolated or coastal sites.....	244
7.3. Public facilities.....	246
7.4. High-rise buildings .....	252
8. CREATION OF AN OPEN ACCESS LIBRARY OF WIND ENERGY DEVICE MODELS ON A COLLABORATIVE BIM PLATFORM .....	261
6. GENERAL CONCLUSION.....	263
APPENDIX 2: DATA SHEETS OF WIND ENERGY CAPTURE DEVICES.....	278
APPENDIX 3: EXISTING BUILDING-INTEGRATED WIND ENERGY SYSTEMS .....	292
APPENDIX 4: EXAMPLE OF A WIND TURBINE STUDY USING A GENERATIVE DESIGN TOOL (FUSION 360).....	298
APPENDIX 5: A CALCULATION REPORT OF THE STARCCM+ SIMULATION .....	301
BIBLIOGRAPHIC REFERENCES .....	317
INDEX OF ILLUSTRATIONS.....	325

## 5.1. INTRODUCTION

Over the years, an architect develops his own way of conceiving spaces, and a working method that stems from this vision. For him, each **building is a prototype**. It is therefore not easy for us to imagine standardized architectural solutions without really accompanying him in his sketches or in his project approach.

However, since the post-war period, with the emergence of a large number of products to simplify the reconstruction and transformation of the country, architects have gradually **become assemblers of industrialized building products**. (Facade cladding, masonry blocks, plaster panels and ceilings,)

Would the aerodynamic simulations and the analysis method developed in this research allow us to produce **a set of architectural solutions** or design tools that builders could have at their disposal from the beginning of their project? In spite of the complexity of the flow around a building<sup>135</sup>, in spite of the diversity of urban contexts and the uniqueness of each building<sup>136</sup>, could architects have at their disposal **principles of aerodynamic analysis and integration of wind systems for their building?**

This is the objective of this sequence of our research which aims to design wind turbine models with their integration support structure and to insert them in existing or future architectural projects.

I have established an open access **catalog of 3D objects and models** (BIM-like) (online shared library at [www.RevitCity.com](http://www.RevitCity.com)) for the efficient integration of these devices into the work of architects. This database is open, and includes a pre-sizing of the **energy produced by these devices**. These typologies are grouped into **action dendrograms or decision trees** (see Figure 259) to guide architects and builders.

This work is then illustrated with a large number of **insertions of 3D models in contemporary architectural projects**, and we propose a **nomenclature of product typologies with the mode of assembly and implementation** on the building.

This design method, in order to be accurate, will also have to be based, in a second step, on a **specific aerodynamic simulation** that takes into account the exact volumetry of the building, the topography of the surrounding context and these possible buildings, and the urban wind corridors.

Not all of these virtual insertions have been numerically simulated, rather they are designed as **possible extrapolations of our research**.

## 5.2. PRESENTATION OF THE ARCHITECTURAL DESIGN METHOD

---

<sup>135</sup> Sinisa STANKOVIC, Neil CAMPBELL, and Alan HARRIES, *Urban Wind Energy*, Reprint, Routledge, 2015, 200 pp.

<sup>136</sup> K. R. RAO, "Wind Energy: Technical Considerations - Contents," in K. R. RAO (ed.), *Wind Energy for Power Generation: Meeting the Challenge of Practical Implementation*, Cham, Springer International Publishing, 2019, pp. 1-426.

In this chapter, we will study several scenarios of integration of wind devices to simple and then more complex buildings. Each of these studies is carried out using **numerical models for the design of the device and for the aeraulic simulation**. Physical models at reduced scales (1/5th and 1/10th) have been realized to test each prototype. They have not been the subject of experimental tests with air velocity readings by Pitot tubes in physical wind tunnel (pandemic context), but many experiments in real wind and wind tunnel have allowed to test and improve prototypes (3D printing of turbines, with mini-generator and piano wire supports) by reading the energy produced. In a second step, these studies will be compared to a simulation in digital wind tunnel of 3D models of the same devices.

In order to be able to compare the study in numerical simulation and the study in physical model and in particular the increase of the air velocity, the scale factors and in particular the Reynolds number<sup>137</sup> have been carefully defined between physical model and numerical model. We compared solutions against each other in each of these experimental models in order to progressively improve the choice of solutions and the implementation of devices on the building.

### 5.2.1. The aerofoil, a wind gas pedal and stabilizer

After having been able to precisely locate the wind turbine on the areas of highest wind speeds, we studied the increase of energy production by a wind "**amplifier**" in addition to the wind turbine. The "**aerofoil**<sup>138</sup>" allows to accelerate locally the wind speed, but also to stabilize the turbulences, and to integrate **the wind device in a "blade", or a "frame"** which, applied on the building, allows to let appear **a slot of air intake**.

We have also studied other examples of **foils and fins** developed by the nautical industry or by the automotive industry and **the modes of integration or design** of these systems. Despite the grid on the front of a car body, **automobile grills** have gradually become **the visual identity of a product and sometimes the emblem of a brand**.

In the hands of designers, purely technical elements without aesthetic quality have become **notable marks of difference** or identity of the product.

The study carried out here concerns several types of buildings which were selected and classified according to their scale, their use, their interactions with their urban environment. They present only a sample of the great diversity of buildings. The selected architectures are rather buildings of great **conceptual clarity and strongly articulated volumes**.

We did not study monolithic architecture in which the overall clean volume of the building lends itself more difficult to the integration of additional components.

### 5.2.2. Design of air intakes on a surface

The main function of a vehicle's grille is to admit cooling air to the car's radiator. But over the years and the design of vehicles by brands this purely technical and relatively unsightly

---

<sup>137</sup> Relationship between inertial forces and viscous forces, highlighted by Osbourne Reynolds in 1883

<sup>138</sup> English term for airfoil, from the old French feuille. A wing that controls the impact of the wind, either by lifting, by leaning, or by regulating turbulence.

device (a metal grille) has become one of the main visual components at the front of vehicles. As automotive designer Angelo Young puts it, "*an inspired design of the grille makes for an attractive car and shapes its identity by linking it to the history and reputation of the car manufacturer*"<sup>139</sup> " and has gradually played an important commercial role in seducing drivers. The aesthetics of the vehicle's grille "*is much more important than whether the design features actually serve.*"<sup>140</sup>

The grille has become a main identification element for car brands. For example, Rolls-Royce with its Parthenon grille straightens the angle of the bars so that they appear perfectly vertical; Bugatti is known for its horseshoe-shaped grille, BMW (nostril-shaped), Ford, Jaguar or Aston Martin are inspired by fighter jet engine style grilles for their cars Porsche, a manufacturer of air-cooled cars, continues to crush and minimize the importance of a grille on its modern vehicles (see figures 225 and 226). Tesla has simply made them disappear in favor of a simple slit in place of the bumper, which is non-existent since Lidar sensors prevent any impact on the car.



Figure 226 : Comparaison de Calandres automobiles présentant comment une grille de ventilation est devenu un symbole de marque



Figure 227 Examples of air intakes on the fuselage of a jet aircraft

### 5.2.3. Relative position of the turbine and the "aerofoil"

During the study of the installation of a horizontal axis wind turbine on the ridge of a double slope house roof, we compare the position of this turbine and an aerofoil type wind gas pedal. This gas pedal is made of a folded steel or composite sheet whose roughness will be defined to limit the turbulences in the air flow. The foil constitutes a shell fixed on the structure of the

<sup>139</sup> Does Your Car Look Happy To You? Designers Talk About The Evolution Of Lights, Grilles And Bumpers, <https://www.ibtimes.com/does-your-car-look-happy-you-designers-talk-about-evolution-lights-grilles-bumpers-1491974>, accessed May 23, 2020.

<sup>140</sup> *Ibid.*

building by a triangulated support<sup>141</sup> in order to guarantee a great rigidity of the surface and to limit the vibratory effects of this structure.

The relative position of the foil, the roof geometry and the turbine of the wind device is an important issue in this research. We experimented, in the numerical model and in the physical model, the different angles between these elements, but also progressive shifts of the respective position of these 3 elements: the roof, the turbine and the foil.

We sought to increase the steady-state wind speed. Our numerical simulations show a significant potential for a 2-3 fold increase in wind speed when the aerofoil and roof are accurately positioned.

The support structures of the aerofoil and the turbine will be made of steel, aluminium or composite tubes braced by triangulation of the elements. In the reduced scale prototypes, we used piano wire whose rigidity and fine diameters limit the vibratory forces with the wind.

The numerical studies were confirmed in different physical models which integrated micro-turbines. By comparing the electrical power (in volts) generated by each of these devices, after adjusting the position of the foil and the turbine, we gradually obtained results comparable to the simulations.

#### 5.2.4. The architectural volumes studied

In the framework of this study we studied 4 typologies of buildings:

1. Small scale typology of 1 to 3 levels (scale of the individual house or a small collective)
2. Typology of medium scale from 3 to 7 levels (scale of the urban collective building)
3. Large-scale typology of 7 to 15 levels (scale of a building-island type IGH)
4. Very large scale typology of 15 to 30 levels (scale of exceptional buildings or residential or office towers)



---

<sup>141</sup> Triangulation of the wind turbine support structures increases the rigidity of the assembly and the bracing of the device

Figure 228. Exemples de volumes architecturaux d'échelles différentes étudiées pour l'intégration de micro-éoliennes et de foils.



Figure 229. Exemples de volumes architecturaux de grande échelle étudiés pour l'intégration de micro-éoliennes et de foils. (Ecole Architecture Paris-Val-de-Seine, Paris 13ème/ la Grande Arche de la Défense, Puteaux (92))

### 5.2.5. Aggregation of wind devices Redundancy rather than optimization

The choice of wind device, the mode of aggregation of devices, the type of context or the type of architectural integration are all parameters that allow, not only to define the productivity or the performance<sup>142</sup> of energy extraction but also the very low nuisance of these devices on the environment.



Figure 230 Mode de mise en « cluster » de dispositifs éoliens (fonctionnement en groupes de turbines rapprochées)

We have worked on a paradigm of micro-wind turbines, whose energy performance is reduced, but whose quantity and mode of aggregation participate in the regulation of the energy produced and in the reduction of wind turbulence at the exit of the devices.

We take as a basic principle the **redundancy of distributed wind devices at reduced cost**, rather than the energetic optimization of isolated devices (taking for granted a territory of implantation

<sup>142</sup> Jorge L. ACOSTA, Kevin COMBE, Saša Ž DJOKIC, and Ignacio HERNANDO-GIL, "Performance Assessment of Micro and Small-Scale Wind Turbines in Urban Areas," *IEEE Systems Journal*, March 2012, vol. 6, n°1, pp. 152-163.

without limits and without pollution constraints). The Caltech study<sup>143</sup> shows that vertical axis micro-wind turbines limit the resulting wind turbulence, and this allows the densification of their aggregation on a given area.

In this study, we studied two aggregation scenarios:

- A scenario of **grouping devices in a linear series**
- A **field assembly** scenario, respecting precise distribution rules

For serial grouping, the devices are plugged into each other in a linear fashion to create a continuous line of assembled devices (e.g., wind devices integrated into guardrails or along the sides of a building). This strategy allows, during wind turbulence, to capture the movement of the wind over a large height or length and to multiply the sources and continuity of energy production, despite the small diameter of the turbines.

The other type studied is that of wind fields that are grouped (in a "cluster") on the roof or on a surface of a building and thus allow to increase, by their redundancy, the capture of wind energy accelerated by the building.

This method of implementation is based on the principle of redundancy of devices rather than on **the optimization of a few more efficient but fewer systems**. Some plant or tree structures, for example, often use multiple branches and leaves and flowers, rather than reducing the number of components<sup>144</sup>.

This paradigm is very different from the one used for the design of our energy infrastructure in the post-war period, namely the **centralized production of energy** on a few points of the territory and distributed by a complex network to a whole country.

#### 5.2.6. The interest of using vertical axis micro wind turbines

Several interesting studies conducted by the Environmental Engineering Department of Princeton, Stanford and Caltech Universities on the synergistic aggregation<sup>145</sup> of multiple wind turbines on the same site show that, contrary to all expectations, grouping wind turbines according to precise aggregations based on studies of aeraulic turbulence, or biomimetic studies of the behavior of fish schools do not produce less energy, or even demonstrate an increase in their performance.

---

<sup>143</sup> Robert W. WHITTLESEY, Sebastian LISKA, and John O. DABIRI, "Fish schooling as a basis for vertical axis wind turbine farm design," *op. cit.*

<sup>144</sup> Janine M. BENYUS, *Biomimicry: When Nature Inspires Sustainable Innovation*, 1<sup>re</sup>ed. Paris, HARMONIA MUNDI, 2011, 408 pp.

<sup>145</sup> Seyed Hossein HEZAVEH, Elie BOU-ZEID, John DABIRI, Matthias KINZEL, Gerard CORTINA, and Luigi MARTINELLI, "Increasing the Power Production of Vertical-Axis Wind-Turbine Farms Using Synergistic Clustering," *Boundary-Layer Meteorology*, November 1, 2018, vol. 169, n °2, pp. 275-296.

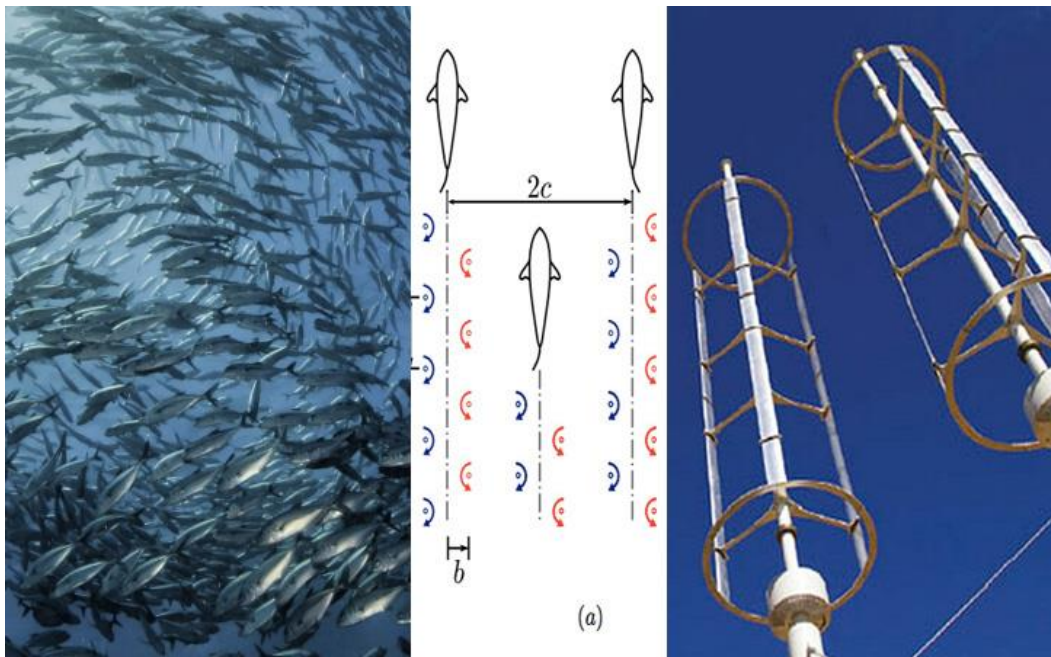


Figure 231 Dabiri biomimetic model of fish schools to define the aggregation mode of wind turbines<sup>146</sup>

*"The simulations confirm that vertical-axis wind turbines have a positive influence on each other when packed in well-designed clusters: such configurations increase the power generation of a single turbine by about 10 percent. In addition, the cluster designs allow for closer turbine spacing resulting in about three times the number of turbines for a given land area compared to conventional configurations. Therefore, both the turbine and wind-farm efficiencies are improved, leading to a significant increase in the density of power production per unit land area."<sup>147</sup>*

Most wind farms consist of horizontal axis wind turbines (HAWT) because of the high power coefficient of an isolated turbine.<sup>148</sup> However, in the vicinity of neighboring turbines, HAWTs suffer from a reduced power coefficient. In contrast, research from this lab on vertical axis wind turbines (VAWTs) suggests that closely spaced VAWTs suffer **only small decreases (or even increases)** from the power coefficient of an individual turbine when placed in close proximity to neighbors, producing much higher powers for a given terrain.

<sup>146</sup> Robert W. WHITTLESEY, Sebastian LISKA, and John O. DABIRI, "Fish schooling as a basis for vertical axis wind turbine farm design," *op. cit.*

<sup>147</sup> *Ibid.*

<sup>148</sup> Mechanical power divided by the power of the free air through the turbine cross section.

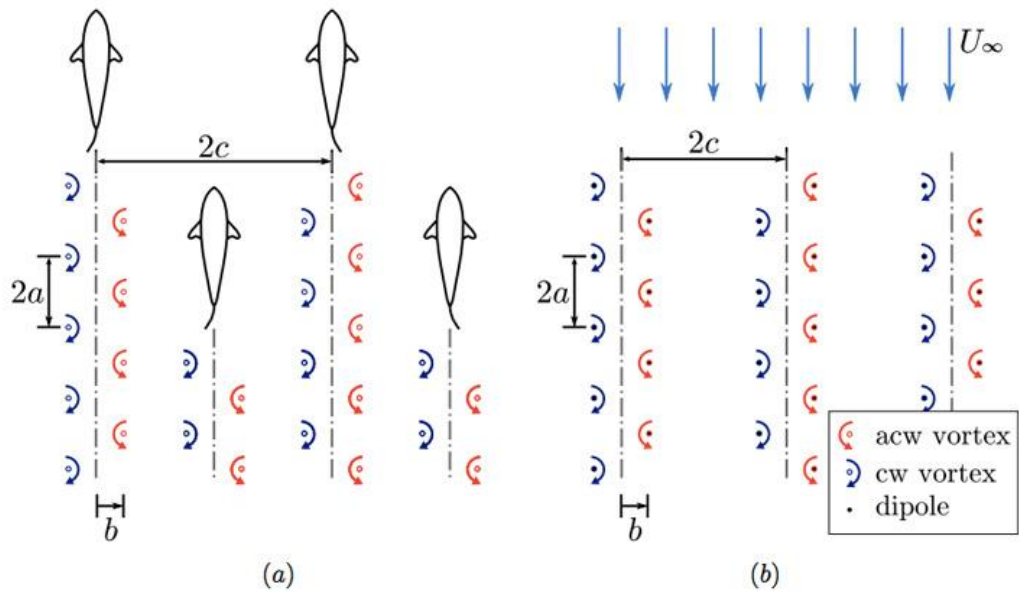


Figure 232 Study of turbulence generated by the group effect of fish and wind turbines taken from the mentioned research<sup>149</sup>

A **potential flow model of vertical-axis wind turbine (VAWT) interactions** is developed in this study by John Dabiri<sup>150</sup> and his team at the Caltech Field Laboratory for Optimized Wind Energy (FLOWE) in California. To investigate the effect of changes in the spatial arrangement of VAWT turbines on the coefficient of performance of the close group of turbines, he compares the expected average power coefficient of turbines in an array to a spatially isolated turbine. A planar layout based on the **biomimetic configuration of fish school wakes**<sup>151</sup> significantly increases the coefficient of performance of the array (cluster) based on a  $16 \times 16$  wind turbine array. The results confirm a **doubling of the extracted energy power for a given area compared to horizontal axis wind turbines.**

### 5.2.7. Aerofoil based gas pedals

Derived from the Latin *folia*, (leaf) foils are wind control surfaces that accelerate the speed of movement of vehicles and or sailboats.

In the case of the nautical industry, the first foils were developed by Eric Tabarly and his foiling trimaran: the Paul Ricard<sup>152</sup>. The foils really became widespread in the 2000s with the appearance of hydrofoils<sup>153</sup>; these hydrofoil multihulls can reach extremely high speeds thanks to their foils:

<sup>149</sup> Robert W. WHITTLESEY, Sebastian LISKA, and John O. DABIRI, "Fish schooling as a basis for vertical axis wind turbine farm design," *op. cit.*

<sup>150</sup> Ibid.

<sup>151</sup> Ibid.

<sup>152</sup> Tabarly : the foil history of the Paul Ricard trimaran,

<https://www.voileetmoteur.com/voiliers/actualite-voile/regates-courses/tabarly-la-foil-histoire-de-paul-ricard/72662>,

<sup>153</sup> Jean-Mathieu BOURGEON, Stéphane DYEN, Davy MOYON, Daniel SCHMÄH, Robin AMACHER, Damien COLEGRAVE, Martin CALMON, Mohamed FARHAT, Pascal FUA, Konstantin STARTCHEV, Guillaume BONNIER, Jan-Anders MÅNSEN, Véronique MICHAUD, Antoine SIGG, Marc OGGIER, Michel DEVILLE, Olivier BRAUN, Mark

more than this 100km/h<sup>2</sup>. The sailing speed record was newly set in 2012 by the Vestas Sailrocket 2 (See Figure 6), a foil-powered craft. A top speed of 121 km/h was measured in 2012 in Namibia by Paul Larsen, an Australian sailor.



Figure 233 Vestas Sailrocket 2, piloted by Paul Larsen and designed by the English naval architect Malcolm Barnsley



Figure 234. The Greenbird, a wind-powered car, breaks the speed record in the Nevada desert at 201 km/H, piloted by the Englishman Richard Jenkins. It also uses a rigid carbon sail of the Foil type to reach 3 to 5 times the wind speed.

The speed of travel generates **hydrodynamic lift** on the foil capable of lifting the hull(s) of the boat partially or totally out of the water. The purpose of this lift transfer is to **reduce hull drag** (friction and waves) and to reduce the power required for cruising speed.

The shape of the foils<sup>154</sup> (profile and length) is generated for hydrodynamic reasons, a strong elongation allows to reduce the drag induced by the lift. In the case of sailboats (bending beam, bending moment), the profiles are thickened and lengthened.

According to the Coanda effect<sup>155</sup> and Newton's law, due to the viscosity of the medium, the moving air mass that encounters a cambered airfoil follows the surface of this airfoil; the air mass

---

SAWLEY, Luc BLECHA, and Joël CUGNONI, *L'Hydroptère: A story of a dream*, <https://infoscience.epfl.ch/record/161566><https://infoscience.epfl.ch/record/161566>, accessed May 24, 2020.

<sup>154</sup> Matthew SHEAHAN, "The foiling phenomenon - how sailing boats got up on foils to go ever-faster," p. 19.

<sup>155</sup> *The Coandă effect, (named after the Romanian engineer born in 1886 Henri Coandă, is the attraction or attachment of a fluid to a convex surface on which it flows. The fluid follows the surface and*

is deflected, this is the Coanda effect. In reaction to the momentum of the air mass deflected in one direction (downwards for a load-bearing airfoil), the wing is pulled in the other direction (upwards).

For a positive incidence (leading edge above the trailing edge), the dissymmetry of the profile creates higher speeds on the upper surface and lower on the lower surface. The assumption of incompressibility of the studied fluid allows to explain this. Indeed, this assumption allows to show the conservation of the volume flow of the flow. On the extrados, the flow lines are tightened, the surface decreases so the speed increases by conservation of the volume flow and the opposite occurs on the intrados. According to **Bernoulli's theorem**<sup>156</sup>, usable only under certain hypotheses supposedly verified when a foil is working, (homogeneous, incompressible and stationary flow) the pressure decreases when the speed increases and vice versa. Thus, an overpressure is created on the lower surface and a depression on the upper surface, which leads to an upward lift force and allows the foil to rise. Airfoils are generally defined by their main geometric characteristics and their hydrodynamic characteristics (lift coefficients, drag, pitching moment).

#### 5.2.7.1. Hydrodynamic coefficients

The  $C_z$  or lift coefficient, depends on the weight, the bearing surface and the speed. Frequent value: 0,4 to 0,7 at cruising speed. The lift is  $F = q S C_z$  with  $q = \text{dynamic pressure} = 1/2 \rho V^2$  and  $\rho = \text{density of the fluid}$ .

The  $C_x$  or drag coefficient of the foil, depends :

- The profile and its surface condition. The surface roughness influences the frictional drag coefficient (effect of laminarity),
- Drag induced by lift (influence of aspect ratio, planform, interactions),
- The proximity of the surface (influence of the immersion on the wave field).
  - *Rake is the angle between the chord of the airfoil (the line joining the leading edge to the trailing edge) and the position reference (usually the nominal operating attitude at cruising speed). The pitch can be adjusted to modify the lift.*
  - *Angle of incidence of a foil*

The angle of *attack* (AoA) of a foil is the angle between the chord of the airfoil (the line joining the leading edge to the trailing edge) and the flow (the local velocity vector). When the attitude increases, the incidence and the lift increase.

The lift increases with the incidence (lift slope). From a certain angle, whose value varies according to the profile and the elongation of the bearing surface, there is a separation of the flow called *stall and loss of lift*.

---

*undergoes a deflection before detaching from it with a different trajectory than the one it had upstream. This phenomenon is a stationary bifurcation in a fluid flow.*

<sup>156</sup> Established in 1738 by Daniel Bernoulli, states that in the flow of a homogeneous and incompressible fluid subject only to the forces of pressure and gravity, an acceleration occurs simultaneously with the decrease in pressure.

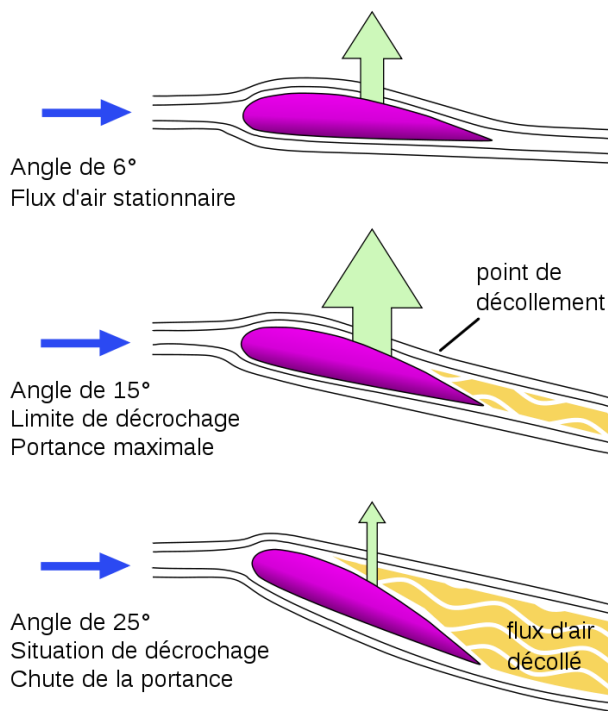


Figure 235. Angle of incidence of a foil ( source : Wikipedia, lift)

### 5.2.8. Aerofoil integration method

The insertion of wind power generation devices into buildings poses a real challenge to architects.

The devices need to be widely exposed to the wind by being located at the ends of the buildings (roofs and envelopes), but architects do not want to show them today and users, despite their interest in passive buildings, do not want to see any movement in their environment and hear any noise. How can one really propose a wind device without **disfiguring the urban landscape or altering the architect's architectural project?**

It is important to know if a wind energy system is relevant and cost-effective at the project design stage. The architect and the design team could, from the first sketches and the implementation of the building profile in the site, think about this relationship between energy system and project. We can cite the example of the **elevator**, which is now installed from the first sketches of the project as a structuring element of the building, whereas for years it was only a technical addition on the periphery or at the back of the building. We can also mention elements such as roof overhangs, sunbreaks, acroteria, which are all devices invented by modern architects and have become the basis of contemporary architectural language. The construction rules certainly influence the systematization of the use of these devices, but the innovative architectural image and the **massive prescription assistance of the building industry will stimulate their emergence and their commonplace.**

Thus, the principles of implementation should be simple and didactic enough for architects to include them in their design process from their first sketches.

We can also consider another hypothesis of development of these systems: The architecture would not be conceived with these devices, they would be grafted to it. That is to say that the time of the conception of the project would remain a different time from that of the question of the energy production. In this case, **how to transmit the bases and the principles to propose a great diversity and a freedom of implementation?**

2 types of method of integration can be considered: a method by the addition, by grafting of the device; This can be realized either by the design of a device or **an architecture which treats the technical systems like a mechanic** in the thought of the architects-builders, one speaks about the hi-tech architecture, or the technical systems are made readable, they reveal with transparency, the fact that any architecture is built from an assembly of components, equipment and systems. Some architects such as Renzo Piano or Richard Rogers have even made it an architectural approach, visible in the Centre Pompidou in Paris or in the Madrid Barajas airport. This is expressed in oversized air vents that become elements of urban furniture (Centre Georges Pompidou, Paris), or lighting fixtures that are elements supported by a vault (Barajas Airport, Madrid).

The second method would be to work in **complete integration of the gas pedal or turbine**, treating them as recessed in the building, to make **the element non-visible and non-discernible**. This is the principle of the integrated aerator, which can be found on car grills or jet engines, where a simple slot on the surface of the objects allows to profile and regulate the constant air flow.

#### 5.2.9. Study of the aeraulic systems on the racing cars



Figure 236 Aeraulic study of a McLaren F 1, 2019 ( Soucre : MacLaren entreprise)

- *Aerodynamic support*

At such high speeds, race cars interact strongly with the air around them. Engineers have used this interaction to keep the car on the ground. If an airplane wing generates a vertical force, called lift, due to its speed through the air, a car's wing points toward the

ground to generate a force toward the ground. This vertical force towards the ground is the **aerodynamic lift**.

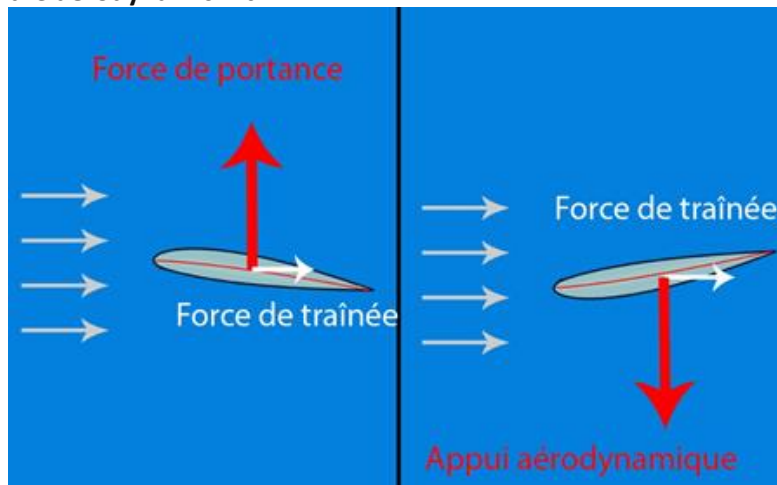


Figure 237 Wing profile on the left: lift force, upside down wing profile on the right : aerodynamic support.

The **spoiler** can also be tilted at the driver's discretion to increase or decrease this vertical force. But the higher the vertical force that slams the car to the ground, the higher the air resistance force (drag force). In order to go fast in the corners, a high aerodynamic downforce is necessary, which increases the grip in the corner. However, a force of air resistance (drag force) is also present. The latter opposes the movement of the car, which slows it down in a straight line. The angle of these fins must therefore be precisely adjusted. This is why the aileron setting is specific to each vehicle and each race track.

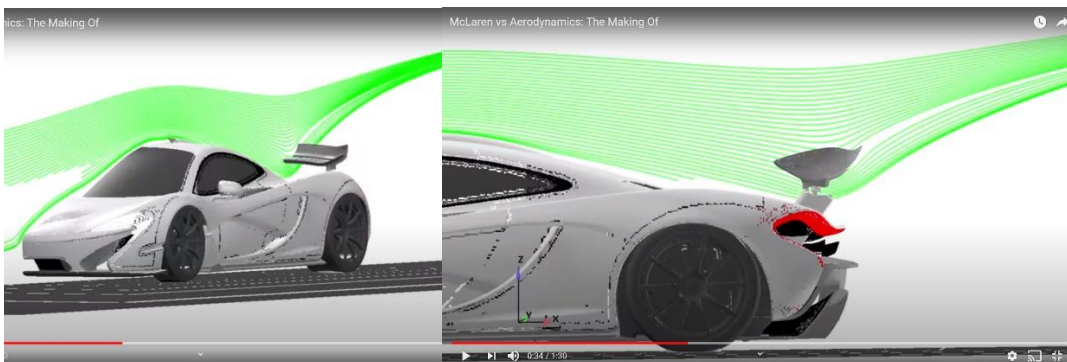


Figure 238 Aerodynamic simulation of a rear wing on the aerodynamic support of a McLaren F1 ( Source McLaren)

- Spoiler, lower body, DTM blades, ...

In designing a car, the two essential aerodynamic elements for an automobile are drag and lift. Most cars have an airfoil-like profile with a curved top and a nearly flat bottom. This difference between the air above the car and the air below creates a vacuum that lifts the car, which is called lift. The objective of the aileron design is to decrease the lift with several solutions:

- Fins



Figure 239 Examples of car fins integrated into the car body

The spoiler offers an alternative to the lift by providing a compensating force. Its design is specially studied to add weight on a part of the body (rear in general). Indeed, its semi-circular cut directed upwards recovers the air. The higher the speed, the stronger the pressure and the heavier the weight. The only drawback is that its design does not favor air penetration and slows down the vehicle that is equipped with it. The shape of the fins is specially designed to be effective from a certain speed and beyond. Vehicles with too little power will not benefit from the qualities but only the defects. Advice: for the rear spoiler, the adjustment will concern the inclination. The more it is inclined, the more weight there will be on the rear and the more stable the car will be (but also braked).

- *Spoilers and side skirts*

The role of spoilers is twofold, they profile the car to improve its Cx (coefficient of penetration) which has the effect of reducing drag. They also reduce lift by lowering the front of the vehicle. Thus, less air is rushed underneath and therefore the lifting force decreases. Finally, the various ribs that often point upwards act (at high speeds) as small spoilers to support the front end. However, the spoilers are designed not to create aerodynamic turbulence, otherwise they may generate an imbalance at high speed and/or an increase in drag. The side skirts play a similar role but in a less important way. They reduce lift and drag by improving the Cx and lowering the sides of the vehicle. In addition, they channel air from the front wheels to the rear wheels.

- *DTM blades*



Figure 240 Examples of DTM blades on the front of a car

The DTM (Deutsche Tourenwagen Masters) blade, named after the German Grand Touring trophy, is low to the ground and cuts through the air. Its role is once again to reduce lift. Its horizontal design allows the air coming from the front to be channeled to the sides: the bumper, the grille, ... There is less air underneath, so ... less lift.

Discovered on the Enzo, the new aerodynamic appendages of this car are controlled by electronics. According to all the information collected by the sensors: speed, steering angle, ... the electronics will define an inclination for the mini spoilers placed in the front and rear spoiler.

These new elements are reactive and allow the car to be 70% more efficient than a standard vehicle.

#### 5.2.10. Wind turbines on measures profiled on the architecture and on the real site

The objective of this part of the thesis is to be able to schematize simple and efficient design principles for architects and engineers, to propose integration modes based on wind data (from wind mapping or anemometric site surveys), to be able to custom build the device to fit the architecture, and to evaluate the performance of the extracted energy when the wind speed increases. We will then talk about **tailored** wind devices.

- *Variable angle aerofoils to accelerate and control the airflow*

We can compare this to the way the fins of racing cars use aerodynamic support at high speed (over 220km/h) to keep the car on the ground and compensate for the effect of aerodynamic lift that tends to lift the car off the ground.

We can also compare this to the foils under the ship of a catamaran of profiles to make sailing boats of more than 7 tons of weight go out of the water at more than 1 meter high. These foils limit the frictional forces between the hull surface and the water at the high speeds of the sailing boat.

**Can we imagine an architectural profiling where fins on the external volumes could adjust the wind speed and the improvement of energy production but also other performances of the facade as sunshade, rainwater collection, technical network path (such as wiring and water network, privacy or protection screen), element of silhouette refinement, element of natural ventilation of the building, element of pressure and depression of the earth on the wall of the architecture?**

### 5.3. TYPES OF INTEGRATED TURBINES AND EXPERIMENTAL STUDY MODELS

In spite of our intensive research, we could not present here **all the existing types of wind turbines<sup>157</sup> today as they are so** numerous and diverse. From the wind systems in the 19th century, to pump water, to the vertical axis turbines (Savonius and Darrieus)<sup>158</sup> and to the gearless direct drive wind turbines<sup>159</sup> and it is surprising to note, that despite a use that remains marginal, there is a very large quantity of new products on the market.



Figure 241. 4 2 Types of vertical axis wind turbines

However, our study shows that **robotic manufacturing technologies** such as **3D digital printing<sup>160</sup>** allows us to imagine the manufacturing of efficient wind turbines<sup>161</sup> precisely adapted to the type of wind, the type of aerofoil and the type of building to be built.

These technologies make it possible to consider **custom manufacturing** according to the needs of the building or the constructors with **the possibility of a fast replacement in case of damage**, thanks to digital printing. However, the different forces that apply to the blades during high winds now require the use of **carbon fiber, glass fiber or bent metal blades** to reinforce these products. The turbine will be chosen according to the different implantation situations.

---

<sup>157</sup> D. A. SPERA, "Wind Turbine Technology," *The U.S. Department of Energy's Office of Scientific and Technical Information*, 1994.

<sup>158</sup> Ion PARASCHIVOIU, *Wind Turbine Design. With Emphasis on Darrieus Concept - Ion Paraschivoiu*, Polytechnic International Press, 2002.

<sup>159</sup> B.J. CHALMERS and E. SPOONER, "An axial-flux permanent-magnet generator for a gearless wind energy system," *IEEE Transactions on Energy Conversion*, June 1999, vol. 14, n<sup>o</sup>2, pp. 251-257.

<sup>160</sup> K. BASSETT, R. CARRIVEAU and D. S. -K. TING, "3D printed wind turbines part 1: Design considerations and rapid manufacture potential," *Sustainable Energy Technologies and Assessments*, 1 September 2015, vol. 11, pp. 186-193.

<sup>161</sup> Nuomin HAN, Dan ZHAO, Jorg U. SCHLUTER, Ernest Seach GOH, He ZHAO, and Xiao JIN, "Performance evaluation of 3D printed miniature electromagnetic energy harvesters driven by air flow," *Applied Energy*, September 15, 2016, vol. 178, pp. 672-680.

5.3.1. Main types of wind turbines

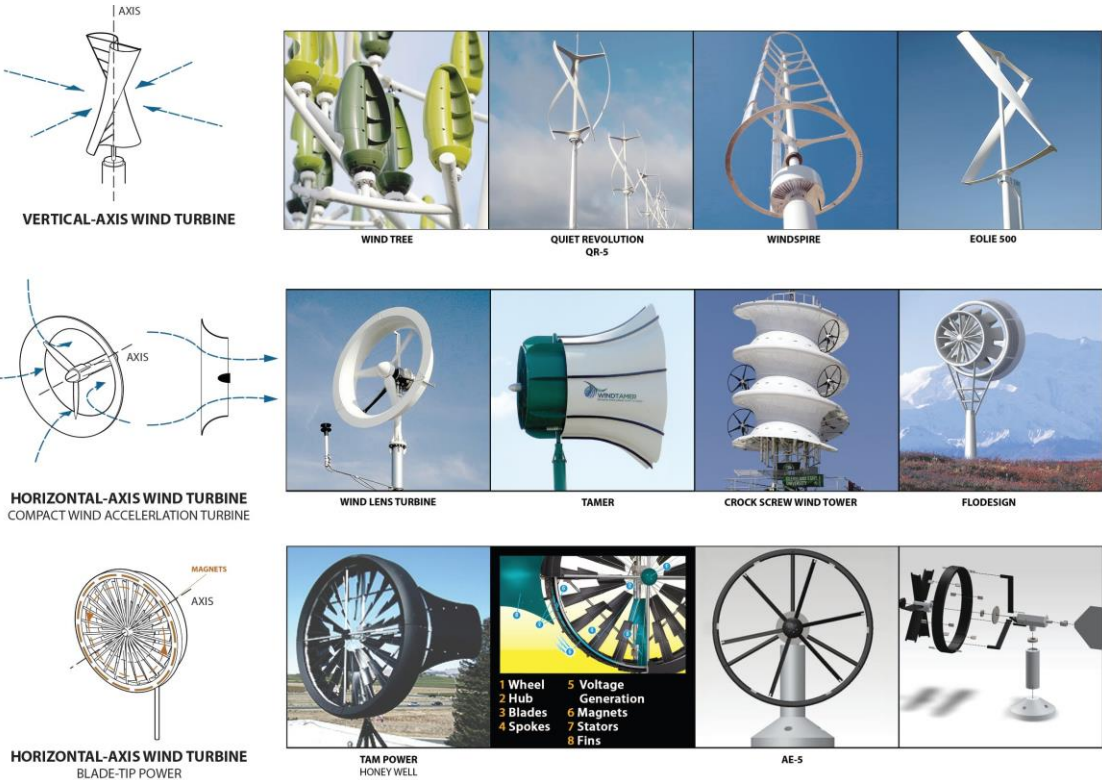


Figure 242 Main typologies of wind energy devices that can be integrated into buildings

For the types of turbines (refer to this subject, in part 2)

• *Nomenclature of the integrated wind turbines studied*

IMAGE	TAMI TURBINE	HELIX WIND S594	WIND TREE	QR6 Quiet Revolution wind turbine	POWER FLOWERS	HORIZONTAL WIND TURBINE (conventional)	MOTORWIND	CSU	AEROCAM	520H AEROTURBINE
TYPE	Blade Tip Power	Vertical	Vertical	Vertical	Vertical	Horizontal	Horizontal	CWAT	Horizontal/Vertical	Horizontal/Vertical
LOCATION	Charleston, SC, US Rooftop	Chicago, US Roof Top: recommend 2 ft above roof line.	Paris, France Open space	London, UK Rooftop (6m tall) Ground (15-18 m tall)	Deft, the Netherlands Open space	Manama, Bahrain World Trade Center Bridge between skyscrapers	Hong Kong Rooftops of buildings Balconies at home	Roof top of a baseball stadium	Rooftops of buildings	Chicago, US Rooftops of buildings
DIMENSIONS	1,8 m in diameter	Rotor dimension: 4,87 m x 1,2 m	The steel tree stands 11 m tall and 8 m in diameter	5,5m tall, 3,1m diameter, 16m <sup>2</sup> swept area	3,4 m tall Each unit is 3m in diameter	Blade Diameter: 3,7 m	Unit: 26 cm in diameter Frame: 1,02 l x 0,54 m h x 0,14 m	1,83m in diameter, 3,04m long for each unit	2-2,5 m in diameter, 3-3,5 m tall	1,83m in diameter, 3,04m long for each unit
ECHELLE / WIND RANGE	0,2- 15,7 m/s	> 2 m/s	2,5 m/s	3,5 - 26 m/s	12- 33 m/s	7,5 m/s	> 2 m/s	wind amplification to be at about 1,5 times the regular rate	2-17 m/s	11 m/s
GENERATION / ENERGY OUTPUT	6,67 kW/h	4,5 kW/h	3,1 kW/h	8,5 kW/h	152 kW/h	7 kW/h	1,2 kW/h	83 kW/h	35 - 93 kW/h	1,5 kW/h
INVENTEURS / RESEARCH TEAM	TAMI Energy Charleston, SC, US	HOK United States	Jérôme Michaud- Larivière France	Quietrevolution United Kingdom	NL Architects The Netherlands	Atkins UK	Lucien Gambarota / Hong Kong University Hong Kong	Majid Rashidi, Ph.D Cleveland State Univ. U.S.	BroadStar TX, CT, United States	Aerotechture International Murphy/Jam Architects United States
DATE	2011	2010	2015	2011	2011	2007	2007	2012	2007	2007

### 5.3.2. Working method: Physical model studies as a source of design

Physical models are a tool for architects to develop the space and volume of a building. In particular, they allow the study of issues of scale and proportion of that building in its context. In this research, the model was used instead as a prototype<sup>162</sup>, to modify and sculpt the elements of the envelope, evaluating its performance in the wind of a single fan. Without precisely quantifying the air velocities or energy extracted, we were able to quickly improve the layout **and gas pedal type of these devices.**

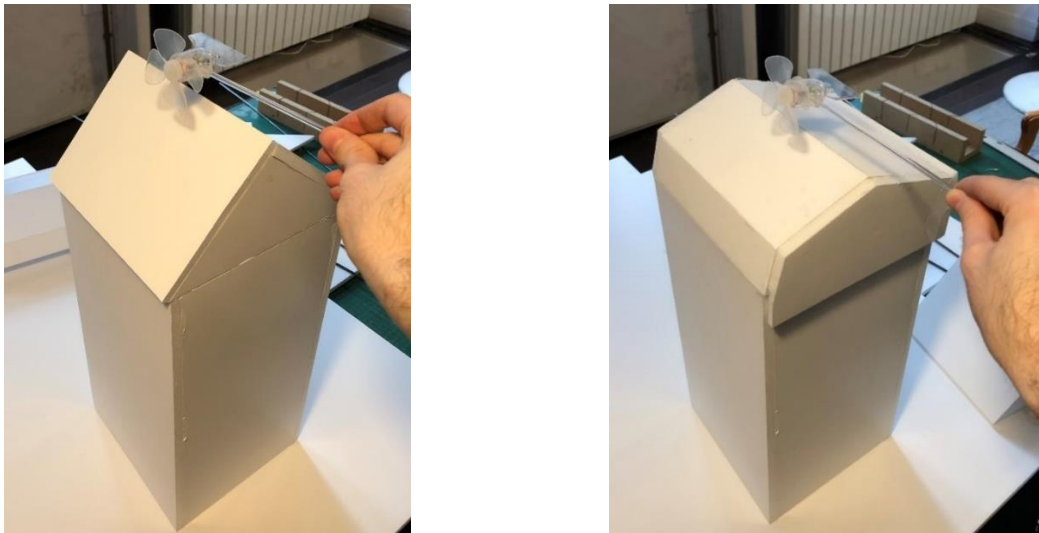


Figure 243. First physical study models with horizontal axis wind turbine test

Study of the possible locations (double slope roof, Mansard roof, flat roof) of the turbine on the roof with and without Foil:



Figure 244. Evolution of the models and studies of possible locations

<sup>162</sup> Design mode of the designers

The design of the device and in particular, its fairing and its low profile, was improved by simple tests in wind tunnel, without taking measurements, in the way designers modify the prototype of a chair to improve its ergonomics (fig 242, then fig 245).

### 5.3.3. 3D modeling of vertical axis turbines optimized for urban wind

For the realization of study models, we modeled in 3D and then printed turbines at the scale of the model and integrated micro-generators. This mock-up allows us to test the extracted energy and the number of revolutions per minute depending on the turbine's implantation on the building and the type of gas pedal associated with this device.

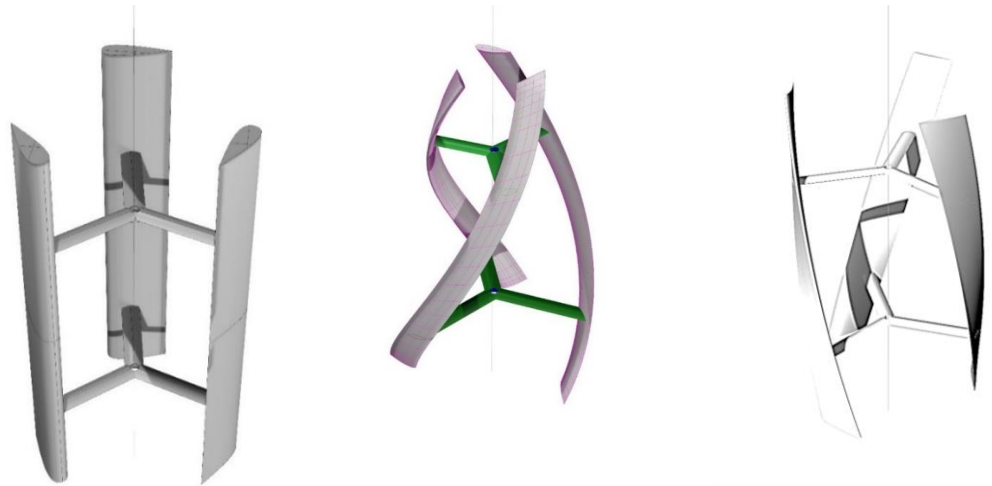
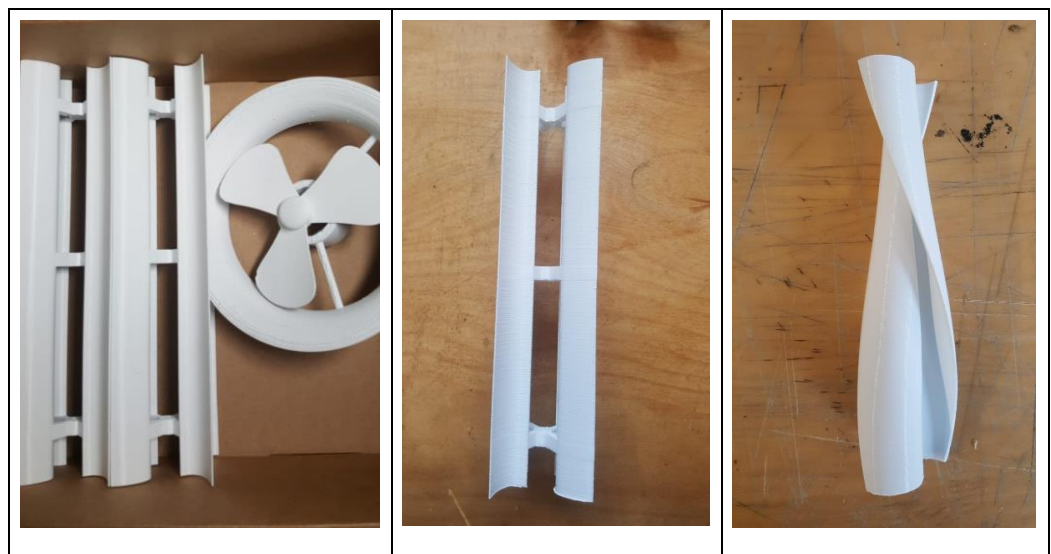


Figure 245. 3D model of the studied turbines modeled on Rhinoceros software

### 5.3.4. 3D printing of optimized vertical axis turbines

The work in model consisted in analyzing the power or the speed of the wind accelerated by the building and to propose the installation of a turbine with its structure-support on this one. It is thus a work of experimentation with trials and errors which made it possible to improve with the wire of the models each of these parameters.



*Figure 246 3d printing of the wind turbines for the realization of models of study of integration of the device ; Intermediate stage*

The scale of the turbines has been reduced in diameter and lengthened in order to be able to adjust it more easily in the volume of the studied architecture. The gas pedals have become thinner, more elongated, and especially much more precisely located in the areas of increased wind speed (identified as red zones by the numerical simulation). ( see point 3.2, on the Reynolds number concerning the scale ratio between the reduced scale model and the wind behavior at scale 1)

Increased by 2 to 3 times depending on the typology, the wind speed was then progressively controlled, redirected to the wind device to increase the air flow. The device was then refined to integrate with elegance and harmony in the building. Each of these models was the subject of a digital simulation in order to be able to work in parallel on an experimental study in model, and a digital aeraulic study more precise and faster to realize than a study in wind tunnel.

The turbines that have been progressively selected have gone from fine-bladed Darrieus type turbines, then to fine Windspire type turbines, then to a twisted type to limit the effects of vibrations, then to Savonius type turbines whose speed is generally lower but whose start-up at reduced wind speed allows a greater regularity of operation. It should be noted that these turbines offer the advantage of starting up alone with the wind, whereas Darrieus systems can only start up at very high wind speeds with the help of a starter.

We then, starting from the Savonius type wind turbine, progressively twisted its geometry allowing a greater regularity of the rotation and a reduction of the vibrations of the turbine.

We present here several 3D printing researches, made during the mock-ups.



*Figure 247 Development of the study models in the wind tunnel with G. Bouchet*



Figure 248 Maquettes d'étude pour soufflerie



Figure 249. Maquette d'étude initiale avec 2 turbines. Leur géométrie n'est pas adaptée au foil avec un régime moins important sur la turbine en hélice.



Figure 250. Maquette finale optimisée avec allongement de la turbine et contreventement du foil de l'étude

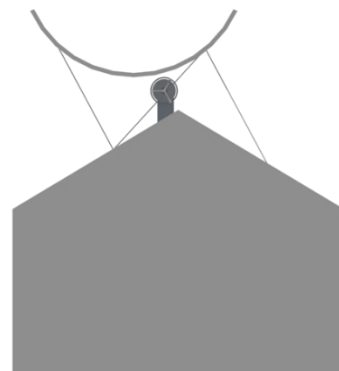
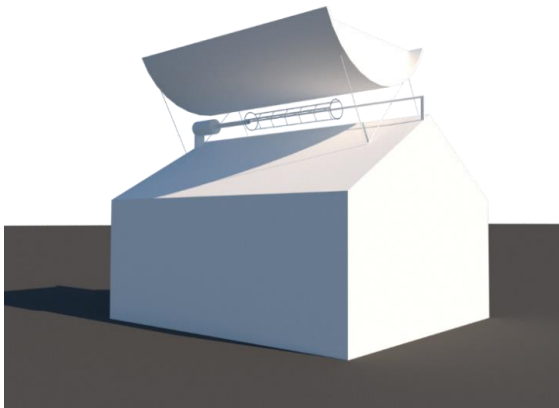


Figure 251. Modélisation 3d du dispositif de foil d'amplification du vent

### 5.3.5. Study models of integrated wind devices

The models were made of white cardboard and featherboard, both very light and resistant. They are weighted with lead weights in order to remain stable during the wind tunnel tests. The mini-wind turbines and the aerofoil were also the object of the implementation of mini-tubes in lattice realized with welded piano wire and which allows a very great rigidity of the prototype and the turbine with a very weak catch in the wind. This tubular structure of model could express a structure of welded steel tubes for the support of wind turbines at scale 1.

In the models, a voltmeter was integrated into the turbine and shows in real time the electrical power released by each solution. This low cost device allowed the realization of a very large number of models in a low technical environment and a very strong improvement of the design of the scale of the implementation of the elements on the space.



Figure 252. LED Voltmeter Ampere, Current/Voltage Indicator (KKmoon New DC1-100V 10A Digital Multimeter)

In an extension of this study, we could have a progressive increase in the scale of these models and a refined evaluation of the turbine and gas pedal performance with respect to the energy produced.

Each of these models was the subject of the realization of a digital 3D model at the same scale so as to be used for the numerical simulation and to compare precisely the results between **experimental study in small scale model and numerical study aeraulic** in a software such as **STAR-CCM+** to specify the operation and the integration of the devices.



Figure 253. Visualization of flag clusters on a Parisian building (Horizontal and vertical). This device captures the winds induced by the corridor effect of dense and homogeneous fabric streets , but is too "foreign" to the architecture present.

This digital model was then used to reprint the turbine and gas pedal from the 3D model of the device. It was also used for the realization of photorealistic virtual insertion in the buildings in order to verify **architecturally the integration and the elegance of the system**.

### 5.3.6. Study in mock-up and profiling of devices



Figure 254. Study of the small-scale building model.

### 5.3.7. Physical wind tunnel study



Figure 255 Physical wind tunnel at ENPC<sup>163</sup>

The proposal is to make a simple prototype type model that allows with the minimum of implementation to evaluate the wind devices. These studies will be compared with a numerical wind tunnel study.

### 5.3.8. Results and comparison with digital wind tunnel

In this chapter, we resume the studies carried out in wind tunnel from simulation in digital wind tunnel of 3D model. The method of simulation consists in the realization of a 3D model on the software Rhinoceros at the scale 1/20. This model is then exported to the digital wind tunnel

---

<sup>163</sup> For your information, the characteristics of the ENPC wind tunnel (Ecole Nationale des Ponts et Chaussées)...: Air vein 80cmX80cm with plexiglass box, Free air vein with aspiration, Length of the vein 15m, Wind speed from 5m/s to 30m/s

software **STAR-CCM+**. We then realized a 3D model mesh in section by increasing the number of meshes to be studied in periphery of the zone of implementation of the turbine and the foil and by limiting the number of global meshes. This simulation allows to visualize the wind speed by a false color view. The creation of red zones shows an increase of 2 to 3 times the wind speed. In this study we did not model the turbine and its ability to rotate as a function of wind speed this step and outside of our initial study.

In summary, the following diagram summarizes the 3 models of analysis and simulation of airflow, the traditional physical wind tunnel model, the numerical simulation model, and the simplified dendrogram model.

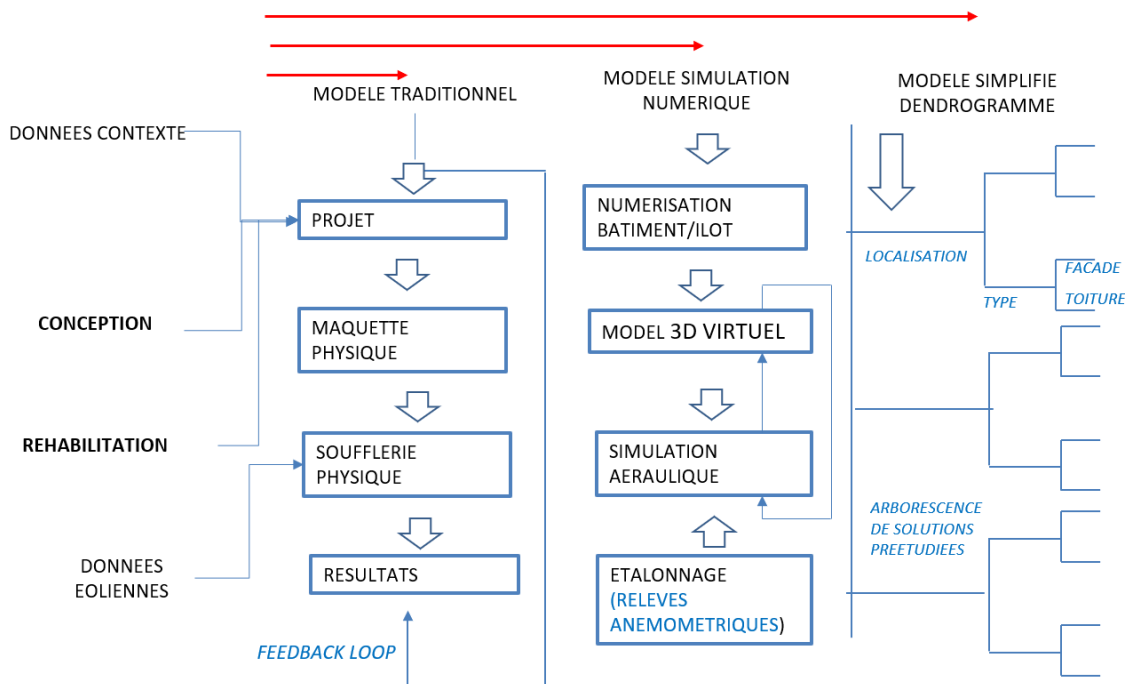


Figure 256 Comparison of airflow simulation methods, D. Serero

### 5.3.9. The modes of integration of wind devices

The wind devices have been categorized by their type of positioning (vertical, horizontal) by their mode of integration (surface mounted, embedded, associated with a gas pedal) or their mode of aggregation (independent, in series, in group...)

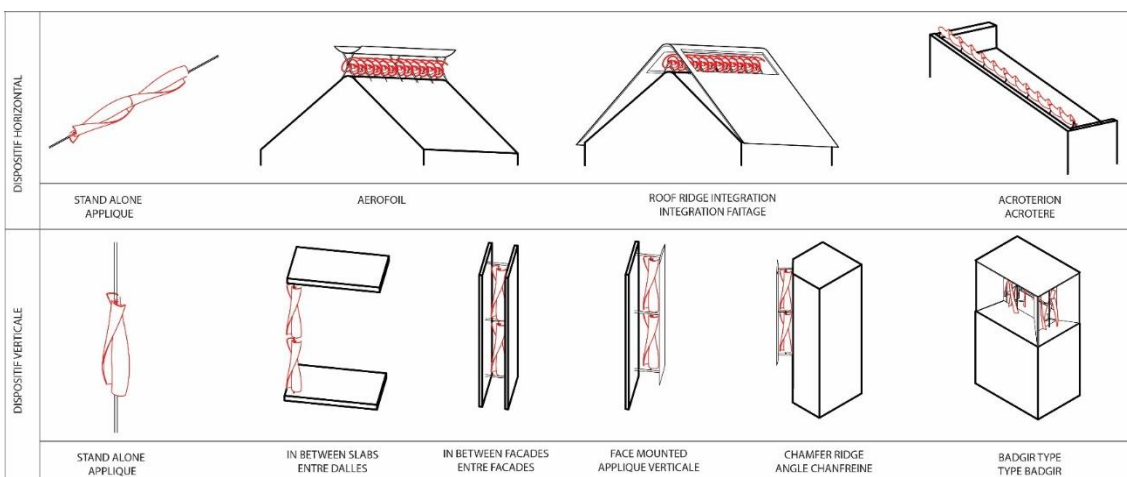


Figure 257 Main typologies of wind energy devices that can be integrated into buildings

## 5.4. QUANTIFICATION OF THE POWER OF THE DEVICES

The quantification of the energy produced is based on several principles related to the dimensioning of the wind turbines and the context. The generator data is related to the rotating force produced by the turbine blades. The statistical distribution of wind speeds varies from place to place as it depends on the local climatic conditions, the surrounding landscape (especially the topography) and the roughness of its surface. The Weibull distribution<sup>164</sup> therefore tends to vary, both in shape and in mean value. Wind intermittency and the Weibull distribution (Figure 255), allowing the statistical distribution of winds at a site to be identified and the sales elements to be sized.

The calculation is therefore made by multiplying the number of devices distributed over the height of the building or the width of a roof according to the knowledge of the wind intermittency at that location.

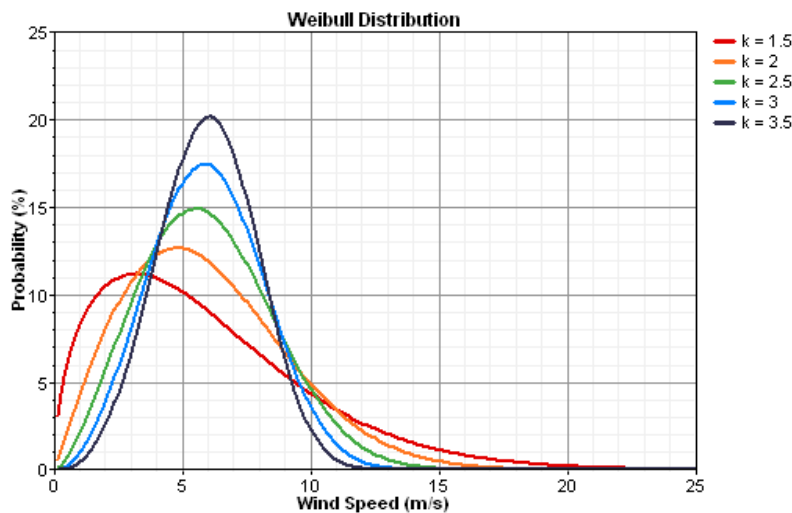


Figure 258 Example of a Weibull distribution for estimating the wind distribution over the year, where  $k$  is the shape parameter.

These calculations allow a relatively precise dimensioning of the extracted energy. However, more specific elements such as the climatic behavior or the precision of the input of the context of the device can make evolve in positive or negative the quantity of energy produced.

The quantification of the power is specified in chapter 5.4 Estimation of the energy produced in a typical city and in chapter 5.6 Examples of architectural integration of energy production devices.

We can however specify here that a theoretical power can be estimated by the multiplication of :

---

<sup>164</sup> Law of probability of wind speeds over the year, named after the Swedish mathematician Waloddi Weibull. The Weibull curve is a statistical representation of the wind present at a site. The two coefficients  $A$  and  $K$  allow to characterize the wind on any site.

The coefficient  $A$  corresponds to the point where the wind is the most important of the curve.

The coefficient  $K$  corresponds to the shape of the curve, it varies between 1 and 3. The smallest values of this coefficient correspond to a curve very tight on the value of  $A$ .

The peak power X the wind efficiency coefficient X the number of devices.

In our case studies, we will take a device power reference for a 1m length of wind turbine blades. This length will be multiplied by the developed length of the devices on the facade or roof of the building.

## 5.5. PRINCIPLE ESTIMATION OF THE GLOBAL ENERGY PRODUCED IN A TYPICAL CITY

Knowing now the energy production of a wind turbine, can we evaluate what their performance would be if they were deployed following the studies we did on a whole city?

We sketch here an evaluation of the number of households that could be supplied by this type of wind device in a large city such as Paris. This evaluation is not based on a numerical simulation of the whole city, but on an extrapolation from several studied typologies. We can estimate the following elements:

### Calculation of the energy consumption of a city:

- Let's take the example of a city of 2 million inhabitants or  $2 \times 10^6$  (Paris Intramuros)
- The area per capita is  $25 \text{ m}^2$
- Annual consumption per capita:  $50 \text{ kw.h/m}^2 / \text{inhab.}$
- Calculation of the consumption for  $25 \text{ m}^2$  :  $50 \times 25 = 1\,250 \text{ kw.h/inhab/year}$ , that is  $1,25 \text{ Mw.h/inhab/year}$
- Calculation of the consumption per day:  $1,25 \text{ Mw.h/inhab}/365 \text{ d} = 3,42 \text{ kw.h/inhab}$
- Let's calculate the energy consumed by all the inhabitants of the city:
- $3,4 \text{ kw.h/inhab} \times 2 \times 10^6 = 6,8 \text{ Gw.h/day}$

### The consumption of 2 million inhabitants is 6.8 Gw.h/day

If we install a micro-wind turbine with a power of  $500 \text{ w.h}$  with an efficiency of 0.25.

The energy produced by the wind turbine is about  $125 \text{ w/h}$

So to generate  $6,8 \text{ Gw.h/day}$ , we would need to install about 54 400 wind turbines of this type.

### How much roof or facade area would be required for this amount of devices?

Knowing that there are 100 889 buildings in Paris, we could either put a wind turbine every 2 buildings, or 2 wind turbines on the roof of one building out of 4.

But these buildings have very different surfaces from each other. If we approximate the surface of the roofs and facades above the urban boundary layer of a city like Paris to 70 million  $\text{m}^2$ , it would then be necessary to implant a wind turbine every:  $70 \times 10^6 / 54400 = 1286 \text{ m}^2$

This calculation shows that, for a very densely populated city such as Paris ( $20754 \text{ inhabitants/km}^2$ ) the density of wind devices on the roof to reach a 100% compensation of the energy consumed by the city would be realistic with the studies of air flow carried out in

urban site around the buildings as well as at the level of the densification in cluster of the wind turbines limiting the impact of turbulences related to the adjacent wind turbines

As presented in the MIT study<sup>165</sup> by Bossanyi et al. on cluster densification of vertical axis wind turbines, these typologies have a low impact on the air turbulence generated by the blades. A densification of their number on a space is thus feasible (60 to 80m<sup>2</sup> per wind turbine) and this grouping, as seen in chapter 5.1 .7 can under certain conditions, improve their performance by an implantation in biomimetic configuration to that of the fish schools.

We could also study the hypothesis of distributing these wind turbines over a doubling of the surface of the urban territory (200 million m<sup>2</sup> instead of 100 million m<sup>2</sup> ).

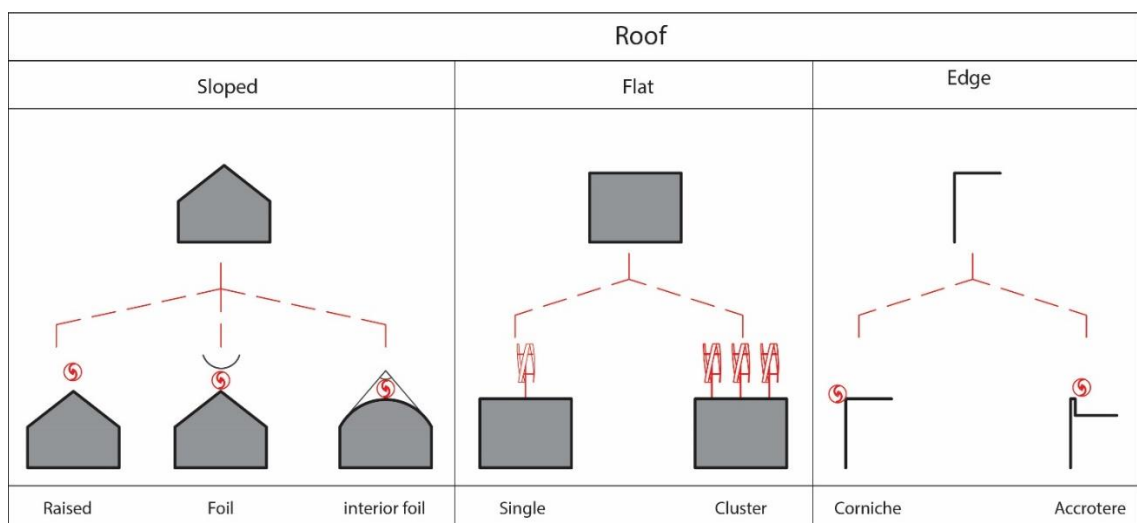
## 5.6. ACTIONABLE DENDROGRAMS FOR DESIGN SUPPORT

Could we, at the end of this research, propose a method to help architects and building engineers in the architectural and technical integration of wind energy production systems?

We have identified the most common typologies encountered in architectural projects and have analyzed the optimal design solutions for these systems. These implementations compared with the increase in wind speed on the large number of building aeraulic simulations that we have performed, allows us to categorize ideal typologies of implementation and operation of integrated wind turbines.

These results are aggregated in a decision tree or **dendrogram** type guide, which by successive steps advises the designers in their choice. However, the dendrogram cannot present all types of architecture or all types of integration.

In these simulations and in the model experimentation, we quickly identified **the edge and surface effects of the building envelope** (see Figure 256). Roof typologies such as acroteria or double roofs allow to significantly accelerate the air velocity and thus to take advantage of a wind field on the roof.



<sup>165</sup> E. A. BOSSANYI, G. E. WHITTLE, P. D. DUNN, N. H. LIPMAN, P. J. MUSGROVE and C. MACLEAN, "The efficiency of wind turbine clusters," 1980, pp. 401-416.

Figure 259. Typologies for integrating wind energy devices into rooftop buildings

Concerning the facades, **the edges of the architecture, the corners and the edges of these volumes constitute sources of increase of the wind speed** which are taken advantage of in many prototypes by elongated and linear aerofoil devices over the whole height or the whole periphery of a building (see figure 257).

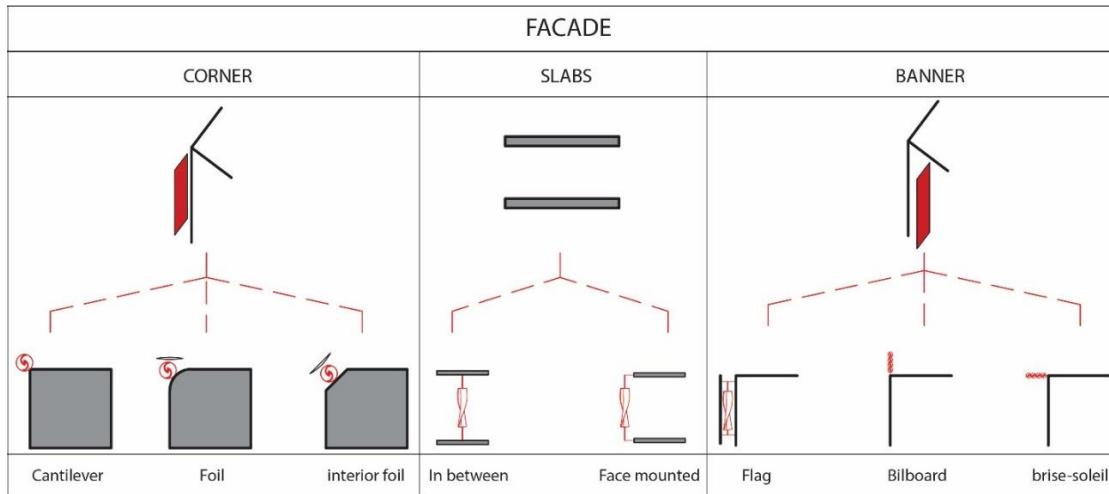


Figure 260 Typologies of integration of wind devices to buildings on facade

The most interesting typologies **should be developed with the building design so that energy production, space ventilation, solar protection or air cooling chimneys participate in the functional and architectural concept of the building.** This represents an important challenge for architects in their current and future projects.

Our research allows us to propose a catalog of integrated wind devices that can be easily added by architects in buildings and in their design. Air movement around a building is a force that cannot be ignored in future designs given the democratization of access to airflow simulation software (CFD).

From the sketch, the dendrogram and the catalog of wind devices that we have shared allow a quick and simple design of these devices. The STAR CCM+ numerical simulation allows the architect or the environmental engineer of the building to propose a study in **numerical aeraulic simulation** first from the action dendrogram and then from a complete 3D model to evaluate and adjust the performance of the chosen device.

This study combined with a wind survey over a period of 6 to 18 months thanks to digital anemometers allows to consider a very precise evaluation of the possible energy to be extracted on a building, an urban block or a city.

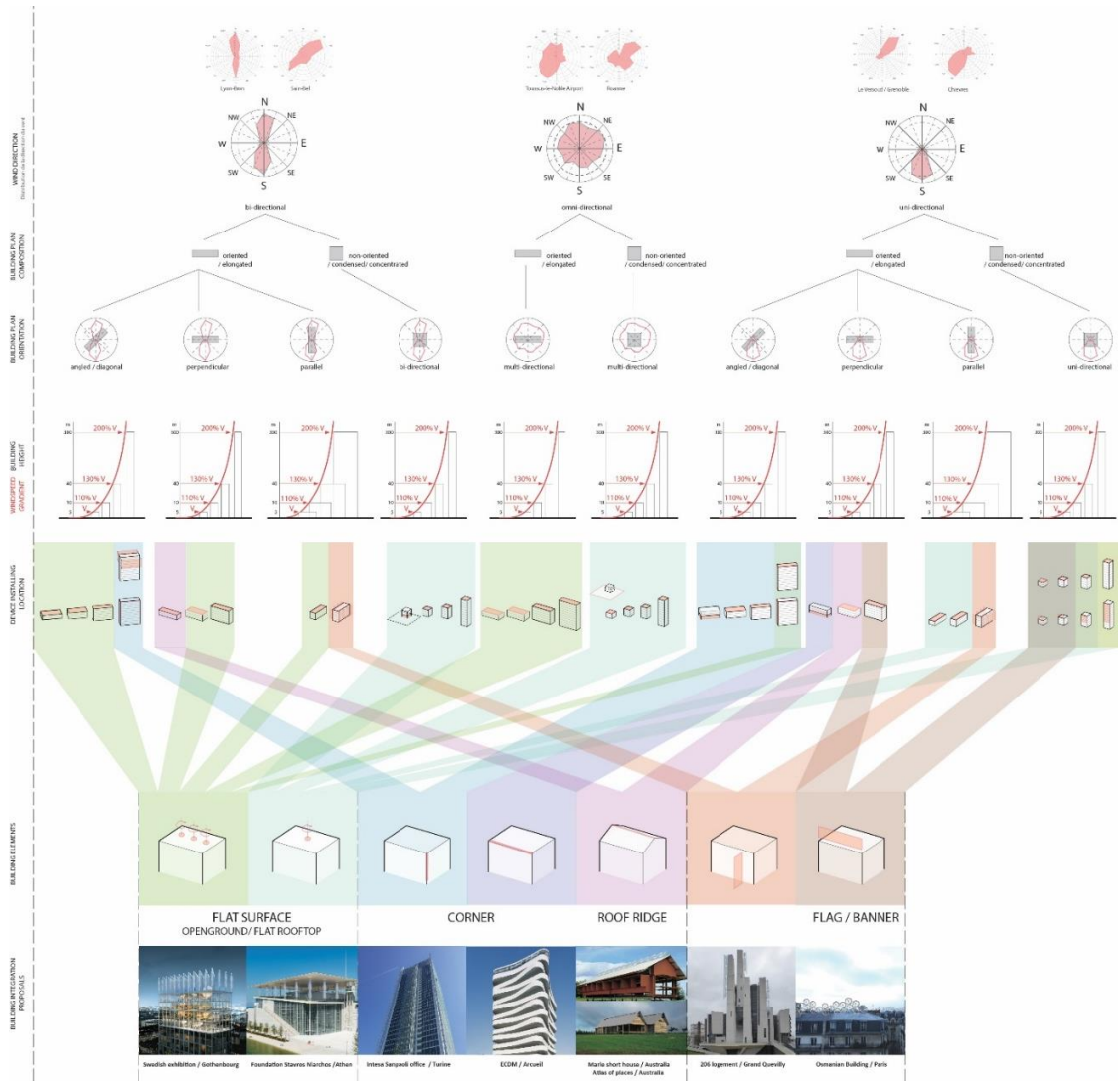


Figure 261. Wind action dendrogram for architects and engineers

This dendrogram, from top to bottom, allows to guide the designer in the choice of the device to be implemented on the building according to filtering questions at each line. We show in the following diagram the path of the approach by marking in red line an option and in green line an alternative if the prevailing winds are parallel to the length of the building.

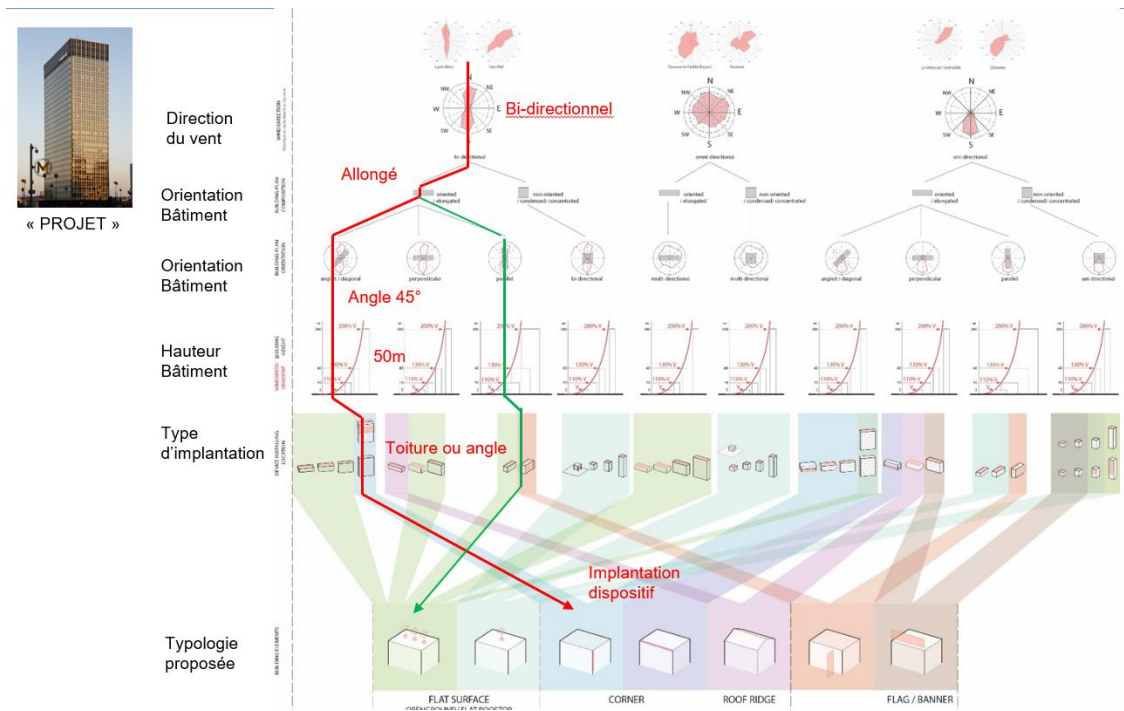


Figure 262 Example of a wind device siting analysis on a tower building.

## 5.7. EXAMPLES OF ARCHITECTURAL INTEGRATION OF WIND POWER GENERATION DEVICES

In this part, architectural and performative simulations were made on many international examples (see illustrations chapters 5.6.1 to 5.6.4) in order to measure the impact that this research could have on construction.

The insertion of wind power generation devices into buildings poses a real challenge to architects.

The devices need to be widely exposed to the wind by being located at the ends of the buildings (roofs and envelopes), but architects do not want to show them today and users, despite their interest in passive buildings, do not want to see any movement in their environment and hear any noise. How can one really propose a wind device without **disfiguring the urban landscape or altering the architect's architectural project?**

It is important to know if a wind energy system is relevant and cost-effective at the project design stage. The architect and the design team could, from the first sketches and the implementation of the building profile in the site, think about this relationship between energy system and project. We can cite the example of the **elevator**, which is now installed from the first sketches of the project as a structuring element of the building, whereas for years it was only a technical addition on the periphery or at the back of the building. We can also mention elements such as roof overhangs, sunbreaks, acroteria, which are all devices invented by modern architects and have become the basis of contemporary architectural language. The construction rules certainly influence the systematization of the use of these devices, but the innovative architectural image and the **massive prescription** assistance **of the building industry will stimulate their emergence and their commonplace.**

Thus, the principles of implementation should be simple and didactic enough for architects to include them in their design process from their first sketches.

We can also consider another hypothesis of development of these systems: The architecture would not be conceived with these devices, they would be grafted to it. That is to say that the time of the conception of the project would remain a different time from that of the question of the energy production. In this case, **how to transmit the bases and the principles to propose a great diversity and a freedom of implementation?**

2 types of integration methods can be considered:

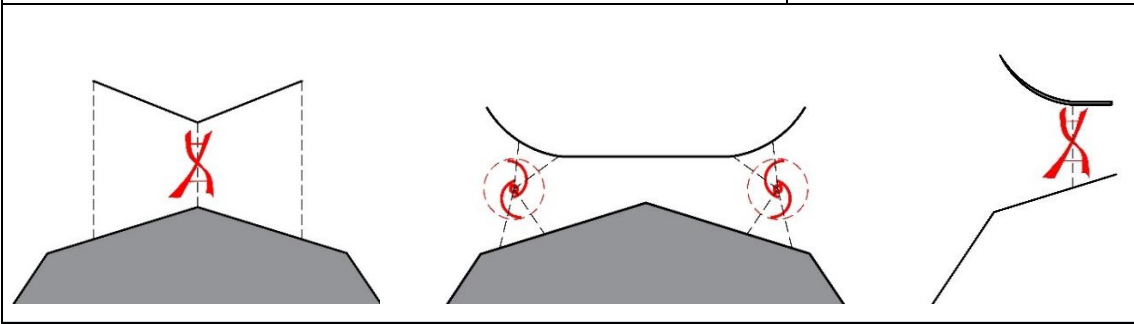
- This can be achieved either by the design of a device or **an architecture that treats technical systems as a mechanism** in the thinking of architect-builders, we speak of high-tech architecture, where technical systems are made legible, they reveal with transparency, the fact that all architecture is built from an assembly of components, equipment and systems. Buildings like the architecture of Renzo Piano or Richard Rodgers even envisage an over-articulation of all these devices with the architecture. This is expressed in oversized air vents that become elements of urban furniture (Centre Georges Pompidou, Paris), or lighting fixtures that are elements supported by a vault (Barajas Airport, Madrid).
- The second method would be to work in **complete integration of the gas pedal or turbine**, treating them as recessed in the building, to make **the element non-visible and non-discernible**. This is the principle of the integrated aerator, which can be found on car grills or jet engines, where a simple slot on the surface of the objects allows to profile and regulate the constant air flow.

5.7.1. Old or heritage buildings

- *Hausmanian Housing building, height 21m, Paris 11<sup>th</sup> district*



DIB Nb : 6 ( 10LM)  
DEVICE LENGTH : 1,50M  
TOTAL LENGTH : 9 M  
DIAMETER : 80 CM  
TYPE : DARRIUS TWISTED  
AEROFOIL : YES  
LOCALIZATION : PARIS (75)  
ANNUAL WIND SPEED MEAN :  
10M/s  
DEVICE POWER : 500W  
EST. EXTRACTED POWER :  
 $500 \times 0,25 \times 9 = 1125W$

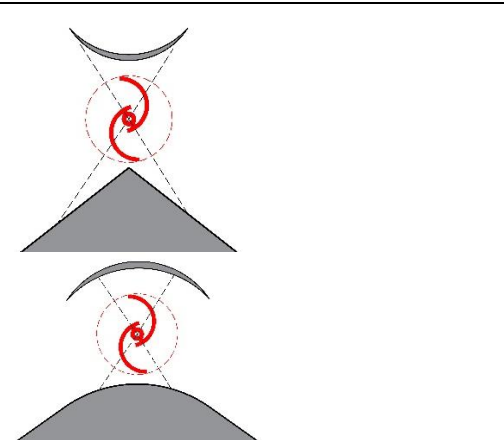
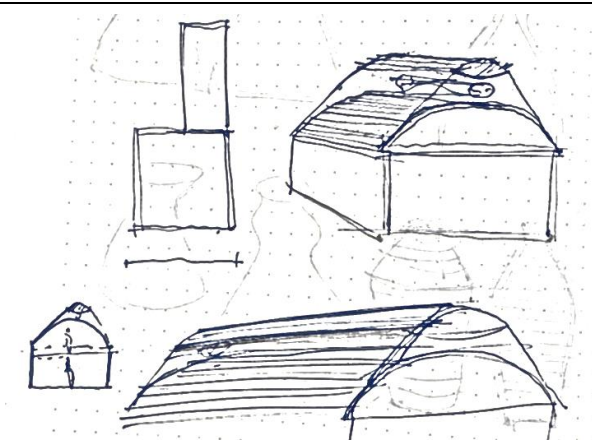




- Windy coast line houses



DIB Nb : 1 ( 10LM)  
 DEVICE LENGTH : 1,20M  
 TOTAL LENGTH : 10 M  
 DIAMÈTER : 80 CM  
 TYPE : STRAIGHT SAVONNIUS  
 AEROFOIL : YES  
 LOCALIZATION : LORIENT (56)  
 ANNUAL WIND SPEED MEAN : 15M/S  
 DEVICE POWER : 500W  
 EST. EXTRACTED POWER :  $500 \times 0,25 \times 10 = 1250W$

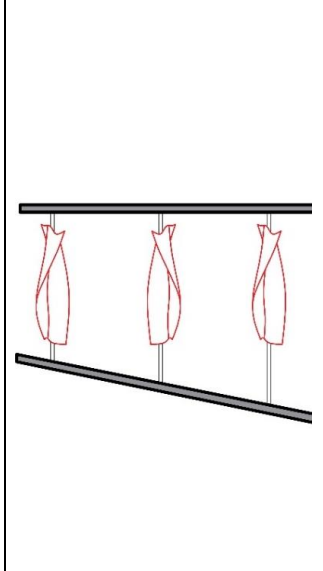


### 5.7.3. Public Facilities

- *Stavros Niarchos Foundation, Arch. Renzo Piano, 2016, Athens, Greece*



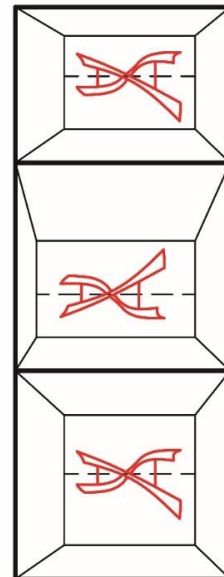
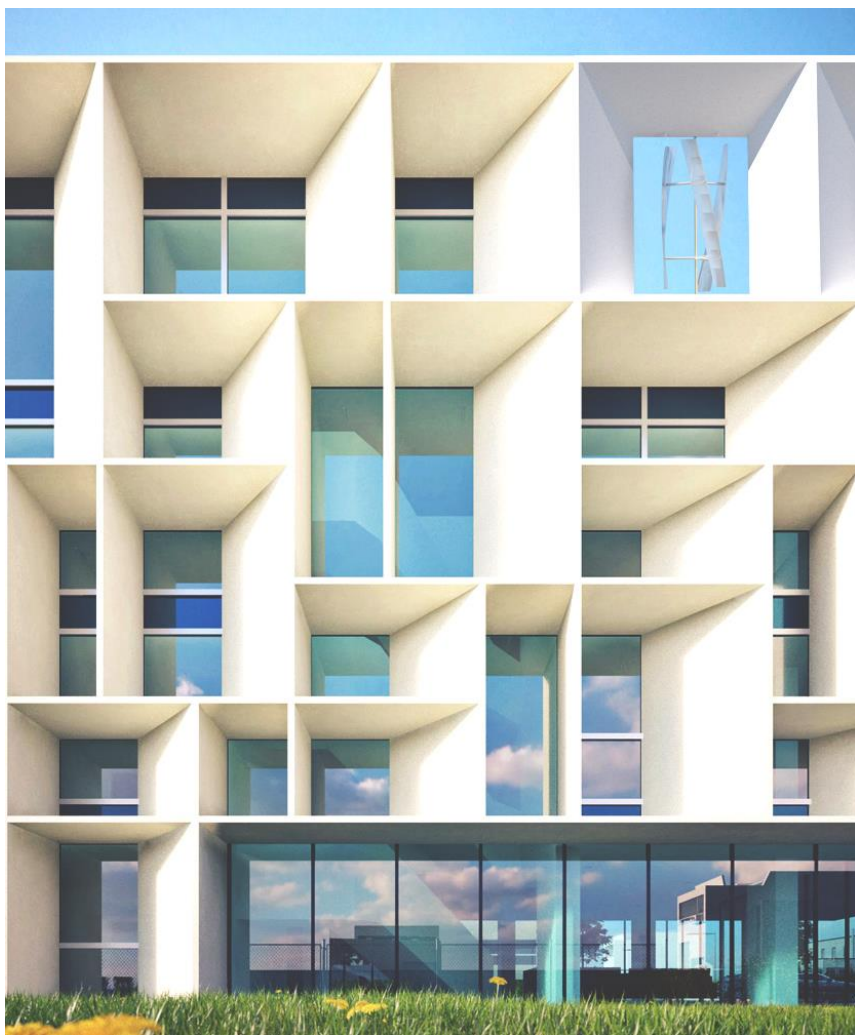
DIB Nb : 16 ( 2LM)  
DEVICE LENGTH : 16M  
TOTAL LENGTH : 32 M  
DIAMETER : 80 CM  
TYPE : DARRIUS TWISTED  
AEROFOIL : YES  
LOCALIZATION : ATHENS  
GREECE  
ANNUAL WIND SPEED  
MEAN : 15M/s  
DEVICE POWER : 500W  
EST. EXTRACTED POWER :  
 $500 \times 0,25 \times 32 = 4\ 000W$



- *Bentini Headquarters, Arch. Piuarch, Faenza, Italie, 2018*



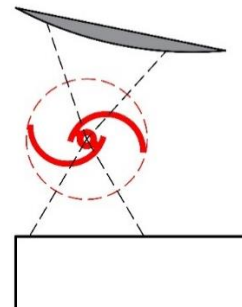
DIB Nb : 12 ( 18LM)  
 DEVICE LENGTH : 1,50M  
 TOTAL LENGTH : 18 M  
 DIAMÈTER : 80 CM  
 TYPE : DARRIUS  
 TWISTED  
 AEROFOIL : YES  
 LOCALIZATION : FAENZA,  
 ITALY  
 ANNUAL WIND SPEED  
 MEAN : 10M/S  
 DEVICE POWER : 500W  
 EST. EXTRACTED  
 POWER : 00X0,25x18  
 = 2 250W



- *University Building ENPC et IFSTTAR, Campus Cité Descartes, Champs-sur-Marne (77), 1983*



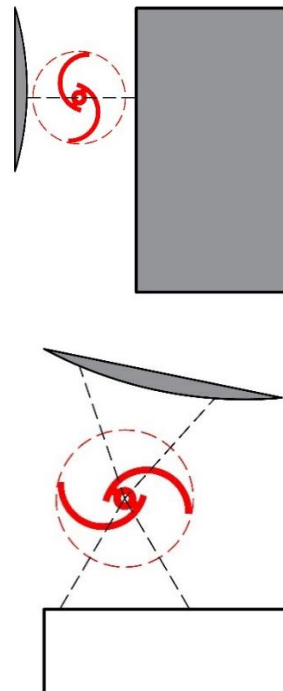
DIB Nb : 8 ( 12LM)  
 DEVICE LENGTH : 1,50M  
 TOTAL LENGTH : 9 M  
 DIAMÈTER : 80 CM  
 TYPE : DARRIUS TWISTED  
 AEROFOIL : YES  
 LOCALIZATION : PARIS (75)  
 ANNUAL WIND SPEED MEAN :  
 10M/S  
 DEVICE POWER : 500W  
 EST. EXTRACTED POWER :  
 $500 \times 0,25 \times 12 = 1500W$



- *Research and innovation Center, Caen, 2016, Arch: Bruther*



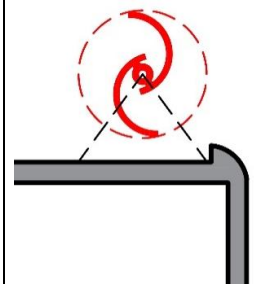
DIB Nb : 10 ( 15LM)  
 DEVICE LENGTH : 1,50M  
 TOTAL LENGTH : 15 M  
 DIAMÈTER : 80 CM  
 TYPE : DARRIUS TWISTED  
 AEROFOIL : YES  
 LOCALIZATION : CAEN (14)  
 ANNUAL WIND SPEED  
 MEAN : 15M/s  
 DEVICE POWER : 500W  
 EST. EXTRACTED POWER :  
 $500 \times 0,25 \times 15 = 1875W$



- Bayeux Media Library, 2018, Arch: SERERO Architectes



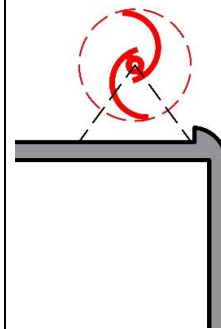
DIB Nb : 30 ( 60LM)  
 DEVICE LENGTH : 2M  
 TOTAL LENGTH : 60 M  
 DIAMETER : 80 CM  
 TYPE : DARRIUS  
 TWISTED  
 AEROFOIL : YES  
 LOCALIZATION :  
 BAYEUX (14)  
 ANNUAL WIND SPEED  
 MEAN : 18M/S  
 DEVICE POWER :  
 500W  
 EST.            EXTRACTED  
 POWER :  
 500X0,25x60       =  
 7500W



- *CLIMATE RESEARCH CENTER, Grenoble Alpes University, Grenoble, 2020, Arch: SERERO Architectes*



DIB Nb : 24( 36LM)  
 DEVICE LENGTH :  
 1,50M  
 TOTAL LENGTH : 36 M  
 DIAMÈTER : 80 CM  
 TYPE : DARRIUS  
 TWISTED  
 AEROFOIL : YES  
 LOCALIZATION :  
 GRENOBLE (38)  
 ANNUAL WIND SPEED  
 MEAN : 15M/S  
 DEVICE POWER :  
 500W  
 EST. EXTRACTED  
 POWER :  
 $500 \times 0,25 \times 36 =$   
 4000 W

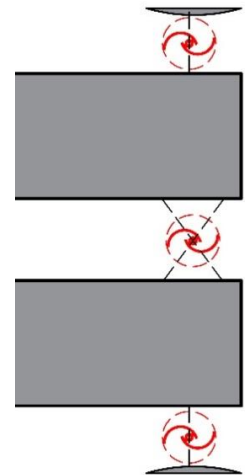


### 5.7.4. High-rise buildings

- *Paris Val de Seine Architecture School, arch : F. Borel, 2008 Paris 13ème*



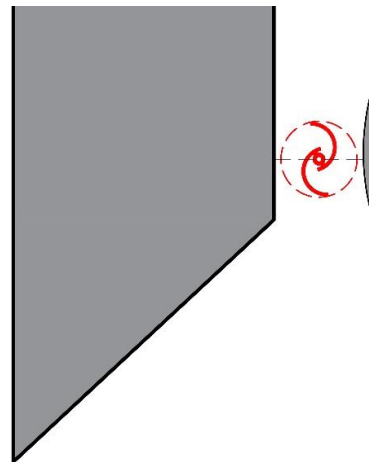
DIB Nb : 15 ( 22,5LM)  
 DEVICE LENGTH : 1,50M  
 TOTAL LENGTH : 22,5 M  
 DIAMÈTER : 80 CM  
 TYPE : DARRIUS TWISTED  
 AEROFOIL : YES  
 LOCALIZATION : PARIS (75)  
 ANNUAL WIND SPEED MEAN :  
 12M/s  
 DEVICE POWER : 500W  
 EST. EXTRACTED POWER :  
 $500 \times 0,25 \times 22,5 = 2\,812\text{W}$



- Grande Arche, Arch. Johan Otto von Spreckelsen, 1985, Puteaux, France



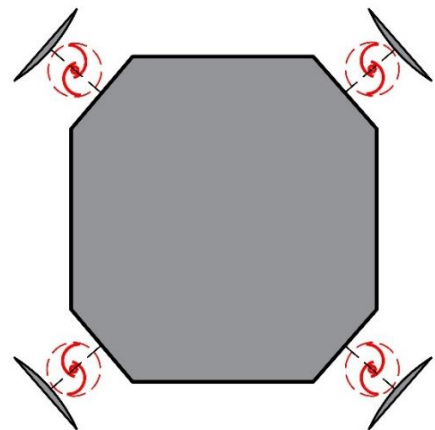
DIB Nb : 22 ( 10LM)  
 DEVICE LENGTH : 2,50M  
 TOTAL LENGTH : 55 M  
 DIAMÈTER : 80 CM  
 TYPE : DARRIUS TWISTED  
 AEROFOIL : YES  
 LOCALIZATION : PARIS (75)  
 ANNUAL WIND SPEED MEAN : 15M/S  
 DEVICE POWER : 500W  
 EST.          EXTRACTED          POWER :  
 500X0,25x55 =6875w



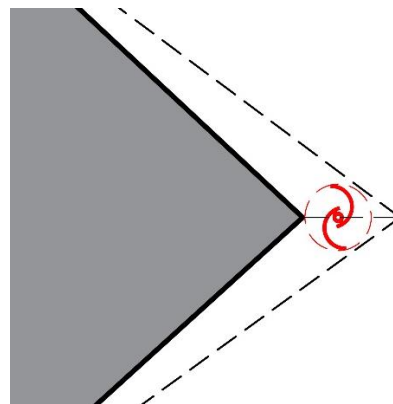
• *One thousand Museum Tower, Arch. Zaha Hadid, 2026, Miami, USA*



DIB Nb : 12 ( 2,50M)  
DEVICE LENGTH : 1,50M  
TOTAL LENGTH : 30M  
DIAMÈTER : 80 CM  
TYPE : DARRIUS TWISTED  
AEROFOIL : YES  
LOCALIZATION : MIAMI USA  
ANNUAL WIND SPEED MEAN : 12M/s  
DEVICE POWER : 500W  
EST. EXTRACTED POWER :  $500 \times 0,25 \times 30 = 3750W$

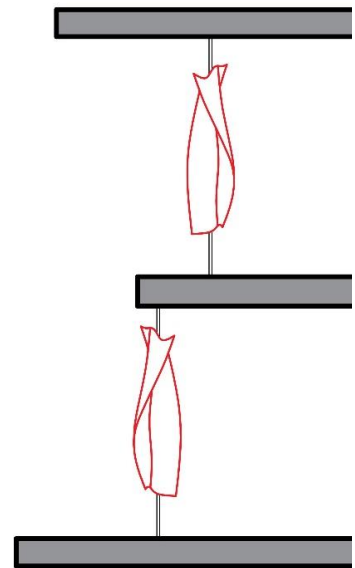


- *Turning Torso Tower, Arch. S. Calatrava, 2001, Malmö, Sweden*



DIB Nb : 16  
 DEVICE LENGTH : 3,50M  
 TOTAL LENGTH : 56M  
 DIAMÈTER : 80 CM  
 TYPE : DARRIUS TWISTED  
 AEROFOIL : YES  
 LOCALIZATION : MALMÖ, SWEDEN  
 ANNUAL WIND SPEED MEAN : 15M/S  
 DEVICE POWER : 500W  
 EST. EXTRACTED POWER :  $500 \times 0,25 \times 56 = 7000W$

- Terrazas, Arch. Herzog et de Meuron, 2009, Beyrouth, Liban

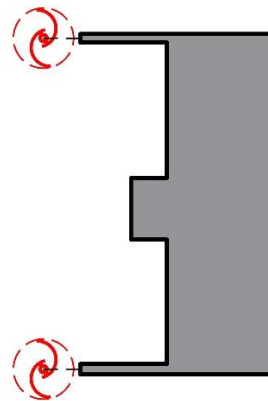


DIB Nb : 18  
 DEVICE LENGTH : 3,50M  
 TOTAL LENGTH : 63 M  
 DIAMÈTER : 80 CM  
 TYPE : DARRIUS TWISTED  
 AEROFOIL : YES  
 LOCALIZATION : BEYROUTH  
 LIBAN  
 ANNUAL WIND SPEED MEAN :  
 15M/s  
 DEVICE POWER : 500W  
 EST. EXTRACTED POWER :  
 $500 \times 0,25 \times 63 = 7\,875\text{W}$

• *Intesa Sanpaolo Office Building, Arch. Renzo Piano, 2011, Torino, Italy*



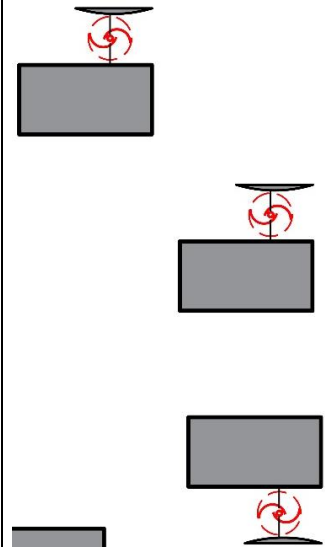
DIB Nb : 30x2  
DEVICE LENGTH : 3,50M  
TOTAL LENGTH : 210 M  
DIAMETER : 80 CM  
TYPE : DARRIUS TWISTED  
AEROFOIL : YES  
LOCALIZATION : TORINO ITALY  
ANNUAL WIND SPEED MEAN :  
16M/s  
DEVICE POWER : 500W  
EST.      EXTRACTED      POWER :  
500X0,25x210 = 26 250W



• 206 Apartments Building, Grand Quevilly, Arch. Frederic Borel, 2014, France



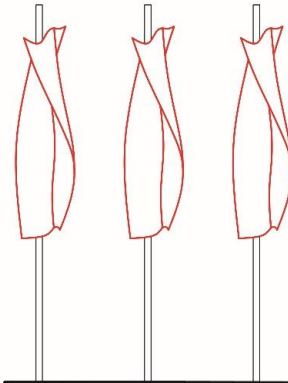
DIB Nb : 22  
 DEVICE LENGTH : 2,50M  
 TOTAL LENGTH : 55 M  
 DIAMÈTER : 80 CM  
 TYPE : DARRIUS TWISTED  
 AEROFOIL : YES  
 LOCALIZATION : GRAND QUEVILLY  
 ANNUAL WIND SPEED MEAN : 12M/S  
 DEVICE POWER : 500W  
 EST. EXTRACTED POWER :  $500 \times 0,25 \times 55 = 6\ 875W$



- Swedish Exhibition & Congress Centre , Arch. Tham & Videgård, 2024, Gothenburg, Sweden



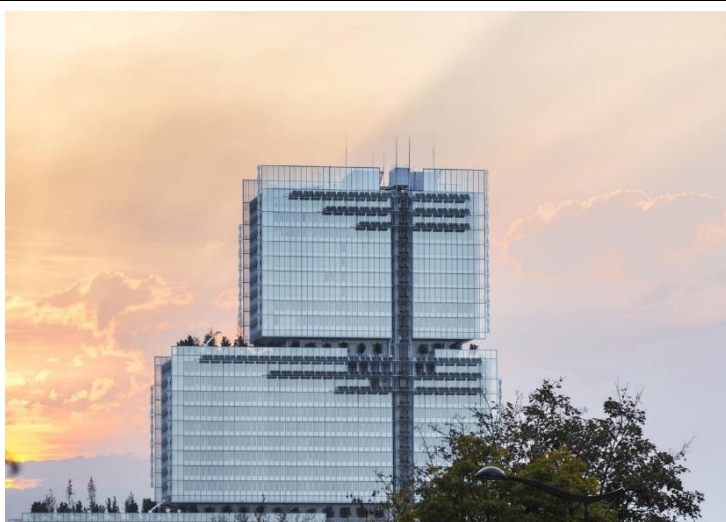
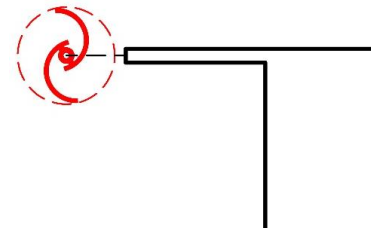
DIB Nb : 48  
 DEVICE LENGTH : 3,50M  
 TOTAL LENGTH : 168 M  
 DIAMÈTER : 80 CM  
 TYPE : DARRIUS TWISTED  
 AEROFOIL : YES  
 LOCALIZATION :  
 GOTHENBURG, SWEDEN  
 ANNUAL WIND SPEED  
 MEAN : 15M/S  
 DEVICE POWER : 500W  
 EST. EXTRACTED POWER :  
 500X0,25X168  
 = 21 000W



- Paris High Court Tower, Renzo Piano Building Workshop, 2018, Paris 17<sup>th</sup> Dist.



DIB Nb : 60  
DEVICE LENGTH : 3,50M  
TOTAL LENGTH : 210 M  
DIAMÈTER : 80 CM  
TYPE : DARRIUS TWISTED  
AEROFOIL : YES  
LOCALIZATION : PARIS  
ANNUAL WIND SPEED MEAN :  
12M/S  
DEVICE POWER : 500W  
EST.      EXTRACTED      POWER :  
500X0,25x168  
= 26 250W



## 5.8. CREATION OF AN OPEN ACCESS LIBRARY OF WIND ENERGY DEVICE MODELS ON A COLLABORATIVE BIM PLATFORM

We have recently seen the emergence of online libraries for sharing 3D models for use by building designers. These platforms offer both examples of projects and products from suppliers to the building industry such as BIM (Building Information Modeling). This is a collaborative work method developed by the construction sector, with the objective of improving the design of buildings, but above all to better anticipate the monitoring of construction sites and the management of building maintenance. All the actors of the construction industry are progressively transforming the digital design of the project, by a multi-actor design of the "BIM" type.

### 5.8.1 Building information modeling

At the heart of the BIM process is a **3D digital model**. This 3D model contains all the data and elements necessary for the construction of a building, but also for the economics of construction. All this information is centralized in a **single digital information model** that integrates several data :

The architect, the structural engineer and the fluid engineer each model their component on the same 3D model. This makes it possible to verify that the foundations, the structure, the networks (water, heating, gas, telecom, electricity) are correctly sized and located without interfering with each other.

Companies can anticipate site problems in a **digital twin of the building** and consult the 3D model during construction to ensure proper execution of the work.

The collaborative aspect of BIM, allows both a **simultaneous design of** actors and a **continuity in the design process**. Several architects can work simultaneously on the same digital document. As the project progresses, the project is progressively refined from a global model, avoiding any problem of technical synthesis<sup>166</sup> .

### 5.8.2 A catalog of 3D models of integrated wind devices

As part of this research, we have made available a catalog<sup>167</sup> of several 3D models of integrated IFC wind turbines. The objective is to allow architects to easily integrate them into their building and design.

As early as the sketch stage, using the action dendrogram and the IFC family catalog, the building design team can evaluate the relevance of a device in terms of energy production, space requirements or aesthetics.

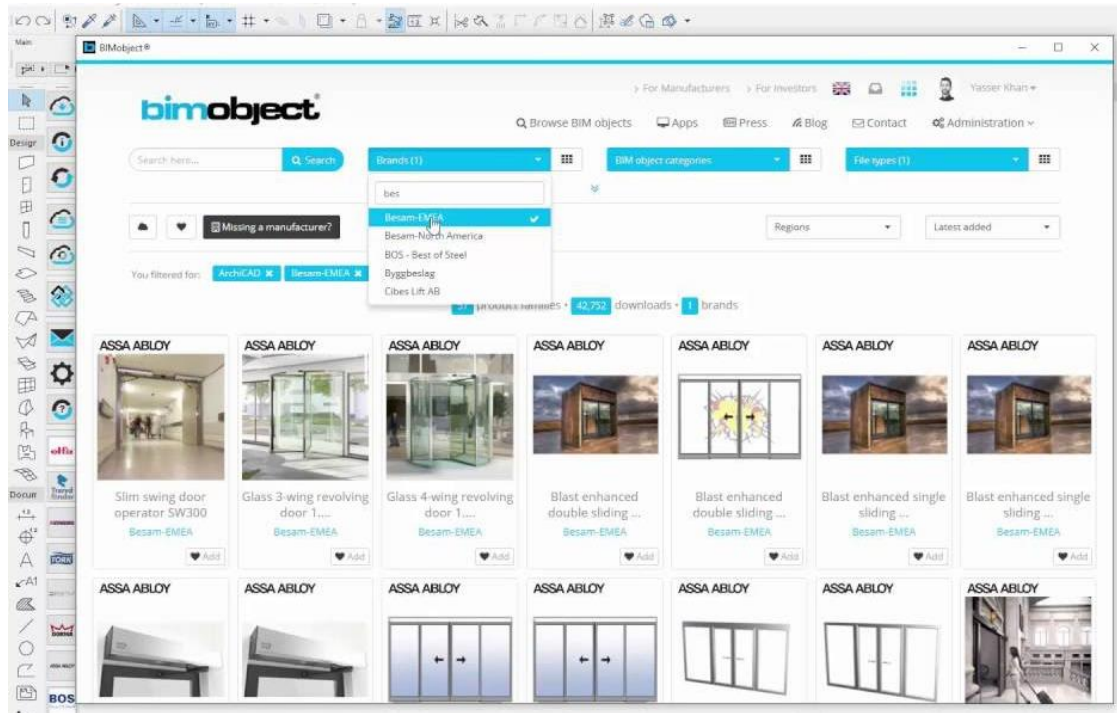
In a 2<sup>ème</sup> time, the standardization and the diffusion of these shared 3D models, will quickly allow to carry out a numerical simulation (of type STAR CCM+) by the aerualic expert or the

---

<sup>166</sup> During the execution study phase, the synthesis mission ensures the spatial coherence of the works of all the trades, in compliance with the architectural, technical, operation and maintenance provisions. It ensures the correlation of the execution details, the passage of the technical networks and the implementation of the terminals and equipment.

<sup>167</sup> Catalog available on [www.bimobject.com](http://www.bimobject.com) and [www.revitcity.com](http://www.revitcity.com) on David Serero's account

environmental engineer of the building, starting from a complete 3D model to evaluate and adjust the performance.



We believe that air movement around a building is **a force that can no longer be ignored** in future designs given the democratization of access to airflow simulation software (CFD).

This study combined with a wind survey over a period of 6 months to 18 months, using the digital anemometers described in this research<sup>168</sup> constitute the basis for a very accurate evaluation of the extractable energy on a project.

<sup>168</sup> See Chapter 2: Wind readings by connected anemometers

## 6. GENERAL CONCLUSION

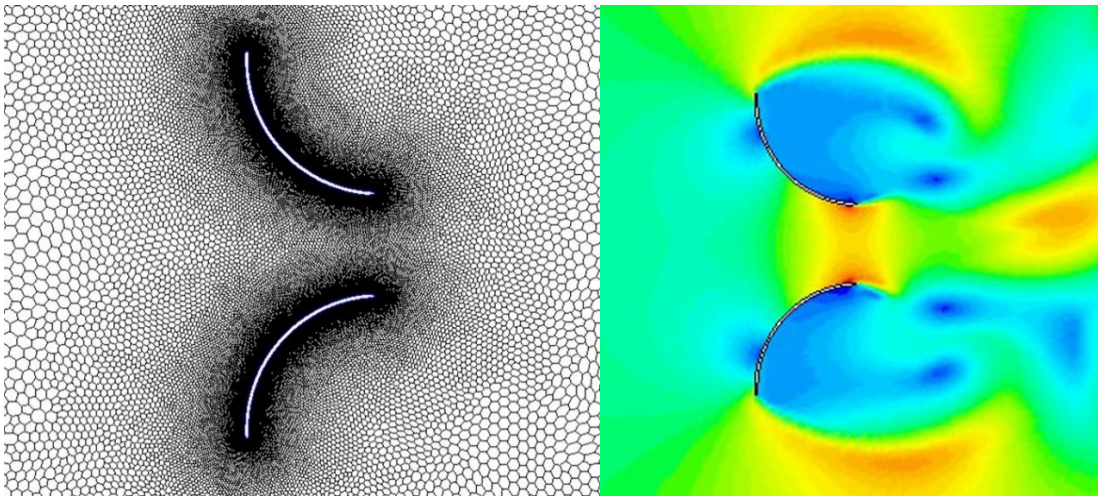


Figure 263 Airflow study on a Foil to accelerate the wind.

These years of research show that the question of **architectural aeraulics** goes far beyond the simple problems of the **vibratory effect of envelopes** or the **aerodynamics of structures** in which architects and engineers have often circumscribed this subject.

In synthesis the main contributions of this research are:

- 1- Creation of wind **data** on airflow around buildings (by surveys and simulation)
- 2- The definition and study of "**aerofoil**" **type gas pedals** to increase the wind speed and stabilize its turbulence locally
- 3- An approach and estimation of **the potential of wind energy extractable from a building and a city**
- 4- The development of a **method of architectural integration of wind energy devices**
- 5- Designing a **dendrogram**, decision tree or **design guide** for architects and engineers

It is now clear that buildings are real "**aeraulic organisms**" and that they have a strong relationship with the physics of their environment and in particular with the airflow around their external envelopes.

Because of **its scale, its important and continuous colonization of new territories**, the architectural and urban design of future environments is a primordial subject to **rethink our relationship to our environment, to local resources and to energy production**. This aspect has often been neglected in architectural design in favor of cost, rationalization of structures, or in favor of a pure formal ideology (Modernism, Minimalism, Regionalism, ...)

However, the location of projects in **extreme climatic zones** (tropical or equatorial climates) or areas with limited resources have forced builders to integrate natural ventilation as a design principle (Badgir in Iran, cross ventilation in Reunion Island, filter walls in Vietnam). A few architects who pioneered **bioclimatic building design** have also developed an approach that **is highly sensitive to their environment** (Glenn Murcutt, Renzo Piano, Lacaton Vassal, etc.), which unfortunately has remained marginal in the vast majority of our built environment today.

This research, combining **numerical analysis of CFD** (computational fluid dynamics) and in-situ measurements by **connected anemometers**, presents the correlations between wind speed and several types of urban conditions in order to predict **the potential of extractable wind energy in cities**.

Any building, any wall, generates by its presence on a plot of land, **an air pressure differential** on its external walls related to the surrounding air movements. This study has shown that **the volumetry and the position of a building** in its context can thus be "**profiled**" and "**oriented**" for an increase and a control of the wind speed in its periphery.

Here we have developed a **building design method** for architects and engineers to integrate **wind energy devices** into their project development. "Aerofoil" type gas pedals are used to locally stabilize wind turbulence and accelerate wind speed. By invoking the **Betz limit** (cubic law between air speed and energy production of a wind device) **a small increase in air speed shows a considerable increase in energy production**.

This research identifies **an urban wind energy source** that remains largely **untapped** to this day. **Turbulence phenomena in urban areas, associated with irregular winds**, have disinterested most of the actors of the renewable energy industry. However, the improvement of **micro-wind turbine technologies** and new research on **their** clustering allow the networking of a large number of low-nuisance devices in urban environments.

This research provides solutions on how to design buildings with these energy harvesting devices, integrating them into the building envelope and design, and **adjusting their structure and envelopes to avoid vibrations and resulting noise pollution?**

The improvement of **bioclimatic design of buildings** associated with global environmental policies to reduce greenhouse gases allows us to envisage the emergence of **an energy sharing ecosystem**.

The emergence of **the Internet of Things (IOT)** which allows these devices to interact with each other, but also with users and building management systems (BMS). It is an emerging infrastructure, **the Internet of Energy (IOE)** which aims to propose an organization for the sharing and exchange of energy locally. This new paradigm projects a vision of smart urban environments where resources, energy production and consumption would be **hyper-localized with a negative environmental impact**.

This approach, by bringing closer **the areas of production and consumption of energy**, by limiting the costs of infrastructure support of wind turbines as well as electro-magnetic losses during the transport of energy (estimated at 30%) is also a new response to the **growing attacks of the energy industry of wind turbines**<sup>169</sup>.

This research has led to the development and sharing of "**actionable dendrograms**" (decision trees) as a **tool for designing embedded energy production systems**, as well as an **architectural profiling method** to stimulate and facilitate the implementation of **zero-energy architecture** among architects and builders.

The realization of a study in the wind tunnel of the Ecole des Ponts (ENPC) could have been carried out to compare the data from numerical simulations with readings in a physical wind tunnel. However, due to the Covid-19 containment and the closure of the Descartes campus

---

<sup>169</sup> Fabien BOUGLE, *Eoliennes : la face noire de la transition écologique*, op. cit.

in Champs-sur-Marne, this study could not be developed. It could be the subject of a future development in order to confirm the studied hypotheses and to refine the design details.

It is also necessary to specify that in the course of this reflection, certain hypotheses were simplified and the parameters of the calculation were adjusted (in particular on the type of turbulence, and on the calculation in unsteady or stationary regime, on the resolution of the calculation), with for objective to go to the principles of implementation, to the general behavior of the wind flow on the building in a specific context.

As presented in the foreword of this document, this work aims to obtain a doctorate in architecture and to propose an answer to questions such as: What is a thesis in architecture? Is it a discipline of the social sciences, or of engineering? Is an architectural work not already an act of research?

This work attempts to generate and share new knowledge on the art of building, in order to reposition the work of the architect in a context of environmental and energy crisis of the architectural act.

Two directions of opening of this research can be envisaged: the development of hybrid energy production devices (solar/wind) and the digital printing of wind turbine blades in order to be able to adapt the wind turbine to the building and the design of the envelope.

- Optimize the energy produced by hybridization of the typologies

In order to improve **the smoothing of energy production**, renewable energy production systems other than wind could be integrated with these wind devices. The energy mix<sup>170</sup> consumed by a building or an urban area could see **its share of renewable energy strongly increased**. A wind energy capture device with an aerofoil gas pedal could combine solar energy production such as photovoltaic energy.

This assembly shows that the foil is an interesting device for driving and increasing the wind. If foils are traditionally conceived as mobile lifting wings, we imagine it here as a fixed element, accelerating the wind. Could we also integrate other uses and functions to this device to allow in specific urban situations to enrich the performance of the device, such as :

- A support for the integration of photovoltaic panels when the wing of the foil is exposed and facing south.

- An air extraction ventilation system, this device uses the geometry of the foil's wing as an air extraction gas pedal using the Venturi effect.

---

<sup>170</sup> The **energy mix** is the distribution of the different primary energy sources consumed in a given geographical area. The share of primary energies in the global consumption of a country, a community or an industry is generally expressed in percentages

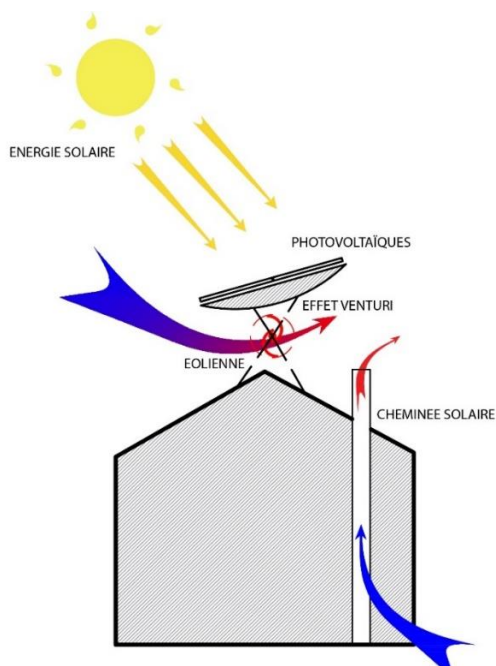


Figure 264. Schéma présentant la possibilité d'un fonctionnement hybride du foil à la fois capteur solaire et accélérateur éolien.



Figure 265. La Girafe de l'entreprise suédoise Innoventrum, un dispositif hybride de production d'énergie éolien et photovoltaïque créant aussi un carport

This assembly of 2 systems offers an air guiding surface (aerofoil) as well as a surface-support of solar radiation sensor. If this device, by combining different sources of energy production, is the subject of many studies including that of Elhadidy and Shaahid for the city of Dhahran in Saudi Arabia<sup>171</sup>, it is however complex to find the position and angle of the foil optimal for both the course of the sun and the direction of the winds.

- Digital 3D printing of wind turbines

With the development of digital manufacturing technologies, and 3D printing of large parts, it is possible to consider precisely adjusting the energy device to the architecture and not the other way around. This is an important paradigm shift from the current situation, where DEI wind turbines are diverted from a design for another use and adapted to a use in urban sites. 3D printing technologies, which have undergone a recent acceleration in their use, particularly during the Covid-19 containment period when a large number of products were manufactured to address access and supply issues in certain regions of the world.

This method could have several forms, 3D printing after digital simulation of a vertical wind turbine, whose type, length and diameter are precisely dimensioned according to an implantation, a wind, an assembly or an architecture.

The printing can allow the manufacture of a mold for the manufacture of the reinforced blade (carbon fiber, fiberglass ...), the printing of a support part of reinforcement of fibers and resins,

<sup>171</sup> M. A. ELHADIDY and S. M. SHAAHID, "Feasibility of hybrid (wind + solar) power systems for Dhahran, Saudi Arabia," *Renewable Energy*, January 1, 1999, vol. 16, n°1, coll. "Renewable Energy Energy Efficiency, Policy and the Environment," pp. 970-976.

or directly the final blade of the wind turbine (printing of materials highly resistant to wear such as ABS, or using a formal and structural optimization using artificial intelligence<sup>172</sup> .

To realize the study models of this research we used different digital printing technologies (SLA, Filaments, sintering, ABS, ...), today the technologies do not simply allow to print a prototyping or molding, but really to print a final part for the use of products of good performance or high durability such as those used in the automotive or aerospace industry

One example is the Charles de Gaulle aircraft carrier, which in 2020 acquired an FDM 3D printer, a piece of equipment that helps sailors on board to create all sorts of small everyday parts and to be able to immediately repair any parts damaged during the crossing. This device avoids the transport of important spare parts stock, improves the speed of repair of parts and limits the weight of the equipment needed during long trips.



Figure 266. Porte Avion Charles de Gaulle qui abrite un atelier d'impression 3D de pièces pour réparation/entretien

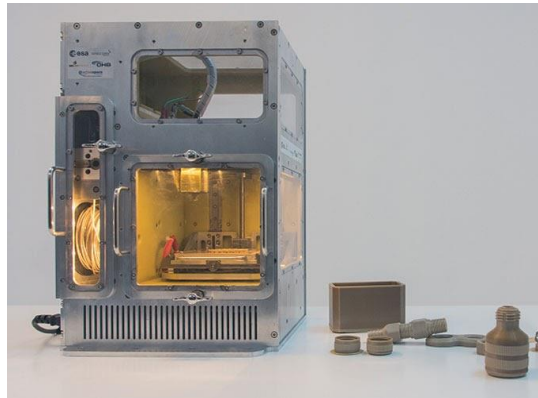


Figure 267. Imprimante 3D de ASE qui fonctionne en situation d'apesanteur.

The European Space Agency (ESA) has also developed a 3D printer<sup>173</sup> capable of operating in zero gravity, designed by various international partners such as SONACA and BEECREATIVE. It was made to print technical polymers with high mechanical and thermal properties allowing astronauts to design all kinds of parts directly in space. The International Space Station has worked in collaboration with Made in Space<sup>174</sup> to create the first 3D printer capable of operating in zero gravity.<sup>175</sup>

---

<sup>172</sup> Such as Autodesk fusion 360 software

<sup>173</sup> After winning a public tender launched by ESA, the consortium of companies - made up of the Portuguese manufacturer BEECREATIVE, the Germans SONACA Space and OHB-Sytem, and Active Space Technologies - launched the MELT project. The aim of the project was to develop and test a 3D printer that could work on board the ISS, the international space station.

<sup>174</sup> 3D PRINTING IN SPACE, <https://beeverycreative.space/>,

<sup>175</sup> A new 3D printer on the International Space Station? , <https://www.3dnatives.com/imprimante-3d-espace-23052018/><https://www.3dnatives.com/imprimante-3d-espace-23052018/>, accessed on May 24, 2020.

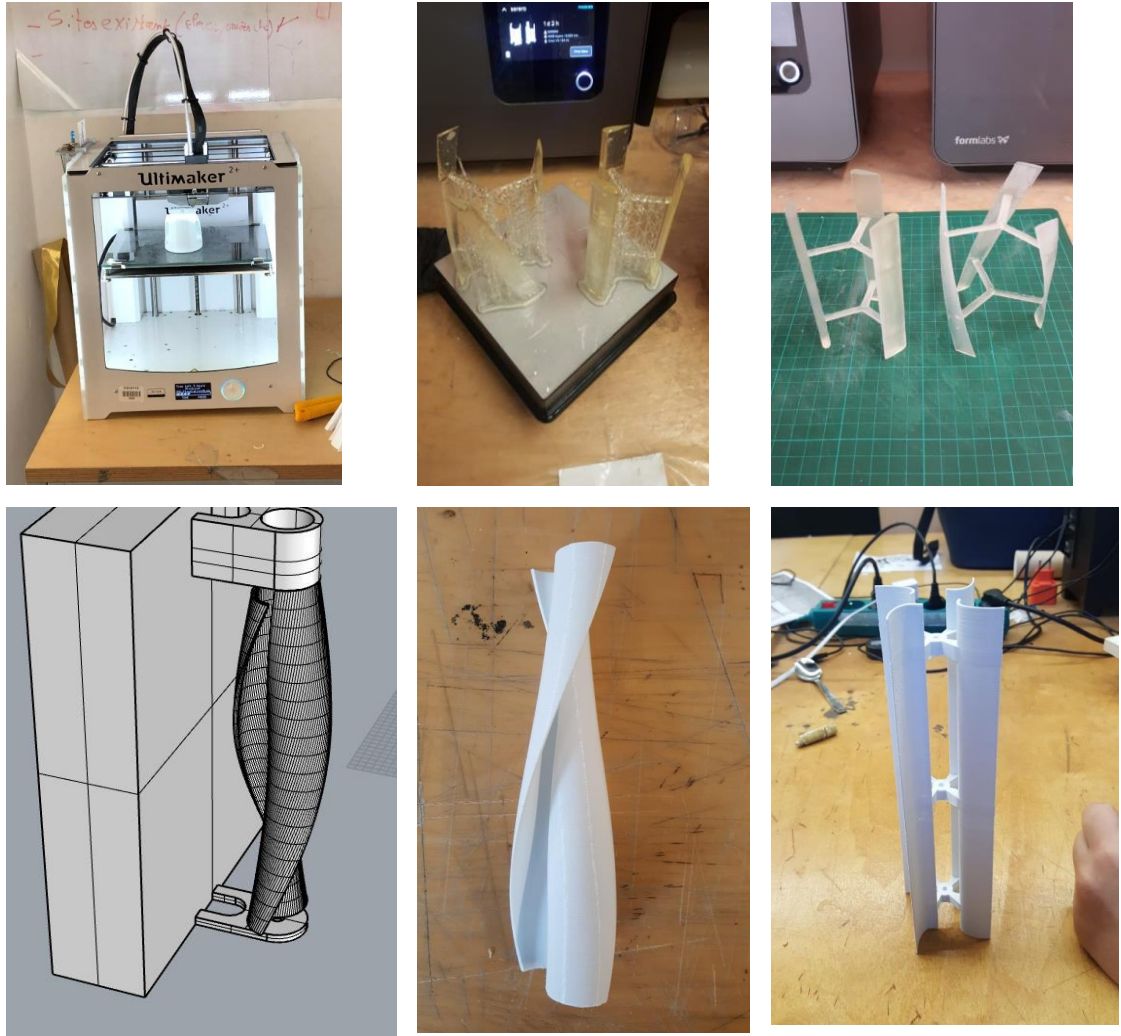


Figure 268. Digital prints for research (SLA, filament, sintering, ...)

Could we imagine these wind devices being printed and repaired using 3D printing of final parts? The devices we propose have diameters less than 1.20m wide with a device length ranging from 1.20m to 3.60m long. This turbine template is adapted to the manufacturing volume of these 3D printers, on the other hand the repairs of these devices can be done locally and immediately. This technology also makes it possible to improve or choose materials according to the required performance, material resistance, product color, or printing time. The aerofoil or gas pedal can also be 3D printed. This technology allows, during the design of the devices, to imagine foils with variable profile in order to improve and control the air speed on a singular point.



## APPENDIX 1: INITIAL STUDY OF THE RESEARCH: CONSTRUCTION OF AN EXPERIMENTAL WIND TUNNEL AND CALIBRATION OF THE NUMERICAL MODEL OF THE SIMULATION

- Calibration of numerical simulation results on an experimental physical wind tunnel

In order to verify and calibrate our virtual wind tunnel, we compared the results with those of an analog wind tunnel that we made in our agency from cardboard and rigid aluminum panels, adhesive strips, and an air extractor and a smoking machine. The power of the air extractor fan does not allow a high speed in the air stream. However, it allows to compare point by point the results, as well as the proportions and the scales of modification of the speeds by the addition of obstacles of type buildings.

- Construction of an experimental wind tunnel prototype (Agency Serero)

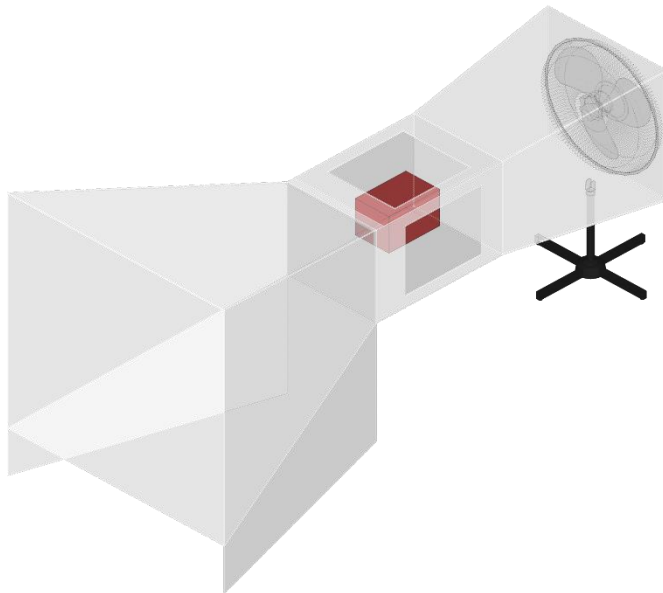


Figure 269. 3D simulation of the experimental wind tunnel prototype

The size of the study chamber is 0.2m(L)\*0.3m(W)\*0.2m(H)



Figure 270. Prototype de tunnel à vent réalisé par D.Serero pour comparer l'échelle des phénomènes



Figure 271. Détail de notre maquette de bâtiment dans la veine d'air

The prototype wind tunnel is an open-ended wind tunnel, sized to set up our study models in the wind tunnel.

Analog test chamber dimensions

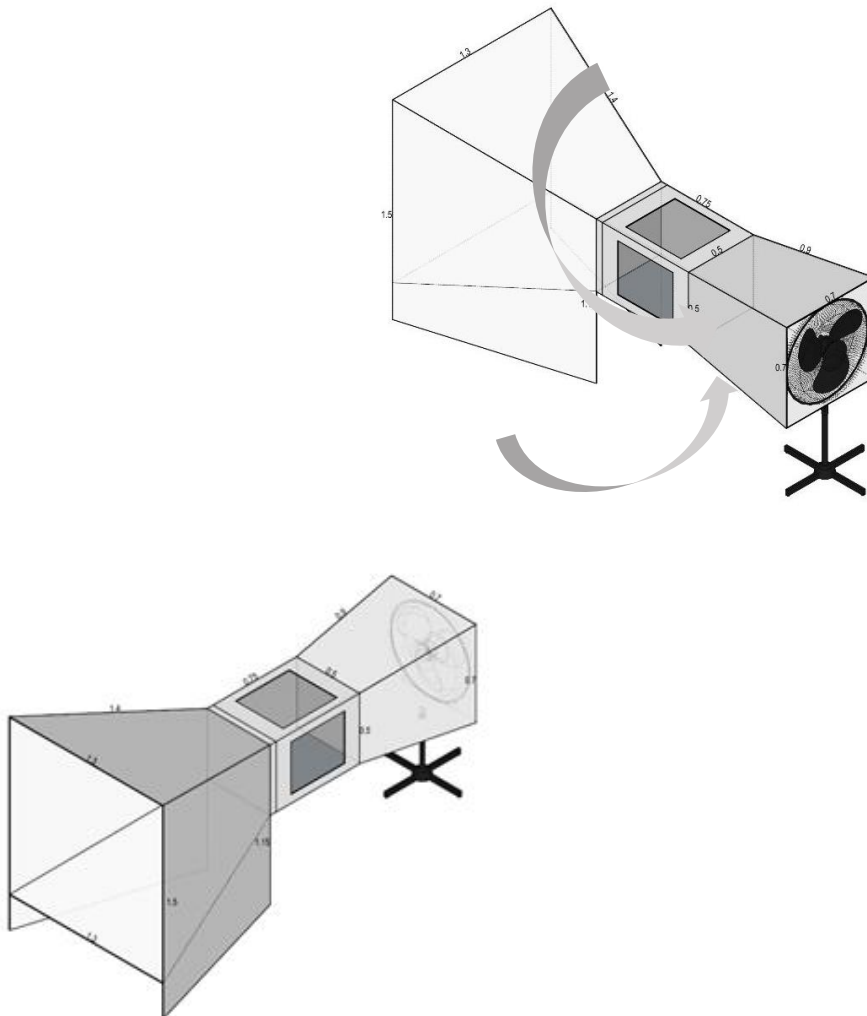


Figure 272. Operating diagram of the analog wind tunnel built for the experiment

- Calculation of the similarity coefficient - Reynolds number

We can here, in order to compare the results, check the similarity coefficient (the number of reynolds)

As a reminder, the Reynolds number is a number without magnitude that allows to verify the similarity between 2 experiments.

$$Re = \frac{VD_H}{\nu}$$

$$Re = (3.41 * 0.666) / (15.23 * 10^{-6}) = 149.266 \rightarrow \text{turbulent regime}$$

$$V \text{ (Wind speed)} = 3.41 \text{ m/s}$$

$$D_H \text{ (hydraulic diameter)} = 4A/P = 0.666 \text{ m}$$

$$A \text{ (cross-sectional area)} = 0.25 \text{ m}^2$$

$$P \text{ (perimeter)} = 1.5 \text{ m}$$

$$\nu \text{ (air viscosity } 25^\circ \text{ c)} = \mu/\rho = 15.23 * 10^{-6}$$

In the case of flat surfaces, the critical point of laminar flow is 30000.

To reduce the Reynolds number to achieve laminar flow, we must follow the steps below:

1. Reduce the wind speed to 1 m / s.
2. Reduce the hydraulic diameter of the test section to 1/2. (New DH = 0.333 m)

After changing the dimensions and the wind speed, the Reynolds number will be reduced to 21,864, which presents a laminar flow.

These modifications, applied to our wind tunnel prototype, would improve the similarity coefficient of the device. However, the reduction of an air flow to 1m/s is not easy to realize in experimental mode and can be subject to errors due to its low speed.

- *Experiment 1: Measurements inside the wind tunnel*

The wind speed inside the air stream is measured with a Voltcraft anemometer, based in (m/s) with a variable temperature of 23.5 °c. to 24.5 °c. The air velocity measured in the air stream is plotted on the following sections and compared to the numerical model.

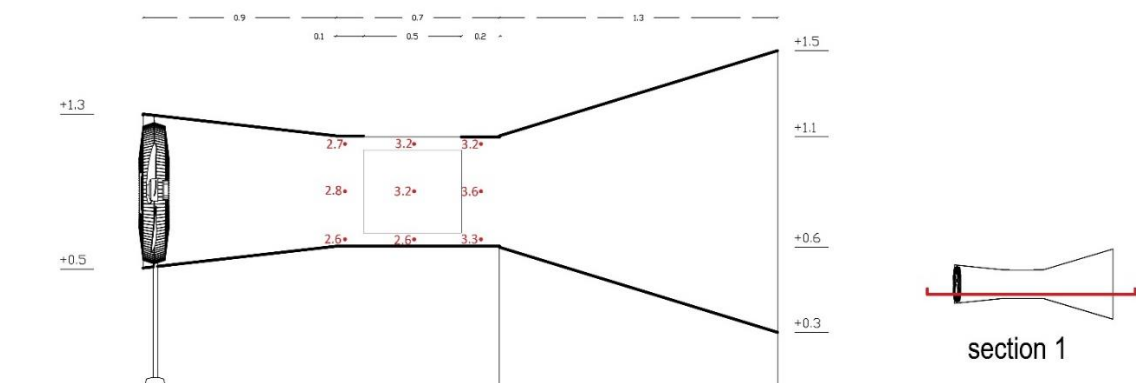


Figure 273. Location of the measurement points on the physical tunnel, GSA Laboratory

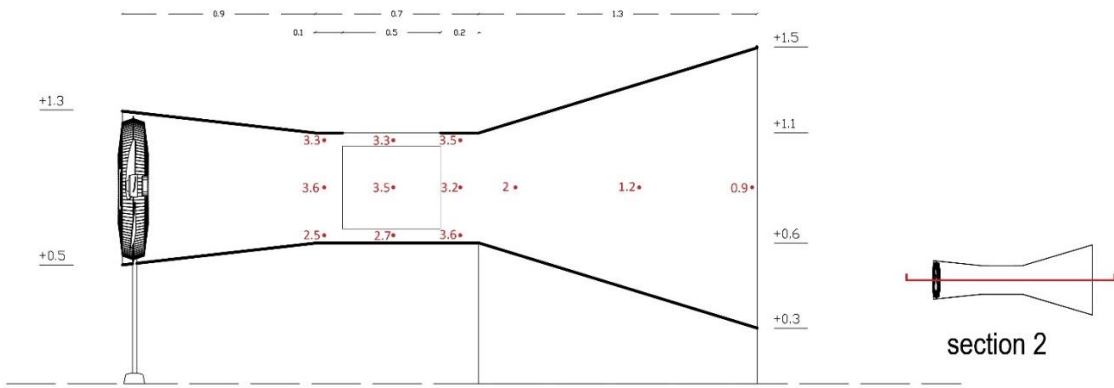


Figure 274. Location of the measurement points on the physical tunnel, GSA Laboratory

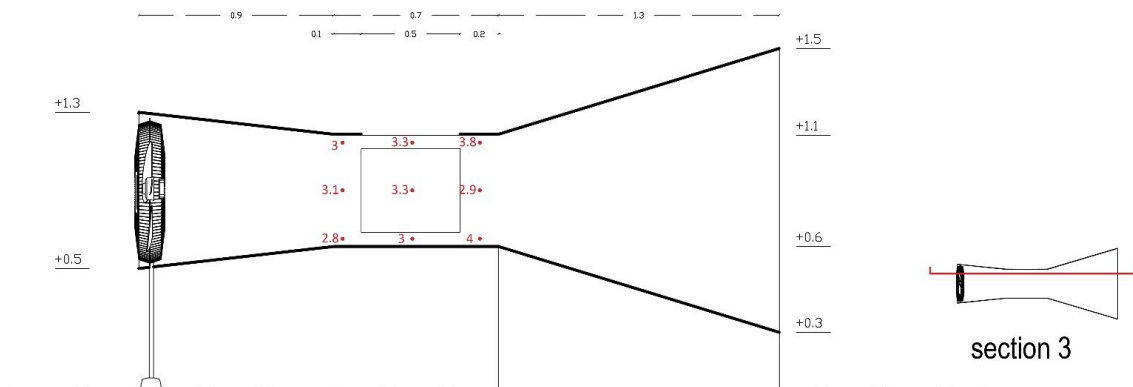


Figure 275. Location of the measurement points on the physical tunnel, GSA Laboratory

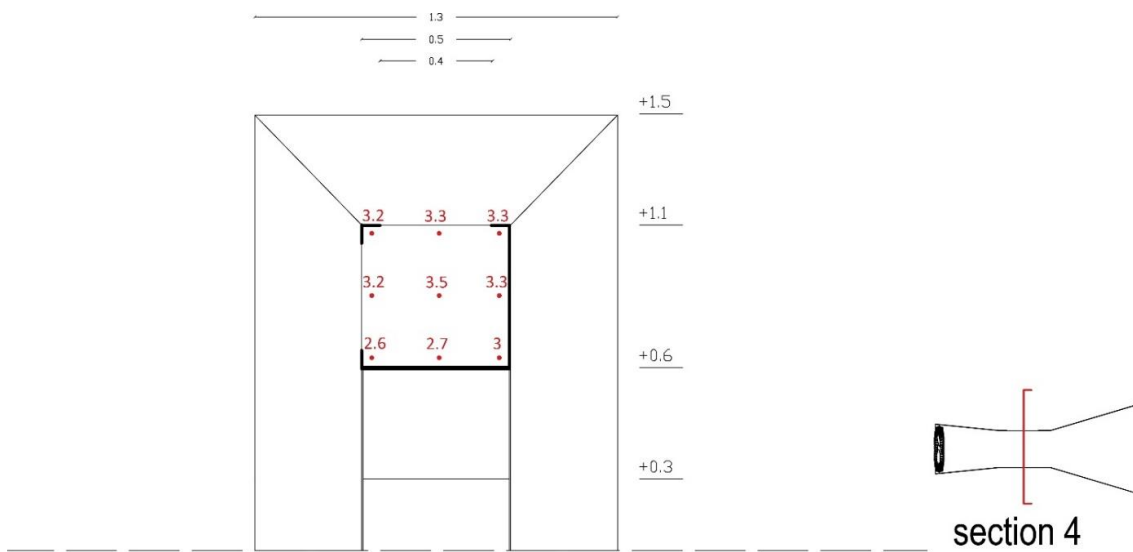


Figure 276. Location of the measurement points on the physical tunnel, GSA Laboratory

- *Boundary Layer*

The boundary layer in our experimental wind tunnel does not affect the results of the wind flow analysis in the studied air section. Considering the air velocity in the studied wind tunnel, there is a 2.5cm boundary layer of all surfaces of the air stream section with air velocity varying between 0 m/s on the surface and 1.62 m/s on the edges.

- *Experiment 2: Wind tunnel modeling and boundary layer comparison*

The wind speed inside the numerical tunnel model is compared to that measured in the physical tunnel. We adjust the computational conditions in order to obtain a boundary layer profile equivalent to the one measured on the physical model under similar conditions. This approach allows a calibration of the numerical model on the parameters of the physical model.

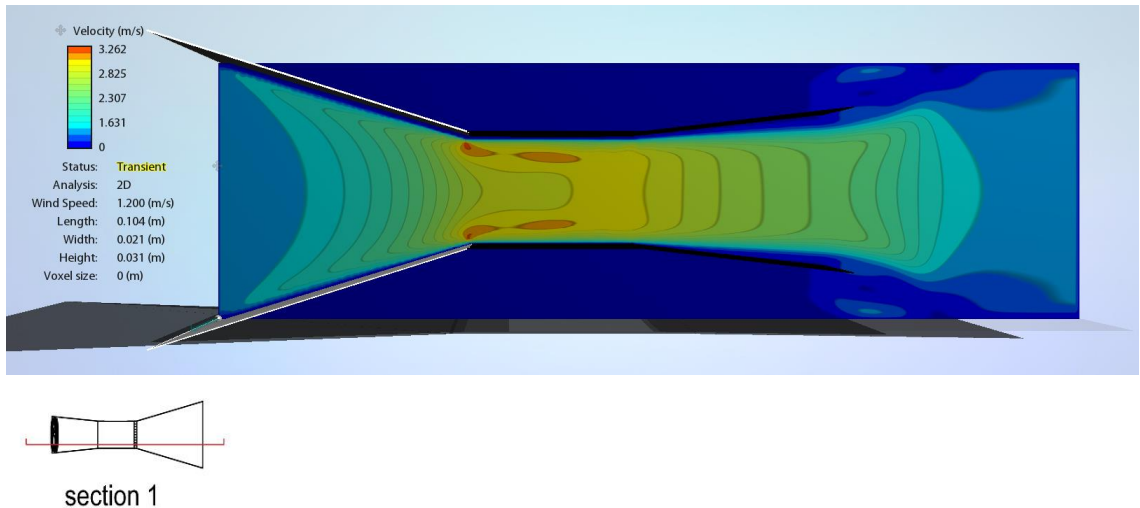


Figure 277. Dynamic simulation of the study physical tunnel model

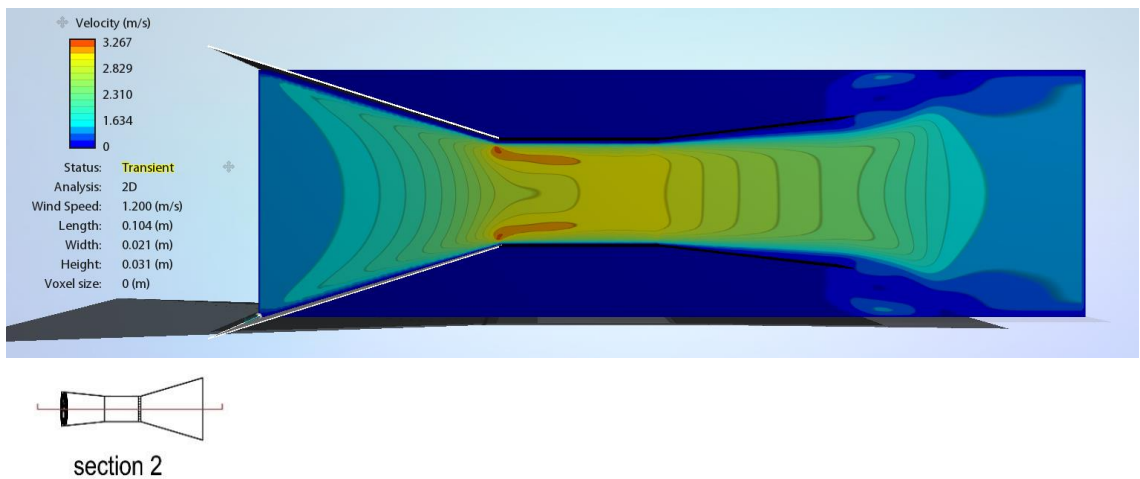


Figure 278. Dynamic simulation of the study physical tunnel model

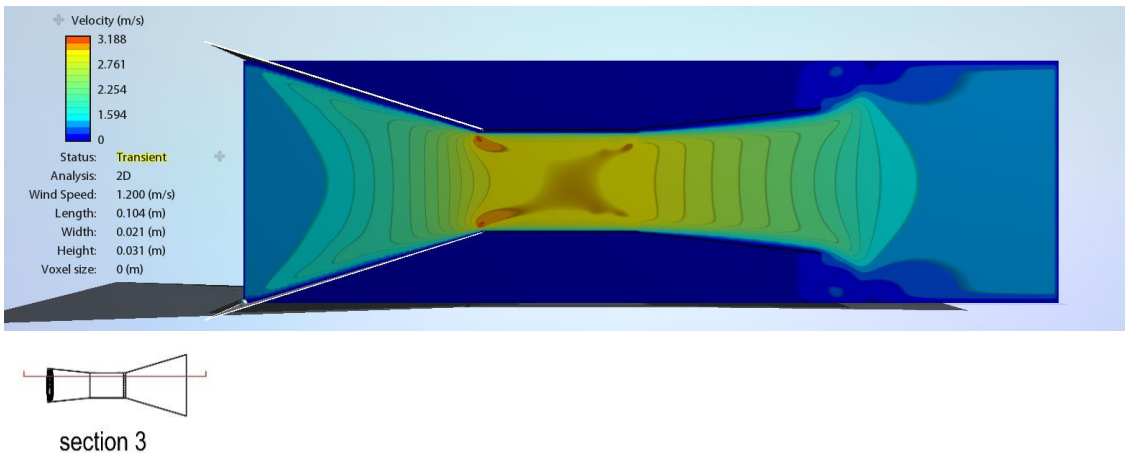


Figure 279. Dynamic simulation of the study physical tunnel model

The wind speed in the fluid simulation is 1.20m/s and is based on the air speed measured on the physical wind tunnel.

- *Experiment 3: Modeling of a 4-story building with a roof wing and comparison with a numerical wind tunnel.*

In this 4th experiment, we modeled a building and a roof wing and compared the results with measurements made on the wind tunnel model. The wind speed inside the numerical model of the tunnel is compared with the one measured in the physical tunnel. This experiment is performed after calibration of the numerical model.



Figure 280. Serero tunnel a vent location

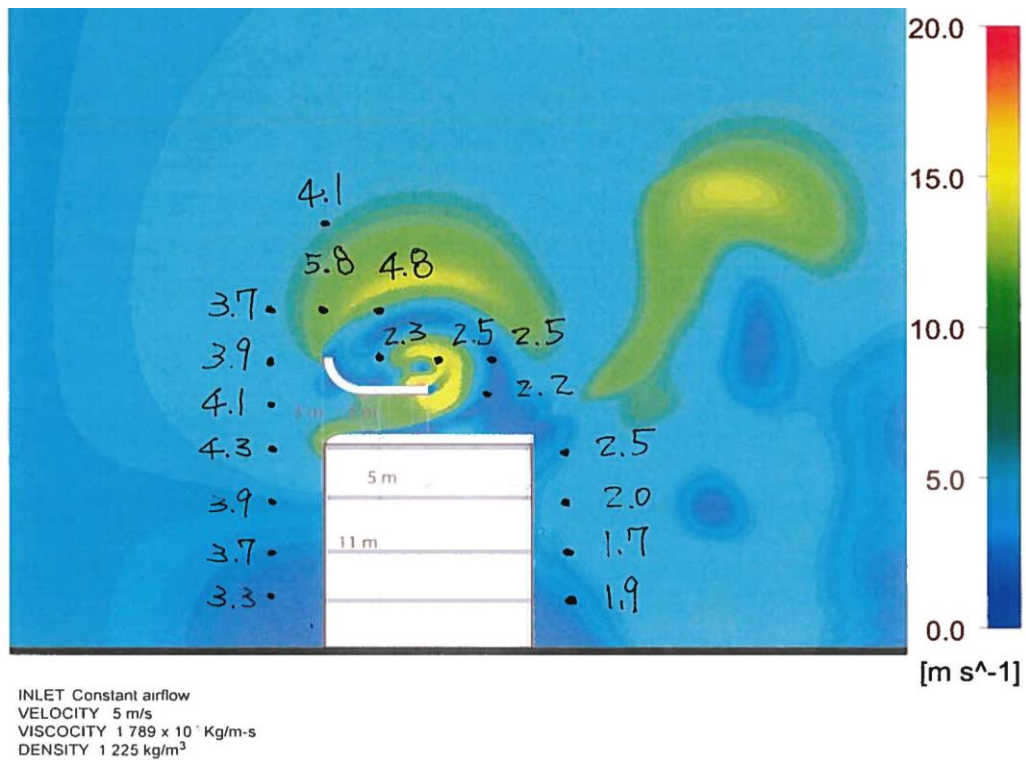


Figure 281. Comparison with a model studied in the analog wind tunnel in the laboratory.

The handwritten annotations on the cross-sectional simulation are the points found in the physical wind tunnel experiment. The very strong coherence between the measurements in a physical environment and the numerical environment (magnitude colors) confirms that our calibration and our initial conditions to the calculation are consistent and very close to the behavior of the physical phenomenon.

## APPENDIX 2: DATA SHEETS OF WIND ENERGY CAPTURE DEVICES

- Modern classic 3-blade wind turbine

- Horizontal axis
- Number of blades : 3

Examples of machines: Enercon E66/2000, Gamesa G80/2000, Nordex N90/2300



Figure 282. Nordex N90/2300

Figure 283. Gamesa G80/2000

Figure 284 Enercon E66/2000

- Modern classic 2 blade wind turbine

- Horizontal axis
- Number of blades : 2

Examples of machines: Vergnet GEV MP 275, Vergnet GEV HP, Vergnet GEV 26/200



Figure 285. Vergnet GEV 26/200

Figure 286. Vergnet GEV HP

Figure 287. Vergnet GEV MP 275

- Single blade wind turbine

Horizontal axis

Number of blades : 1



Figure 288. Eolienne monopale

- Pumping wind turbine

- Horizontal axis
- Number of blades : ~ 20



Figure 289 Pumping wind turbine

- Savonius wind turbine

- Vertical axis
- Number of blades : 2



Figure 290. Wind turbine of Savonius

- Vertical rotor wind turbine

- Vertical axis
- Number of blades : 2-3

Examples of machines: Ropatec Double Vertical, Ropatec Twister, Ropatec Bora Extreme



Figure 291. Ropatec Double Vertical



Figure 292. Ropatec Twister



Figure 293. Ropatec Bora Extreme

- WINDSIDE WIND TURBINE

- Vertical axis
- Number of blades : 2

Examples of machines: Windside WS-12, Windside WS-2B, Windside WS-0,15 C/B



Figure 294. Windside WS-12



Figure 295. Windside WS-2B



Figure 296. Windside WS-0,15 C/B

- NEW WIND INNOVATION

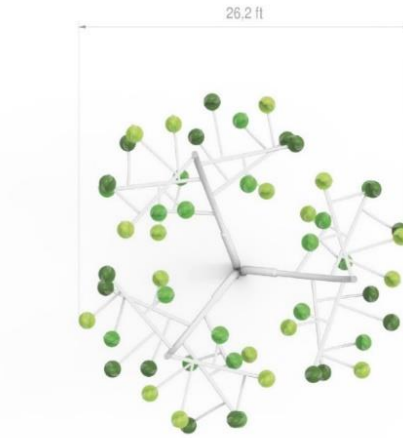
**TECHNICAL CHARACTERISTICS**

Total height	30.2 FT
Diameter	26.2 FT
Total weight (excluding base anchor)	2500 KG
Number of Aeroleaves	54
Aeroleaf's height	3.2 FT
Wind gusts resisting system	121.4 FPS (37 M/S)

DESIGN BY CLAUDIO COLANGELO

**ELECTRICAL CHARACTERISTICS**

Installed capacity	3510 W
Peak power per Aeroleaf	65 W
Output voltage of the inverter	210 / 240 V



130, rue de Lourmel, 75015 Paris, France

**Website:**

<http://www.newwind.fr/en/>

**Contact name: Marie de Jouët**

Sales & Marketing, NewWind R&D

Tel: +33 (0)7 81 81 83 36 1

Email: [mdejouette@newwind.fr](mailto:mdejouette@newwind.fr)

130, rue de Lourmel - 75015 Paris

**Price:** about 30 000 euros; each aero leaf costs 500 euros

**Keys specs:** Cut in: 2.5m/s; cut out: 37 m/s; rated speed (survival speed):

**Dimensions:** 90 cm height X 30 cm diameter?

**Electrical generator:** French

**Types:** direct drive, contains 2 generators

**Height:** 7.5 meters Diameter 6.5 meters;

**Electrical Production:** 65W/ aero leaf, 54 aero leaf per tree, 3,5KW (maximum wind speed)

Can be concentrated in wind farm of 1 every 5 meters

**Advantage:** Elegant and skinny, no noise < 50dB, no turbulence

- GUAL STATO EOLIAN

**Jean-Claude PICCIO**

at 0683532612

**website:** <http://www.stato-windturbine.com>

PS: To avoid the problems generated by the use of power leds, I invite you to visit <http://everlum.fr>

**E-mail:** [anthony.gadet@wanadoo.fr](mailto:anthony.gadet@wanadoo.fr)

<http://www.gual-st atoeolien.com/>

RDV on 18/01/2017 at 4:00 pm

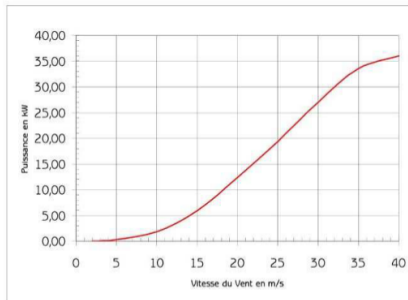
**Keys specs:**

## STATOEOLIEN GSE 8

### Caractéristiques techniques :

Diamètre / Hauteur :	8 m / 3 m
Vitesse de démarrage :	2 m/s (7,2 km/h)
Vitesse maximale :	60 m/s (216 km/h)
Puissance à 15 m/s (54 km/h) :	6 kW
Puissance à 25 m/s (72 km/h) :	19,3 kW
Puissance à 40 m/s (144 km/h) :	36 kW
Vitesse de rotation :	de 0 à 60 tours/min
Génératrice triphasée :	Asynchrone à cage d'écuriel
Régulation de Puissance :	Pilotage électronique direct du couple
Masse :	Environ 2 500 kg
Maintenance :	Inspection annuelle
Garantie :	3 ans

Courbe de puissance



Ces informations sont données à titre indicatif et ne peuvent en aucun cas engager la responsabilité de GUAL Industrie.  
Ces informations peuvent être modifiées par GUAL Industrie sans préavis.

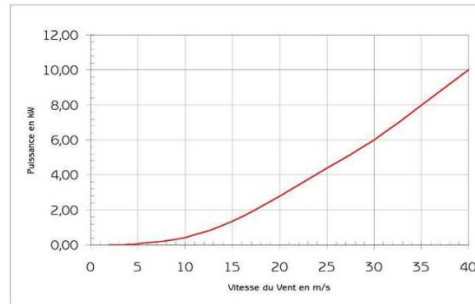
9

## STATOEOLIEN GSE 4

### Caractéristiques techniques :

Diamètre / Hauteur :	4m / 1,5 m
Vitesse de démarrage :	2 m/s (7 km/h)
Vitesse maximale :	60 m/s (216 km/h)
Puissance à 15 m/s (54 km/h) :	1,3 kW
Puissance à 25 m/s (90 km/h) :	4,4 kW
Puissance à 40 m/s (140 km/h) :	10 kW
Vitesse de rotation :	de 0 à 120 tours/min
Génératrice :	Synchrone à aimants permanents
Régulation de Puissance :	Pilotage électronique direct du couple
Masse :	Environ 800 kg
Maintenance :	Inspection annuelle
Garantie :	3 ans

Courbe de puissance



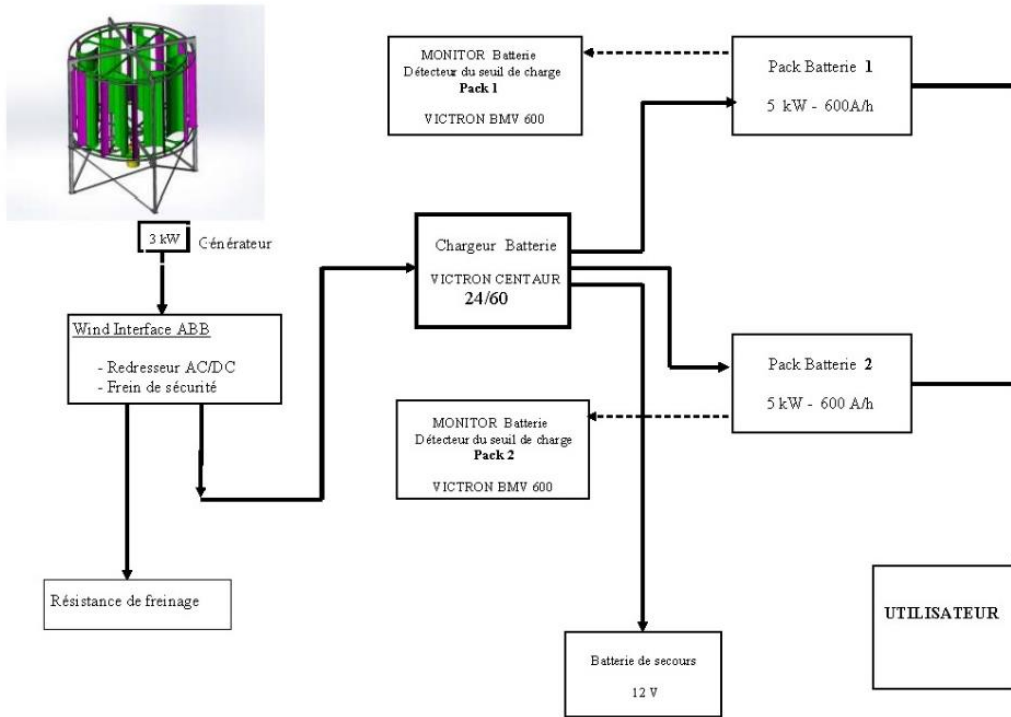
Ces informations sont données à titre indicatif et ne peuvent en aucun cas engager la responsabilité de GUAL Industrie.  
Ces informations peuvent être modifiées par GUAL Industrie sans préavis.

8

### Avantage:

Its characteristics and its aesthetics, allow the opening of a new market for market for the New Renewable Energies (ENR) addressing the greatest number of both in urban and rural areas, and corresponding to :

- Individual housing
- Collective housing
- Industrial, commercial and agricultural sites.



ANNEXE II -- 1/2

ECLAIRAGE PUBLIC, CONSOMMATION ACTUELLE

PUBLIC LIGHTING, CURRENT CONSUMPTION

DESIGNATION DES EQUIPEMENTS	EQUIPMENT NAME	Puissance Wh	Equipements installés sur le port (Quantité)	Durée d'allumage (Heures)	Consommation annuelle en Kwh
		Power Wh	Equipments installed on the port (Quantity)	Duration of lighting (Hours)	Annual consumption in KWh
<i>Etude réalisée en 2004-2010 par jspiccoconsult@free.fr dans le cadre des économies d'énergies dans les ports de plaisance Français</i>	<i>Study carried out in 2004-2010 by jspiccoconsult@free.fr within the framework of energy savings in the French marinas</i>				
Appliques 1 Boule	Wall lamps 1 Ball	150	20	4000 *	12000
Appliques 2 Boules	Wall lamps 2 Balls	300	2	4000	2400
Colonne "Sparkos"	Column " Sparkos "	150	37	1825 **	22200
Cheminement Autour Capitainerie	Way around the port office	50	19	4000	1734
Guirlandes sur le pourtour du port	Garland around the port	10	4000	150 ***	6000
Lampadaires 2 Boules	Lamp posts 2 Balls	300	62	4000	74400
Lampadaires 1 Boule	Lamp posts 1 Ball	150	16	4000	9600
Lampadaires 1 Boule (en Applique)	Lamp posts 1 Ball (In Wall lamp)	150	2	4000	1200
Lampadaires 12 Mètres (4 Projecteurs de 400Watts)	Lamp posts 12 meters (4 Projectors of 400Watts)	1600	8	4000	51200
Appareil d'éclairage Ampoules 9/11 Watts	Lighting device : CFL 9/11 Watts	9	300	4000	10800
Projecteurs (Encastrés)	Fitted spotlights	150	14	4000	8400
Projecteurs	Projectors	150	14	4000	8400
Projecteurs	Projectors	70	1	4000	280
				<b>Total Annuel en KW - Annual total in KW</b>	<b>208614</b>
					PRODUCTION OF CO <sub>2</sub> in kilogram
					<b>20861</b>
				<b>Total Annuel en MW - Annual total in MW</b>	<b>209</b>
<p>GUTRLANDES :4000 ampoules à 10W/Chacune x temps d'éclairage = 15nuits l'été, 15 nuits l'hiver selon les préconisations de l'AFE:4000/365x30=328 heures            GARLANDS:4000 ballbe in 10W/each x Duration of lighting = 15 nights in summer, at 15 nights in winter according to the recommendations of l'AFE:4000 / 365x30 = 328 hours</p>					

- WINDSPIRE

**Website:**

<http://bwegroupusa.wix.com/bwe-group#!vstc0=power-module>

<http://bwegroupusa.wixsite.com/urban-wind>

<http://bwegroupusa.wixsite.com/wind-farms>

<http://bwegroupusa.wixsite.com/windspire-eco>

**Contact name:**

Beach Wind Energy - Windspire

Richard Kline, designer and fabricator

1-803-347-5566

**Price:** about 6000 dollars

**Email:**

**Keys specs:** up to 20 KW per wind spire

**Dimensions:** 5 meters per 1.2 diameter

Electrical generator? German, Swiss, Chinese

Can be concentrated in wind farm of 1 every 5 meters

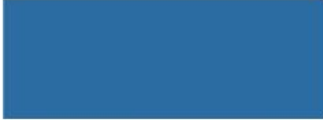
**Advantage:** Elegant and skinny, no noise < 50dB, no turbulences

**Disadvantage:** very high,

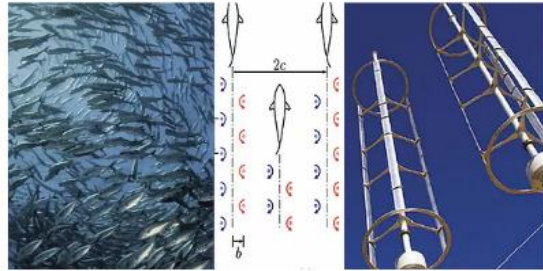
**Note:** Kline can fabricated any product we need vertical from the USA

# Windspire Wind Farms

HOME



## How fish can make wind farms more efficient



Wind-turbine Placement Produces Tenfold Power Increase, Caltech Researchers Say –

- AEOLOS wind turbine

**Website:** <http://www.windturbinestar.com>

**Contact name:** Susan Yin

Lotus Energy Technology Co.

No.16, Shandong Road, Qingdao, CHINA

**Tel:** +86 532 8090 3375

**E-mail:** susan@windturbinestar.com

**Price:**

5kw(grid-on): \$17,750

5kw(grid-off): \$16,910

The prices are to be understood EXW, including packing. Shipment and installation are excluded.

**Quantity discount:**

1--2 units of Aeolos-V 5-10kW turbines (whole system) net

3--5 units of Aeolos-V 5-10kW turbines (whole system) 5%

More than five sets, the special discount can be considered further.

**Validity:**

The quotation is valid until 31st January, 2017.

**Delivery time:**

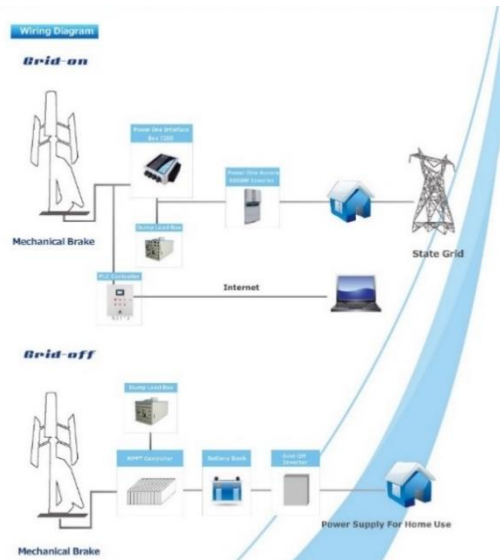
Production time: for 5-10kW, 20 working days after receipt of order,

Delivery time: By shipment, depends on different port with different distance.

**Payment method:**

With T/T - 30% down payment at order confirmation; With T/T - 70% before shipment.

**Keys specs:**



- QUIET REVOLUTION

**Website:** [www.vwtpower.com](http://www.vwtpower.com)

**Contact name:** Tracey Newland, Business Development Manager  
 11 Edison Road  
 St.Ives  
 Cambridgeshire  
 PE27 3LF  
 United Kingdom

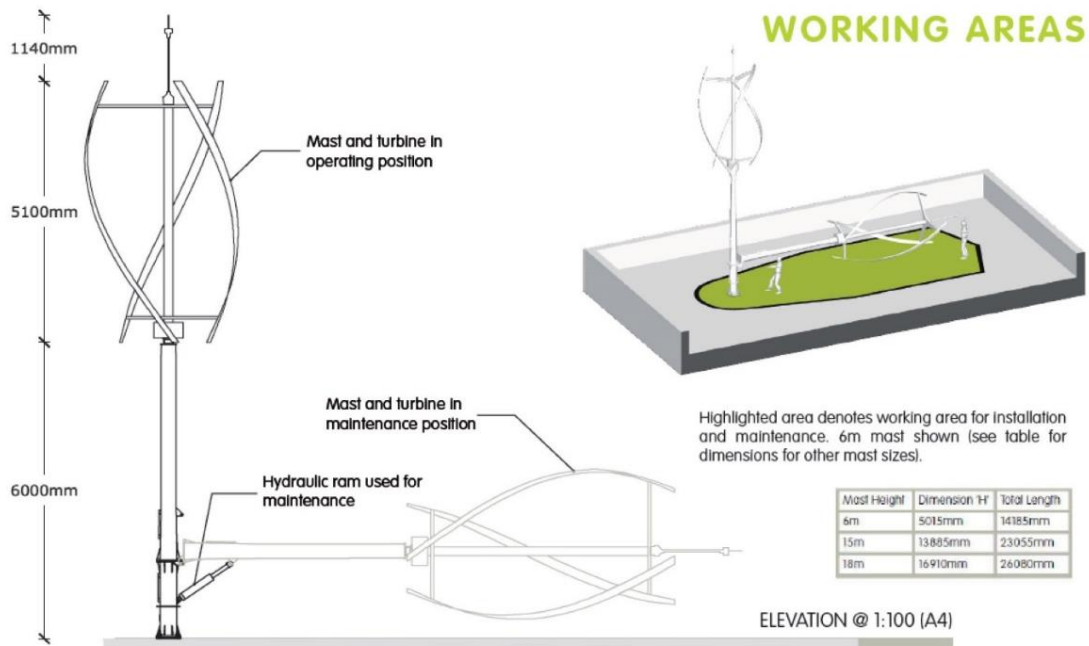
**TEL:** +44 (0) 1480 277360

**Mobile:** +44(0) 7831 197492

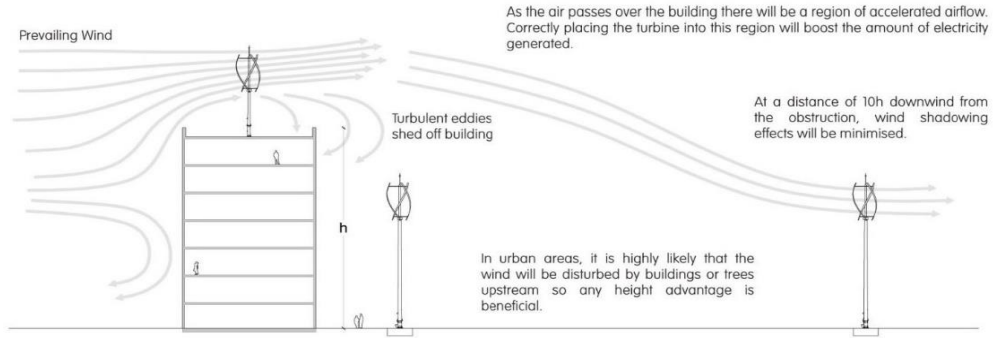
**Email:** [tracey.newland@vwtpower.com](mailto:tracey.newland@vwtpower.com)

**Price:** 35,000 pounds + installation, foundation work and etc.

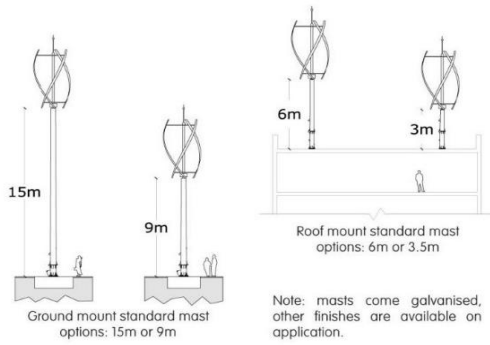
**Keys specs:**



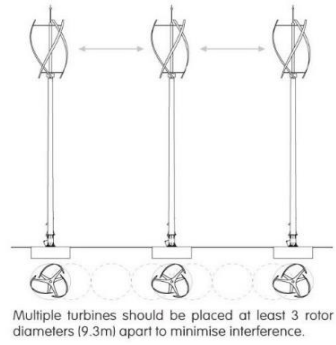
## Optimising Wind Energy in the Urban Environment



## Installation Options



## Turbine Spacing



● FORTIS WIND ENERGY

Website: [www.fortiswindenergy.com](http://www.fortiswindenergy.com)

E-mail: [jahn@fortiswindenergy.com](mailto:jahn@fortiswindenergy.com)

Contact name: Eric F.W. JAHN  
Business Development Director (CCO)

Skype ID: Eric.Jahn

Keys specs:

Mobile: +31 614 424 930

TECHNICAL SPECIFICATIONS				
				
Model:	Passaat	Montana	Montana-Q	Alizé
Type	Upwind rotor with fixed pitch			
Maximum power <sup>1</sup>	1.4 kW	5.0 kW	6.0 kW	10 kW
Rated wind speed	16 m/sec	14 m/sec	14m/sec	13 m/sec
Cut-in wind speed	2.5 m/sec	2.5 m/sec	2.5 m/sec	3 m/sec
Output@11m/sec	0.9 kW	3.4 kW	4.45 kW	8.5 kW
Rotor diameter	3.12 m	5.0 m	5.25 m	6.3 / 6.6 / 6.9 m
Number of blades	3	3	3	3
Swept area	7.64 m <sup>2</sup>	19.63 m <sup>2</sup>	21.63m <sup>2</sup>	31.2 m <sup>2</sup> / 34.2m <sup>2</sup> / 37.4m <sup>2</sup>
Blade material	Fibreglass-reinforced epoxy			
Yaw control	Passive aligned by tail vane			
Speed regulation	Ecliptic safety system by inclined hinged vane, 90 degree setting of tail. Short circuit of generator			
RPM operation range	180 - 775	120 - 450	120 - 450	75 - 300
Generator Type	Permanent Ne-Fe-Br magnets producing 3 phase AC			
Battery regulator	Available for 24VDC / 48VDC	Available for 48VDC	Available for 48VDC	On request
Grid feed inverter	1P-230VAC+N+PE	1P-230VAC+N+PE 3P-230VAC+N+PE 3P-400VAC+N+PE	3P-230VAC+N+PE 3P-400VAC+N+PE	3P-230VAC+N+PE
Guyed tower	12-18 m	12-24 m	12-24 m	18-30 m
Free standing tower	12-18 m	12-24 m	12-24 m	12-24 m
Head weight	75 kg	200 kg	210 kg	385 kg
Unique features	<ul style="list-style-type: none"> <li>• Conforms to IEC 61400-2 international standard</li> <li>• Upwind, direct drive, fixed pitch, overvoltage protection and emergency braking</li> <li>• Maintenance free, 5 year warranty, installation by Fortis Certified System Partner</li> <li>• Average lifetime for Fortis Wind Turbines is over 20 years</li> <li>• Made in The Netherlands</li> </ul>			
<sup>1</sup> ] maximum power output @ rated wind speed				

- KINGSPAN ENVIRONMENTAL

Website: [www.kingspanwind.com](http://www.kingspanwind.com)

Contact name:

Blair Caldwell

Wind Sales Representative

TEL: +44 1560 486 570

Mobile: +44 7990 080 916

Email: [blair.caldow@kingspan.com](mailto:blair.caldow@kingspan.com)

Keys specs

Small Wind Energy Solutions

Kingspan Wind

UNIQUE DESIGN

## TECHNICAL PRODUCT SPECIFICATIONS

- SELF REGULATING
- MINIMAL VISUAL IMPACT
- NO GEAR BOX
- ANTI OVER-SPEED CONTROL

UNRIVALED WIND ENERGY SOLUTIONS  
BUILT ON EXPERTISE

### KW3 PRODUCT SPECIFICATION

Peak Power	3.2kW
Reference Annual Energy @ 5m/s	4700kWh
Application	Residential, Commercial, On- & Off-Grid, Platform, Remote, Island, On-Grid
Gridless	Grid Tied, Battery Charge, 24V, 48V, 300V
Grid Options	Single / Split / Dual / Three Phase
Architecture	Commercial, 3 Blades, Self-Regulating
Blade	5.0m Spanner / Maximum 3000 RPM
Blade Material	Glass Reinforced Composite
Generator	Brushless Direct Drive Permanent Magnet
Tower Height Options	6.5m / 7m / 8m / 9m / 10m / 11m
Tower Specification	Class 1 Rated / Galvanized Steel
Foundation Option	Pad / Bolt / Rock Anchor
Cut In Speed	2.5 m/s
Rated Wind Speed	Rated - Continuous Operation
Survival Wind Speed	Designed to Class 1 (70km/h)
Warranty	5 Year Parts & Labour
Grid Cable Options	Available on Request
Colour Options	White (RAL 9002) Black (RAL 9005)

### KW3 ANNUAL ENERGY PRODUCTION

\* The KW3 Annual Energy Production Curve illustrates the energy that will be generated under the given average wind speed. The ability to calculate the power allowed for the installation of a turbine is subject to local conditions.

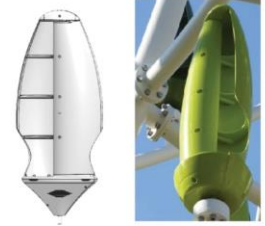
### KW6 PRODUCT SPECIFICATION

Peak Power	6kW
Reference Annual Energy @ 5m/s	6200kWh
Application	Residential, Commercial, On-Grid, Platform, Remote, Island, On-Grid
Gridless	Grid Tied, Battery Charge, 48V, 300V, 600V
Grid Options	Single / Split / Dual / Three Phase
Architecture	Commercial, 3 Blades, Self-Regulating
Blade	5.6m Spanner / Maximum 3000 RPM
Blade Material	Glass Reinforced Composite
Generator	Brushless Direct Drive Permanent Magnet
Tower Height Options	6.5m / 7m / 8m / 9m / 10m / 11m
Tower Specification	Class 1 Rated / Galvanized Steel
Foundation Option	Pad / Bolt / Rock Anchor
Cut In Speed	2.5 m/s
Rated Wind Speed	Rated - Continuous Operation
Survival Wind Speed	Designed to Class 1 (70km/h)
Warranty	5 Year Parts & Labour
Grid Cable Options	Available on Request
Colour Options	White (RAL 9002) Black (RAL 9005) Grey (RAL 9006)

### KW6 ANNUAL ENERGY PRODUCTION

\* The KW6 Annual Energy Production Curve illustrates the energy that will be generated under the given average wind speed. The ability to calculate the power allowed for the installation of a turbine is subject to local conditions.

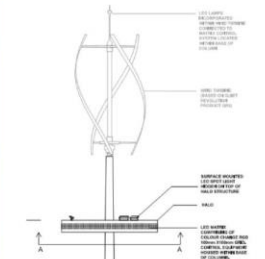
## APPENDIX 3: EXISTING BUILDING-INTEGRATED WIND ENERGY SYSTEMS



Project: WIND TREE  
Paris, France  
Design: Jérôme Michaud-Larivière

The Wind tree uses tiny blades that are housed in the leaf units. The blades turn inwards, which enables the units to turn in the wind, regardless of wind direction. Jerome told Microsoft the units respond to wind as low as 2 meters per second. The units are silent, which is a bonus, as other wind turbine technology can be very noisy and unsuitable for urban areas. The team therefore claim the wind tree to be less obtrusive than other designs and could be used in many locations such as gardens, squares, parks and shopping centers. The units will cost around £23,000 and can be linked together. Since they look like sculptures, the trees could be used as street art that also powers the city.

DAVID SERERO - DISPOSITIFS EOLIENS INTEGRES



THE q5  
QuietRevolution wind turbine

The q5 was designed in response to increasing demand for wind turbines that work well in environments close to people and buildings. The elegant helical (twisted) design of the q5 ensures a robust performance even in turbulent winds. It is also responsible for virtually eliminating noise and vibration. At five metres high and three metres in diameter, it is compact and easy to integrate, and with just one moving part, maintenance can be limited to an annual inspection.

EXISTING WIND HARVESTING DEVICES - VERTICAL AXIS WIND TURBINE

DAVID SERERO - DISPOSITIFS EOLIENS INTEGRES



**Project: POWER FLOWERS**  
Location: the Netherlands  
Design Team: NL Architects

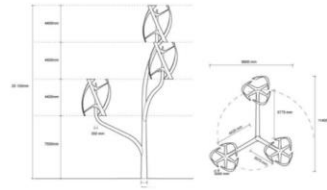
The Power Flower comes in two designs: uw3 (urban windmill) and uw12. The uw3's are around 19 meters in diameter and can be placed just about anywhere from backyards to building tops. One uw3 can power a typical US household a year and a uw12 can power 5 US households a year. Although the Power Flowers' lower heights decreases effectiveness as compared to a full size HAWT turbine, efficiency is made up by their close proximity to households, no wind direction requirements and minor spacing requirements.

### uw3

type of windturbines used: URBAN GREEN ENERGY 4kW  
number of turbines: 3  
rated power: 12 kW  
annual power at average wind speed 5 m/s: 13 680 kWh  
generated noise at 12 m/s: 42.8 dB  
blade materials: carbon fibre and fibreglass  
tower material: steel hollow profile



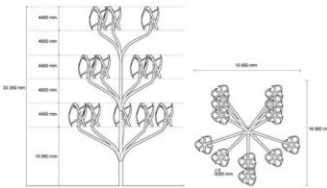
branches of the turbine are ordered in shape of a spiral  
this ensures low torque moment for the highest turbine  
creates natural design resembling a flower



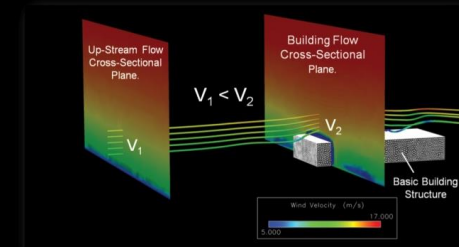
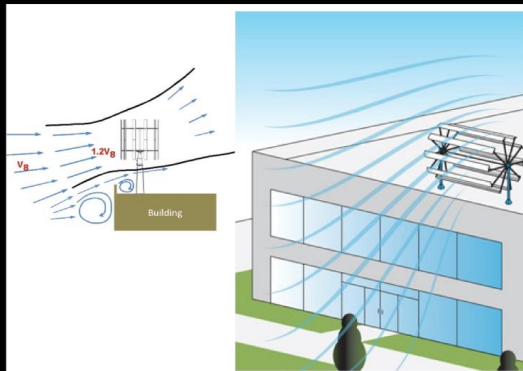
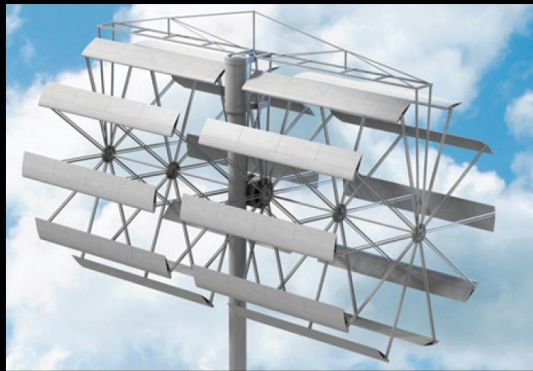
### uw12

generates even more power than uw3  
the shape of branches of the windmill are inspired by simple geometrical shapes: pentagon, square, triangle  
horizontal distance between each turbine on the branch has to be at least 10 meters

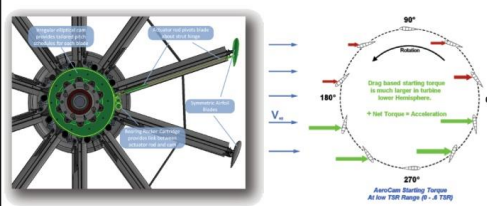
type of windturbines used: URBAN GREEN ENERGY 4kW  
number of turbines: 12  
rated power: 48 kW  
annual power at average wind speed 5 m/s: 55 000 kWh  
generated noise at 12 m/s: 48.8 dB  
blade materials: carbon fibre and fibreglass



DAVID SERERO - DISPOSITIFS EOLIENS INTEGRÉS



Compared to a conventional three-blade turbine, the AeroCam has more wing area working to produce power, but in a significantly smaller package. This effectively generates more power from the same wind speed. The AeroCam's blades use the natural flow of air to create lift, effectively minimizing drag and optimizing mechanical efficiency.



**Project: AeroCam**  
Location: US  
Design Team: Broadstar Wind Corporation

The AeroCam technology is the first truly viable renewable wind energy solution for the commercial environment. The proprietary AeroCam wind turbine technology can be mounted on rooftops or free-standing towers at commercial and industrial sites with moderate wind conditions. The modular wind energy system integrates multiple 11kW AeroCam wind turbines to accommodate site-specific energy needs.

EXISTING BUILDING INTEGRATED WIND HARVESTING DEVICES - AEROCAM

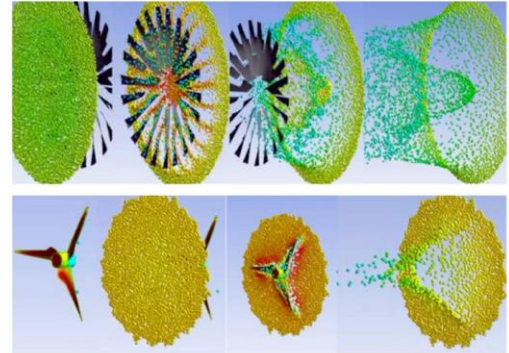
DAVID SERERO - DISPOSITIFS EOLIENS INTEGRÉS



Blade Tip Power Production the magnets, and copper stators on the tip of the blade are producing a 'flywheel' effect.



- 1: Wheel
- 2: Hub
- 3: Blades
- 4: Spokes
- 5: Voltage Generation
- 6: Magnets
- 7: Stators
- 8: Fins



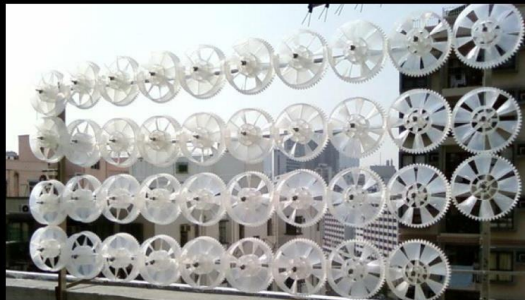
The TAM Turbine is producing the power at the tip of the blade where the speed and energy are up to 9-10 times greater than the center of the Turbine. The TAM turbine's magnets and stators are at the blade tip of the Turbine and are protected by a shroud or casing. Traditional Turbines are center gear shaft driven, which means that the blades turn and the power is generated at the center of blades, the multi-stage blade system is able to take a much higher percentage of energy from the wind than that of a traditional Turbine.



Project: TAM Turbine  
Location: US  
Design Team: TAM Energy

The TAM Wind Turbine produces clean renewable energy where the energy is used, at your home or commercial building. Its BTPS (Blade Tip Power System) unique design of multi-stage blades allows the system to react quickly to changes in wind speed. This ensures that the maximum wind energy is captured without the typical noise and vibration associated with traditional wind turbines.

DAVID SERERO - DISPOSITIFS EOLIENS INTEGRÉS



The first micro-turbine array set up in Hong Kong. It includes 49 turbines, which has daily production capacity of 960Wh with average wind speeds of 5.5 m/s. This installation was made in November, 2009, and is large enough to power all of the lights in the apartment below. If space is available, it is suggested to spread these turbines along a single row, instead of four rows. This is because the anchoring with the posts will be easier and more secure. The taller the display is, the stronger the posts and anchoring system needs to be.



EXISTING BUILDING INTEGRATED WIND HARVESTING DEVICES - MOTORWIND

Motorwind Home

Home > 10 Turbines set with generator

10 Turbines set with generator

Item# TG1017  
US\$1,000.00  
Color: Blue

Add to cart

**Product Description**  
10 micro turbines with generator rated 60W for 10m/s wind, daily production : 1.2 kWh. Output 12 to 48 volts  
Best application between 1m/s and 10m/s wind speeds.  
Frame: 1.02 meter long x 0.54 m height x 0.14 m wide. Stainless steel main support, with 2 aluminum posts (0.82 m long)  
Volume : 0.075 CBM Measurement : Weight :12 Kgs  
20'container = approx 410 pcs -----40' container = approx 840 pcs

Motorwind Home

Home > 12 Turbines 360 degrees directional set bi-generator

12 Turbines 360 degrees directional set bi-generator

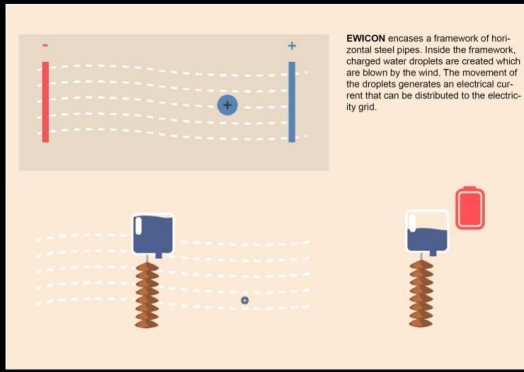
Item# AT1234  
US\$1,200.00  
Color: Blue

Add to cart

**Product Description**  
12 micro turbines with 2 generators rated 100W for 10 m/s wind. Output 12 to 48 VDC volts non regulated.  
2.1 meters span. Works from 2 m/s wind speed.  
Volume: 0.10584 CBM Gross weight: 18 Kgs  
(for shipment by container: 20' = approx. 240 sets, 40' = approx. 510 sets)

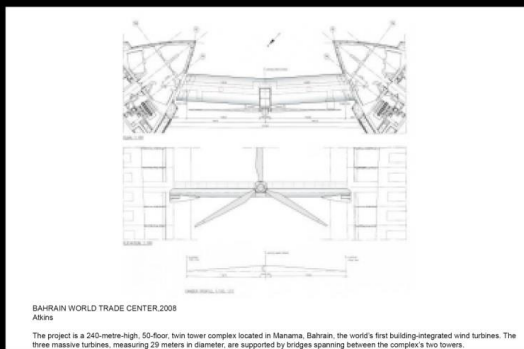
Project: Motorwind  
Location: Hong Kong  
Design Team: Lucien Gambarota (inventor), CHRISTAN MASSET, Dr Michael Leung, Dr Dennis Leung

DAVID SERERO - DISPOSITIFS EOLIENS INTEGRÉS



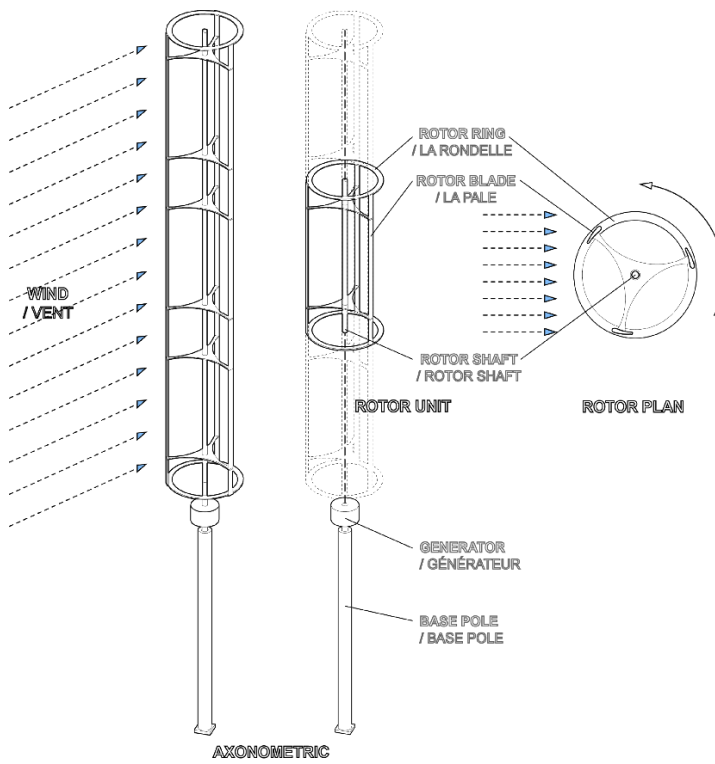
EXISTING BUILDING INTEGRATED WIND HARVESTING DEVICES - EWICON

DAVID SERERO - DISPOSITIFS EOLIENS INTEGRÉS



EXISTING BUILDING INTEGRATED WIND HARVESTING DEVICES - HORIZONTAL AXIS WIND TURBINE

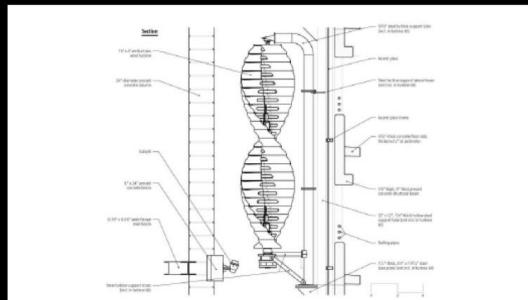
DAVID SERERO - DISPOSITIFS EOLIENS INTEGRÉS



San Francisco Public Utilities  
Commission  
(SFPUC)  
San Francisco, 2012  
KMD/ Stevens+ Associates  
Mariah Windspire turbines: five  
turbines  
Swept area: 4.89 m<sup>2</sup>  
Energy production: 227 Mwh/ year



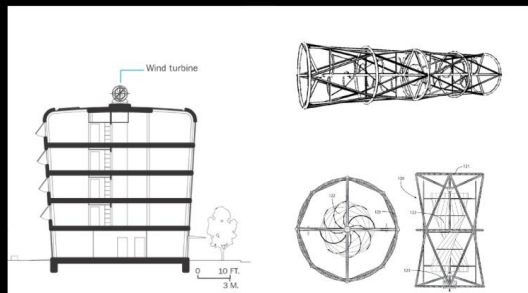
Figure 297. San Francisco Public Utilities Commission



**GREENWAY SELF PARK**  
HOK Architect

The vertical turbines are located on the southwest corner of the garage to take full advantage of Chicago's summer winds. The turbines will harvest the wind to power the exterior wall lighting of the facility, as well as contribute excess power to the city grid.

EXISTING BUILDING INTEGRATED WIND HARVESTING DEVICES - VERTICAL AXIS WIND TURBINE



**520H AEROTURBINES ON MERCY HOUSING**  
Murphy/Jahn Architects, Aerostucture International

This installation features eight 520H Aeroturbines mounted horizontally to the roof of this 96-unit single-resident housing development. The building, designed by Murphy/Jahn Architects, is a fine example of building-integrated wind energy technology. The geometry and orientation of the building was designed specifically to increase the speed of the wind as it flows over the roof.

EXISTING BUILDING INTEGRATED WIND HARVESTING DEVICES - VERTICAL AXIS WIND TURBINE

DAVID SERERO - DISPOSITIFS EOLIENS INTEGRÉS

## APPENDIX 4: EXAMPLE OF A WIND TURBINE STUDY USING A GENERATIVE DESIGN TOOL (FUSION 360)

Fusion 360 is a complete parametric CAD (computer aided design) tool developed by Autodesk. This tool is intended to draw and design 3D parts, both mechanical and design. A powerful CAM solution is integrated to the tool to drive the CNC<sup>176</sup>.



Figure 298. Example of generative work on the chassis of a vehicle and on the structure of a chair



Figure 299. 3D printing of wind turbines with generator turbines

<sup>176</sup> Jon McCORMACK, Alan DORIN, and Troy INNOCENT, "Generative design: a paradigm for design research," p. 8; Sivam KRISH, "A practical generative design method," *Computer-Aided Design*, January 1, 2011, vol. 43, n°1, pp. 88-100.

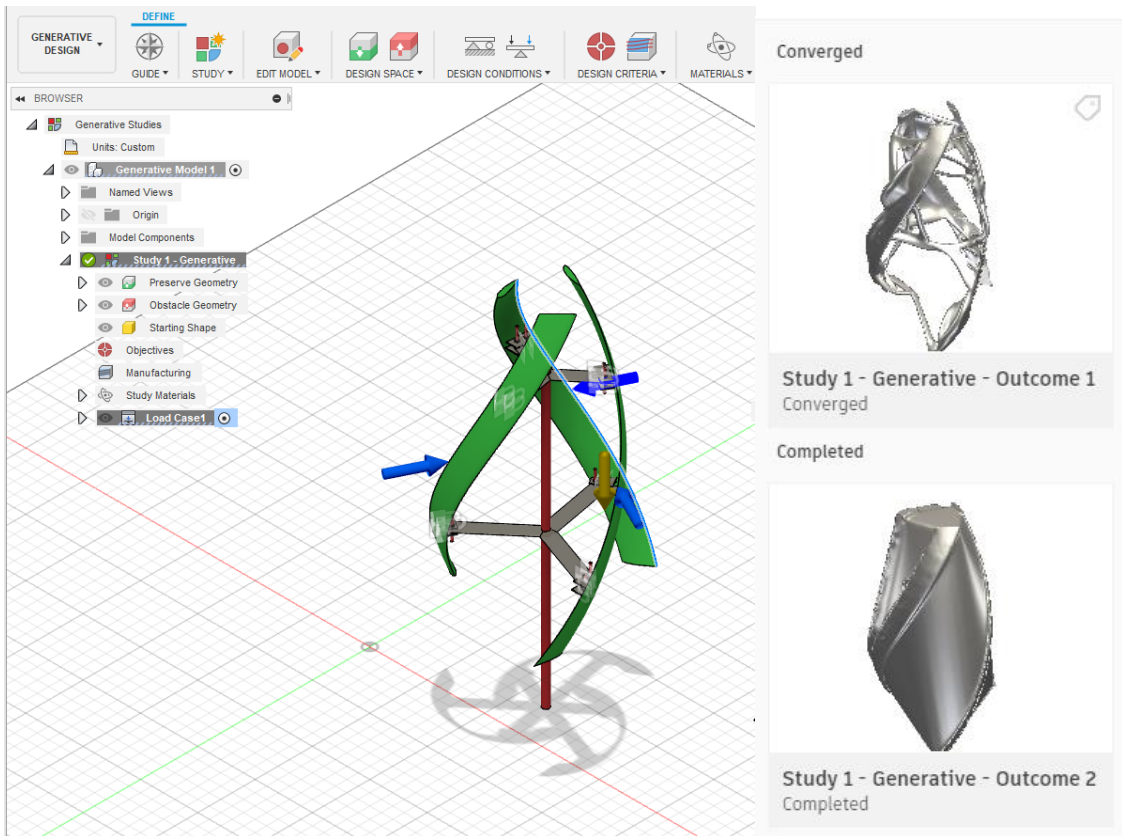


Figure 300. Generative study of a wind turbine design in Fusion 360

### Generation 1: from 3 blades

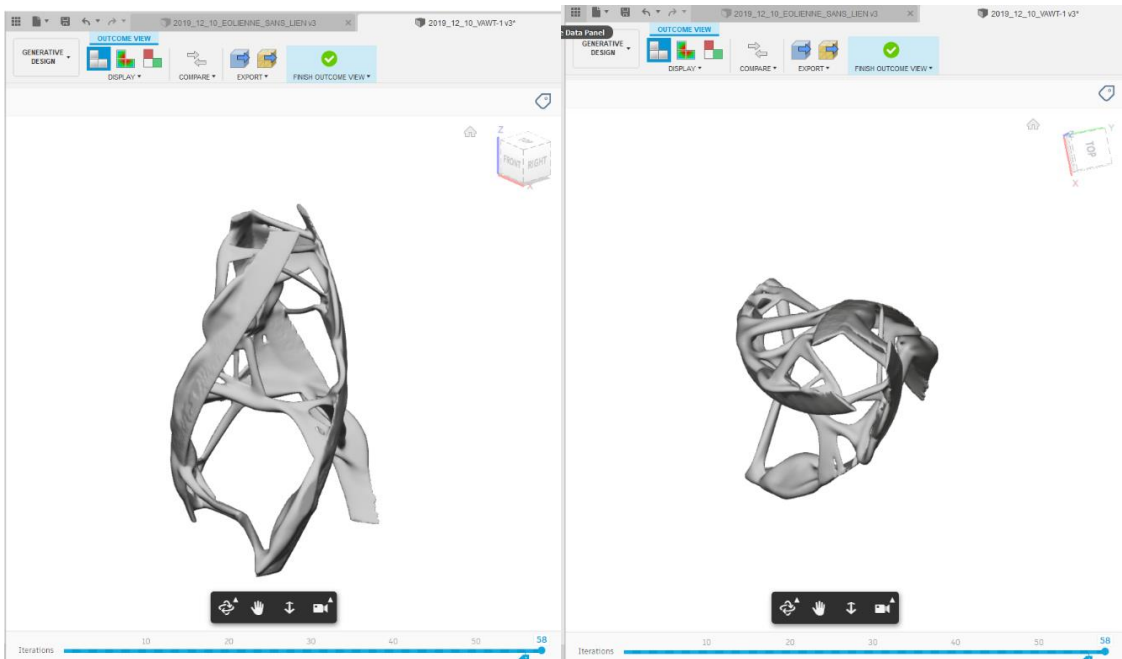


Figure 301. Generative study of a wind turbine design in Fusion 360

### Generation 2: from 3 spiral blades

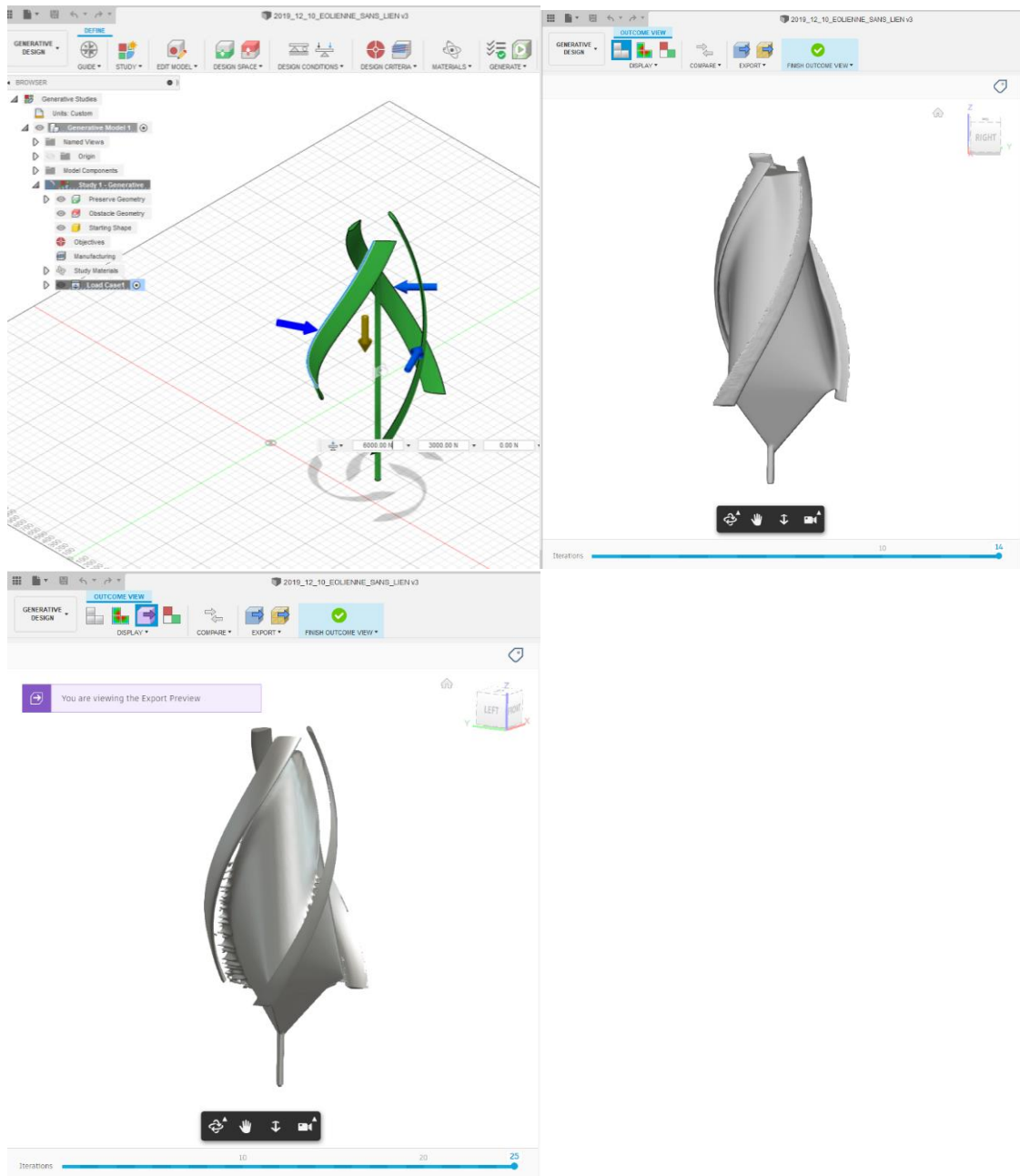


Figure 302. Generative study of a wind turbine design in Fusion 360

## APPENDIX 5: A CALCULATION REPORT OF THE STARCCM+ SIMULATION

1 SECTION			
ROOF			
WITHOUT			
DEVICE			
+1	Continua	Continua	2
	+1	Units	Regions
			[Region]
Meshes			
			Interfaces
			Tags
			Interfaces
			Tags
	2	Physics 1	Regions
			[Region]
			Interfaces
			Point Sets
			Active
			true
			Tags
			[]
+-1 Models			
		+1	
Constant			
Density			
	+2	Coupled	Integration
		Flow	IMPLICIT
			Positivity Rate Limit
			0.2
			Explicit Relaxation
			1.0
			Active Explicit Relaxation
			1.0
			Preconditioning Enabled
			true
			Unsteady Low-Mach Preconditioning
			true
			Unsteady Preconditioning Max Factor
			0.95
			Pressure Difference Scale Factor
			2.0
			Minimum Reference Velocity
			1.0E-10 m/s
			Maximum Reference Velocity
			1000000.0 m/s
			Flow Boundary Diffusion
			true
			Secondary Gradients
			We
			Coupled Inviscid Flux
			Roe FDS
			Discretization
			2nd-order
+-3 Gas			
		-1	Air
			Database Material
			Air (Air) [Standard/Gases]
			Tags
			[]
		-1	
Material			
Properties			
		+1	Method
			Constant
Density			
		-1	Value
			1.18415 kg/m^3
Constant			

		^-2	Method	Constant
Dynamic Viscosity				
		^-1	Value	1.85508E-5 Pa-s
Constant				
		+4	Gradient Method	Hybrid Gauss-LSQ
Gradients				
			Limit Method	Venkatakrishnan
			Custom Accuracy Level Selector	2.0
			Verbose	false
			Least-Squares Quality Criterion	true
			Flat Cells Curvature Criterion	true
			Cell Skewness Criterion	true
			Chevron-Cell Criterion	true
			Least-Squares Tensor Minimum Eigenvalues Ratio	0.1
			Normalized Flat Cells Curvature Factor	1.0
			Maximum Safe (Positive) Skewness Angle (deg)	75.0
			Minimum Unsafe (Positive) Skewness Angle (deg)	88.0
			Use TVB Gradient Limiting	false
			Acceptable Field Variation (Factor)	0.05
	+5	Implicit	Continuum Iteration	215000
Unsteady				
			Continuum Physical Time	21.500000000003293
	+6	K-	Epsilon	Turbulence
		+7	Buoyancy Production of Dissipation	Boundary Layer Orientation
Realizable Epsilon Two-Layer				
			Cmu	0.09
			C1e	1.44
			C2e	1.9
			Ct	1.0
			Sigma_k	1.0
			Sigma_e	1.2
			Sarkar	2.0
			Tke Minimum	1.0E-10
			Tdr Minimum	1.0E-10
			Secondary Gradients	We
			Convection	2nd-order
			Normal Stress Term	false
			Curvature Correction Option	Off
			Two-Layer Type	Shear Driven (Wolfstein)
			Two-Layer ReY*	60.0

	Two-Layer Delta ReY	10.0
	+8 Reynolds-Averaged Navier-Stokes	
	+9 Turbulent	
	+10 Two Dimensional	
	+11 Two-Layer All y+ Wall Treatment	Iterative Ustar false
	`-12 Wall Distance	Wall Distance Method Implicit Tree
	+2 Reference Values	
	+1 Minimum Allowable Wall Distance	Value 1.0E-6 m
	+2 Maximum Allowable Absolute Pressure	Value 1.0E8 Pa
	+3 Minimum Allowable Absolute Pressure	Value 1000.0 Pa
	-4 Reference Pressure	Value 101325.0 Pa
	3 Initial Conditions	
	+1 Pressure	Method Constant
	`-1 Constant	Value 0.0 Pa
	+2 Turbulence Intensity	Method Constant
	`-1 Constant	Value 0.01
	+3 Turbulence Specification	Method Intensity + Viscosity Ratio
	+4 Turbulent Velocity Scale	Method Constant
	`-1 Constant	Value 1.0 m/s
	+5 Turbulent Viscosity Ratio	Method Constant
	`-1 Constant	Value 10.0
	6 Velocity	Method Constant
	Coordinate System	Laboratory

`-1 Constant	Value	[0.0, 0.0] m/s
+2 Regions	Part Selection Priority	[Region]
	Regions	1
`-1 Region	Index	0
	Mesh Continuum	Meshes shares
	Physics Continuum	Physics 1
	Shares	[Body 1]
	Type	Fluid Region
	Allow Per-Part Values	false
	Tags	[]
+1 Boundaries	Part Surface Selection Priority	[Region: Body 1.Building, Region: Body 1.Entry, Region: Body 1.Floor, Region: Body 1.Top, Region: Body 1.Exit]
	Boundaries	5
+1 Body 1.building	Index	12
	Interfaces	
	Share Surface area	[Body 1.Building]
	Type	Wall
	Allow Per-Surface Values	false
	Tags	[]
+1 Physics Conditions		
+1 Reference Frame Specification	Option	Region Reference Frame
+2 Shear Stress Specification	Method	No-Slip
+3 Tangential Velocity Specification	Method	Fixed
4 Wall Surface Specification	Method	Smooth
`-2 Physics Values		
`-1 Blended Wall Function	E	9.0
	Kappa	0.42
+2 Body 1.input	Index	13
	Interfaces	
	Share Surface area	[Body 1.Entry]
	Type	Velocity Inlet
	Allow Per-Surface Values	false

	Tags		[]
+-1 Physics Conditions			
	+1 Option	Reference Frame Specification	Lab Frame
	+2 Method	Turbulence Specification	Intensity + Viscosity Ratio
3	Velocity Method	Specification	Components
^-2 Physics Values			
	+1 Method	Turbulence Intensity	Constant
	^-1 Value	Constant	0.01
	+2 Method	Turbulent Viscosity Ratio	Constant
	^-1 Value	Constant	10.0
^-3	Velocity Method		Constant
	Coordinate System		Laboratory
	^-1 Value	Constant	[5.0, 0.0] m/s
+3	Body Index	1.Top	15
	Interfaces		
	Share Surface area		[Body 1.Top]
	Type		Pressure Outlet
	Allow Per-Surface Values		false
	Tags		[]
+-1 Physics Conditions			
	+1 Direction	Backflow Specification	Extrapolated
	Pressure		Environmental
	+2 Option	Pressure Outlet Option	None
	-3 Method	Turbulence Specification	Intensity + Viscosity Ratio
^-2 Physics Values			
	+1 Method	Pressure	Constant

^-1	Value	0.0 Pa
Constant		
+2	Method	Constant
Turbulence Intensity		
^-1	Value	0.01
Constant		
-3	Method	Constant
Turbulent Viscosity Ratio		
^-1	Value	10.0
Constant		
+4	Body Index	14
1.Sol		
	Interfaces	
	Share Surface area	[Body 1.Sol]
	Type	Wall
	Allow Per-Surface Values	false
	Tags	[]
+1 Physics Conditions		
+1	Option	Region Reference Frame
Reference Frame Specification		
+2	Method	No-Slip
Shear Stress Specification		
+3	Method	Fixed
Tangential Velocity Specification		
4	Wall Method	Smooth
Surface Specification		
^-2 Physics Values		
^-1	Blended E	9.0
Wall Function		
	Kappa	0.42
-5	Body Index	16
1.Output		
	Interfaces	
	Share Surface area	[Body 1.Output]
	Type	Pressure Outlet
	Allow Per-Surface Values	false
	Tags	[]
+1 Physics Conditions		

+1	Direction	Extrapolated
Backflow Specification		
	Pressure	Environmental
+2	Option	None
Pressure Outlet Option		
-3	Method	Intensity + Viscosity Ratio
Turbulence Specification		
`2 Physics Values		
+1	Pressure Method	Constant
-1	Value	0.0 Pa
Constant		
+2	Method	Constant
Turbulence Intensity		
-1	Value	0.01
Constant		
-3	Turbulent Viscosity Ratio Method	Constant
-1	Constant Value	10.0
+2	Feature Curves Part Curve Selection Priority	[Region:Feature Curve]
	Feature Curves	1
-1	Feature Curve Part Curves	[Body 1.Default]
	Tags	[]
+3 Physics Conditions		
+1	Initial Condition Option	Use Continuum Values
+2	Mass Source Option	false
+3	Momentum Source Option	None
-4	Turbulence Source Option	None
4 Physics Values		
+1	Axis Coordinate System	Laboratory
	Origin	[0.0, 0.0] m
	Direction	[0.0, 0.0, 1.0]
2	Motion Specification Motion	Stationary
	Reference Frame	Lab Reference Frame

+3

Representations

+1 Latest Surface/Volume	Representation	Volume Mesh
	Tags	[]
+2 Geometry	Tags	[]
^-1 Latest Surface	Tags	[]
3 Volume Mesh	Cells	572414
	Interior Faces	1706838
	Vertices	1138034
	Tags	[]
+1 Finite Volume Regions		
^-1 Region	Cells	572414
	Interior Faces	1706838
	Vertices	1138034
	Edges	0
^-1 Finite Volume Boundaries		
+1 Body 1.building	Faces	1648
+2 Body 1.input	Faces	90
+3 Body 1.Top	Faces	398
+4 Body 1.Sol	Faces	1368
-5 Body 1.Output	Faces	105
2 Cell Sets		
+4 Contacts		
+5 Units		
+1 Block	Metadata	{}
	Index	4
	Region	[]
	Contacts	[]
	Descriptions	[Root]
	Face Count	12
	Coordinate System	Laboratory
	Corner 1	[-1.0, -0.2, 0.0] m,m,m
	Corner 2	[3.5, 1.0, 0.005] m,m,m

	Tags	{}
+-1 Surfaces		
`~1 Block Surface	Index	62
	Metadata	{}
	Boundary	{}
	Tags	{}
`~2 Curves		
`~1 Block Curve	Index	4
	Feature Curve	{}
	Tags	{}
`~2 Body 1	Metadata	{}
	Index	3
	Region	[Region]
	Contacts	{}
	Descriptions	[Root]
	Face Count	44
	Tags	[Region (2D Mesh)]
+-1 Surfaces		
+-1 Building	Index	54
	Metadata	{}
	Boundary	[Region: Body 1.Building]
	Tags	[Boundary (2D Mesh)]
+-2 Input	Index	57
	Metadata	{}
	Boundary	[Region: Body 1.Entree]
	Tags	[Boundary (2D Mesh)]
+-3 Top	Index	60
	Metadata	{}
	Boundary	[Region: Body 1.Top]
	Tags	[Boundary (2D Mesh)]
+-4 Wall_oppose	Index	55
	Metadata	{}
	Boundary	{}
	Tags	{}
+-5 Sol	Index	58
	Metadata	{}
	Boundary	[Region: Body 1.Sol]
	Tags	[Boundary (2D Mesh)]
+-6 Output	Index	61

	Metadata	{}
	Boundary	[Region: Body 1.Sortie]
	Tags	[Boundary (2D Mesh)]
Symmetry	-7 Index	56
	Metadata	{}
	Boundary	[]
	Tags	[Region (2D Mesh)]
2 Curves		
-1 Default	Index	3
	Feature Curve	[Region:Feature Curve]
	Tags	[]
+6 3D-CAD Models		
-1 Model 1	3D-CAD Part Update Method	UPDATE_GEOMETRY
	Tags	[]
+1 Body Groups		
-1 Body 1	Name	Body 1
	Color	java.awt.Color[r=128,g=128,b=128]
	Opacity	1.0
	Tags	[]
+2 Features		
+1 XY	Error Message	
	Origin	[0.0, 0.0, 0.0] m
	X-Axis	[1.0, 0.0, 0.0]
	Y-Axis	[0.0, 1.0, 0.0]
	Tags	[]
+2 YZ	Error Message	
	Origin	[0.0, 0.0, 0.0] m
	X-Axis	[0.0, 1.0, 0.0]
	Y-Axis	[0.0, 0.0, 1.0]
	Tags	[]
+3 ZX	Error Message	
	Origin	[0.0, 0.0, 0.0] m
	X-Axis	[0.0, 0.0, 1.0]
	Y-Axis	[1.0, 0.0, 0.0]
	Tags	[]
+4 Global Origin	Error Message	
	Position	[0.0, 0.0, 0.0]
	Tags	[]

	+5	Lab	Error Message	
Coordinate System				
			Origin	[0.0, 0.0, 0.0]
			X-axis Direction	[1.0, 0.0, 0.0]
			Y-axis Direction	[0.0, 1.0, 0.0]
			Tags	[]
	+6	Sketch 1	Error Message	
			Tags	[]
	`-7	Extrude 1	Error Message	
			Sketch	Sketch 1
			Method	Blind
			Direction Type	Normal
			Extrusion Options	OneWay
			Distance	0.005 m
			Asym. Distance	0.1 m
			Draft	None
			Draft Angle	10.0 deg
			Offset Distance	0.1 m
			Body Type	Solid
			Body Interaction	Merge
			Bodies To Interact	All
			Tags	[]
	3	Design	Parameters	
+-7 Operations				
	+1	Badge	Input Parts	[Body 1]
for 2D Meshing				
			Tags	[]
	2	Automated Mesh (2D)	Per-Part Meshing	false
			Mesher Execution Mode	Serial
			Input Parts	[Body 1]
			Preserve Surface Perimeters	None
			Verbose Output	false
			Tags	[]
+-1 Meshers				
	+1	Polygonal Mesher	Perform Curvature Refinement	true
			Perform Proximity Refinement	true
			Perform Compatibility Refinement	false

	Create Aligned Meshes	true
	Minimum Face Quality	0.05
-2 Prism Layer Mesher	Stretching Function	Geometric Progression
	Fashion distribution	Stretch Factor
	Boundary March Angle	50.0
	Gap Fill Percentage	25.0
	Minimum Thickness Percentage	10.0
	Layer Reduction Percentage	50.0
	Concave Angle Limit	0.0
	Convex Angle Limit	360.0
	Near Core Layer Aspect Ratio	0.0
+2 Default Controls		
+1 Base Size	Base Size	0.1 m
	Base Size	0.1 m
+2 CAD Projection	Project to CAD	true
+3 Target Surface Size	Size Type	Relative to base
	Percentage of Base	100.0
	Absolute Size	0.1 m
+4 Minimum Surface Size	Size Type	Relative to base
	Percentage of Base	10.0
	Absolute Size	0.01 m
+5 Surface Curvature	Enable Curvature Deviation Distance	false
	# Pts/circle	72.0
	Max # Pts/circle	200.0
	Curvature Deviation Distance	0.01 m
+6 Surface Proximity	Search Floor	0.0 m
	# Points in gap	2.0
	Enable Search Ceiling	false
	Search Ceiling	1.0E10 m
+7 Surface Growth Rate	Surface Growth Rate	1.01
+8 Number of Prism Layers	Number of Prism Layers	5
+9 Prism Layer Stretching	Prism Layer Stretching	1.2

-10 Layer Thickness	Prism Total	Size Type	Relative to base
		Percentage of Base	20.0
		Absolute Size	0.02 m
3	Custom Controls		
+1 Control	Surface	Enable Control	true
		Controls Display Mode	All
		Share Surface area	[Body 1.Building]
		Apply Only to Contacting Area	false
		Tags	[]
+1	Controls		
+1	Target Surface Size	Target Surface Size	Custom
+2	Minimum Surface Size	Minimum Surface Size	Custom
+3	Surface Curvature	Curvature	Custom
+4	Surface Proximity	Proximity	Parent
+5	Edge Proximity	Proximity	Parent
+6	Surface Growth Rate	Surface Growth Rate	Custom
+7	Dominant Element Type	Dominant Element Type	Parent
+8	Prism Layers	Prism Layers	Custom
^-1	Customize	Customize Number of Layers	true
		Customize Total Thickness	true
		Customize Distribution	true
		Override Boundary Defaults	false
-9	Wake Refinement	Specify wake refinement options	false
^-2	Values		
+1	Target Surface Size	Size Type	Absolute
		Percentage of Base	0.7999999999999999
		Absolute Size	0.8 mm
+2	Custom Prism Values		

+1	Number of Prism Layers	7
+2	Prism Layer Stretching	1.5
`3	Prism Layer Total Thickness	Size Type Absolute
	Percentage of Base	0.7999999999999999
	Absolute Size	0.8 mm
+3	Minimum Surface Size	Size Type Absolute
	Percentage of Base	0.08
	Absolute Size	0.08 mm
+4	Surface Curvature	Enable Curvature Deviation Distance false
	# Pts/circle	72.0
	Max # Pts/circle	200.0
	Curvature Deviation Distance	0.01 m
-5	Surface Growth Rate	Surface Growth Rate 1.2
2	Volumetric Control	Enable Control true
	Controls Display Mode	All
	Shares	[Block]
	Tags	[]
+1	Controls	
+1	Surface Remesher	Customize Size true
-2	Prism Layer Mesher	Customize Number of Layers true
	Customize Total Thickness	true
	Customize Stretching	true
`2	Values	
+1	Custom Size	Size Type Absolute
	Percentage of Base	5.0
	Absolute Size	0.005 m
2	Custom Prism Values	
	Number of Prism Layers	Number of Prism Layers 5
+2	Prism Layer Stretching	Prism Layer Stretching 1.2

3	Prism	Size Type	Relative to base
Layer	Total		
Thickness			
		Percentage of Base	20.0
		Absolute Size	0.02 m
+8		Number of Children	3
Descriptions			
+-1	Root	Described Parts	[Body 1, Block]
+-2	Latest	Described Parts	[Body 1, Block]
Surface			
		Faces	56
		Vertices	32

Solution

Accumulated CPU Time over all processes (s)	1462790.8300024234
Elapsed Time (s)	36603.323249816895
Time Level	21500
Solution Time	21.500000000003293



## BIBLIOGRAPHIC REFERENCES

### BOOKS, THESES AND DISSERTATIONS

**BETZ Albert**, *Windenergie und ihre Ausnutzung durch Windmühlen*, Göttingen, Vandenhoeed & Ruprecht, 1926. A detailed presentation of the blade element theory is given in: **JOURIEH Munif**, *Développement d'un modèle représentatif d'une éolienne afin d'étudier l'implantation de plusieurs machines sur un parc éolien*, Thèse de Doctorat de Mécanique, Arts et Métiers ParisTech, Paris, 2007, p. 51-57. <https://pastel.archives-ouvertes.fr/pastel-00003390/>, 1926.

**BOSSANYI E. A.** , **WHITTLE G. E.** , **DUNN P. D.** , **LIPMAN N. H.** , **MUSGROVE P. J.** and **MACLEAN C.** , "The efficiency of wind turbine clusters," 1980, pp. 401-416.

**BENYUS Janine M.** , *Biomimicry: When Nature Inspires Sustainable Innovation*, 1<sup>re</sup> ed., HARMONIA MUNDI, Paris, 2011, 408 p.

**CARRIVEAU Rupp**, *Fundamental and Advanced Topics in Wind Power*, BoD - Books on Demand, 2011, 438 pp.

**ARTHUR L.** and **LEMAIRE M.** , *Les Chauves-souris de France Belgique Luxembourg et Suisse*, BIOTOPE, coll. " Collection Parthénopé ", 2009.

**DEGHAN KAMARAGI Gholamreza**, *Ventilation and cooling systems in traditional Persian Gulf architecture: device history, modeling, performance evaluation.* , These in Architecture, GSA Laboratory, Université Paris Est, 2012.

**FERRUCCI Margherita**, *Natural ventilation in architecture: methods, tools and design rules*, These de doctorat, Paris Est, 2017.

**JOURIEH Munif**, *Développement d'un modèle représentatif d'une éolienne afin d'étudier l'implantation de plusieurs machines sur un parc éolien*, phd thesis, Arts et Métiers ParisTech, 2007.

**MOSHTAGHE GOHARI Kambiz**, *Morphogenesis of Iranian windmills, techniques of managing wind in an architectural way*, PhD thesis, Paris Est, 2018.

**MORIARTY Mark**, *FEASIBILITY OF SMALL-SCALE URBAN WIND ENERGY GENERATION*, Thesis, University of Pittsburg, 2015

**EDWARD NG**, "Improving the wind environment in high-density cities by understanding urban morphology and surface roughness: a study in Hong Kong," 2011.

**SCOFFIER Richard**, *Frédéric Borel*, 01 ed, Norma, Paris, France, 2004, 224 p.

**SCOFFIER Richard**, *Ecole nationale supérieure d'architecture de Paris Val-de-Seine*, Archibooks, 148 p.

**WANG Biao**, *The impacts of urban morphology on wind: wind energy performance at the neighborhood scale*, 2015.

**WILCOX David C.** *Turbulence Modeling for CFD*, 2nd edition, D C W Industries, La Cãnada, Calif, 1998, 540 pp.

**WANG Biao**, *The impacts of urban morphology on wind: wind energy performance at the neighborhood scale*, 2015.

**WHITTLESEY Robert W. , LISKA Sebastian and DABIRI John O. ,** "Fish schooling as a basis for vertical axis wind turbine farm design," *Bioinspiration & Biomimetics*, August 2010, vol. 5, n° 3, p. 035005.

**WILCOX David C.** *Turbulence Modeling for CFD*, 2nd edition, D C W Industries, La Cãnada, Calif, 1998, 540 pp.

#### ARTICLES ON AIR STUDIES

**ABD RAZAK, HAGISHIMA, and TANIMOTO,** "Analysis of airflow over building arrays for assessment of urban wind environment," *Building and Environment*, 2013.

**AL-BAHADLY Ibrahim,** "Building a wind turbine for rural home," *Energy for sustainable development* 13.3, 2009.

**ANNIE-CLAUDE BAYEUL-LAINÉ,** "Three-dimensional modeling of the hydrofoil of Mr. Gérard WILLS using the Star CCM+ calculation code", 2011.

**BAHADORI,** "Passive Cooling Systems in Iranian Architecture," *in* , 1978, p. 144.

**BASKARAN Appupillai and KASHEF Ahmed,** "Investigation of air flow around buildings using computational fluid dynamics techniques," *Engineering Structures*, November 1, 1996, vol. 18, n° 11, pp. 861-875.

**BASSETT K. , CARRIVEAU R. and TING D. S. -K. ,** "3D printed wind turbines part 1: Design considerations and rapid manufacture potential", *Sustainable Energy Technologies and Assessments*, 1 September 2015, vol. 11, pp. 186-193.

**ELIASSON and OFFERLE,** "Wind fields and turbulence statistics in an urban street canyon," *Atmospheric Environment*, 2006, vol. 40, n° 1, pp. 1-16.

**HAN Nuomin, ZHAO Dan, SCHLUTER Jorg U. , GOH Ernest Seach, ZHAO He, and JIN Xiao,** "Performance evaluation of 3D printed miniature electromagnetic energy harvesters driven by air flow," *Applied Energy*, September 15, 2016, vol. 178, pp. 672-680.

**HELOISE Mme, ALAIN M, BRUNO M, VANESSA Mme, BONIFACE M, STEPHEN M, and SOPHIA-ANTIPOLIS INRIA,** "Numerical simulation of flows around non-profil'es bodies by hybrid turbulence models and a multi-rate scheme," p. 210.

#### ARTICLES ON URBAN WIND POWER

**ACOSTA Jorge L. , COMBE Kevin, DJOKIC Saša Ž, and HERNANDO-GIL Ignacio,** "Performance Assessment of Micro and Small-Scale Wind Turbines in Urban Areas," *IEEE Systems Journal*, March 2012, vol. 6, n° 1, pp. 152-163.

**AHMADIKIA Hossein, MORADI Amir, and HOJJATI Mohammad,** "Performance Analysis of a Wind-Catcher With Water Spray," *International journal of green energy*, February 1, 2012, vol. 9.

**CHALMERS B.J. and SPOONER E. ,** "An axial-flux permanent-magnet generator for a gearless wind energy system," *IEEE Transactions on Energy Conversion*, June 1999, vol. 14, n° 2, pp. 251-257.

**CHAPMAN Lee, BELL Cassandra and BELL Simon**, "Can the crowdsourcing data paradigm take atmospheric science to a new level? A case study of the urban heat island of London quantified using Netatmo weather stations," *International Journal of Climatology*, 2017, vol. 37, n° 9, pp. 3597-3605.

**CHEN James**, *Internet of Energy (IoE)*, <https://www.investopedia.com/terms/i/internet-energy-ioe.asp>, accessed July 15, 2020.

**EIFFEL Gustave**, *Scientific works executed at the 300-meter tower: From 1889 to 1900*, BnF collection ebooks, 2016, 318 pp.

**ELERT Glenn**, *Flow Regimes*, <https://physics.info/turbulence/>, accessed July 20, 2020.

**ELHADIDY M. A. and SHAAHID S. M.**, "Feasibility of hybrid (wind + solar) power systems for Dhahran, Saudi Arabia", *Renewable Energy*, 1 January 1999, vol. 16, n° 1, coll. "Renewable Energy Efficiency, Policy and the Environment", pp. 970-976.

**HEZAVEH Seyed Hossein, BOU-ZEID Elie, DABIRI John, KINZEL Matthias, CORTINA Gerard, and MARTINELLI Luigi**, "Increasing the Power Production of Vertical-Axis Wind-Turbine Farms Using Synergistic Clustering," *Boundary-Layer Meteorology*, November 1, 2018, vol. 169, n° 2, pp. 275-296.

**JARRY Laura**, *Carmen storm. Bouin wind turbine on the ground: "It would be a mini-tornado,"* <https://www.ouest-france.fr/pays-de-la-loire/challans-85300/tempe-te-carmen-eolienne-de-bouin-au-sol-ce-serait-une-mini-tornade-5480134>, accessed July 23, 2020.

**KRISH Sivam**, "A practical generative design method," *Computer-Aided Design*, January 1, 2011, vol. 43, n° 1, pp. 88-100.

**MCCORMACK Jon, DORIN Alan, and INNOCENT Troy**, "Generative design: a paradigm for design research," p. 8.

**MCLAREN, DUNCAN, AGYEMAN, and JULIAN**, "Intelligent city," in *Sharing cities*.

**MILLER L. M. , GANS F. and KLEIDON A. ,** "Estimating maximum global land surface wind power extractability and associated climatic consequences," *Earth System Dynamics*, 11 February 2011, vol. 2, n° 1, pp. 1-12.

**O'KANE**, "The Madrasa al-GhiyāsÂiyya at Khargird," in , 1976, p. 85.

**PARASCHIVOIU Ion**, *Wind Turbine Design. With Emphasis on Darrieus Concept - Ion Paraschivoiu*, Polytechnic International Press, 2002.

**RAO Dr. S. Srinivasa, SHANMUKESH Kota, NAIDU M. K., and KALLA Praveen**, "Design and Analysis of Archimedes Aero-Foil Wind Turbine Blade for Light and Moderate Wind Speeds," *International Journal on Recent Technologies in Mechanical and Electrical Engineering*, August 31, 2018, vol. 5, n° 8, pp. 01-05-01-05.

**RAO K. R. ,** "Wind Energy: Technical Considerations - Contents," in K. R. RAO (ed.), *Wind Energy for Power Generation: Meeting the Challenge of Practical Implementation*, Springer International Publishing, Cham, 2019, pp. 1-426.

**REMY Tom and MBISTROVA**, "Offshore Wind in Europe Key trends and statistics 2017," *windeurope*.

**RICCIAR DELLI F, POLIMENO S. JWIND ENG IND AERODYN**, "Some characteristics of the wind flow in the lower urban boundary layer," 2006.

**ROAF S**, "Windcatchers," in *Windcatchers in Living with the Desert*, 1982, pp. 57-70.

**ROY DENOON, BRAD COCHRAN, DAVID BANKS, GRAEME WOOD**, *Harvesting Wind Power from Tall Buildings*, 2008.

**SCOFFIER Richard**, *Frédéric Borel*, 01 ed, Norma, Paris, France, 2004, 224 p.

**SCOFFIER Richard**, *Ecole nationale supérieure d'architecture de Paris Val-de-Seine*, Archibooks, 148 p.

**SERERO David**, "Dômes Acoustiques à géométrie variable", *Journal de l'Académie de France à Rome Villa Médicis*, 04/2006 p.

**SHEAHAN Matthew**, "The foiling phenomenon - how sailing boats got up on foils to go ever-faster," p. 19.

**SNOW D. J.**, *Low frequency noise and vibration measurements at a modern wind farm*, Powergen - Ratcliffe Technology Centre, 1997.

**SPERA D. A.** "Wind Turbine Technology," *The U.S. Department of Energy's Office of Scientific and Technical Information*, 1994.

**STANKOVIC Sinisa, CAMPBELL Neil, and HARRIES Alan**, *Urban Wind Energy*, Reprint, Routledge, 2015, 200 pp.

**TOMINAGA Yoshihide, AKABAYASHI Shin-ichi, KITAHARA Takuya, and ARINAMI Yuki**, "Air flow around isolated gable-roof buildings with different roof pitches: Wind tunnel experiments and CFD simulations," *Building and Environment*, January 1, 2015, vol. 84, pp. 204-213.

**UCHIDA and OHYA**, "Micro-siting technique for wind turbine generators by using large-eddy simulation," *Wind Engineering and Industrial Aerodynamics*, 2008, pp. 2121-2138.

**WOOD Curtis R**, "Wind observations above an urban river using a new lidar technique, scintillometry and anemometry," *The Science of the total environment*, 2013.

## STUDY REPORTS

**ALBA Dominique**, *Analysis of the thermal performance of Parisian housing*, <https://www.apur.org/fr/nos-travaux/analyse-performance-thermique-logements-parisiens>, accessed October 6, 2020.

**ALBA Dominique**, *Analysis of the thermal performance of Parisian housing built between 1801 and 1850*, 2011.

**ALBA Dominique**, *Analysis of the thermal performance of Parisian housing built between 1851 and 1914*, 2011.

**ALBA Dominique**, *Analysis of the thermal performance of Parisian housing built between 1918 and 1939*, 2011.

**ALBA Dominique**, *Analysis of the thermal performance of Parisian housing built between 1945 and 1974*, 2011.

**ALBA Dominique**, *Analysis of the thermal performance of Parisian housing built between 1975 and 2000*, 2011.

"Report 17-03. Health Nuisances of Onshore Wind Turbines - National Academy of Medicine | An Institution in its Time".

**BOUGLÉ Fabien**, *Wind turbines: the dark side of the ecological transition*, Éditions du Rocher, 2019.

**BOURGEON Jean-Mathieu, DYEN Stéphane, MOYON Davy, SCHMÄH Daniel, AMACHER Robin, COLEGRAVE Damien, CALMON Martin, FARHAT Mohamed, FUA Pascal, STARTCHEV Konstantin, BONNIER Guillaume, MÅNSON Jan-Anders, MICHAUD Véronique, SIGG Antoine, OGGIER Marc, DEVILLE Michel, BRAUN Olivier, SAWLEY Mark, BLECHA Luc, and CUGNONI Joël**, *L'Hydroptère: A story of a dream*, <https://infoscience.epfl.ch/record/161566>, accessed May 24, 2020.

**BRUYERRE Philippe**, " Power of windmills ", *Le Monde des Moulins*, 08/07/2019 p.

**DANCETTE Mael**, *What is the purpose of the multi-annual energy program (PPE)? PPE (programmation pluriannuelle de l'énergie): definition and objectives*, <https://www.connaissancedesenergies.org/quoi-sert-la-programmation-pluriannuelle-de-lenergie-ppe-170324>, accessed July 15, 2020.

**UNITED NATIONS ENVIRONMENT PROGRAMME**, *Guidelines for the consideration of bats in wind projects. Update 2014*, UNEP/EUROBATS, Bonn, 2016.

## PRESS ARTICLES

**LENOIR Luc**, *Le (polluant) recyclage des vieilles éoliennes allemandes*, <https://www.lefigaro.fr/economie/le-scan-eco/decryptage/2019/01/29/29002-20190129ARTFIG00141-le-polluant-recyclage-des-vieilles-eoliennes-allemandes.php>, accessed 23 July 2020.

"Do wind turbines increase CO2 emissions?", *Le Monde.fr*, 10/01/2012 p.

*Wind turbines: 30 million tons of concrete to save biodiversity - Economie Matin*, <http://www.economiematin.fr/news-eoliennes-beton-artificialisation-sol-biodiversite>, accessed July 23, 2020.

*Tabarly : the foil history of the Paul Ricard trimaran*, <https://www.voileetmoteur.com/voiliers/actualite-voile/regates-courses/tabarly-la-foil-histoire-de-paul-ricard/72662>, accessed on May 24, 2020.

*A new 3D printer on the International Space Station?* <https://www.3dnatives.com/imprimante-3d-espace-23052018/>, accessed on May 24, 2020.

## WEB SITES

**AGAFONKIN Vladimir**, *How I built a wind map with WebGL*, <https://blog.mapbox.com/how-i-built-a-wind-map-with-webgl-b63022b5537f>, accessed July 15, 2020.

**WINDFINDER.COM**, *Windfinder - wind, wave & weather reports, forecasts & statistics worldwide*, <https://www.windfinder.com>, accessed 15 July 2020.

*Endangerment of protected species: FNE sues EDF Energies Nouvelles*, <https://www.fne.asso.fr/actualites/mise-en-p%C3%A9ril-d%E2%80%99esp%C3%A8ces-prot%C3%A9g%C3%A9es-fne-assigne-edf-energies-nouvelles>, accessed on 23 July 2020.

*Myth: All renewable electricity generation is intermittent*, <https://www.connaissancedesenergies.org/toutes-les-energies-renouvelables-productrices-delectricite-sont-intermittentes-141105>, accessed July 15, 2020.

*Does Your Car Look Happy To You? Designers Talk About The Evolution Of Lights, Grilles And Bumpers*, <https://www.ibtimes.com/does-your-car-look-happy-you-designers-talk-about-evolution-lights-grilles-bumpers-1491974>, accessed May 23, 2020.

*Transmission of electricity AC or DC? Explanation*, <https://www.connaissancedesenergies.org/est-il-preferable-de-transporter-l-electricite-en-courant-alternatif-ou-continu-130830>, accessed July 15, 2020.

*Grenelle de l'Environnement: stakes, actors, laws of 2009 and 2010*, <https://www.connaissancedesenergies.org/fiche-pedagogique/grenelle-environnement>, accessed on July 15, 2020.

*Onshore Wind Turbines: Operation, Issues and Major Players*, <https://www.connaissancedesenergies.org/fiche-pedagogique/eoliennes-terrestres>, accessed July 15, 2020.

*Onshore Wind Turbines: Operation, Issues and Major Players*, <https://www.connaissancedesenergies.org/fiche-pedagogique/eoliennes-terrestres>, accessed July 15, 2020.

*The World at War with Wind Turbines*, <https://www.territoire-energie.com/article/le-monde-en-guerre-contre-les-eoliennes/>, accessed July 23, 2020.

*BĀDGĪR - Encyclopaedia Iranica*, <http://www.iranicaonline.org/articles/badgir-traditional-structure-for-passive-air-conditioning>, accessed February 26, 2019.

*BNEF 2016 wind turbine manufacturers ranking*, <https://about.bnef.com/blog/vestas-reclaims-top-spot-annual-ranking-wind-turbine-makers/>, accessed July 17, 2020.

*Offshore Wind*, <https://www.ecologique-solidaire.gouv.fr/eolien-en-mer-0>, accessed July 15, 2020.

*Eiffel Aerodynamics Laboratory*, <http://www.aerodynamiqueeiffel.fr/detail.php?id=45>, accessed July 15, 2020.

*Energy & Environmental Science*, <https://www.rsc.org/journals-books-databases/about-journals/energy-environmental-science/>, accessed July 23, 2020.

*Federation Environnement Durable - Vent du Bocage*, <https://ventdubocage.net/sante3.htm>, accessed July 23, 2020.

*Schomer, et al, Wind Turbine Noise Conference, Denver, August 2013 | Waubra Foundation*, <https://waubrafoundation.org.au/resources/schomer-et-al-wind-turbine-noise-conference-denver-august-2013/>, accessed 23 July 2020.

*Anses - Agence nationale de sécurité sanitaire de l'alimentation, de l'environnement et du travail*, <https://www.anses.fr/fr>, accessed 23 July 2020.

*Wind Power and Bird Studies*, <http://www.currykerlinger.com/studies.htm>, accessed July 23, 2020.

*LPO (Ligue pour la Protection des Oiseaux)*, <https://www.lpo.fr/>, accessed 23 July 2020.

*Impacts of Wind Turbines on Birds - Wind Biodiversity*, <https://eolien-biodiversite.com/impacts-connus/article/eoliennes-et-oiseaux>, accessed 23 July 2020.

*Impacts of Wind Turbines on Bats - Wind Biodiversity*, <https://eolien-biodiversite.com/impacts-connus/article/eoliennes-et-chauves-souris>, accessed 23 July 2020.

*How to recycle wind turbine blades?*

<https://www.livingcircular.veolia.com/fr/industrie/comment-recycler-les-pales-des-eoliennes>, accessed July 23, 2020.

*Limoux. Eoliennes du Limousis : on les démonte*,

<https://www.ladepeche.fr/article/2010/04/21/820617-eoliennes-du-limousis-on-les-demonte.html>, accessed on July 23, 2020.

*What is the Internet of Energy?* <https://www.nesgt.com/blog/2019/05/what-is-the-internet-of-energy>, accessed July 15, 2020.

*5 problems the internet of energy can solve | Greenbiz*, <https://www.greenbiz.com/article/5-problems-internet-energy-can-solve>, accessed July 15, 2020.

*Grid edge - where the energy system of the future takes off*,

<https://new.siemens.com/global/en/company/stories/infrastructure/grid-edge-where-the-energy-system-of-the-future-takes-off.html>, accessed July 15, 2020.

*Transforming Singapore*, <https://www.smartnation.gov.sg/why-Smart-Nation/transforming-singapore>, accessed July 15, 2020.

*1650 Jansson Wind Rose, Anemographic Chart, or Map of the Winds*,

<https://www.geographicus.com/P/AntiqueMap/Anemographica-jansson-1650>, accessed 15 July 2020.

*Features of the Smart Weather Station*, <https://www.netatmo.com/fr-fr/weather/weatherstation/specifications>, accessed July 17, 2020.

*Smart Weather Station and Accessories - How does wind measurement work? | Netatmo*

*Helpcenter*, <https://helpcenter.netatmo.com/fr/station-meteo-intelligente-et-ses-accessoires/mesures-et-calibrations/la-mesure-du-vent-comment-ca-marche>, accessed July 17, 2020.

*Mesh concept in Star-CCM+*, <http://hmf.enseeiht.fr/travaux/beiepe/book/export/html/1108>, accessed July 20, 2020.

*Connected Anemometer*, <https://www.netatmo.com/fr-fr/weather/weatherstation/anemometer>,

accessed May 26, 2020.

*3D PRINTING IN SPACE*, <https://beeverycreative.space/>, accessed May 24, 2020.



# INDEX OF ILLUSTRATIONS

All simulations, 3D models, building photos and field photos were made by D. Serero

Known sources are cited in the legend of each figure.

Some sources have not been found. If you are the author of one of these unidentified views, please contact us so that we can specify the origin of the sources: david.serero@paris-valdeseine.archi.fr

<a href="#">Figure 1: Mapping of currently unused renewable energy sources in buildings By D. Serero</a> .....	11
<a href="#">Figure 2. Raw earth windmills in the city of Nashtifan in eastern Iran</a> .....	22
<a href="#">Figure 3. The vertical blades of the raw earth windmills partly go up against the wind and limit the speed of the device, src: National Geographic, photo Reza Azizfarkhani</a> .....	22
<a href="#">Figure 4: Nashtifan mills operation diagram, surveyed by WHC UNESCO</a> .....	22
<a href="#">Figure 5. Cross-sectional drawings of five typical wind tower types in Yazd city at the vent level. A. Unidirectional. B. Bidirectional. C. Four-way. D. Octagonal with two vents on each side. E. Four-way with two "false" vents on opposite sides.</a> .....	23
<a href="#">Figure 6. A wind turbine in Yazd with wooden poles on which scaffolding is attached for maintenance purposes.</a> .....	23
<a href="#">Figure 7. Cross section through a wind catcher serving the main summer rooms of a house in Yazd. A. Tālār. B. Basement. C. Courtyard with pool by H. Ahmadikia.</a> .....	24
<a href="#">Figure 8. Schematic of the wind tower operation according to day and night (drawn by D. Serero)</a> .....	25
<a href="#">Figure 9. Windmill in Schiedam, the Netherlands (photo D. Serero)</a> .....	26
<a href="#">Figure 10. The Moidrey mill in Pontorson (Manche), Photograph D. Serero on May 27, 2018, it is a "tower mill" type mill</a> .....	27
<a href="#">Figure 11. Detail of the blades whose angle can vary according to the wind speed (D. Serero)</a> .....	27
<a href="#">Figure 12. The Cassel (North) "pivot" type mill (Photo by PAT 2013, www.moulins-a-vent.net)</a> .....	27
<a href="#">Figure 13. The "cavier" type mill-cavier of Aigremonts in Bléré (Indre-et-Loire) (Photo by PAT 2013, www.moulins-a-vent.net)</a> .....	27
<a href="#">Figure 14 Power curves of three main types of mills ( black, Flemish mill; red, symmetrical wing mill and variable inclination; green, symmetrical wing mill and constant inclination.</a> .....	29
<a href="#">Figure 15 Power of different types of windmills in a 6.5 m/s wind</a> .....	29
<a href="#">Figure 16. 1888 The Cleveland Wind Turbine, an Electrical First</a> .....	30
<a href="#">Figure 17. Portrait of Charles Brush, the inventor of the first electricity-generating wind turbine</a> .....	30
<a href="#">Figure 18. 35 m machine, 1,000 kW, Neyrpic wind turbines in Saint-Rémy-des-Landes. (Source: <a href="http://eolienne.cavey.org/communs">http://eolienne.cavey.org/communs</a>).</a> .....	31
<a href="#">Figure 19. Model of the BEST double helix wind turbine, by engineer Lucien Romani in 1963, EDF Research and Studies Department, a wind turbine project (Source: <a href="http://eolienne.cavey.org/communs">http://eolienne.cavey.org/communs</a>)</a> .....	31
<a href="#">Figure 20. Gedser turbine in Denmark, on a reinforced concrete mast - the origin of today's wind turbines (source: <a href="https://fr.wind-turbine-models.com/">https://fr.wind-turbine-models.com/</a>)</a> .....	32
<a href="#">Figure 21. Danish engineer Johannes Juul (1887 -1969) (source: <a href="http://www.windsofchange.dk/JohannesJuul.png">http://www.windsofchange.dk/JohannesJuul.png</a>)</a> .....	32
<a href="#">Figure 22. Kentish Flats offshore wind farm, off the British coast of Kent (@Vattenfall-Robin Dawe)</a> .....	33
<a href="#">Figure 23. Evolution of the size and power of offshore wind turbines (@Connaissance des Énergies / <a href="https://www.connaissancedesenergies.org/sites/default/files/eolien_offshore.infographie_zoom.png">https://www.connaissancedesenergies.org/sites/default/files/eolien_offshore.infographie_zoom.png</a>)</a> .....	34
<a href="#">Figure 24. Eiffel wind tunnel, longitudinal section of the initial configuration of the wind tunnel. Source: © Laboratoire Eiffel, with the kind permission of Mr Martin Peter</a> .....	39
<a href="#">Figure 25. Motorization of the Eiffel wind tunnel, Photo D. Serero of 18/09/2016. Source © Eiffel Laboratory, courtesy of Mr. Martin Peter</a> .....	39
<a href="#">Figure 26. Eiffel wind tunnel by Gustave Eiffel. The wind tunnel chamber of the aerodynamic laboratory created by Gustave Eiffel in 1911. Paris, 16th district, 67, rue Boileau. Source © Laboratoire Eiffel, courtesy of Mr. Martin Peter</a> .....	39
<a href="#">Figure 27. Eiffel wind tunnel by Gustave Eiffel, study of an aircraft, Source © Laboratoire Eiffel, courtesy of Mr Martin Peter</a> .....	40

<a href="#">Figure 28. Aerodyne wind tunnel, Association d'études réalisations en optimisation Dynamique&amp; Energétique ; Source : <a href="https://aerodyne-cachan.blogspot.com/">https://aerodyne-cachan.blogspot.com/</a>, with the kind permission of the association.</a>	41
<a href="#">Figure 29. Aerodyne wind tunnel. Source: <a href="https://aerodyne-cachan.blogspot.com/">https://aerodyne-cachan.blogspot.com/</a>, courtesy of the association.</a>	41
<a href="#">Figure 30. Wind tunnels of Saint Cyr. Source: Souffleries S2A; <a href="http://www.soufflerie2A.com">www.soufflerie2A.com</a></a>	42
<a href="#">Figure 31. Visual impact on the landscape of a wind farm in San Gorgonio Pass, USA, source: Stock Photos &amp; Images (662)</a>	44
<a href="#">Figure 32. Comparative height of wind turbines to heritage buildings in intermediate scale cities.</a>	44
<a href="#">Figure 33. In Coutances, Normandy, a wind turbine is located in the axis of the city's cathedral and distorts the urban panorama of the city</a>	44
<a href="#">Figure 34. Noise impact comparison (source: <a href="https://reporterre.net/Quel-est-l-impact-des-eoliennes-sur-l-environnement-Le-vrai-le-faux">https://reporterre.net/Quel-est-l-impact-des-eoliennes-sur-l-environnement-Le-vrai-le-faux</a>)</a>	45
<a href="#">Figure 35. Internet of Things (IoT) connected devices installed worldwide from 2015 to 2025 in billions</a>	55
<a href="#">Figure 36. The example of the internet of energy for new urban mobility</a>	56
<a href="#">Figure 37. Example of a Smart city model, MIT Senseable City Lab, Carlo Rati</a>	57
<a href="#">Figure 38. Distribution of global smart city markets, 2014 - 2019, MIT Senseable City Lab, Carlo Rati</a>	58
<a href="#">Figure 39. "Intelligence" rankings of mid-sized cities in Europe, based on IESE Cities in Motion Index, 2018</a>	59
<a href="#">Figure 40. Strategic national projects for Singapore by Institute Smart Nation, an organization for transforming the relationship between citizens and governance.</a>	60
<a href="#">Figure 41: Collective housing buildings built in Paris before 1800, source: Apur</a>	63
<a href="#">Figure 42. Block consisting of residential buildings built before 1800, model D. Serero</a>	63
<a href="#">Figure 43. Buildings built before 1800, rue Saint-Martin, 1st district, source: Apur</a>	63
<a href="#">Figure 44. Collective housing buildings built in Paris between 1801 and 1850 ( <a href="https://www.apur.org/fr">https://www.apur.org/fr</a> )</a>	65
<a href="#">Figure 45. Block consisting of residential buildings built from 1801 onwards, model D. Serero</a>	65
<a href="#">Figure 46: Buildings constructed between 1801 and 1850, rue de Trévis, Paris, 9th Arrondissement, Source: Apur</a>	65
<a href="#">Figure 47. Collective housing buildings built in Paris between 1851 and 1914</a>	66
<a href="#">Figure 48. Block consisting of apartment buildings built from 1851 onwards, model D. Serero</a>	67
<a href="#">Figure 49. tenement buildings, built between 1851 and 1914, rue de Châteaudun, 9th, photo D. Serero.</a>	67
<a href="#">Figure 50. Rue de Dunkerque and rue de Guérande, 9th district. Apartment buildings, subdivision operation, Source: Geoportail.</a>	67
<a href="#">Figure 51. Multi-family housing buildings built in Paris between 1918 and 1939 (<a href="https://www.apur.org/fr">https://www.apur.org/fr</a>)</a>	69
<a href="#">Figure 52. Block of residential buildings built from 1920 onwards, Modeling D. Serero</a>	69
<a href="#">Figure 53. 1924-1930 H.B.M. housing building, C. Heubès architect, Avenue Simon Bolivar, 19th arrondissement, photo: D. Serero</a>	70
<a href="#">Figure 54. Housing building of the I.L.M. type, 1924-1926 boulevard Jourdan, 14th arrondissement. (<a href="https://www.apur.org/fr">https://www.apur.org/fr</a>)</a>	70
<a href="#">Figure 55. Multi-family housing buildings built in Paris between 1945 and 1974 (<a href="https://www.apur.org/fr">https://www.apur.org/fr</a>)</a>	72
<a href="#">Figure 56. Block made up of M.R.U.* type apartment buildings built from 1945 onwards, Modelling D. Serero</a>	72
<a href="#">Figure 57. Apartment building, rue Dunois and boulevard Vincent Auriol, 13th arrondissement.</a>	73
<a href="#">Figure 58. Place des Fêtes (XIXth arrondissement): large complex under construction, erasing the existing urban grid, 1971 (<a href="https://www.apur.org/fr">https://www.apur.org/fr</a>)</a>	73
<a href="#">Figure 59. Multi-family housing buildings built in Paris between 1975 and 2000 (<a href="https://www.apur.org/fr">https://www.apur.org/fr</a>)</a>	74
<a href="#">Figure 60: Block of residential buildings built from 1975 onwards</a>	75
<a href="#">Figure 61. Apartment building, 1982, Labro and Orzoni architects, rue des Écluses-Saint-Martin, 10th arrondissement. (<a href="https://www.apur.org/fr">https://www.apur.org/fr</a>)</a>	75

<a href="#">Figure 62: ZAC Citroën-Cévennes, 15th arrondissement, 1989-2006, Source: SEMEA 15, aerial mission 2004.</a>	76
<a href="#">Figure 63. Mapping of buildings in Paris based on their typology and date of construction (<a href="https://www.apur.org/fr">https://www.apur.org/fr</a>).</a>	76
<a href="#">Figure 64. Heating power required per unit area of housing, source Ademe</a>	77
<a href="#">Figure 65. Heating power required per unit area of a dwelling in Europe in kWh/m<sup>2</sup> / , Source Ademe</a>	77
<a href="#">Figure 66. Summary of electricity generation in the world (source: EDF/IEA 2013)</a>	84
<a href="#">Figure 67. Sources of electricity generation in France and projection to 2050 ( source: OECD/IEA 2014)</a>	84
<a href="#">Figure 68. Visualization of a possible reappropriation of Parisian roofs with micro-generators, Photomontage: D. Serero</a>	85
<a href="#">Figure 69. This wind map was published in 1650 in the Maritime Atlas, or volume 5 of the Atlantis Majoris, by Janssonius, source: Geographicus.com</a>	86
<a href="#">Figure 70. The Windfinder.com website presents a real-time mapping of wind speed over the entire globe</a>	88
<a href="#">Figure 71. The Windfinder site is cross-platform, Source: windfinder.com</a>	88
<a href="#">Figure 72. The site is dedicated to real-time wind visualization and prediction for snow sports aficionados</a>	88
<a href="#">Figure 73. Surface wind per 18 hours in February 18, 2019, Source: Météo France</a>	89
<a href="#">Figure 74 Maps of climate data available in Ladybug</a>	89
<a href="#">Figure 75.Extraction of the layers constituted by the weather data, the projection media of a real time mapping</a>	91
<a href="#">Figure 76. Data linkage model between wind mapping and satellite data.</a>	91
<a href="#">Figure 77: Global weather and anemometer observation system, source: World Meteorological Organisation, 2019</a>	92
<a href="#">Figure 78. Two resolutions of interactive global wind mapping (source: mapbox.com).</a>	93
<a href="#">Figure 79. Connected weather station used by D. SERERO</a>	94
<a href="#">Figure 80. Ultrasonic anemometer and real-time data presentation interface tablet or smartphone, source: netatmo.com</a>	94
<a href="#">Figure 81. Measuring device mounted on a rigid support 2 m above the roof.</a>	95
<a href="#">Figure 82. Manipulation of the data presentation screens</a>	95
<a href="#">Figure 83. Operating diagram of the ultrasonic anemometer connected by Netatmo site</a>	95
<a href="#">Figure 84. Diagrams of wind speeds measured at the site 136 avenue Parmentier, 75011 Paris in 2018, Vertical axis: speed in M/s. The black curve represents the wind speed and the blue line the minimum winds recorded over the same period.</a>	95
<a href="#">Figure 85. Plan, elevation, cross-section of the anemometer used</a>	96
<a href="#">Figure 86. General data visualization interface, Netatmo application, weather station</a>	96
<a href="#">Figure 87. Map of Netatmo connected weather stations in Paris (real-time data on the NETATMO website)</a>	97
<a href="#">Figure 88 Wind measurement stations show the main directions in the City of Paris, by the Windfinder site.</a>	97
<a href="#">Figure 89 Geolocation of connected anemometers as of 1/12/2017 in Paris on the Netatmo website...</a>	98
<a href="#">Figure 90. Location of the wind survey weather stations, installed by Serero that are compared daily, 2016-2020.</a>	99
<a href="#">Figure 91.Installation of the anemometer on the roof of the building 136 avenue Parmentier, Paris 11<sup>ème</sup>. A TV antenna was used to support the device.</a>	100
<a href="#">Figure 92. Location of the wind survey station - 136 avenue Parmentier - Paris, D. Serero</a>	100
<a href="#">Figure 93. 3D model of the Parmentier building showing the schematic wind flows and the position of the measuring anemometer, 3D model D. Serero</a>	101
<a href="#">Figure 94. Comparison of wind speed in the Paris area measured at national weather stations (Roissy, Orly), and anemometers connected at 22 m above ground level on the roof of a "Faubourg" type building. (in m/s, compared over 4 daily time slots).</a>	102
<a href="#">Figure 95. Parmentier weather station reading (monthly average winds in 2018) at 22m height from the street in a dense urban "Faubourg" environment.</a>	102
<a href="#">Figure 96. Location plan of the house in the Maison des examens neighborhood in Arcueil, D. Serero</a>	102
<a href="#">Figure 97. Wind direction distribution in annual percentage, site 39 rue de Chinon, Arcueil 94110</a>	103

<a href="#">Figure 98. View of the new anemometer at a height of 8 meters above the ground of the Roméra house in Arcueil</a> .....	103
<a href="#">Figure 99: Extract from a sheet of wind speed data in the Paris region measured at national weather stations (Roissy, Orly), and anemometers connected at 8 m above ground level on the roof of a single-family building, D. Serero (in m/s, compared over 4 daily time slots)</a> .....	104
<a href="#">Figure 100. Location of the new anemometer at ENSAPVS</a> .....	
<a href="#">Figure 101. View of the device inserted on the roof of the building (Paris 75013)</a> .....	105
<a href="#">Figure 102. Wind direction distribution in annual percentage, Ecole d'Architecture Paris Val-de-Seine. Paris 75013</a> .....	105
<a href="#">Figure 103. Comparison of wind speed in the Paris area measured at national weather stations (Roissy, Orly), and anemometers connected 30 m above ground on the roof of a complex building. Each reading indicates wind speed and wind direction (in m/s, compared over 4 daily time slots)</a> .....	106
<a href="#">Figure 104. Comparison chart of the wide variety of wind devices that exist to date</a> .....	108
<a href="#">Figure 105. Integration of wind devices in roof wings (roof reversal) to accelerate the airflow</a> .....	109
<a href="#">Figure 106. Preliminary vision for an old Parisian building, renovated with different devices studied</a> .....	110
<a href="#">Figure 107. Integration of wind devices in these funnel type cells to accelerate the airflow</a> .....	110
<a href="#">Figure 108. Electricity generation by "wind arrow" with horizontal axis (Windspire) L= 3m, 0.6m diameter, drawings D. Serero</a> .....	111
<a href="#">Figure 109. Electricity generation by "wind arrow" with horizontal axis (Windspire) L= 2m, 0.6m diameter, drawings D. Serero</a> .....	111
<a href="#">Figure 110. Electricity generation by "wind arrow" with vertical axis ( Windspire) H= 3m, 0.6m diameter, drawings D. Serero</a> .....	111
<a href="#">Figure 111. Micro-wind turbine electricity generation with vertical axis H= 1m, 0.7m diameter, drawings D. Serero</a> .....	112
<a href="#">Figure 112. Changes in urban wind flow related to architectural volumes</a> .....	117
<a href="#">Figure 113. Different turbulence typologies in the wind flow</a> .....	118
<a href="#">Figure 114. Wind effects on high-rise buildings</a> .....	118
<a href="#">Figure 115. Dynamic aeraulic simulation of wind on a section of a building on piles. Simulation by D. Serero</a> .....	120
<a href="#">Figure 116. The Venturi effect</a> .....	121
<a href="#">Figure 117. Experiment of O. Reynolds: presentation of the device (left) and representation of the main A, B and C behaviors of the obtained colored fluid nets</a> .....	124
<a href="#">Figure 118. Flow regimes</a> .....	125
<a href="#">Figure 119. <math>Re &lt; 0.5</math>: No separation, creeping flow</a> .....	125
<a href="#">Figure 120. <math>5 &lt; Re &lt; 40</math>: Pair of symmetrical recirculation vortices</a> .....	125
<a href="#">Figure 121. <math>40 &lt; Re &lt; 180</math>: Transition to turbulence in the wake</a> .....	126
<a href="#">Figure 122. Subcritical regime: <math>300 &lt; Re &lt; 3 \times 10^5</math></a> .....	126
<a href="#">Figure 123. The average lift coefficient is nonzero in the critical regime <math>3 \times 10^5 &lt; Re &lt; 3.5 \times 10^5</math></a> .....	126
<a href="#">Figure 124. The diagram on the left shows a better distribution of cell volume changes</a> .....	129
<a href="#">Figure 125. The deformation angle of the cell</a> .....	130
<a href="#">Figure 126. Definition of the analysis domain and domain boundary conditions</a> .....	132
<a href="#">Figure 127 Detail on a mesh generated around the building under study</a> .....	133
<a href="#">Figure 128 Detail of the mesh in the area around the building</a> .....	133
<a href="#">Figure 129 Detail of a general mesh of the domain</a> .....	134
<a href="#">Figure 130 Extract from the simulation programming window</a> .....	135
<a href="#">Figure 131. Air velocity distribution in the model</a> .....	138
<a href="#">Figure 132. Pressure distribution in the numerical model</a> .....	139
<a href="#">Figure 133 Extract from the STAR CCM+ window for solver definition</a> .....	140
<a href="#">Figure 134. Star CCM+ Screenshot of the profile model to be studied</a> .....	141
<a href="#">Figure 135. Star CCM+ - Profile and 2D mesh view</a> .....	143
<a href="#">Figure 136. Star CCM+ -Magnitude of velocities following the launch of the simulation</a> .....	143
<a href="#">Figure 137. Fig. 86: Star CCM+ - Initial conditions</a> .....	144
<a href="#">Figure 138. Star CCM+, residue curves of the equation not converged in the first calculations</a> .....	145
<a href="#">Figure 139. Analysis of the computational "Residues" on the first 500 iterations. The calculation was not extended to 10,000 iterations because of the computation times exceeding several weeks</a> .....	145

<a href="#">Figure 140. 2D mesh shape</a> .....	146
<a href="#">Figure 141. Velocity Magnitude</a> .....	146
<a href="#">Figure 142. STAR CCM+ -Initial Conditions</a> .....	147
<a href="#">Figure 143. Analysis of the "Residues" of the calculation.</a> .....	147
<a href="#">Figure 144. 2D mesh shape</a> .....	148
<a href="#">Figure 145. Magnitude of the velocities</a> .....	148
<a href="#">Figure 146. STAR CCM+, Condition Setting Window: "PHYSICS</a> .....	149
<a href="#">Figure 147 Location of the 3 study sites with wind survey weather stations installed by Serero from 2016 to 2020.</a> .....	158
<a href="#">Figure 148 Study of a low architectural volume for the integration of micro wind turbines and foils (H=9m)</a> .....	159
<a href="#">Figure 149 Study of a building in an urban block of intermediate scale (H=35m)</a> .....	159
<a href="#">Figure 150 Study of a large-scale building-island along the Seine (H=75m)</a> .....	159
<a href="#">Figure 151 Complementary study of a very large scale building in an open space (Esplanade La Défense) (H=110m)</a> .....	159
<a href="#">Figure 152 - Installation of a connected anemometer on a house in Arcueil (92) by D. Serero</a> .....	160
<a href="#">Figure 153 Roof view of the anemometer connected to a house in Arcueil (92) by D. Serero</a> .....	160
<a href="#">Figure 154 Wind map of Paris measured by Netatmo anemometers</a> .....	161
<a href="#">Figure 155. Mesh of the 2D model of the typical house.</a> .....	163
<a href="#">Figure 156. False color study of wind speed around the house</a> .....	163
<a href="#">Figure 157. Dimensional study of the digital/physical model of the house with foil.</a> .....	164
<a href="#">Figure 158. Mesh of the 2D model of the house with foil type 1</a> .....	165
<a href="#">Figure 159. False color study of wind speed around the house with foil type 1</a> .....	165
<a href="#">Figure 160. Mesh of the 2D model of the typical house with foil type 2</a> .....	166
<a href="#">Figure 161. False-color study of the wind speed around the house with foil type 2. The red rectangle shows the enlarged area in Figure 167.</a> .....	166
<a href="#">Figure 162. False color zoom of wind speed around the house with foil type 2</a> .....	167
<a href="#">Figure 163: Vector field of wind over the house with foil type 2</a> .....	167
<a href="#">Figure 164. Mesh of the 2D model of the typical house with foil type 3</a> .....	168
<a href="#">Figure 165. False color study of wind speed around the house with foil type 3</a> .....	168
<a href="#">Figure 166. Mesh of the 2D model of the typical house with foil type 4</a> .....	169
<a href="#">Figure 167. False color study of wind speed around the house with foil type 4</a> .....	169
<a href="#">Figure 168. Mesh of the 2D model of the typical house with foil type 5</a> .....	170
<a href="#">Figure 169. False color study of wind speed around the house with foil type 5</a> .....	170
<a href="#">Figure 170 3D studies of a 45° aerofoil on a rounded corner of a building</a> .....	172
<a href="#">Figure 171 3D architectural studies of 45° aerofoil implementation on a pointed building</a> .....	172
<a href="#">Figure 172. Dimensional Study Vertical Foil Type H1, Scale 1/20</a> .....	172
<a href="#">Figure 173. Dimensional study of the vertical foil Type H2, Scale 1/20</a> .....	172
<a href="#">Figure 174. Mesh of the 2D model of the building study area without foil</a> .....	173
<a href="#">Figure 175. False color study of wind speed without foil</a> .....	173
<a href="#">Figure 176. 2D model mesh of the building study area with integrated V1 type foil</a> .....	174
<a href="#">Figure 177. False color study of wind acceleration around the integrated vertical foil type V1.</a> .....	174
<a href="#">Figure 178. 2D model mesh of the building study area with integrated foil type 2</a> .....	175
<a href="#">Figure 179. False color study of wind speed around the integrated vertical foil type 2. This simulation shows that this choice of recessed volume has no benefit in accelerating the air in place</a> .....	175
<a href="#">Figure 180. 2D model mesh of the building study area with integrated V3 type foil</a> .....	176
<a href="#">Figure 181. False color study of wind speed around the integrated vertical foil type V 3</a> .....	176
<a href="#">Figure 182. 2D model mesh of the building study area with integrated V4 foil type</a> .....	177
<a href="#">Figure 183. False color study of wind speed around the integrated vertical foil type V4.</a> .....	177
<a href="#">Figure 184. 2D model mesh of the building study area with integrated foil type 5</a> .....	178
<a href="#">Figure 185. False color study of wind speed around the integrated vertical foil type 5</a> .....	178
<a href="#">Figure 186. Dimensional study of the building with acroterial device type 1</a> .....	179
<a href="#">Figure 187. 2D model mesh of the building study area with integrated type 1 acroterion device</a> .....	179
<a href="#">Figure 188. False color study of the wind speed around the acroterial device type 1</a> .....	180
<a href="#">Figure 189. Dimensional study of the building with acroterial device type 1</a> .....	180

<a href="#">Figure 190. Mesh of the 3D model of the building study area with integrated type 1 acroterion device</a>	180
<a href="#">Figure 191. False color study of wind speed increase around the type 1 acroterial device</a>	181
<a href="#">Figure 192 Figure 191: Installation of the anemometer on the roof of the building 136 avenue Parmentier, Paris 11ème. A TV antenna was used to support the device</a>	182
<a href="#">Figure 193. Location of the wind survey station - 136 avenue Parmentier, Paris 11ème</a>	182
<a href="#">Figure 194 Gauge - unlined roadside envelope for airfoil installation on a roadway of 12 m or more but less than 20 m in width</a>	182
<a href="#">Figure 195. Comparison of wind speed measured at the site and at 22m above ground and the wind measured in the CFD model</a>	183
<a href="#">Figure 196. Comparison of wind speed in the Paris area measured at national weather stations (Roissy, Orly, Montsouris), and anemometers connected at 22 m above ground level on the roof of a compressed air plant</a>	184
<a href="#">Figure 197. Wind speed reading from the Parmentier weather station (monthly average winds in 2018) at 22m height from the street in a dense urban "Faubourg." In m/s on the vertical ave</a>	184
<a href="#">Figure 198. Mesh of the 3D model of the study area of the mansard roof without device</a>	185
<a href="#">Figure 199. Simulation of wind speed around the building roof without a device</a>	185
<a href="#">Figure 200. 3D model mesh with device</a>	186
<a href="#">Figure 201. Simulation of the increase in wind speed around the Haussmann building with a</a>	186
<a href="#">Figure 202. Location of the new anemometer at ENSAPVS</a>	188
<a href="#">Figure 203. View of the device inserted on the roof of the building (Paris 75013)</a>	189
<a href="#">Figure 204. Wind direction distribution in annual percentage, Ecole d'Architecture Paris Val-de-Seine. Paris 75013</a>	189
<a href="#">Figure 205. Study of the winds measured by all the connected weather stations showing the main wind directions in Paris. By Windfinder</a>	189
<a href="#">Figure 206. The ENSAPVS building in its large urban context (source: 3D modeling by D. Serero)</a>	190
<a href="#">Figure 207. Aerial view of the different buildings that constitute ENSAPVS (source idem)</a>	190
<a href="#">Figure 208. Position of the 9 areas identified for the connected anemometer survey</a>	191
<a href="#">Figure 209. Urban section of ENSAPVS showing the relationship between the Seine and Avenue de France at the top of the site. (Source: Section drawn by D. Serero)</a>	191
<a href="#">Figure 210. Definition of the aeraulic analysis mesh on the 3D model of ENSAPVS, according to an East-West vertical section</a>	192
<a href="#">Figure 211. Airflow simulation with an average speed of 5m/s, on a North-South section of the ENSAPVS building (on a chimney) Calculation at 10 000 iterations</a>	193
<a href="#">Figure 212. Aeraulic simulation on a North-South section of the ENSAPVS building (with wind speed of 5 m/s, West-East wind direction)</a>	193
<a href="#">Figure 213 Aeraulic simulation on a North-South section of the ENSAPVS building (with wind speed of 5 m/s, West-East wind direction)</a>	194
<a href="#">Figure 214. Analysis plane mesh of the ENSAPVS building with increased densities on areas near the building at 12m</a>	195
<a href="#">Figure 215. Aeraulic simulation on a horizontal section at 12 m elevation of the ENSAPVS building (with an air speed of 5 m/s, West-East wind direction)</a>	195
<a href="#">Figure 216. ENSAPVS building analysis plan mesh with increased densities on areas near the building</a>	196
<a href="#">Figure 217. Aeraulic simulation on a horizontal section at 12m elevation of the ENSAPVS building (with an air speed of 5 m/s, West-East wind direction)</a>	196
<a href="#">Figure 218. Study mesh on a horizontal section at +70m altimetry of the ENSAPVS building (tower dimensions: 25m wide X45m long, scale: 1/1000th)</a>	197
<a href="#">Figure 219. Aeraulic study of a detail of the space between the 2 towers (at altitude + 70m)</a>	197
<a href="#">Figure 220. Study mesh on a horizontal section at +70m elevation</a>	198
<a href="#">Figure 221. Airflow simulation at the 2 towers with the addition of aerofoils</a>	198
<a href="#">Figure 222. Study mesh on a horizontal section at +70m altimetry of the ENSAPVS building</a>	199
<a href="#">Figure 223. Airflow simulation at the 2 towers with the addition of aerofoils</a>	199
<a href="#">Figure 224 3D study of the wind devices integrated into the ENSAPVS building</a>	202
<a href="#">Figure 225. Device study on the ENSAPVS building</a>	202
<a href="#">Figure 226: Comparison of automotive grills showing how a ventilation grille became a brand symbol</a>	209

<a href="#">Figure 227 Examples of air intakes on the fuselage of a jet aircraft</a> .....	209
<a href="#">Figure 228. Examples of architectural volumes of different scales studied for micro-wind turbine and foil integration</a> .....	211
<a href="#">Figure 229. Examples of large-scale architectural volumes studied for the integration of micro-wind turbines and foils (Ecole Architecture Paris-Val-de-Seine, Paris 13ème/ la Grande Arche de la Défense, Puteaux (92))</a> .....	211
<a href="#">Figure 230 Clustering of wind energy devices (operation in groups of turbines close together)</a> .....	211
<a href="#">Figure 231 Dabiri's biomimetic model of fish schools to define the mode of wind turbine aggregation</a> .....	213
<a href="#">Figure 232 Study of turbulence generated by the group effect of fish and wind turbines extracted from the mentioned research</a> .....	214
<a href="#">Figure 233. Vestas Sailrocket 2, piloted by Paul Larsen and designed by English naval architect Malcolm Barnsley</a> .....	215
<a href="#">Figure 234. The Greenbird, a wind-powered car, breaks the speed record in the Nevada desert at 201 km/H, piloted by the Englishman Richard Jenkins. It also uses a rigid carbon sail of the Foil type to reach 3 to 5 times the wind speed</a> .....	215
<a href="#">Figure 235. Angle of incidence of a foil (source: Wikipedia, lift)</a> .....	217
<a href="#">Figure 236 Aeraulic Study of a McLaren F1, 2019 (Soucre: Maclaren entreprise)</a> .....	218
<a href="#">Figure 237 Wing profile on the left: lift force, Inverted wing profile on the right: aerodynamic support</a> .....	219
<a href="#">Figure 238 Aeraulic simulation of a rear wing on the aerodynamic support of a McLaren F1 (Source Maclaren)</a> .....	219
<a href="#">Figure 239 Examples of car fins integrated into the car body</a> .....	220
<a href="#">Figure 240 Examples of DTM blades on the front of a car</a> .....	220
<a href="#">Figure 241. 4 2 Types of vertical axis wind turbines</a> .....	222
<a href="#">Figure 242 Main types of wind energy devices that can be integrated into buildings</a> .....	223
<a href="#">Figure 243. First physical study models with horizontal axis wind turbine test</a> .....	225
<a href="#">Figure 244. Evolution of the models and studies of possible locations</a> .....	225
<a href="#">Figure 245. 3D model of the studied turbines modeled on the Rhinoceros software</a> .....	226
<a href="#">Figure 246 3d printing of wind turbines for device integration study mock-ups; Intermediate stage</a> .....	226
<a href="#">Figure 247 Development of study models in the wind tunnel with G. Bouchet</a> .....	227
<a href="#">Figure 248 Wind tunnel study models</a> .....	228
<a href="#">Figure 249. Initial study model with 2 turbines. Their geometry is not adapted to the foil with a lower rpm on the propeller turbine</a> .....	228
<a href="#">Figure 250. final optimized model with turbine elongation and study foil bracing</a> .....	228
<a href="#">Figure 251. 3d modeling of the wind amplification foil device</a> .....	228
<a href="#">Figure 252. LED Voltmeter Ampere, Current/Voltage Indicator (KKmoon New DC1-100V 10A Digital Multimeter)</a> .....	229
<a href="#">Figure 253. Visualization of flag clusters on a Parisian building (Horizontal and vertical). This device allows to capture the winds induced by the corridor effect of dense and homogeneous streets, but is too "foreign" to the present architecture</a> .....	229
<a href="#">Figure 254. Study of the small-scale building model</a> .....	230
<a href="#">Figure 255 Physical wind tunnel at ENPC</a> .....	230
<a href="#">Figure 256 Comparison of airflow simulation methods, D. Serero</a> .....	231
<a href="#">Figure 257 Main typologies of wind devices that can be integrated into buildings</a> .....	232
<a href="#">Figure 258 Example of a Weibull distribution for estimating the wind distribution over the year, where k is the shape parameter</a> .....	233
<a href="#">Figure 259. Typologies for integrating wind devices into rooftop buildings</a> .....	236
<a href="#">Figure 260 Typologies for integrating wind devices with buildings on facades</a> .....	236
<a href="#">Figure 261. Wind action dendrogram for use by architects and engineers</a> .....	237
<a href="#">Figure 262 Example of a wind device siting analysis on a tower building</a> .....	238
<a href="#">Figure 263 Airflow study on a Foil to punctually accelerate the wind</a> .....	260
<a href="#">Figure 264. Schematic showing the possibility of hybrid operation of the foil as a solar collector and wind gas pedal</a> .....	263

<a href="#">Figure 265. The Giraffe from the Swedish company Innoventrum, a hybrid wind and photovoltaic power generation device that also creates a carport</a>	263
<a href="#">Figure 266. Charles de Gaulle Aircraft door housing a 3D printing workshop for repair/maintenance parts</a>	264
<a href="#">Figure 267. ASE 3D printer that operates in a weightless situation</a>	264
<a href="#">Figure 268. Digital prints for research (SLA, filament, sintering, ...)</a>	265
<a href="#">Figure 269. 3D simulation of the experimental wind tunnel prototype</a>	267
<a href="#">Figure 270. Prototype wind tunnel made by D.Serero to compare the scale of the phenomena</a>	267
<a href="#">Figure 271. Detail of our building model in the air stream</a>	267
<a href="#">Figure 272. Operating diagram of the analog wind tunnel built for the experiment</a>	268
<a href="#">Figure 273. Location of the Measurement Points on the physical tunnel, GSA Laboratory</a>	269
<a href="#">Figure 274. Location of the Measurement Points on the physical tunnel, GSA Laboratory</a>	269
<a href="#">Figure 275. Location of the Measurement Points on the physical tunnel, GSA Laboratory</a>	270
<a href="#">Figure 276. Location of the Measurement Points on the physical tunnel, GSA Laboratory</a>	270
<a href="#">Figure 277. Dynamic simulation of the study physical tunnel model</a>	271
<a href="#">Figure 278. Dynamic simulation of the study physical tunnel model</a>	271
<a href="#">Figure 279. Dynamic simulation of the study physical tunnel model</a>	271
<a href="#">Figure 280. Serero tunnel a vent location</a>	272
<a href="#">Figure 281. Comparison with a model studied in the analog wind tunnel in the laboratory</a>	272
<a href="#">Figure 282. Nordex N90/2300</a>	275
<a href="#">Figure 283. Gamesa G80/2000</a>	275
<a href="#">Figure 284: Enercon E66/2000</a>	275
<a href="#">Figure 285. Vergnet GEV 26/200</a>	275
<a href="#">Figure 286. Vergnet GEV HP</a>	275
<a href="#">Figure 287. Vergnet GEV MP 275</a>	275
<a href="#">Figure 288: Single-bladed wind turbine</a>	276
<a href="#">Figure 289: Pumping Turbine</a>	276
<a href="#">Figure 290. Savonius wind turbine</a>	277
<a href="#">Figure 291. Ropatec Double Vertical</a>	277
<a href="#">Figure 292. Ropatec Twister</a>	277
<a href="#">Figure 293. Ropatec Bora Extreme</a>	277
<a href="#">Figure 294. Windside WS-12</a>	278
<a href="#">Figure 295. Windside WS-2B</a>	278
<a href="#">Figure 296. Windside WS-0.15 C/B</a>	278
<a href="#">Figure 297. San Francisco Public Utilities Commission</a>	291
<a href="#">Figure 298. Example of generative work on the chassis of a vehicle and on the structure of a chair</a>	293
<a href="#">Figure 299. 3D printing of wind turbines with generator turbines</a>	293
<a href="#">Figure 300. generative study of a wind turbine design in Fusion 360</a>	294
<a href="#">Figure 301. Generative study of a wind turbine design in Fusion 360</a>	294
<a href="#">Figure 302. Generative study of a wind turbine design in Fusion 360</a>	295